

Alma Mater Studiorum – Università di Bologna

DOTTORATO DI RICERCA

Science for Conservation

Ciclo **XXII**

Settore/i scientifico disciplinari di afferenza: CHIM/12

TITOLO TESI

**DURABILITY OF MONUMENTAL STONES TREATED
WITH SILOXANE-BASED WATER REPELLENTS**

Presentata da: Ana Bogdana Simionescu

Coordinatore Dottorato

Prof. Rocco Mazzeo

Relatore

Prof. Modesto Montoto

Prof. Rosa M. Esbert

Esame finale anno 2009

Alma Mater Studiorum – Università di Bologna

DOTTORATO DI RICERCA
Science for Conservation

Ciclo **XXII**

Settore/i scientifico disciplinari di afferenza: CHIM/12

TITOLO TESI

**DURABILITY OF MONUMENTAL STONES TREATED
WITH SILOXANE-BASED WATER REPELLENTS**

Presentata da: Ana Bogdana Simionescu

Coordinatore Dottorato

Prof. Rocco Mazzeo

Relatore

Prof. Modesto Montoto

Prof. Rosa M. Esbert

Esame finale anno 2009

To a special person I admire, respect and love. You are the initial reason why this was possible, since I have learned English due to you. You have taught me about what really matters in life, changing my way, my priorities, my vision and making me a better person. Your enormous talent, faith, integrity, courage and beliefs will always be my guide. To Michael Jackson.

Table of Contents

Table of Contents	i
Summary	v
I. Introduction. State of the art	1
II. Objectives	13
III. Methods	14
III. 1. Microscopic and instrumental techniques	14
III. 2. Chemical composition	17
III. 3. Determination of the velocity of propagation of ultrasonic waves	19
III. 4. Pore space structure	20
III. 4. 1. Mercury intrusion porosimetry	21
III. 4. 2. Nitrogen adsorption on specific surface	22
III. 5. Hydraulic properties	25
III. 5. 1. Water absorption / desorption	25
III. 5. 2. Water absorption by capillary suction	27
III. 5. 3. Water vapor permeability	27
III. 6. Color measurements	29
III. 7. Chemical characterization of water repellent treatments as liquids and films	30
III. 7. 1. FT-IR spectroscopy	30
III. 7. 2. NMR spectroscopy	33
III. 8. Thermal stability and properties of water repellent treatments	34
III. 8. 1. Thermogravimetric analysis	34
III. 8. 2. Differential scanning calorimetry	35
III. 8. 3. Rheological analysis	36
III. 9. Swelling and solubility test of the polymeric films	39

III. 10. Contact angle measurements	39
III. 11. Artificially accelerated ageing tests	40
III. 11. 1. Artificially accelerated ageing under UV irradiation	40
III. 11. 2. Resistance to salt mist action	40
III. 11. 3. Resistance to SO ₂ action the in presence of humidity	41
IV. Stones selection and sampling	43
IV. 1. Laspra	48
IV. 2. Repedea	50
V. Stones characterization	58
V. 1. Introduction	58
V. 2. Macro and micro observation	58
V. 2. 1. Laspra	59
V. 2. 2. Repedea	64
V. 3. Chemical composition	69
V. 3. 1. Laspra	69
V. 3. 2. Repedea	72
V. 4. Velocity of propagation of the ultrasonic waves	74
V. 4. 1. Laspra	74
V. 4. 2. Repedea	75
V. 5. Pore space structure	77
V. 5. 1. Mercury intrusion porosimetry (MIP)	78
V. 5. 2. Nitrogen adsorption on specific surface (BET method)	83
V. 6. Hydraulic properties	84
V. 6. 1. Water absorption / desorption	85
V. 6. 2. Water absorption by capillary suction	92
V. 6. 3. Water vapor permeability	93
V. 7. Color measurements	95
VI. Water repellent treatments	98
VI. 1. Introduction	98
VI. 2. Characterization of three selected worldwide used water repellent products (Lotexan-N, Silres® BS 290, Tegosivin HL 100)	102
VI. 2. 1. Chemical characterization	103
VI. 2. 1. 1. NMR spectroscopy and FT-IR spectroscopy	103

VI. 2. 2. Thermal stability and properties	110
VI. 2. 2. 1. Thermogravimetric analysis and differential scanning calorimetry analysis	110
VI. 2. 2. 2. Rheological properties	114
VI. 3. Synthesis and characterization of a new water repellent product	121
VI. 3. 1. Introduction	121
VI. 3. 2. Synthesis	123
VI. 3. 3. Chemical characterization	124
VI. 3. 4. Thermal stability	134
VI. 3. 5. Rheological properties	137
VI. 4. Conclusions	141
VII. Treated stones characterization	146
VII. 1. Introduction	146
VII. 2. Characterization of the treated stones	147
VII. 2. 1. Microscopic investigation	147
VII. 2. 2. Contact angle measurements	150
VII. 2. 3. Water vapor permeability measurements	152
VII. 2. 4. Color measurements	155
VII. 2. 5. Mapping of the treatments distribution	156
VII. 3. Conclusions	167
VIII. Artificially accelerated ageing	171
VIII. 1. Introduction	171
VIII. 2. Artificially accelerated ageing under UV irradiation	173
VIII. 2. 1. Artificially accelerated ageing under UV irradiation – polymeric films	173
VIII. 2. 1. 1. FT-IR spectroscopy	173
VIII. 2. 1. 2. Swelling and solubility tests	178
VIII. 2. 2. Characterization of the treated stones after the artificially accelerated ageing under UV irradiation	182
VIII. 2. 2. 1. Contact angle measurements	182
VIII. 2. 2. 2. Water absorption by capillary suction	185
VIII. 2. 2. 3. Conclusions	191
VIII. 3. Resistance to salt mist action	192

Summary

The thesis investigates the effect of siloxane-based water repellents on the durability of monumental stones. Laspra, a micritic limestone typical for the Spanish region of Asturias, and Repedea, an oolitic limestone from Moldavia, Romania were selected for the present study, due to their regional / national significance and level of usage. As for the siloxane-based water repellents, three worldwide used products, namely Lotexan-N, Silres® BS 290 and Tegosivin HL 100 and a newly synthesized nanocomposite material, TMSPMA, obtained starting from the 3(trimethoxysilyl)propyl methacrylate as a precursor were investigated.

The limestones and the water repellents were thoroughly characterized using specific techniques. The coating of the two monumental stones with the mentioned products and the investigation of coating efficiency yielded to the conclusion that all treatments induce good water repellent properties.

The treated limestones were afterwards submitted to different artificially accelerated ageing tests – resistance against UV irradiation, resistance to salt mist action and resistance to SO₂ action in the presence of humidity –, the results being analyzed according to standardized evaluation methods.

The durability of the treated stones was proved to depend on both stone characteristics and water repellent chemical structure. All four water repellents induced a good protection against UV irradiation, no significant differences among them being noticed. As far as the resistance to salt mist action is concerned, the product that afforded the best results when applied on Laspra was TMSPMA, and on Repedea, Silres® BS 290 or / and TMSPMA showed the highest efficiency. The best resistance to SO₂ action in the presence of humidity was conferred by Tegosivin HL 100 and TMSPMA when applied on Laspra, while Silres® BS 290 and TMSPMA afforded better results in the case of Repedea.

1. Introduction. State of the Art

The cultural heritage is the legacy of physical artifacts and intangible attributes of groups or societies that are inherited from past generations, maintained in the present and preserved for the benefit of future generations. What may be considered cultural heritage by one generation may be rejected by the next, only to be revived by a succeeding one. The *cultural heritage* concept is an extremely vast one, this topic being possible to see, analyze and study from many perspectives.

Some general definitions, ideas, statements and classifications of the concept became generally accepted. *Physical or tangible cultural heritage* refers to buildings and historic places, monuments, artifacts etc., considered worthy of preservation for the next generations. All include objects significant to the archaeology, architecture, science or technology of a specific culture. *Natural heritage* – that includes the countryside and natural environment, flora and fauna (scientifically know as biodiversity) – is also an important part of a culture. The heritage that survives from the past is often unique and irreplaceable and requires the responsibility of the current generation. Smaller and transportable objects (artworks and other cultural masterpieces) are collected and exposed in museums and art galleries.

The Convention Concerning the Protection of World Cultural and Natural Heritage, adopted by the General Conference of UNESCO in 1972, is significant from this perspective. 878 World Heritage Sites – 678 cultural, 174 natural, and 26 mixed properties – were listed in 2008 in 145 countries. Each of these sites is considered to be important to the international community.

A broader definition of cultural heritage includes *intangible aspects of a particular culture*, often maintained by social customs during a specific historical period. These include social values and traditions, customs and practices, artistic expression, aesthetic and spiritual beliefs, language and other wide aspects of human activity, and are much more difficult to preserve than the *tangible cultural goods*. The importance of physical artifacts can be interpreted against the backdrop of socio-economic, political, religious, ethnic, and philosophical values of a particular group of people.

The concept of *cultural heritage* has been continually broadened over the past decades. The Venice Charter (1964) made reference to *monuments and sites* and discussed the *architectural heritage*, a notion that covers groups of buildings, vernacular architecture, industrial and XXth century built heritage, the concept of *cultural landscape* underlining the interpenetration of culture and nature.

The historic and artistic monuments are the most visible aspects of the world's cultural heritage. Almost all important cultures shared a special interest in building stones. Primitive societies set up stones to memorize the site of important events or to highlight the routes. More advanced cultures used the stones to construct monuments and buildings. Abundant limestone and marble in classic Greece enabled the architect to develop a unique style that combined sophisticated use of marble with delicate decorative detail. The Romans developed massive stone structures, as well as many concepts and systems, such as accumulation of stocks, mass production, prefabrication and standardization of qualities of building stones. The modern society advanced from buildings constructed from stones to less expansive and easier to handle materials, such as steel and concrete.

A *monument*¹ may be defined as a type of structure either explicitly created to commemorate a person or an important event or which has become significant to a social group as a part of their remembering of past events. The monuments are often

¹ Monuments are also often designed to convey historical or political information related to a specific epoch, being used to reinforce the primacy of contemporary political power, e.g. the column of Traian in Rome or the numerous statues of Lenin in the former Soviet Union. However, the social meanings of monuments are rarely considered to be certain and are frequently "contested" by different social groups. Monuments have been created for thousands of years, and they are the most durable and famous symbols of ancient civilizations. Some of them, such as the Greek Parthenon and the Egyptian pyramids, have become authentic symbols of their civilizations. In modern times, monumental structures such as the Statue of Liberty and the Eiffel Tower have become emblems of the present nation-states.

represented by stone works and are threatened by environmental conditions, pollution, urbanization, public access and other natural and man-made phenomena. The deterioration of stones is influenced by their composition, structure and surface conditions, by the interactions of the surrounding microclimate and environment with the stone, as well as by the efficiency of the conservation methods.

Conservation and maintenance of stone monuments are notions that can not be separated, although they obey to significantly different requirements.

The final results of conservation processes can be judged only after a long period of time. Conservation² is a difficult interdisciplinary field for scientists, and stone conservation is to be considered as one of the most problematic. Numerous variables / parameters are to be taken into account (especially for items directly exposed to the environment), deadlines can be stringent, and decisions on possible alternatives can be sometimes risky. Nevertheless, fundamental and technological research proved, in time, to have a significant contribution to stone conservation.

Building stones deterioration is often compared to the effects of an illness. The first step is to analyze the item's background, to check and clarify the symptoms, this allowing the identification of possible secondary reactions that appeared following the previous treatments. After establishing a diagnosis, treating the symptoms may produce an immediate, but short-term improvement in appearance and condition, this approach certainly being a less fortunate one. Understanding all the aspects of "stone illness", treating the cause and not the effects, assessing the condition and associating an accurate, holistic diagnosis could represent the solution for an effective treatment, able to prevent further deterioration.

A coherent set of rules must be followed during the conservation interventions³.

² The modern principles that govern the conservation interventions have taken centuries of philosophical, aesthetic and technical progress to develop. The conservation of cultural property also demands wise management of resources and consists in an interdisciplinary activity coordinating a range of aesthetic, historic, scientific and technical aspects.

³ The condition of the stone / monument under conservation / restoration, together with all the methods and materials used during the (previous) intervention(s) must be documented; the interventions must be performed continuously respecting the aesthetic, historical and physical integrity of cultural heritage; historical evidence must be recorded and not removed, falsified or destroyed. The interventions should be reversible, not prejudice a future intervention, involve materials compatible with the original one in terms of color, texture, form, scale, and allow the maximum amount of material to be retained.

The building stones, used over the centuries, can be generally classified as sedimentary rocks (such as limestone and sandstone), igneous rocks (such as granite) and metamorphic rocks (such as marble and slate). While there are a few stones that seem to be little affected by centuries of weather / environment exposure, the majority of stones are subjected, in time, to gradual degradation. This may not be important if the stone is situated in an undecorated part of a massive wall – for example, in a castle or a cathedral; however, a slight deterioration in an intricately carved piece of stone can completely destroy a sculpture.

Stone decay may take many different forms⁴. Before acting to prevent or to remedy the deterioration of stone, one has to understand the factors causing it. The cause can be obvious, or, on the contrary, there may be several different factors acting at once, making the diagnosis difficult. In an attempt to clarify the significance and interdependency of individual causes, the principles of system dynamics have been proposed [1].

The plausible degradation causes are wide ranging⁵.

According to many experts, air pollution is the prime reason of stone decay. The effects of air pollution on stone have received enormous attention in the past decades⁶. Even though it was shown that air pollution is a problem that dates since antiquity [2], it is generally accepted that, due to its increasing importance, it is also a very modern problem. Several reports attempt to correlate pollution levels with the damage observed by examining the effects of pollution on individual historic buildings over several centuries. However, most research is focused on the "traditional" pollutants, i.e. sulfur oxides, nitrogen oxides, and carbon dioxide. All these oxides are soluble in water

⁴ The stone can weather away gradually, leaving a sound surface behind or drop away very fast; the stone surface may erupt into blisters or sometimes the stone loses all integrity, simply crumbling away; the stone may look perfectly sound to the naked eye, while below the surface it has lost its cohesion.

⁵ They include earthquake, fire, flood, terrorism, vandalism, neglect, tourism, previous treatments, temperature fluctuations, wind, rain, frost, chemical attack, salt growth, pollution, biodeterioration, a.s.o. Some of the causes – like those at the beginning – are sudden and rapid in their effect, while others – like those toward the end – are slow and more insidious.

⁶ Major programs on the effects of air pollution on stone were initiated and coordinated by the European Union through its STEP and Environment initiatives, NATO Committee for the Challenges of Modern Society, the United Nations Economic Commission for Europe (UNECE), U.K. National Materials Exposure Programme, the German Bundesministerium für Forschung und Technologie (BMFT), the U.S. National Acid Precipitation Assessment Program (NAPAP), a.s.o.

forming acidic solutions, therefore are capable to react with calcareous materials such as limestone, marble and lime mortar. All are naturally occurring, but human activity has greatly increased the amounts and impact especially in crowded urban areas.

The effects of acidic pollutants on calcareous stones strongly depend on the immediate environment of the stone. If the stone monument is situated in an exposed position and regularly washed by rain, the stone – acidic solution reaction products are washed away. On the contrary, if the stone monument is located in a more or less sheltered position, the reaction products accumulate and may form a dense black crust on the surface.

A great deal of research, particularly in Italy, focused on the nature and the origins of the black crust [3-5]. The investigations proved that carbonaceous particles, especially fly ash (resulting from the combustion of fossil fuels), are responsible for the blackness of the crust. The particles are not passive components of the crust – they contain metal oxides that catalyze the oxidation of sulfur dioxide and hence promote formation of the crust in the first place.

Along with air pollution, soluble salts represent one of the most important causes of stone decay. The growth of salt crystals within the pores of a stone can generate stresses that are sufficient to overcome the stone's tensile strength and turn the stone, in time, into powder. Many of the world's greatest monuments have been severely deteriorated by salts. Stonework can become contaminated with salts in various circumstances⁷.

Basically, salt damage can be attributed to the crystallization of salts from solution and the hydration of salts. Any salt, in principle, can cause crystallization damage, whereas hydration damage can be caused only by salts existing in more than

⁷ Air pollution is considered to be a major source of sulfates and nitrates. Other sources include the soil – from which salts may be carried into masonry by rising damp, salts transported by the wind from the sea or the desert, unsuitable cleaning materials, incompatible building materials, chemical plants and, in the case of some medieval buildings, the storage, during decades, of salts for meat preservation or even for gunpowder.

one hydration state⁸. A third way in which salts could cause damage is through thermal expansion, but this mechanism has received little attention and is not well understood.

Salt damage⁹ occurs in outdoor environment, due to cycles of rainfall and subsequent drying, but also indoors, through the hygroscopic action of the salts, or even in uncontrolled museum environments [13].

Growth of microorganisms on stone represents both an advantage and a problem. Colorful lichens and creepers can give an air of age and romance to a monument, and their removal can leave the stone looking stark and denuded. However, many organisms contribute to the deterioration of stone, and it is necessary to find the right balance between appearance and longevity. The biological degradation of rocks has been known and studied for a long time as one of the weathering mechanisms responsible for soil formation. However, the deterioration of stone in buildings and monuments through the action of biological organisms has received increasing attention only recently. Most papers are primarily concerned with the influence of organisms on the appearance of stone surfaces, while only few concentrate with the deterioration of the stone itself¹⁰.

To restore a stone monument by replacing parts of it is an important and sometimes underestimated task. Selecting the most suitable type of natural stone to act as a replacement is difficult in most cases. When the original stone used in a certain monument is no longer available, available stones with properties similar to the original one represent a fair solution. The use of alternative stone can solve problems such as

⁸ For example, sodium chloride is capable only of crystallization damage, while sodium sulfate – which can exist as either the anhydrous salt thenardite (Na_2SO_4) or the decahydrate mirabilite ($\text{Na}_2\text{SO}_4 \cdot 10\text{H}_2\text{O}$) – can cause both crystallization damage and hydration damage.

⁹ Using scanning electron microscopy to supplement macroscopic observation, some researchers have described the actual crystallization process [6, 7]. Four different stages of crystal growth, which depend primarily on the humidity of the stone, were identified. The investigations demonstrated [6-9] the breakdown of large crystals during dehydration to form submicrometer aggregates. Subsequent hydration-dehydration cycles in the absence of excess water lead to the formation of a highly porous salt structure whose dissolution in liquid water yields the formation of large crystals, this causing serious damage. The development of microfissures during the hydration of sodium sulfate was monitored by acoustic emission techniques [10]. Salt-induced stresses were related to stone porous structure in early reports [11, 12].

¹⁰ In 1932, in his classic report on *The Weathering of Natural Building Stones*, Schaffer wrote: “Living organisms also contribute to the decay of stone and similar materials and, although their action is, generally, of somewhat less importance than certain of the other deleterious agencies which have been considered, their study presents numerous features of interest. The effect of certain organisms, such as bacteria, is still a matter of controversy, but the effect of others, such as the growth of ivy, is generally considered to be detrimental”.

stone availability, but may not be always a desirable solution, because the properties that differ between the two stones may induce dissimilar weathering behaviors. Stone durability is also a matter of consideration.

Although it represents a possible solution, *preventive conservation* – i.e., acting on the environment in which the stone is placed – is not a simple concept, being connected to legislation to protect individual buildings and monuments, pollution and ground water control, visitor management, and disaster planning.

Preventive conservation measures of more immediate effect are usually concerned with keeping water out of the stone and with controlling the relative humidity¹¹ and temperature of the air surrounding the stone. This can be a relatively easy task for stone artifacts situated within a museum, and it may even be feasible for stone masonry that is exposed on the interior of a building [14].

Protective shelters (likely to be visually intrusive) are frequently used on the outside of buildings to protect those features that are particularly important. Their purpose is to reduce the amount of rain that reaches the stone and to stabilize the temperature and moisture content within the stone.

Stone conservation often begins with cleaning. Removing the dirt allows the direct visualization of the condition of the underlying stone and thus judge what further conservation may be necessary. Cleaning may also serve in some circumstances to remove harmful materials from the surface¹². Nowadays, modern technology offers a wide range of techniques¹³ for stone cleaning, ranging from those that are intended for use on large facades to those that are intended for meticulous use on finely carved and delicate sculpture [15-17].

¹¹ The main purpose of controlling the relative humidity is prevention of salt damage. While the humidity regime required to prevent damage in a stone contaminated with a single salt is well established, the situation is much more complicated in the common case of stones contaminated with a mixture of salts.

¹² The primary reason for cleaning often consists in the dramatic change in stone appearance – a dirty building or monument look quite neglected, and the dirt may well obscure both fine detail and major architectural features. Nevertheless, some specialists argue that cleaning contravenes one of the fundamental principles of conservation – *reversibility* – and that by removing the dirt one is removing both the sense and the evidence of history.

¹³ Although more sophisticated, the basic cleaning techniques have remained largely the same during the last decades due to an increasing awareness of the damage that may be caused by inappropriate or unnecessary cleaning, and also of the posed environmental issues.

The effectiveness of a cleaning technique is usually assessed subjectively, although objective procedures have been described by many authors [18-20]¹⁴.

In situations where soluble salts are a major contributor to decay, removing the salts – quite difficult in practice – could represent a solution, at least a temporary one¹⁵.

Where stone is severely weakened by decay, some form of consolidation may be necessary to restore its strength. The ideal would be to make the stone at least as strong as it was originally, so it might resist further decay. The treated stone will have to have almost the same mechanical and thermal properties – moisture expansion, thermal expansion, and elastic modulus – as the untreated stone, in order to avoid internal stresses, and the treatment must be completely invisible.

Some inorganic materials (calcium hydroxide (slaked lime) and barium hydroxide) deserve a particular mention as stone consolidants. However, the majority of materials that have been tested are represented by organic polymers – from natural compounds, such as linseed oil and cactus oil, to synthetic polymers. It should be mentioned that, at the beginning, materials have been selected more on the grounds of availability than of any predetermined characteristics. The majority of researchers believe that stone needs to "breathe", meaning that the stone should remain permeable to water vapor, in order to avoid any buildup of moisture at the interface between the treated zone and the untreated stone below, and this opinion influences both academic and technological research. The total filling of stone pore space with poly(methyl methacrylate), although this process is used only on stone objects that are not an integral part of a building [24], represents, for a few decades, a successful commercial approach.

Alkoxysilanes, or "silanes" and, in particular, methyltrimethoxysilane (MTMOS) and tetraethoxysilane (TEOS) have been the most widely used stone consolidants¹⁶.

¹⁴ Different researchers emphasized the damage that can be caused by cleaning – loss of surface, staining, deposition of soluble salts, or making the stone more vulnerable to pollutants or biological growth [21, 22]. It is clear that very severe damage can arise, but, according to some opinions, a degree of skepticism would perhaps be justified over "damage" that is observable only using the scanning electron microscope.

¹⁵ As early as in 1975, Bowley [23] showed that it was possible to extract a worthwhile quantity of salt from masonry through the repeated use of clay poultices, although little would be gained in the long run unless one could eliminate the source of further salt.

¹⁶ The popularity of MTMOS and TEOS is also due to their commercial availability, a large number of products that are based on these two compounds existing on the market. A number of other silanes, usually involving substitution of the methyl group with more bulky alkyl or aryl groups, have also been tried.

Silanes are hydrolyzed by water to form silanols, which then polymerize in a condensation reaction to give a silicone polymer. The condensation reaction, and often the hydrolysis reaction, also, takes place after the treatment has penetrated into the stone, the resulting polymer/polymer network imparting the required strength to the stone.

The bonding that takes place between a consolidant and the substrate is still a subject of interest. It is widely argued, for example, that alkoxy silanes will form primary chemical bonds to the Si – OH groups on the surface of sandstones, but that they will not be able to form primary bonds with a limestone substrate. The lack of bonding doesn't necessarily mean failure, an unbonded network of consolidant proving, in different cases, to provide strength properties.

The use of epoxy resins as consolidants is a subject of debate. Many conservators see them as viscous, brittle, yellowing materials that act as efficient adhesives in some circumstances, but can not be taken into consideration as consolidants. Review papers summarized the use of epoxies as consolidants, describing the successes and failures [25], also presenting the two different paths adopted to treat relatively small objects and large facades, respectively. The choice of the solvent, application techniques, and post-application procedures are considered to be important to a successful result.

As for methyl methacrylate and other acrylic / methacrylic monomers, their *in situ* polymerization has its advantages, but the high rigidity and glass transition temperatures of the resulting polymers are considered to diminish their interest as stone consolidants¹⁷. More attention was given, last years, to the use of acrylic resins dissolved in solvents.

A lot of research in the 70's and 80's has focused on finding a single treatment that would both consolidate and protect the stone. In the 90's, different authors reported the damage to certain stones following treatment with tetraethoxysilane (TEOS), unless

¹⁷ Organic consolidants usually rely on the loss of volatile reaction products or solvents during the curing process. However, this can make application impracticable in hot climates and poses a hazard to the environment. The development of aqueous emulsions to be used as consolidants and as surface coatings represents a serious alternative.

the stones were also treated with a water-repellent coating [26-27]. The surface coating has to be renewed at regular intervals, but the initial consolidation lasts much longer.

Water repellency represents a target property in surface coating. Water is involved in most forms of stone decay, and treatments preventing the ingress of water should help to reduce it. Water repellency is widely provided by alkoxysilanes, silicones, and fluoropolymers¹⁸.

Water repellent coatings prevent the penetration of liquid water, but they do not prevent the passing through of water vapor. Moreover, many surface coatings are also permeable to harmful gases such as sulfur dioxide [30].

The evaluation of the lasting results of different treatments is based on a range of tests [31, 32], but it seems that the applied evaluation procedure should be tailored to suit a particular stone and environment [33].

Regardless the techniques and the materials applied for the conservation of stone cultural heritage, one needs to measure the extent to which these ones prove their efficiency. To evaluate the effectiveness of the treatments applied on stones (water repellents, consolidants, pollution deterrents, etc.), different specific tests are taken into consideration¹⁹.

In the science for conservation of cultural heritage, as far as stone conservation is concerned, nanotechnology and nanomaterials are being now used for many purposes [34-37].

¹⁸ Fluoropolymers are close relatives of polytetrafluoroethene (PTFE, or Teflon), well known for its nonstick properties. Early fluoropolymer coatings yielded good results, except for a rather poor ability to stick to the stone. The preparation of compounds containing functional groups able to adhere to the stone surface, thereby providing more persistent protection [28], was an alternative development. Fluorinated polyurethanes have been also reported at the beginning of the 90's [29].

¹⁹ The tests may be grouped in three categories: tests intended only to characterize the extend and nature of the treatment, those using accelerated ageing chambers and those aimed to assess the extend to which the treatments meet previously stated objectives. The accelerated ageing tests are widely used in order to evaluate the durability of the chemical treatments. The chambers are capable to simulate a variety of environmental conditions, either singly or in combination. Porosity and pore size distribution of the treated stone, its appearance, and the depth of penetration are some of the properties of interest in building up an overall picture of the treated stone. However, the majority of tests are concerned with measuring properties known to change as the stone decays, or with assessing the extent to which the treatment has met certain objectives.

No matter the applied treatment, one can not be completely sure that it will not lead to unexpected problems in the future. Natural exposure provides the only "true" test. Conservators invariably pay homage to the *principle of reversibility* – no treatment should be used unless it can be removed at some future date, if necessary. However, for obvious reasons, the principle of reversibility is considered to be a more or less idealistic concept in stone conservation. In practice, to remove even the most soluble treatments could be extremely difficult. This dilemma underlines the significance of *preventive conservation*, but there are situations where preventive conservation is not enough, therefore it is necessary to reach a carefully balanced decision, taking into account all aspects of each individual case.

Conservation is not immune to fashion that varies according to time and place²⁰.

Numerous attempts have been made to codify conservation principles and to introduce international uniformity. The International Charter for the Conservation and Restoration of Monuments and Sites (the "Venice Charter", 1964) and the more recent Burra Charter (ICOMOS, 1988) are the most representative examples. Shaping a conservation policy involves the architect, the art historian, the scientist, the archaeologist, the conservator, the owner, and ultimately the general public.

The number of published papers related to stone conservation is very high and continues to grow yearly. While most of them are dealing with the same topics or materials and procedures / techniques, the design and development of new chemical treatments seems to be a scientific and technologically evolving process. As for the materials, those used so far in order to conserve stone include epoxies, acrylics, polyesters, urethanes, silicones, alkoxy silanes and other organic/inorganic polymers [38, 39].

As a general comment related to the present study, one has to underline that, while many stone conservation approaches proved their efficiency for well selected

²⁰ For instance, one hundred years ago in UK it was fashionable to replace decayed sculpture with "copies". On the contrary, the current normal philosophy is to "conserve as found", i.e. to keep original material and prevent further deterioration as far as is practicable. A further approach is common in the Far East, where the emphasis is more on preserving a monument function as a monument than on preserving the materials from which it was built.

problems, limestone conservation continues to represent a challenge, due to the chemical composition and pore structure of the limestones. The properties desired by the conservation community for a protective treatment are an increased chemical resistance against dissolution, strengthening or consolidation of the weakened limestone, hydrophobicity accompanied by permeability to water vapor, reversibility and environmental friendliness. In addition, the main drawbacks of conventional treatments, either for consolidation, strengthening or water repellency, to be overcome consist in the weakness of the chemical bond between the limestone and the protective treatment, discoloration, UV degradation and poor penetration [39, 40].

11. Objectives

The present study is aimed to evaluate two different types of monumental limestones in terms of their durability; the main purpose is to estimate the durability of these monumental limestones, subjected to several protective water repellent treatments applied on their surface, against certain environmentally aggressive factors.

The aims of this research are:

- to evaluate the durability of two porous monumental limestones, namely Laspra and Repedea, treated with siloxane-based worldwide used water repellent products (Lotexan-N (KEIM), Silres® BS 290 (WACKER) and Tegosivin HL 100 (GOLDSCHMIDT)), against the environmental conditions the monuments built from may be surrounded by;
- to find, characterize and propose new, improved chemical recipes to be used as an alternative to the commercially available ones;
- to determine and substantiate the connections existing between the applied chemical treatment and the durability of each of the two monumental stones;
- to conclude which of the selected chemical treatments is the most appropriate and yields the most significant results in the conservation of the investigated limestones.

The study supposes (a) the selection and characterization of the two limestones, (b) the selection and structural, thermal and rheological characterization of the three worldwide water repellents, in both liquid and polymeric film form, (c) the synthesis and characterization of a new water repellent product, (d) the characterization of the limestones coated with the mentioned products, (e) the investigation of the durability of the treated limestones, submitted to artificially accelerated ageing tests, i.e. UV irradiation, salt mist action and SO₂ action in the presence of humidity.

III. Methods

III. 1. Microscopic and instrumental techniques (POL, ESEM)

Optical microscopy

For a petrophysical study, the first step is to observe, map and evaluate the rock-forming components. Many imaging techniques are microscopy-based and provide images formed under various radiations: electrons, photons, acoustic waves, a.s.o. [41].

Polarizing microscopy is the basic tool in use in petrography.

The polarized light optical microscopy serves for the study of stones mineralogy, revealing detailed textural, mineralogical and grain interlocking information. Thin sections of the two selected stones were used in this study, these ones being obtained through perpendicular to the stone surface cutting in order to analyze the stratigraphy. The investigation was performed by using a Leica DM 4500 P optical microscope.

ESEM

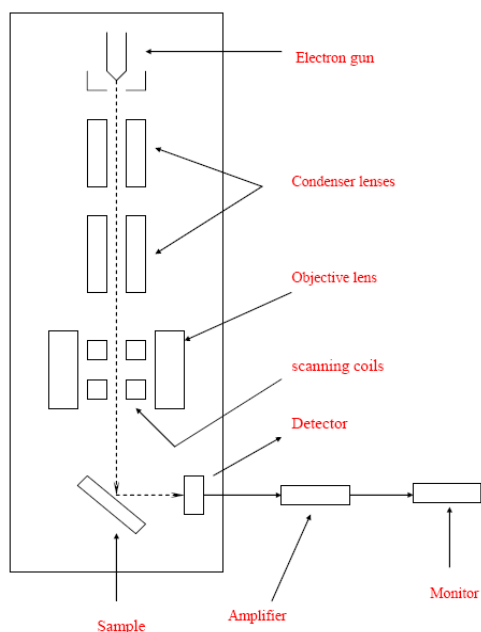
In the cultural and historical heritage field, the (environmental) scanning electron microscopy represents a powerful tool for (a) the characterization of the building and ornamental materials used for the construction of monuments [42, 43], (b) the diagnosis of the deterioration processes suffered by the materials [44, 45], (c) the identification of the contaminating substances existing in monumental buildings [46, 47], (d) the identification of patinas [48]. This technique can be also used for the evaluation of the effectiveness of applied chemical treatments or for the assessment of the aggressiveness of cleaning methods towards stone materials [49, 50].

Principle

An electron beam is focused onto the sample surface, kept in vacuum, by electromagnetic lenses (since electron possesses a dual nature with both particle and wave properties, an electron beam can be focused or condensed like ordinary light). The beam is then rastered or scanned over the surface of the sample. The scattered electron from the sample is then fed to the detector and then to a cathode ray tube through an amplifier, where the images are formed, which gives the information on the surface of the sample.

Instrumentation

The instrumentation consists of a heated filament as source of electron beam, condenser lenses, an aperture, an evacuated chamber for placing the sample, the electron detector, amplifier, CRT with image forming electronics, etc.



Scanning electron microscopy has been applied to study the surface of metals, ceramics, polymers, composites and biological materials for both topography as well as compositional analysis. Depending on the type of detectors used, this method is classified into Energy Dispersive Spectrometry (EDS) and Wavelength Dispersive Spectrometry (WDS). The technique is extensively applied in the analysis of metallic

and ceramic inclusions, inclusions in polymeric materials, diffusion profiles in electronic components.

In the present research, this method allowed the investigation of the natural stone samples, the focus being oriented on the morphology and crystals size, as well as on stone samples porosity and fissures. Following the analysis of the natural stones, the technique was applied for the investigation of the stone samples submitted to several water repellent treatments. This approach allowed the evaluation of the influence of chemical treatments on the two selected limestones – surface coverage, polymeric film formation and continuity, possible polymeric film fissures, a.s.o. The treated and artificially aged stone samples were also investigated using scanning electron microscopy – after each artificial accelerated ageing test, the samples were analyzed through ESEM in order to assess the stones and chemical treatments behavior after performing the durability tests. The stone samples were studied in terms of changes of surface morphology, polymeric film fissures, material loss as well as other textural modifications.

The ESEM micrographs were obtained with a Quanta 200 scanning probe microscope, the specimens being fixed with adhesive past on cylindrical-shaped Al conducting supports and then sputtered-coated with gold.

The Quanta 200 ESEM is equipped with an Energy Dispersive Spectroscopy (EDS) system that detects the x-rays emitted from a sample during electron imaging. The system consists of three main components: an x-ray detector, separated from the SEM chamber by a very thin polymer window; pulse processing circuitry, which determines the energy of the detected x-rays; and analyzer equipment, which interprets the x-ray data and displays it on a computer screen. In practice, EDS is most often used for qualitative elemental analysis, simply to determine which elements are present and their relative abundance.

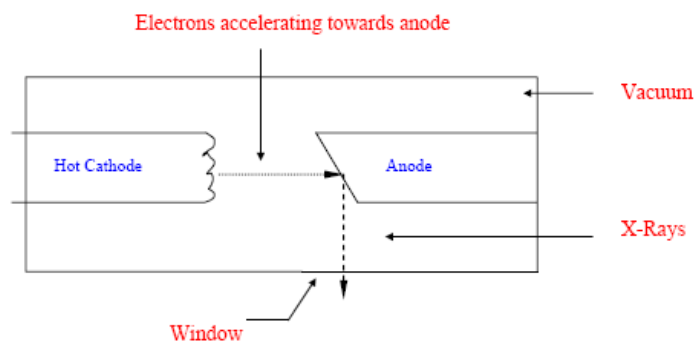
The microscope is equipped with an Oxford Inca Energy Dispersive X-ray (EDX) system for chemical analysis. Qualitative and quantitative analysis, elemental mapping and linescans can be performed. The microscope can also be equipped with a Peltier stage for studies of wet samples *in situ*. There are two heating stages available for *in situ* heating experiments up to 1500° C. This can be done in combination with having an external gas present in the chamber, e.g. air, for studying chemical reactions.

III. 2. Chemical composition (XRD)

X-rays Diffraction

When metals, like copper, molybdenum, tungsten etc. are bombarded directly with a stream of high energy electrons or radioactive particles, X-rays (wavelengths of the order $0.1 - 100 \text{ \AA}$) are emitted due to the transitions involving K-shell and L-shell electrons. This can be simply expressed as follows: a cathode in the form of a metal wire when electrically heated gives off electrons. If a positive voltage, in the form of an anode (target comprised of the metals mentioned above), is placed near these electrons, the electrons are accelerated toward the anode. Upon striking the anode, the electrons transfer their energy to the metallic surface, which then gives off X-ray radiation. This is referred as *primary X-rays*.

The following is the schematic diagram for the process:

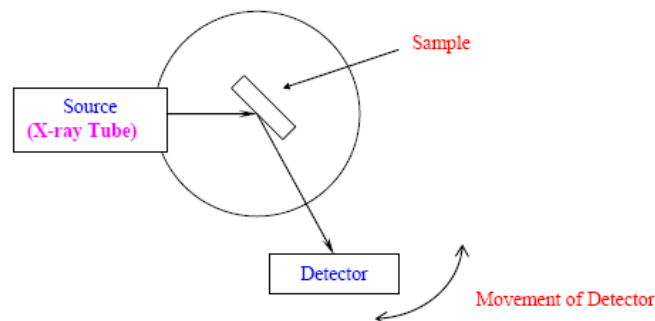


Principle

The primary X-rays are made to fall on the sample substance under study. Due to their wave nature, like light waves, they get diffracted to a certain angle. The angle of diffraction, which differs from that of the incident beam, will give the information regarding the crystal nature of the substance. The wavelength of the X-rays can be varied for specific applications by using a grating plate.

Instrumentation

The instrumentation consists of the X-ray tube for the source, a monochromator and a rotating detector.



The diffraction of X-rays is a good tool to study the nature of the crystalline substances. In crystals the ions or molecules are arranged in well-defined positions in planes in three dimensions. The impinging X-rays are reflected by each crystal plane. Since the spacing between the atoms and hence the planes can not be the same or identical for any two chemical substances, this technique provides vital information on the arrangement of atoms and the spacing in between them and also to find out the chemical composition of crystalline substances. The sample under study can be of either a thin layer of crystal or in a powder form. Since the power of a diffracted beam is dependent on the quantity of the corresponding crystalline substance, quantitative determinations are also possible.

In the present investigation, the X-rays diffraction method was used (a) to analyze the mineralogical phases of the two limestone samples, and (b) to establish the degree of crystallinity of the samples. The mineralogical analysis was performed on powdered samples. Small pieces of limestone were powdered in an agate recipient until they reached 0.053 mm in dimensions. The obtained stone powder was transported in an aluminium recipient, which was then introduced in the diffractometer.

The XRD patterns were recorded with a D8 Advance Bruker AXS diffractometer (Bragg-Bretagno geometry) equipped with a scintillation detector. X-rays were generated using a $\text{CuK}\alpha$ source with an emission current of 40 mA and a voltage of 36 kV. A 0.6 mm fixed divergence slit was used for all samples to improve the signal-to-noise ratio. Scans were collected over the range $5 - 70^\circ$ using a step size of 0.01° and a count time of 0.5 s/step. Instrument's calibration was carefully made by using the provided SRM1976 corundum sample.

III. 3. Determination of the velocity of propagation of ultrasonic waves – UNE – EN 14579 (2005)

One of the non-destructive techniques of investigation of the stone cultural heritage consists in the determination of the velocity of propagation of ultrasonic waves (20,000 Hz frequency) through the stone. Porosity decreases exponentially with velocity while compressive strength increases exponentially, being proved that properties of stones change after weathering and can be detected by measuring the longitudinal wave velocity, a non-destructive method.

This methodology has been developed by Thompson and Thompson [51] and allows the physical characterization of different materials, rocks being among these ones. In a solid material, the velocity of the transmission of elastic waves is conditioned by various factors such as the density of the material, the amount of pores and voids and the amount of humidity existing in the material's pores. The velocity of propagation of ultrasonic waves therefore depends on the nature of the material, i.e. its composition and texture.

The European standard deals with the determination of the velocity of propagation of the impulses of the longitudinal ultrasonic waves within the natural stone, both in the laboratory and *in situ*.

Principle

An impulse of longitudinal vibrations is generated with the help of an electro-acoustic transducer put in contact with stone surface. After recurring a full length stone longitude, the impulse of the vibrations is transformed in an electrical signal within a second transducer, a few electronic circuits allowing the measurement of the impulse propagation time.

Equipment

The equipment (C. N. S. Electronics Ltd. London RS 232) mainly consists in a generator of electrical impulses, a few transducers, an amplifier and an electronic device for the measurement of the time interval between the initiation of an impulse generated by the emitting transducer and the detection of its arrival to the receptor transducer.

The equipment also involves a device for the measurement of the samples weight (with a 0.01% precision) and a ventilated oven able to maintain the temperature of 70° C.

Sample preparation

At least six stone samples must be selected for this laboratory test. The stone samples must be cut in prisms of 300 mm x 75 mm x 50 mm, with a more or less 2 mm of tolerance, and dried at 70° C until they reach a constant weight. It is considered that a sample has reached a constant weight when the weight difference from two weight measurements performed in a 24 hours interval is less than 0.1%.

Experimental procedure

It is possible to measure the velocity of propagation of the impulse by arranging the two transducers on opposite sample surfaces (direct transmissions) or on adjacent surfaces (semidirect transmissions) or on the same surface (indirect or surface transmissions). The instrument must have an adequate acoustic coupling between the stone sample and the surface of each transducer. Certain products, such as vaseline, liquid soap or glycerol paste, meant to facilitate the interaction, can be used by pressuring the transducer against the stone surface.

The velocity of the impulse can be calculated with the equation $V = L / T$, where V is the impulse velocity (km/h), L is the distance (mm), and T is the time (μ s) necessary for the impulse to transit the distance.

III. 4. Pore space structure

The porous system characteristics and the volume and size of the voids are strongly related to the deterioration of the stones. The study of the porous system of monumental building stones allows the understanding of the effect of different factors (environmental conditions, chemical treatment, cleaning treatments) on the building stones durability. Mercury injection or intrusion porosimetry, saturation in liquids and gas adsorption are the most known methods in the characterization of the pore space structure.

III. 4. 1. Mercury intrusion porosimetry

Mercury intrusion porosimetry (MIP) is based on the premise that a non-wetting liquid (a liquid having a contact angle value higher than 90°) will only intrude capillaries under pressure [52]. A progressively increased pressure is applied to mercury in order to fill the open porosity space – mercury invades first the bigger pores and afterwards the smaller pores.

The principles of this method are based on the technique of mercury introduction, at different pressures, in the porous system of a stone sample. This liquid doesn't moisture many natural substrates, therefore putting it in contact with a porous material and submitting it to increasing pressure is successively forcing it to penetrate even small dimensioned pores. The method offers information on the total porosity of a material, as well as on the distribution and sizes of the accessible to mercury pores, based on the necessary pressures applied to realize the penetration of the mercury inside the porous stone sample.

This investigation method is widely used for the porosity characterization of monumental stones, as well as for the assessment of their deterioration degree [52, 53], a.s.o.

A Carlo Erba Strumentazione 2000 WS Porosimeter was used. The stone samples were cut as cubes of 1 x 1 x 1 cm in dimension, then weighted and introduced in the porosimeter sample compartment. Once the mercury intrusion process is finished, various data can be obtained.

The ink-bottle effect

If a small pore of a radius r is connected to a larger pore of a radius R , the mercury can enter in the large pore only when the pressure P_r is reached to enter the smaller pore according to Laplace law. Both pores are invaded simultaneously and the volume considered is only the one of the pore class r . Therefore, large pores can be underestimated and *vice versa*, smaller pores class can be overestimated. The interpretation might be validated by cross-checking the results with other, complementary methods as BET. The mercury porosimetry does not estimate the real pore space geometry as it is based on the model of cylindrical pores.

A number of factors affect the MIP results, the important ones being the method of sampling, sample conditioning (oven drying), rate of pressure increase, maximum

intrusion pressure applied assumed values of the contact angle and surface tension of mercury.

III. 4. 2. Nitrogen adsorption on specific surface – BET method

The specific surface area in m^2/g is defined as the sum of the area developed by each particle composing a mass unit of the porous material. The most accurate information on a material specific surface can be obtained measuring the adsorption of an inert gas on a solid material surface at a reduced temperature as well as the corresponding gas desorption at room temperature. The obtained adsorption isotherms can be interpreted using the equation developed by Brunauer, Emmett and Teller, also known as the BET method [54].

The quantity of gas or vapor which is adsorbed by a porous solid material in function of the applied pressure strongly depends on the pore size distribution of the solid. In these types of techniques, various gases/fluids can be used as adsorbents, but the best results, as far as porous stones are concerned, were registered with nitrogen. The advantage of this method in the investigation of solid materials microporosity was underlined [55].

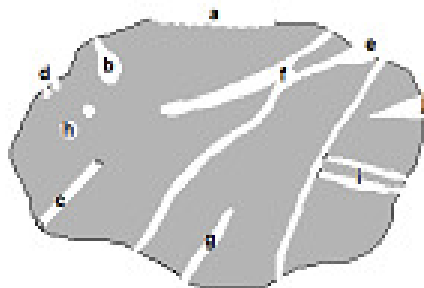
The form in which a material adsorbs a gas can be compared to an adsorption isotherm.

Principle

The pore size distribution, as well as specific surface area, can be estimated from nitrogen adsorption isotherms at liquid nitrogen temperature. To have the isotherms, the adsorbed volume is plotted against relative pressure (equilibrium pressure, p / saturation pressure, p^0).

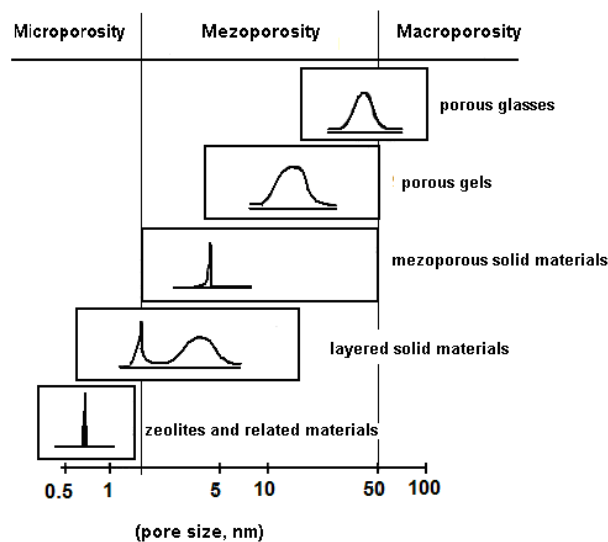
Before performing the gas sorption experiments, the solid surfaces must be freed from contaminants such as water and oils. Surface cleaning (degassing) is most often carried out by placing a solid sample in a glass cell and then heating it under vacuum.

The next figure illustrates cracks and orifices (pores) of different sizes and shapes found in a solid material.



- (a) – not deep or roughness; (b) – ink bottle;
 (c) – cylindrical; (d) – spherical; (e) – funnel;
 (f) – interconnected; (g) – telescope;
 (h) – closed, with parallel walls (i) or in
 fissures (j)

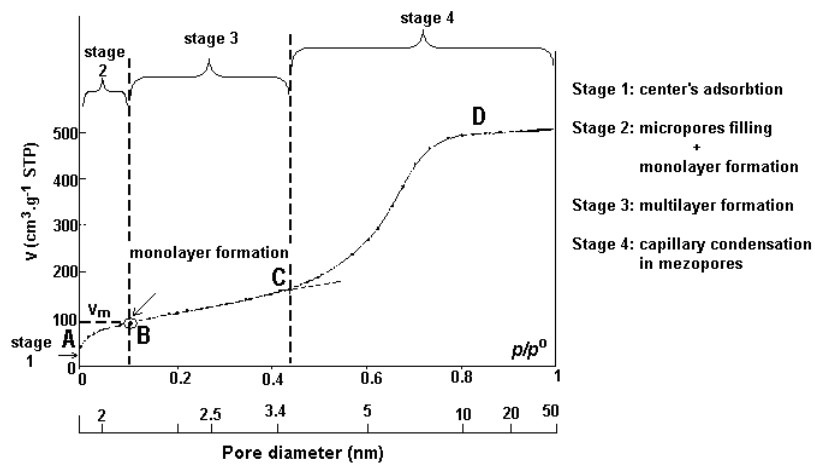
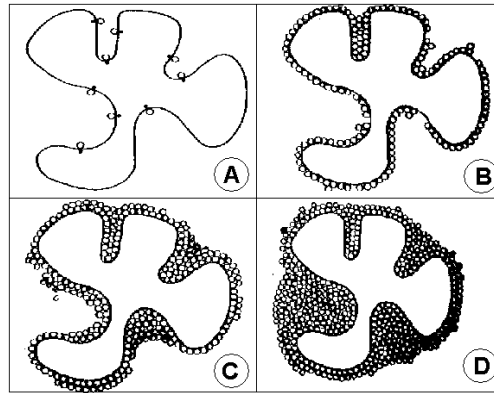
Regarding this method and according to IUPAC classification, porous materials are grouped in three groups depending on the pore size, i.e., microporous materials ($d < 2$ nm), mesoporous materials ($2 \text{ nm} < d < 50$ nm) and macroporous materials ($d > 50$ nm).



Once clean, the sample is brought to a constant temperature by means of an external bath. Small amounts of a gas (the *adsorbate*) are then admitted in steps into the evacuated sample chamber. Adsorbate molecules quickly find their way to the surface of every pore in the solid (the *adsorbent*). These molecules can either bounce off or stick to the surface. Gas molecules that stick to the surface are said to be *adsorbed*. The strength with which adsorbed molecules interact with the surface determines if the adsorption process is to be considered physical (weak) or chemical (strong) in nature.

Physical adsorption (*physisorption*) is the most common type of adsorption. Physisorbed molecules are fairly free to move around the surface of the sample. As more gas molecules are introduced into the system, the adsorbate molecules tend to form a thin layer that covers the entire adsorbent surface. Based on the well-known Brunauer,

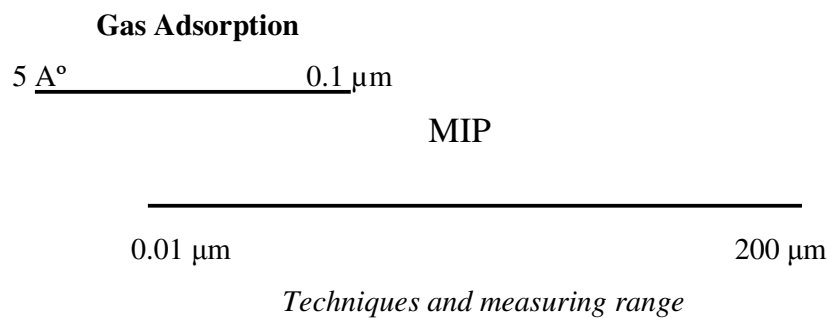
Emmett and Teller (BET) theory, one can estimate the number of molecules required to cover the adsorbent surface with a *monolayer* of adsorbed molecules, n_m .



Multiplying n_m by the cross-sectional area of an adsorbate molecule (16.2 \AA^2 for N_2) yields the sample's *surface area*. Continued addition of gas molecules beyond monolayer formation leads to the gradual stacking of multiple layers (or multilayers) on top of each other. The formation of multilayers occurs in parallel to capillary condensation. The latter process is adequately described by the Kelvin equation, which quantifies the proportionality between residual (or equilibrium) gas pressure and the size of capillaries capable of condensing gas within them. Computational methods such as the one proposed by Barrett, Joyner and Halenda (BJH) allow the computation of pore sizes from equilibrium gas pressures. One can therefore generate experimental curves (or *isotherms*) linking adsorbed gas volumes with relative saturation pressures at

equilibrium, and convert them to cumulative or differential *pore size distributions*. As the equilibrium adsorbate pressures approach saturation, the pores become completely filled with adsorbate. Knowing the density of the adsorbate (0.8081 g.cm^{-3} for N_2), one can calculate the volume it occupies and, consequently, the *total pore volume* of the sample. If at this stage one reverses the adsorption process by withdrawing known amounts of gas from the system in steps, one can also generate *desorption* isotherms. Since adsorption and desorption mechanisms differ, adsorption and desorption isotherms rarely overlay each other. The resulting *hysteresis* leads to isotherm shapes that can be mechanistically related to those expected from particular *pore shapes*.

Nitrogen adsorption was conducted at 77 K on a Quantachrome Autosorb-1 volumetric analyzer. The samples were degassed at 350° C under vacuum for 3 hours prior to the measurement.



III. 5. Hydraulic properties

III. 5. 1. Water absorption / desorption

***Determination of water absorption / desorption at atmospheric pressure –
EN – 13755 (2002)***

Principle

After drying the stone samples until reaching constant weight, each stone sample is weighted and then introduced totally in water at atmospheric pressure, for a specific time period.

Sample preparation

The stone samples must have a cylindrical, prismatic or cubic form of 70 ± 5 mm or 50 ± 5 mm and they have to be obtained by cutting with a diamond saw.

Procedure

Every stone sample must be weighted after drying (m_d), and then placed in a tank on the available supports, each sample being at a minimum distance of 15 mm from the adjacent stone samples. The next step is to add water at $20 \pm 10^\circ$ C up to half of the height of the samples (time t_0). At $t_0 + 60$ minutes one has to add flowing water until it covers $\frac{3}{4}$ parts of the height of the samples. At $t_0 + 120$ minute one has to add some more water until the stone samples are completely covered, under a sheet of 25 ± 5 mm of thickness. At $t_0 + 48$ hours, the samples must be taken out of the water, quickly cleaned with a humid cloth and, in a short interval of one minute, weighted (m_i). Following the weight measurements, the stone samples are submerged in water again, this operation being repeated until the samples are reaching a constant weight. The value of the last weight measurement is considered to be the mass of the saturated samples (m_s).

The water absorption (A_b) at atmospheric pressure for each sample is calculated by means of the equation

$$A_b = [(m_s - m_d) / m_d] \times 100$$

Once finished the water absorption experiment and having the stone samples saturated in water, the desorption process can begin with the weight measurements of the samples at certain time intervals. The weight measurements are intended to evaluate the stone material water loss.

The stone samples were placed in a plastic recipient and then left to dry at room temperature and pressure, until reaching, as in the case of water absorption experiments, a constant weight value. Starting from the obtained values, one can calculate the water content within the stone sample, the process being very similar to the water absorption one.

III. 5. 2. Water absorption by capillary suction

Determination of water absorption coefficient by capillarity –

UNE - EN - 1925 (1999)

Principle

After drying the stone samples until they reach constant weight values, each sample is submerged in (3 ± 1) mm water.

Sample preparation

The stone samples must be cut as cubes of 70 ± 5 mm or 50 ± 5 mm and then dried until constant weight in a ventilated oven at a $70 \pm 5^\circ$ C. It is considered that the samples reached a constant weight when the weight difference between two consecutive measurements is less than 0.1% of the sample mass.

Procedure

The experiment was performed in a plastic recipient, where a thin porous material layer accompanied by a thick filter paper layer was introduced. Distilled water was added until the filter paper was covered and that water level was maintained during all the experiment.

The stone samples were weighted with a 0.01 g precision, after drying (m_d).

After different time intervals, initially short and later longer, the stone samples were taken out of the plastic container, lightly dried with a humid cloth and weighted (m_i), being than placed again in the tank.

The water absorption coefficient by capillarity C was calculated according to

$$C = (m_i - m_d) / (A \times \sqrt{t_i}) \quad [\text{g/m}^2 \times \sqrt{\text{s}}]$$

where A represents the area of the submerged base.

III. 5. 3. Water vapor permeability

Standard test method for water vapor transmission of materials –

ASTM - E 96 - 92 (1992)

The importance of the presence of humidity in the processes of deterioration and durability of stones is very well known, due to the fact that a high humidity level that circulates inside the stones is present in a vapor form. Generally, permeability is linked

to open pathways in the rock sample: open pore throats as connections between pores; open cracks; and networks of open pores and cracks.

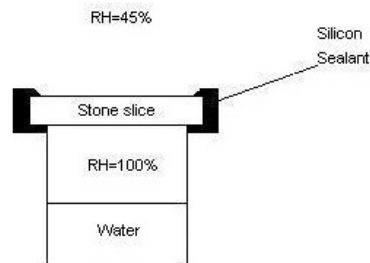
This experiment is based on water vapor mobility through a stone porous system as a response of a partial pressure difference of water vapor, this difference inducing a diffuse movement of water molecules. Through this test one can control the amount of water that travels within a known material, in a determinate time interval, temperature and relative humidity.

Sample preparation

The stone samples must have 5 x 5 x 1 cm in dimension and must belong to (be cut from) a homogeneous stone block.

Equipment

For this experiment, a weighting device with a 0.1 mg of precision is required, as well as standardized sample-cells. The cells are normally made of an impermeable material (poly(vinyl chloride), PVC) and serve as recipients where a determined deionised water volume is placed. Inside the same cell, a small amount of cotton is placed in order to avoid the deposited water to enter into contact with the stone sample. The stone sample is placed between two layers of hermetic material (usually rubber) at a 2 cm distance and the cell is afterwards hermetically closed.



Representation of the water vapor permeability measurement by the wet cup procedure

Procedure

The measuring system consists in controlling the difference in weight registered by the cell – stone sample system. For that purpose, the initial weight of the cell – sample system must be recorded and in order to maintain constant the temperature and relative

humidity, the cell has to be introduced in a plastic container having on its bottom a silica gel layer. The container is then introduced in a constant temperature oven.

The permeability value is calculated based on the weight differences obtained after each weight measurement (every 24 hours) according to

$$(\Delta M_i - \Delta M_{i-1}) \times 100 / \Delta M_i \leq 5 \%$$

where ΔM_i is the weight difference recorded in a specific time interval and ΔM_{i-1} is the weight difference previously registered.

For water vapor permeability measurements, the sample blocks were fixed on the top of identical cylindrical poly(vinyl chloride) containers partially filled with distilled water. The containers were afterwards placed in a desiccator, kept at a value of 25% RH and at constant temperature (20° C). The containers were weighted every 24 h, for 7 days. It was assumed that the vapor flow through the stone had reached a constant value when the difference between two consecutive daily weight variations was less than 5%.

The permeability coefficients (K_v) were calculated according to

$$K_v = -(\Delta M / S) / t \text{ (g/m}^2 \cdot 24\text{h)}$$

where $\Delta M / S = - (M_t - M_0) / S \text{ (g/m}^2)$, M_0 being the initial container mass at $t = 0 \text{ (g)}$, and M_t the container mass at $\Delta t = 24 \text{ h}$; for $t = 0$, $M_t = M_0, \text{ (g)}$; $S = 0.00159 \text{ m}^2$ (standard value).

III. 6. Color

Colorimetry - EN ISO 105-J03:1997

The determination of color parameters is a very significant issue in the area of monumental stone conservation. The aesthetic aspect can not be overlooked when studying a monumental building, from that fact deriving the necessity for a precise and objective evaluation of the changes that certain interventions or chemical products can induce to monumental stone. The amount of work involving color studies in the area of stone conservation is impressive and is continuously growing [50, 56].

In this research, this method was used first for the determination of the natural stones color parameters. The following step was the investigation of the color changes induced by the treatment of the stones with several chemical water repellent products. Finally, this technique was used for the assessment of the stones color changes that

intervened during the artificial accelerated ageing tests. Based on color parameters measurements, the ΔE values were calculated. These values indicate the registered color differences between the natural stone and the treated or treated/aged stone samples.

The optical characteristics were evaluated through color alteration measurements taken on homogeneous spot areas using a portable MiniScan XE Plus (HunterLab Associates Inc., USA) reflectance spectrophotometer and were determined by the use of L^* , a^* and b^* coordinates of the CIE 1976 scale.

Color measurements are expressed using CIE $L^* a^* b^*$ and CIE $L^* C^* h$ systems, where L^* represents the variable lightness, which can vary from 0 (black) to 100 (white), a^* and b^* are the chromatic coordinates, i.e., + a is red, - a is green, + b is yellow and - b is blue. The attributes of chroma are C^* - saturation or color purity, and hue h - color wheel. The global color variation (ΔE) was evaluated using the formula $\Delta E^* = (\Delta L^{*2} + \Delta a^{*2} + \Delta b^{*2})^{1/2}$.

III. 7. Chemical characterization of water repellent treatments as liquids and films

III. 7. 1. Fourier Transform Infrared Spectroscopy (FT-IR)

Principles

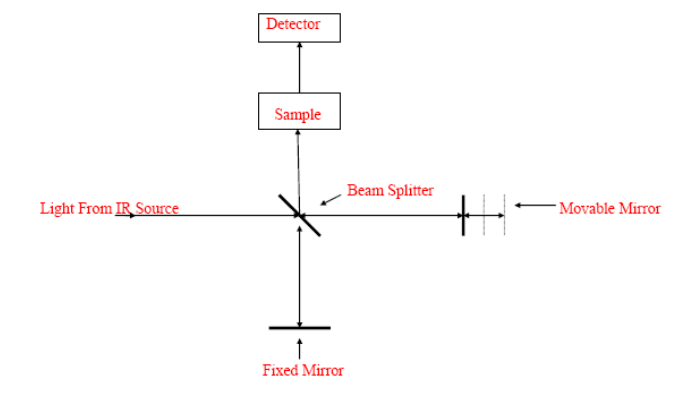
The technique/method involves the absorption of electromagnetic radiation in the infrared region of the spectrum which results in changes in the *vibrational energy* of molecules. Since usually all molecules will be having vibrations in the form of stretching, bending etc., the absorbed energy will be used in changing the energy levels associated with them. It is a valuable and formidable tool in identifying organic compounds which have polar chemical bonds (such as O - H, N - H, C = O, etc.) with good charge separation (strong dipoles).

Instrumentation

The instrumentation was originally designed as a double beam spectrophotometer comprising an IR source (red hot ceramic material), a grating monochromator, a thermocouple detector, cells made of either sodium chloride or potassium bromide, etc. The light is dispersed by the monochromator. In time, this type of basic design for IR measurements has been outdated and a newer technique, termed *Fourier Transform-*

Infrared (FT-IR) was introduced and put in practice. This technique uses a single beam of undispersed light and has the instrument components similar to the previous one.

In FT-IR, the undispersed light beam is passed through the sample and the absorbances at all wavelengths are received simultaneously at the detector. A computerized mathematical manipulation (known as “Fourier Transform”) is performed on this data, to obtain absorption data for each and every wavelength. To perform this type of calculations interference of light pattern is required for which the FT-IR instrumentation contains two mirrors, one fixed and one moveable with a beam splitter in between them. A reference or a blank scanning is required before scanning the sample.



Simplified design of the FT-IR instrument

The method finds extensive use in the identification and structural analysis of organic compounds, natural products, polymers, etc. The presence of particular functional groups in a given organic compound can be identified. Since every functional group has unique vibrational energy, the IR spectra can be seen as their fingerprints.

Fourier transform infrared spectra were recorded on a Bruker Vertex 70 instrument, in the $400 - 4000 \text{ cm}^{-1}$ range, 64 scans, at room temperature, using the KBr pellet technique and the Opus 5 FTIR software.

Attenuated total reflection measurements

Attenuated total reflection (ATR) is based on the principle of total reflection. At the interface between two materials with different refractive index, the incident radiation is in part reflected and in part refracted. In ATR measurements, the IR radiation reflected by IREs, commonly called crystals, is therefore attenuated from a little fraction absorbed by a sample inserted in close contact with these IREs. Different materials have been used

for the fabrication of internal reflection elements. Having the highest refractive index (4.0), germanium is the most commonly used but it is relatively soft and may easily be scratched. Alternatively, the use of silicon, which is a harder material with a refractive index of 3.41, has become important. The use of ATR has been successfully reported for a large variety of samples due to the fact that the spectra obtained in this mode are similar to those recorded in transmission mode. The simplest way to compare ATR and transmission spectra is to create a reference library of known compounds, whose spectra can be afterwards compared with unknown samples.

FT-IR chemical maps / images or functional group maps/images can be obtained by plotting the intensities of characteristic absorption bands against their spatial position on a selected sample area. Possible overlapping between absorbance bands from different compounds with similar chemical features (functional groups) may result in inaccurate images. Mathematical manipulations can enhance the FT-IR map / images providing a possible separation of these features and are also useful to individuate components, which may have not previously been detected due to the large amount of collected data.

Micro-FT-IR spectroscopy

As many of inorganic compounds and organic substances show characteristic absorptions in the 4000 – 600 cm^{-1} mid-IR range, FT-IR microscopy represents one of the first analytical techniques applied to cultural artefacts. A Nicolet Continuum FT-IR microscope²¹ has been used in reflection mode with a micro slide-on ATR (Si crystal) device or in transmission mode with a diamond anvil cell on some particles. The FT-IR microscope is equipped with a MCT (Mercury Cadmium Telluride) detector cooled by liquid nitrogen and a 15 x Thermo-Electron Infinity Refflachromat objective with a tube factor of 10x. Spectra from 4000 to 650 cm^{-1} (ATR / diamond cell) have been registered with a FT-IR Thermo Nicolet Avatar 370, at a resolution of 4 cm^{-1} and a mirror velocity of 1.8988 $\text{cm}\cdot\text{s}^{-1}$. A total of 64 scans have been recorded and the resulting interferogram averaged. Acquisition and post-run processing have been carried out using a Nicolet “Omnic” software.

²¹ μ FT-IR analyses were performed in the Microchemistry and Microscopy Art Diagnostic Laboratory, Ravenna, Italy. The scientific and technical assistance of Prof. Rocco Mazzeo and Miss Elsebeth Kendix is gratefully acknowledged.

III. 7. 2. Nuclear Magnetic Resonance Spectroscopy (NMR)

The application of ^1H -NMR spectroscopy lies mostly in the identification and structural analysis of organic compounds and thus, it is mostly a tool for qualitative analysis. It gives valuable information on the position of the functional groups in a molecule and provides distinct spectra for isomers. Very precise information on the structure of the compounds can be obtained using the same technique with other magnetic nuclei like ^{13}C , ^{17}O , the instrumentation being the same except that the sweep of the magnetic field is varied. The instrumentation is very expensive and complex needing exceptional skills to operate. The usage of the solvents is limited and in most of the situations deuterated solvents are required.

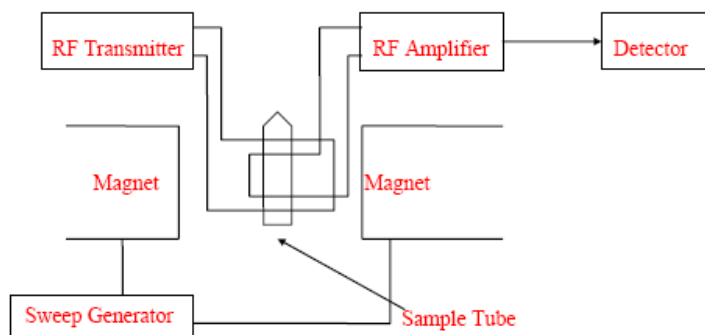
Principle

In NMR substances absorb energy in the radio frequency region of the electromagnetic spectrum under the influence of a strong magnetic field. It is a well known fact that the nuclei of the atoms bonded to each other in molecules spin on an axis like a top. Since nuclei are positively charged, this spin will create a small magnetic field. If an external magnetic field is applied to these nuclei this magnetic field will split into two energy levels. The energy difference is very small and corresponds to a radiofrequency energy which is unique for every molecule and will give the information regarding the nature of the compounds and the presence of various functional groups and their environment.

Since this technique is mostly measuring the spinning of the hydrogen nuclei (almost all organic compounds contain hydrogen atoms!), it is sometimes referred as *Proton Magnetic Resonance (PMR)* or ^1H -NMR spectroscopy.

Instrumentation

The instrumentation for this technique includes a powerful magnet, a radiofrequency signal generator, an amplifier, a detector, etc.



Outline of the NMR instrument

The NMR analyses were performed on a Bruker Avance DRX 400 MHz spectrometer. The attribution of the signals was based on unidimensional and bidimensional spectra.

The following types of spectra were analyzed:

Unidimensional spectra

¹H-NMR spectra: from the chemical shift and from the value of the integral, information on the type of the protons present within the chemical compound (aromatic, aliphatic, alkene, alcohol, acid, ester, a.s.o.) can be obtained.

¹³C-NMR spectra: this type of experiments, based on chemical shifts, yields information on the type of carbon atoms present within the chemical structure.

Bidimensional spectra

COSY: information on the coupling of neighbor protons can be obtained.

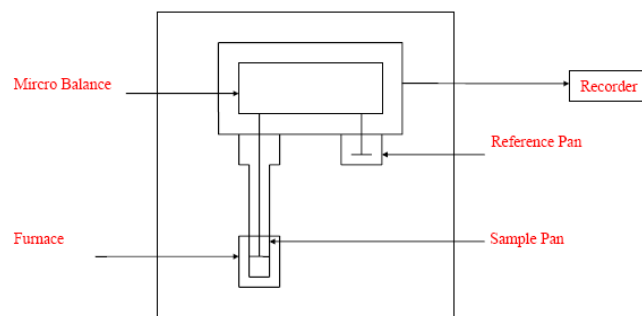
HMQC and HMBC: proton – carbon correlation spectra.

III. 8. Thermal stability and properties of water repellent treatments

III. 8. 1. Thermogravimetric analysis (TGA, DTA)

Thermogravimetric Analysis (TGA)

In this technique, the change in sample weight is measured while the sample is heated at a constant rate (or at constant temperature), under air (oxidative) or nitrogen (inert) atmosphere. The technique is effective for quantitative analysis of thermal reactions accompanied by mass changes, such as evaporation, decomposition, gas absorption, desorption and dehydration.



Simplified diagram of the TGA instrument

The micro-balance plays a significant role, since during measurement the change in sample mass affects the equilibrium of the balance. This imbalance is fed back to a force coil, which generates additional electromagnetic force to recover equilibrium. The amount of additional electromagnetic force is proportional to the mass change.

Thermogravimetric analyses (TGA) were performed²² under nitrogen flow ($20 \text{ cm}^3 \text{ min}^{-1}$) at a heating rate of $10^\circ \text{ C min}^{-1}$ from 25 to 900° C with a Mettler Toledo model TGA/SDTA 851 instrument, the initial mass of the samples being $4 - 5 \text{ mg}$.

Differential Thermal Analysis (DTA)

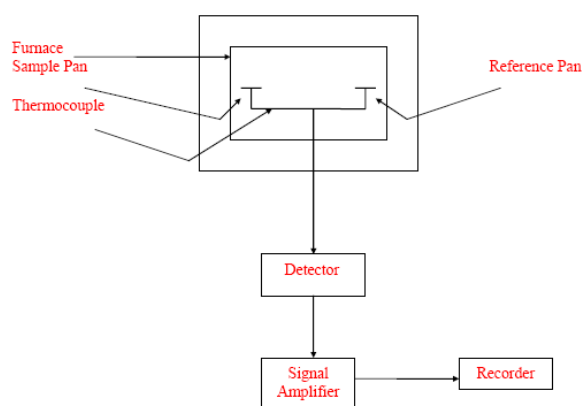
This technique measures the temperature difference between a sample and a reference material as a function of temperature as they are heated or cooled or kept at a constant temperature (isothermal). The sample and reference material are simultaneously heated or cooled at a constant rate. Reaction or transition temperatures are then measured as a function of the temperature difference between the sample and reference. The method provides vital information on materials on their endothermic and exothermic behavior at high temperatures. This technique finds most of its applications in analyzing and characterizing clay materials, ceramics, synthetic and natural polymers, etc.

III. 8. 2. Differential scanning calorimetry (DSC)

Using the differential scanning calorimetry (DSC) technique, the amount of heat absorbed or released by a sample as it is heated or cooled or kept at constant temperature

²² The measurements were performed in the Centre of Polymer and Coal Materials, Polish Academy of Sciences, Zabrze, Poland.

(isothermal) can be measured. The sample and reference material are simultaneously heated or cooled at a constant rate. The difference in temperature is proportional to the difference in heat flow (from the heating source i.e. furnace) between the two materials. This technique is applied to most of the polymers in evaluating the curing process of the thermoset materials as well as in determining the heat of melting and melting point of thermoplastic polymers, glass transition temperature (T_g), endothermic and exothermic behavior. Through the adjunct process of isothermal crystallization it provides information on the molecular weight and structural differences between very similar materials. The instrumentation is exactly similar to that of DTA except for the difference in obtaining the results.



Simplified diagram of the DSC instrument

Differential scanning calorimetry (DSC) analyses were performed using a Mettler Toledo DSC 1 (Mettler Toledo, Switzerland) equipment, operating with a Stare software 9.1 version. The samples (2 – 4 mg) were encapsulated in aluminum pans that had pierced lids to allow escape the volatiles, with a heating rate of $10^{\circ} \text{C min}^{-1}$ and nitrogen purge of 120 mL min^{-1} .

III. 8. 3. Rheological analysis

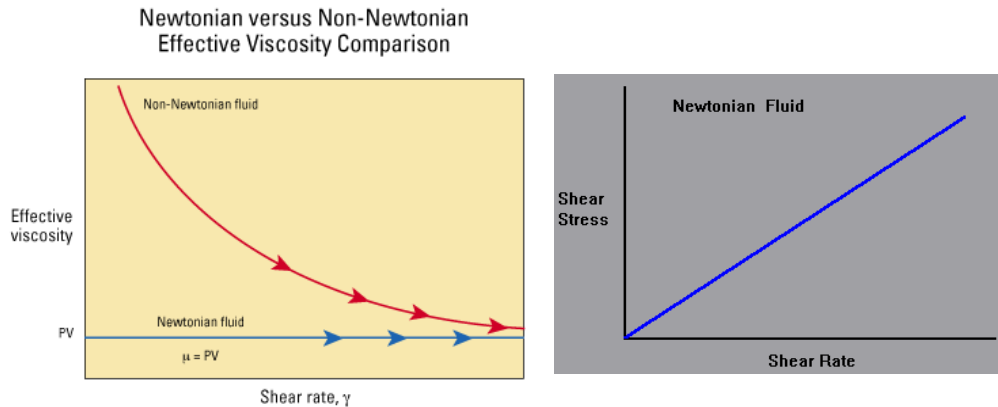
Rheological measurements

Rheology is the science which studies the deformation and flow of materials in liquid, melt, or solid form in terms of the material's elasticity and viscosity. This is accomplished by applying a precisely measured strain to the sample to deform it, and

accurately measuring the resulting stress developed in the sample. The developed stresses are related to material properties through Hooke's and Newton's laws.

Hooke's law. Hooke's law defines the mechanical behavior of an ideal solid, relating the applied strain (ϵ or γ) to the resultant stress (σ or τ) through a factor called the modulus (E or G). Thus, $\sigma = E\epsilon$ (tension, bending) or $\tau = G\gamma$ (shear). The modulus is a measure of material stiffness (i.e., its ability to resist deformation). The linear region in which the modulus does not change when the strain is changed is called the Hookean region.

Newton's law. Newton developed a relationship similar to Hooke's law for ideal viscous fluids, relating stress (τ) linearly to the shear rate ($d\gamma / dt$). Thus, $\tau = \eta d\gamma / dt$, where η is the viscosity coefficient. A fluid is Newtonian if, when sheared, its viscosity does not depend on shear rate.



General rheological behavior of Newtonian fluids

Water and mineral oil are Newtonian, but not many other liquids behave this way. Most fluids are non-Newtonian, their viscosity changing with changes in shear rate. For a Newtonian fluid the viscosity is constant irrespective of the shear stresses and independent of time. Newtonian behavior is approximated by gases and some liquids, notably water and low-molecular weight liquids.

Rheometry refers to a set of standard techniques that are used to experimentally determine rheological properties of (fluid or solid) materials. The idea underpinning rheometry is to realize flows, where the stress and / or strain fields are known in advance, which make it possible to deduce rheological properties from measurements of flow properties.

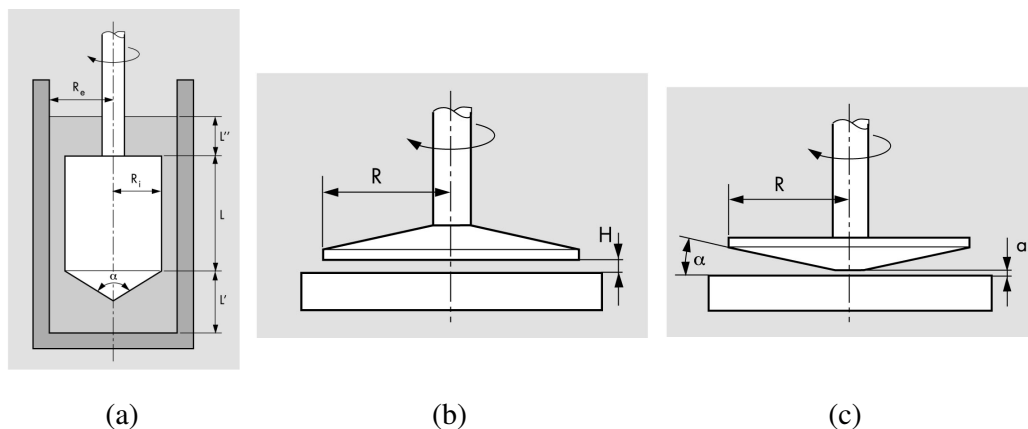
Rheometers measure rheological data on the flow and deformation behavior of substances. Test types include:

Rotational tests for liquids: Flow curves (shear stress and shear rate), viscosity function, yield point, thixotropy (structural decomposition and regeneration), temperature behavior.

Oscillatory tests for all materials – from low viscous liquids to solids: viscoelastic behavior as an amplitude sweep as a function of the deformation or load (or shear stress); as a frequency sweep function of time (speed or frequency); time-dependent behavior (thixotropy, structural decomposition and regeneration), temperature-dependent behavior (glass transition temperature, melting temperature, crystallization temperature, DMTA tests), jellification and hardening behavior.

Creep and relaxation tests – to investigate the viscoelastic behavior and material structure (e.g., molar mass distribution of polymers).

Different types of measuring systems may be used, correlated with the type of the analyzed sample. The usual measuring systems are presented below: coaxial cylinders (a), plate – plate (b) and cone – plate (c).



Measuring systems for rheometers

Rheological measurements were carried out²³ on a Physica MCR 501 rheometer (Anton Paar) equipped with a Peltier device for temperature control. The measurements

²³ Rheological measurements were performed in the Centre of Polymer and Coal Materials, Polish Academy of Sciences, Zabrze, Poland. The scientific and technical assistance of Dr. Constanta Ibanescu is gratefully acknowledged.

were performed using a plate – plate geometry with a diameter of 50 mm. Due to the reduced viscosity of the samples, the gap was fixed at 0.300 mm.

III. 9. Swelling and solubility tests of the polymeric films

Swelling and solubility tests were carried out on unaged and aged polymeric films. The films were obtained by casting the treatment's solutions onto quartz plates and then vacuum dried, at room temperature, for 36 hours. The polymeric films were then aged, for two cycles of 500 hours, in an Angelantoni CH250 climatic chamber, at 40° C, under UV irradiation.

To evaluate the swelling and solubility behavior, the unaged and aged polymeric films were immersed in neutral and modified pH water (i.e., pH = 7.2; pH = 5.5; pH = 8.5) for 24 hours. The swelling degree was determined according to

$$\text{swelling} = 100 (W_s - W_0) / W_0 \quad (\%)$$

where W_s is the weight of the polymeric film after the immersion in water solution and W_0 represents the weight of the dry polymeric film before the immersion in the aqueous solution. The negative values represent partial solubilization of the film and positive values represent the swelling degree.

III. 10. Contact angle measurements

The contact angle measurements, performed on stone samples treated with water repellent products, consist in the deposition of a distilled water drop on the treated stone surface followed by the actual measurement of the angle between the water drop and the treated stone surface. This experiment gives information on the hydrophilic/hydrophobic properties of a surface – for a well determined volume water drop, a lower contact angle value indicates a less hydrophobic surface, while, on the contrary, a higher contact angle value indicates a high surface hydrophobicity. To express it in a different way, a low contact angle between a water drop and a certain surface can be observed when the drop moistures the surface, or, on the contrary, a high contact angle is registered when the water drop remains less extended on the surface, not moisturizing it.

Nowadays, the literature contains many studies involving this technique, due to its use for the assessment of chemical products in stone conservation [57, 58].

The instrument is placed on top of a steady table, the cleaning and media (20° C) adequate conditions being taken into account. The images are registered automatically with major precision.

The contact angle measurements were performed using a Kruss Easydrop Standard Goniometer (DSA 100 Soft). The deposition of water droplets was performed automatically, using a 100 µL Hemilton syringe. Contact angle values were registered automatically during 30 seconds.

III. 11. Artificially accelerated ageing tests

III. 11. 1. Artificially accelerated ageing under UV irradiation

Resistance to ultraviolet irradiation

Principle

The test involves the absorption of electromagnetic radiation by the substances in the ultraviolet and visible regions of the spectrum. This results in changes in the electronic structure of ions and molecules through the excitations of bonded and non-bonded electrons.

Instrumentation

It consists of a dual light source, e.g., a tungsten lamp for visible range and a deuterium lamp for ultraviolet region, grating monochromator, photo-detector, mirrors and glass or quartz cells. Both glass and quartz cells can be used for measurements in the visible region, while for the measurements under ultraviolet region, only quartz cells can be used.

The treated stones as well as the polymeric films were aged, for two cycles of 500 hours in an Angelantoni CH250 climatic chamber, at 40° C, under UV irradiation.

III. 11. 2. Resistance to salt mist artificial accelerated ageing

Resistance to salt mist action – UNE – EN 14147 (2004)

Principle

The stone samples were placed in a specific climatic room where they were sprayed with saline solution (5% NaCl). A spraying cycle took 4 hours and was followed by a drying cycle of 20 hours.

Equipment

A climatic chamber equipped with a spraying device and a ventilator.

Sample preparation

The stone samples were washed and then dried at $70 \pm 5^\circ \text{C}$ until they reached constant weight, weighted and the initial weight values (M_0) were registered.

Procedure

The stone samples are placed in the special climatic chamber, making sure the samples are not very close to each other. The samples are then exposed to 4 hours of salt mist artificially ageing cycle, followed by a 20 hours cycle of drying.

The standard consists in performing 60 artificially ageing cycles, although the experiment can be stopped before if the stone samples are becoming extremely deteriorated.

After the finalization, the samples are washed with deionized water and then dried at $70 \pm 5^\circ \text{C}$ until they reach constant weight (M_n).

For every stone sample the weight loss is calculated with the relation

$$\Delta M = [(M_0 - M_n) / M_0] \times 100 \quad (\%).$$

III. 11. 3. SO₂ action the in presence of humidity artificially accelerated ageing

Resistance to SO₂ action in the presence of humidity – UNE – EN 13919 (2003)

Principle

The resistance of the stone samples against SO₂ action can be determined by placing the stone samples in two acid resistant containers during 21 days, using two different SO₂ concentrations in each container. For the sake of clarity, only the experimental results obtained for the highest SO₂ concentration will be reported in Chapter VIII.

Materials

For a container of 50 liters:

- solution: 500 ± 10 ml H₂SO₃ diluted in 150 ± 10 ml H₂O;
- m_0 – dry sample weight before the experiment (g);
- m_1 – dry sample weight after the experiment (g);

Δm – weight variation (%) ($\Delta m = [(m_0 - m_1) / m_0] \times 100$).

Procedure

The stone samples are submerged in water at $20 \pm 5^\circ \text{C}$ for 24 hours prior to the experiment. The samples are then introduced in the two containers which have, on their bottom, the acidic solutions. The stone samples must be placed at least 100 mm higher than the acidic solution level. The containers must be closed and sealed in order to maintain the SO_2 saturated atmosphere during the 21 days of experiment.

After 21 days, the stone samples are washed and dried until reaching constant weight.

IV. Stones selection and sampling

Sedimentary rocks

Sedimentary rocks form about 75% of Earth surface, but only 5 to 10% of its volume and are covering extensive tracts of the continents surface. Argillaceous rocks are by far the most abundant sedimentary rocks, occupying about 45% of the area, with sandstones forming more or less 30% and limestones about 28% of the surface. All these taken into account, it is logical that sedimentary rocks have been widely used for building and decoration and that sandstones and limestones are the predominant rock types used.

The specialized literature presents many elaborated classifications of the sedimentary rocks, but a more simplified one is based on their origin, i.e. chemical, organic, and clastic or detrital.

Chemical limestones are formed directly by precipitation of calcium carbonate from water. Calcium carbonate is only slightly soluble in water; however, most circulating ground waters contain carbon dioxide. Rain water, which is the source of most groundwater, also contains carbon dioxide. These waters are converting calcium carbonate into calcium bicarbonate ($\text{CaCO}_3 + \text{CO}_2 + \text{H}_2\text{O} + \text{Ca}(\text{HCO}_3)_2$), which has a much higher solubility and exists only in solution. Chemically precipitated limestones were also formed in sea waters. In some areas, warm, tide-swept and wave-agitated shallow sea water in tidal channels and in lagoons calcium carbonate precipitates in concentric layers, commonly round, a fragment of shell or a grain of sand acting as a nucleus. These small, mainly spherical carbonate grains are known as *ooliths*. Some limestones are composed nearly entirely of ooliths; they are called *oolitic limestones* or

oolites. Generally, the ooliths are about 1 mm, more rarely up to 2 mm in diameter. In some rocks they are about the size of a pea, these being called *pisolite*.

Organic limestones largely consist in the fossilized shells of one or more organisms. The organisms removed calcium carbonate from the water in which they lived and used it for their shells or skeletons. For example, reef limestones are composed of a number of organic components, algal limestones originate from algae which secrete lime, shelly limestones are made generally of the fossil remains of shellfish. The spaces between the fossilized organisms may be filled with broken shell matter or with calcareous mud. The fossils in a limestone may range from complete, unbroken shells to those that are completely broken.

Clastic or detrital limestones result from the erosion of pre-existing limestones. The fragments range from fine-grained calcareous mud to pebbles of the original limestone, later consolidated and generally cemented with calcareous material into a new coherent rock.

Although limestone is not quarried for dimension stone on the same huge scale that it is for crushed rock and for industrial use, it has nevertheless contributed greatly and sometimes dramatically to the appearance of many of the world's buildings and towns.

Carbonate stones

The carbonate rocks make up 10 to 15% of sedimentary rocks. They largely consist of two types of rocks, i.e. limestones which are composed mostly of calcite (CaCO_3) or high Mg calcite [$(\text{Ca},\text{Mg})\text{CO}_3$] and dolostones which are composed mostly of dolomite [$\text{CaMg}(\text{CO}_3)_2$].

Commercial limestones are rocks of sedimentary origin primarily composed of calcium carbonate with or without magnesium. Included in this category are calcitic limestone, dolomite, dolomitic limestone, and travertine (a rock that is chemically precipitated from hot springs).

Due to the fact that carbonate minerals are generally soluble in slightly acidic waters, they often present high porosity and permeability, this making them ideal

reservoirs for petroleum. Dolostones tend to weather to a brownish color rock, whereas limestones tend to weather to a white or gray colored rock. The brown color of dolostones appears due to the presence of small amounts of iron, replacing some of magnesium in dolomites.

Two classification schemes are in common use by those working on carbonate rocks: Folk and Dunham classifications. Folk classification divides carbonates into two groups (Fig. 1). Allochemical rocks contain grains brought in from elsewhere. Orthochemical rocks are those in which the carbonates crystallized in place. Allochemical rocks have grains that may consist of fossiliferous material, ooids, peloids, or intraclasts. These are embedded in a matrix consisting of microcrystalline carbonate (calcite or dolomite), called micrite, or larger visible crystals of carbonates, called sparite. Sparite is a clear granular carbonate that has been formed through recrystallization of micrite, or by crystallization within previously existing void spaces during diagenesis.

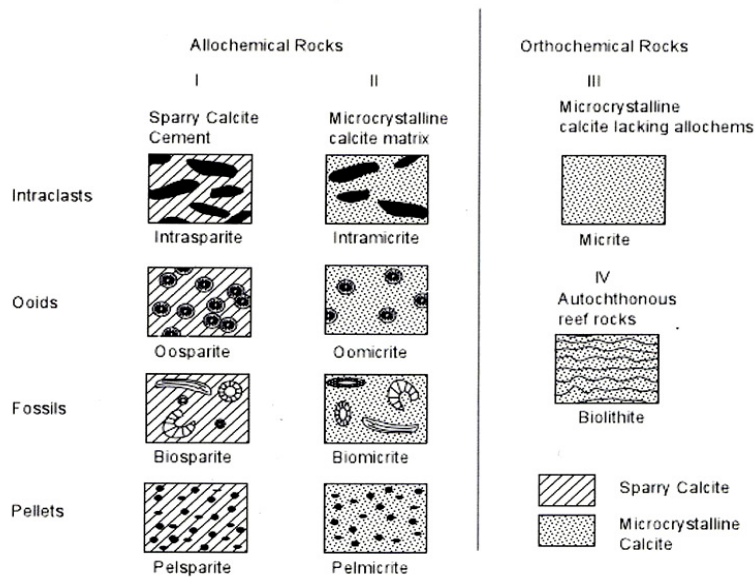


Fig. 1. Classification of carbonates according to Folk

Dunham classification is based on the concept of grain support. This classification divides carbonate rocks into two broad groups, those whose original components were not bound together during deposition and those whose original

components were formed in place and consist of intergrowths of skeletal material. The latter group is called boundstones (similar to biolithites of the Folk classification). The former group is further subdivided as to whether or not the grains are mud-supported or grain-supported. If the rock consists of less than 10% grains it is called a mudstone; if it is mud-supported with more than 10% grains it is called a wackstone; if the rock is grain-supported, two varieties of limestone exist – packstone, when grains have shapes that allow for small amounts of mud to occur in the interstices, and grainstone, if no mud exists between the grains.

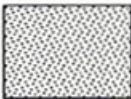
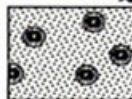
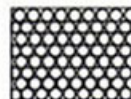
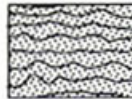
Original components not bound together during deposition				Original components bound together during deposition. Shows intergrown skeletal material, lamination contrary to gravity, or sediment-floored cavities that are roofed over by organic material and are too large to be interstices.
Contains mud (particles of clay and fine silt size)		Lacks mud		
Mud-supported		Grain-supported		
Less than 10% Grains	More than 10% Grains			
Mudstone	Wackstone	Packstone	Grainstone	Boundstone
				

Fig. 2. Classification of carbonates according to Dunham

Being soft and soluble in water, for calcite and aragonite the distance of transport is usually not very far. Unlike other sediments, the degree of rounding and sorting of the grains may not be reflecting the energy of the transporting medium, but may be biologically determined. Grains found in carbonate rocks are as follows:

- Whole or broken skeletons of organisms (fossils). These may range in size from gravel to fine sand, depending on the organism and the degree to which the grains are broken during transport.

- Ooids – spherical sand sized particles that have a concentric or radial internal structure. The central part of each particle consists of a grain of quartz or other carbonate particle surrounded by thin concentric layers of chemically precipitated calcite. The layers or coatings are formed in agitated waters as the grain rolls around.

- Peloids – spherical aggregates of microcrystalline calcite of coarse silt to fine sand size. Most appear to be fecal pellets from burrowing benthic organisms. As these organisms burrow through the muddy carbonate-rich sediment, they ingest material in search of nutritional organic compounds resulting in waste products containing microcrystalline calcite. Due to their small size, the peloids are much easier seen in thin section than in hand specimen.

- Limeclasts – fragments of earlier formed limestone or partially lithified carbonate sediment. Most are intraclasts, originating within the basin of deposition.

The matrix of carbonate rocks consists of either fine-grained carbonate mud, called micrite, or coarser grained calcite crystal formed during diagenesis, called sparite.

The micrite results from recrystallization of carbonate mud during diagenesis or from direct precipitation of calcite, and causes lithification of the sediments. The micrite gives the hazy opaque appearance of most limestones as seen in hand specimen. If the rock consists entirely of fine-grained mud matrix, it implies deposition in a low energy environment just like in siliclastic mudstones. Some of the mud may start out as aragonite needles 5 to 10 mm in length produced by calcareous algae, becoming recrystallized to a microspar 5 to 15 mm in diameter during diagenesis.

Among the existing rocks, the carbonated ones have a special significance, due to their abundance and economical value. This type of rocks is the most used as building material for monumental buildings, especially due to the physical / mechanical properties (durability / resistance) they exhibit. People representing cultures around the world are using limestone to build monuments for thousands of years: the Egyptian pyramids, London's St. Paul's Cathedral, Empire State Building in New York are just a few examples of limestone usage spreading all over the world.

For the present study, two types of rock, from Spain and Romania, were selected. To select the stones, some criteria were taken into account. Two limestones were chosen in order to be comparable from this point of view but, at the same time, these stones have different properties and characteristics, so one expects them to have different behaviors towards the chemical treatments and the durability tests as well. The stones were also chosen due to their regional significance, abundance and importance. Another aspect taken into consideration in the selection of the materials was their level of usage as

building materials in the construction of monuments (churches, monasteries, cathedrals, etc.) that present historic and artistic importance and have significance from the cultural heritage point of view.

IV. 1. Laspra

The first selected stone is a micritic dolomitic limestone, typical from the Spanish region of Asturias, called Laspra. In historical references Laspra's quarry is mentioned under the name of Laspra (1451) and Aspra (1463), and also Amilladoiro (1473), Omilladoiro (1493), and Milladoiro (1505).

This rock can be widely found in Asturias, especially in Oviedo county, being used, for example, as one of the three main building materials of the San Salvador Cathedral of Oviedo (1293-1587) (Fig. 3). Small inner parts of two preromanic churches from the IXth century outside Oviedo, namely Santa Maria del Naranco (Fig. 4) and San Miguel de Lillo (Fig. 5) were built as well using Laspra as building material.



*Fig. 3. San Salvador
Cathedral of Oviedo, Spain
Origin: IXth century
Period: XVIth century
Style: Gothic*



*Fig. 4. Santa María del Naranco
Period: IXth century
Style: Pre-Romanesque
UNESCO's World Heritage Site since 1985*



*Fig. 5. San Miguel de Lillo
Period: IXth century
Style: Pre-Romanesque
UNESCO's World Heritage Site since 1985*

Oviedo's Cathedral is one of the most representative buildings of the late gothic architectural style in the province of Asturias. Historically and artistically, the cathedral presents a significant interest, reflecting all gothic style evolution in Spain. San Salvador Cathedral was the first gothic monumental building in Asturias.

Three types of stones were used for the construction of the cathedral – Laspra, Piedramuelle and Tinana, the first one being found, as building material, in more than 60% of the cathedral.

Laspra was used to build all the interiors (the church and *Sala Capitular*) and an important part of the exterior (*Claustro* and *Portico*), its period of usage having the roots in the XIII century (until the first half of the XVIth century). Laspra was used during the Cathedral's reconstruction works in 1943. The three types of ornamental stones can be

easily distinguished just looking at the monument, Laspra being recognized by its bright white aspect.

Due to the intensive usage of this stone during centuries, no Laspra quarry exists nowadays. This is the reason why a small block remaining from the former restoration of the Cathedral of Oviedo was used for this study (Fig. 6).



Fig. 6. The block of Laspra used in this research

IV. 2. Repedea

The second selected stone is coming from Romania and is a bioclastic oolitic stone, named Repedea.

This type of stone can be found in the east part of Romania, along the Moldavian Platform, the oolitic limestone slate covering a surface of approximately 3000 km². In the north-eastern region of Romania, called Moldova, this limestone is the main building material used for the construction of basically all important churches and monasteries since antiquity until the present time. The most representative churches that can be found in this part of the country were built, in most cases, only from Repedea.

One of the most important monasteries, from both historic and cultural point of view, situated in the north-eastern part of Romania is the Dobrovat monastery (Fig. 7), the whole monastery assembly being built (1503 – 1504) from Repedea limestone. As confirmed by XVth century documents, the choice of the place for building the monastery

was not by chance – the Moldavian *voevod* of that time choose the Dobrovat valley influenced by the ancient monarchal life in the area.

The monarchal assembly, the way it looks today, contains many constructions – The Descending of the Holy Spirit on the Disciples Church (the only church from that period preserved intact in the Moldavian region), the chapel, the entrance tower with the enclosure wall (partially battered) built in the XVIIIth century, the ruins of some constructions from the XVIIIth century, the cell assembly with administrative offices from the XXth century.

The year 1743 marks a new architectonic contribution to this monarchal assembly. On the East side of the enclosure an entrance tower with multiple functions, a guard place, steeple and chapel were build.

The most important monument from the Dobrovat monastery assembly undoubtedly remains The Descending of the Holy Spirit on the Disciples Church. The facades decoration impresses both by sobriety and by the perfect equilibrium of the forms, stressing the monumental effect of the building. The stone wall is built over a profiled stone pedestal, decorated at its superior part with two rows of niches.

The entire establishment is plastered by a thin layer through which one can see the construction materials: quarry and matched stones, set by the ridges.

The great wall assembly from Dobrovat prefigures many iconographic trends of the wall painting in the XVIth century Moldavia.



*Fig. 7. Dobrovat Monastery
Period: XVIth century
Style: Medieval Moldavian*

For this study, a block of Repedea stone was sampled from Gura Bohotin non-active quarry, situated in the proximity of the monastery. Repedea was formed along a continental platform area of the Sarmatic Sea, which could be found starting from Vienna (in the west), in Romania, Crimea and up to beyond the Caspian Sea (Fig. 8)²⁴.

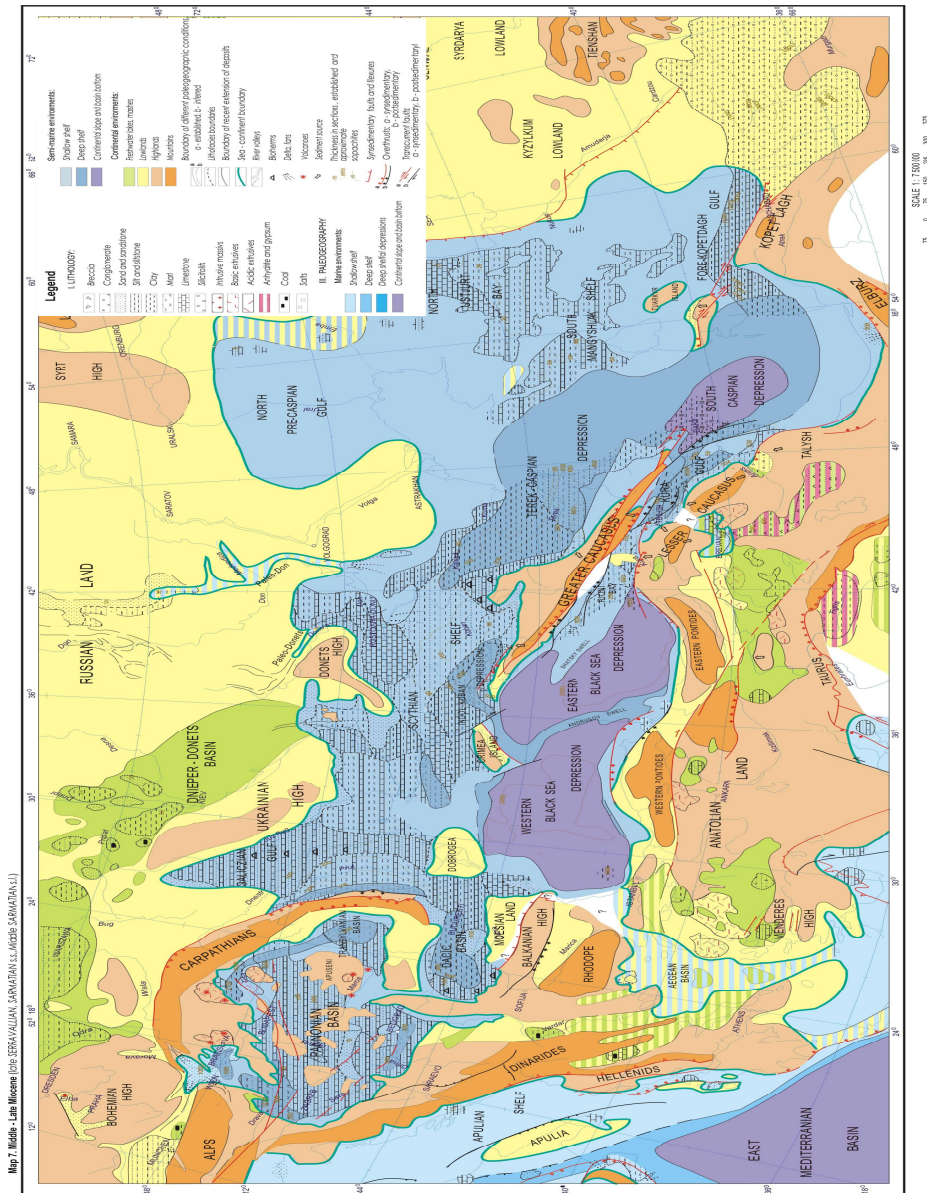


Fig. 8. Geographical localization of the Sarmatic Sea

²⁴ The map was kindly provided by professor I. Petreus, Department of Geology, “Al. I. Cuza” University, Iasi, Romania.

This oolitic limestone was formed through chemical precipitation in a sea-floor during the medium Sarmatian age. The limestone plate, as well as the other rocks forming the sedimentary covering of Moldavian Platform, is presenting a few degrees leaning, from north-west towards south-east. Repedea was formed starting at 400 meters absolute altitude (from the sea level) in the north-western part of this area and continued to up to 85 meters absolute altitude in the south-eastern part, near the city of Husi. A progressive leaning decrease of the limestone plate from north-west towards south-east, with 7-8 m/km, can be observed.

The Gura Bohotin quarry (Fig. 9) is located in Gura Bohotin village, near Prut river, and only 45 km from Iasi, the capital of Moldavia. In this part of Romania, Repedea was the only buiding material used for the construction of houses, fences, cellars, churches and monasteries since antiquity till now.

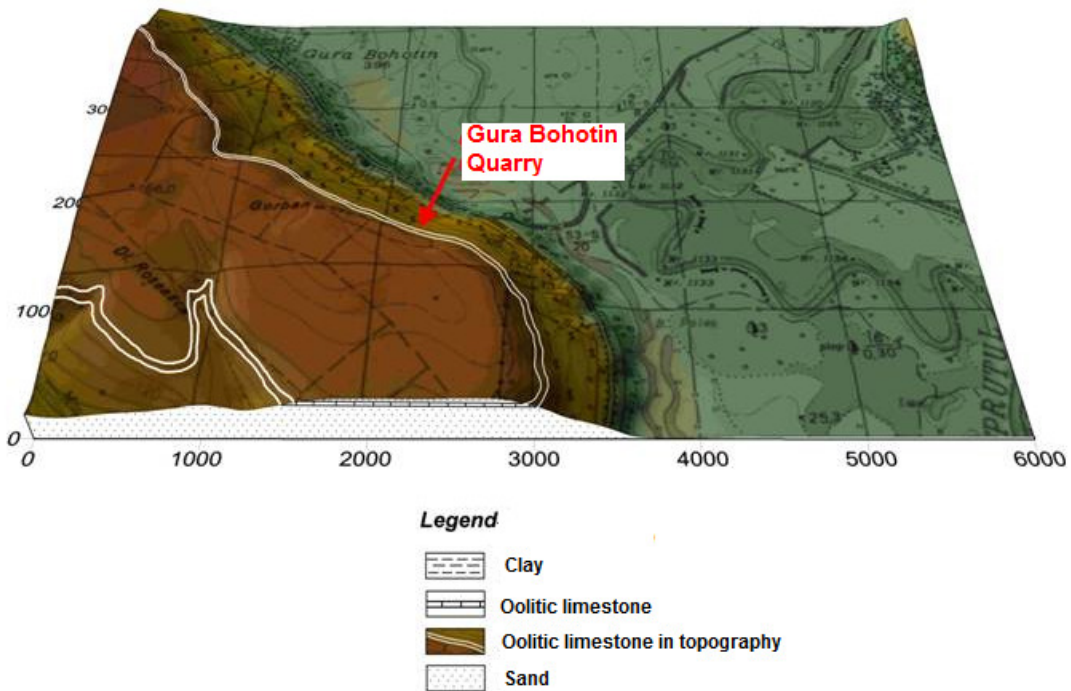


Fig. 9. Block diagram showing the limestone plate (white) and the location of the Gura Bohotin quarry

The limestone quarry is placed exactly on the oolitic limestone plate. In the quarry area the stone layers are not covered for hundreds of meters by any vegetation and the possibility of the extension of the quarry for kilometers does exist.

The Gura Bohotin quarry is not active, the limestone blocks being extracted manually without using any extraction equipment. The used stone block was sampled from the oolitic limestone layer area and had a parallelepiped irregular shape (Fig. 10).



Fig. 10. The sampled Repedea limestone block

The orientation of the sampled limestone block in the rock mass is described in Fig. 11.

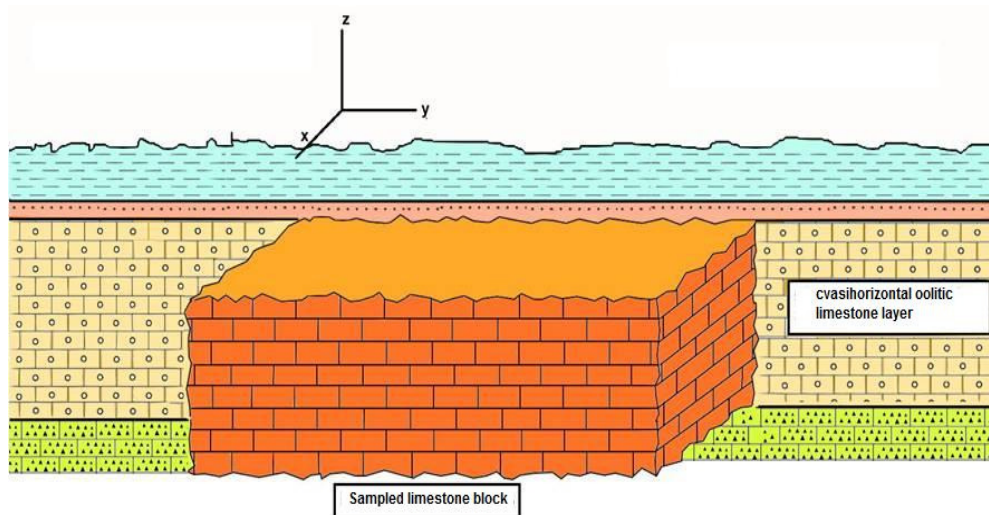


Fig. 11. The orientation of the stone block within the rock mass

The XY plan represents the general stratification plan of the oolitic limestone, of the clay and sand existing in the quarry and in all Moldavian area. The oolitic limestone plate presents a 2-3° recumbence from north-west to south-east. The Z ax is placed perpendicular to the general stratification XY plan.

After sampling, the limestone block was transported to a company specialized in cutting rocks to be cut in slabs (Fig. 12).

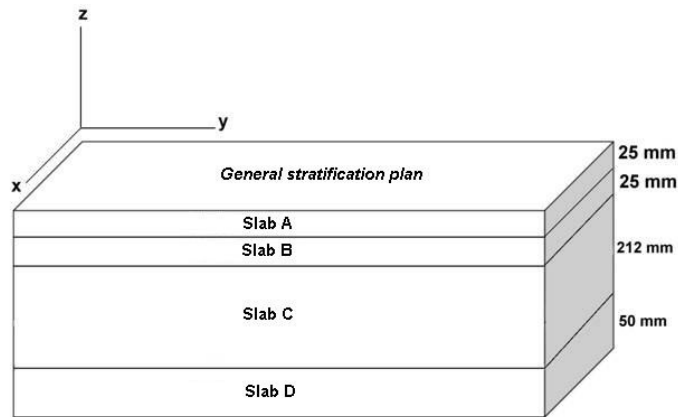


Fig. 12. Orientation of the stone plates in the sampled limestone block

Slab A had a thickness of 25 mm. Samples of 250 x 125 x 25 mm were cut from this slab and named starting from 1 to 16 as in Fig. 13. Every small stone sample was marked with the three directions (X, Y and Z, respectively), indicating the orientation of each sample within the stone block from which it was cut.

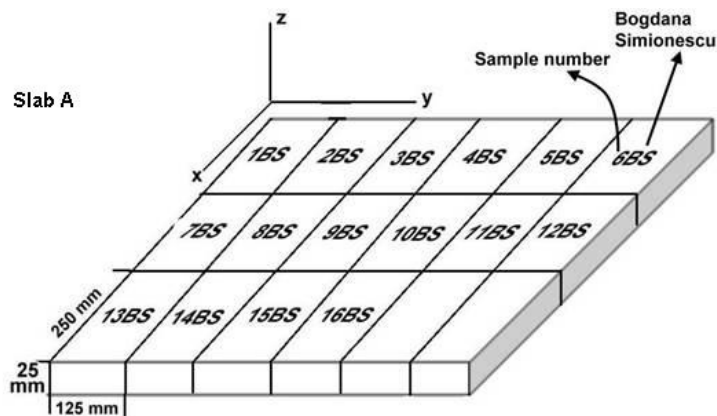


Fig. 13. Slab A and samples 1 to 16

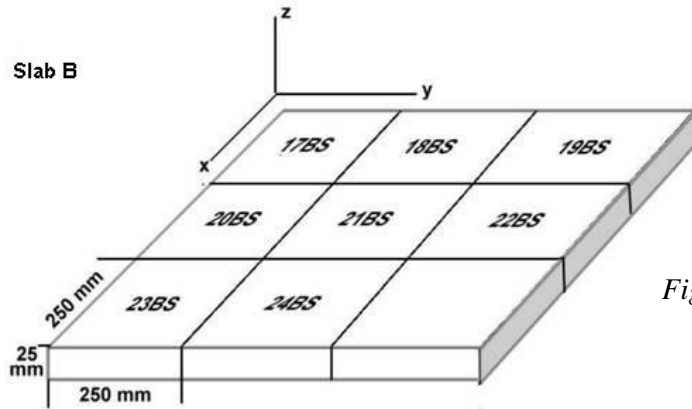


Fig. 14. Slab B and samples 17 to 24

The slab C (Fig. 15), having 212 mm thickness, was used to cut small stone samples with dimensions of 104 x 104 x 212 mm, named with numbers from 25 to 29.

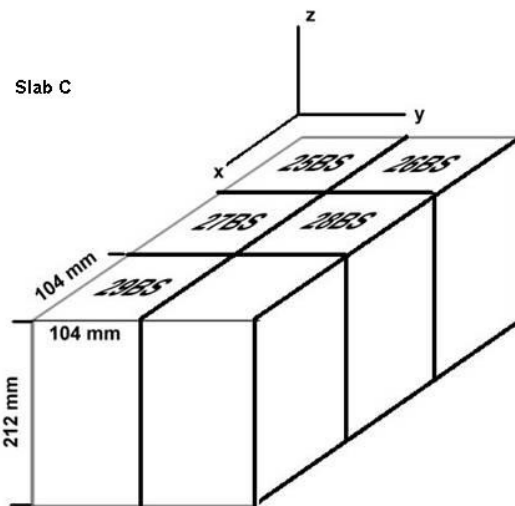


Fig. 15. Slab C and samples 25 to 29

The slab D (Fig. 16), presenting 50 mm thickness, was used for cutting the cubic samples of 50 x 50 x 50 mm in dimensions. 81 stone cubes, noted from 30 to 110, were cut from this slab.

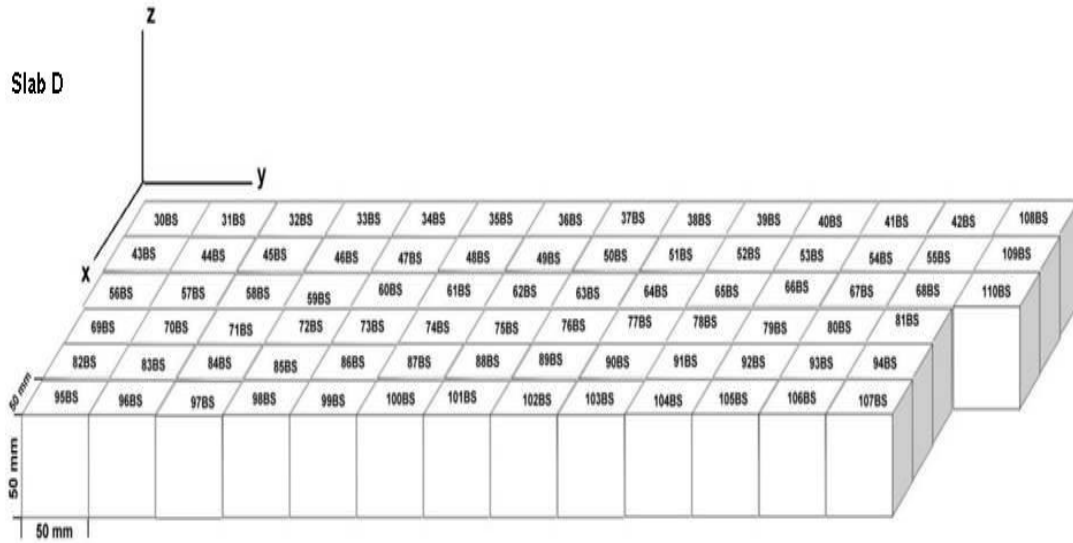


Fig. 16. Slab D and samples 30 to 110

The last slab, E, had a 100 mm thickness and served for the cutting of stone samples with 50 x 100 x 100 mm in dimensions, numbered 111 (Fig. 17).

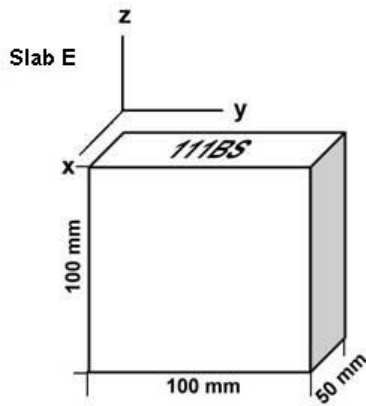


Fig. 17. Sample 111

V. Stones characterization

V. 1. Introduction

The petrography has the role of defining the rock – describing mineralogical composition and the spatial relation between the minerals – texture, pore space structure, fissures.

Both aspects are very important for the further understanding of water movement within the stones, water being the most dangerous weathering agent as far as stones are concerned. For the most common petrographic studies the traditional polarizing microscopy and scanning electron microscopy are the most useful techniques.

Carbonated rocks have in their composition a small variety of minerals, the most important mineral being calcite (or sometimes dolomite).

V. 2. Macro and micro observation

Macroscopic observation refers to the description of the stone with the naked eye, as far as color, texture, porous system and other general characteristics are concerned. The macroscopic description is accompanied by photos, scale 1:1.

Microscopic observation represents the description of the thin section of the stones by using the polarizing light microscope. It gives primary information on stone's composing minerals, its matrix, grain sizes, details about the shape and dimensions of the minerals, as well as stone's texture. Microscopic photos of the thin sections of every type of studied stone are attached to the description.

V. 2. 1. Laspra

Macroscopic observation

Laspra can be described as having a bright white color and being a uniform stone, with very fine grain size. One can observe that this stone has a compact and coherent aspect. Laspra is a microporous stone, the very small pores being visualized even with the naked eye; no fissures can be seen at macroscopic level. Looking closely at the stone, one can identify small traces of iron oxides.

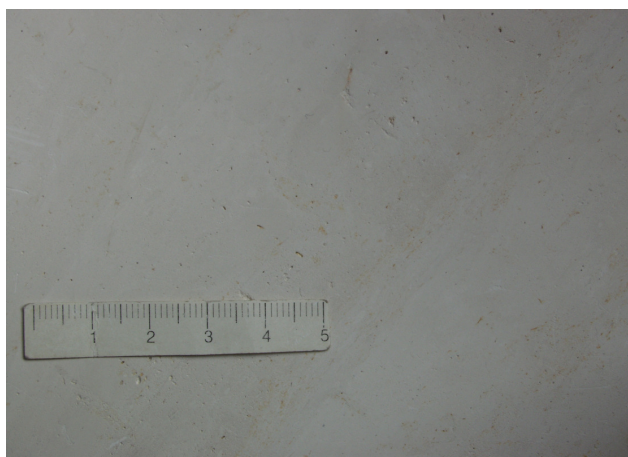
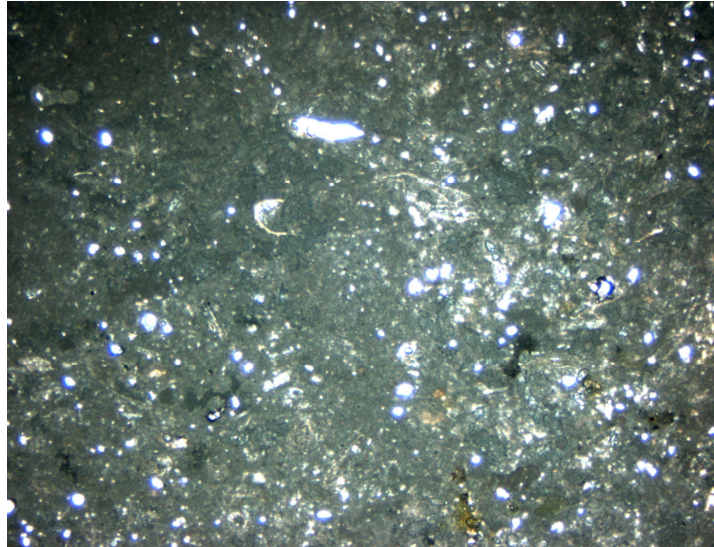


Fig. 18. Macrographs of Laspra

Microscopic observation

From the microscopic point of view, Laspra presents a microcrystalline texture and is composed mainly of dolomite, calcite and ankerite with micritic grain size, as well

as of small amounts of quartz. In some areas, the stone presents microsparitic grain size along the pores.



*Fig. 19. Laspra – micrographs (POL)
(NPx10) and (NCx10)*

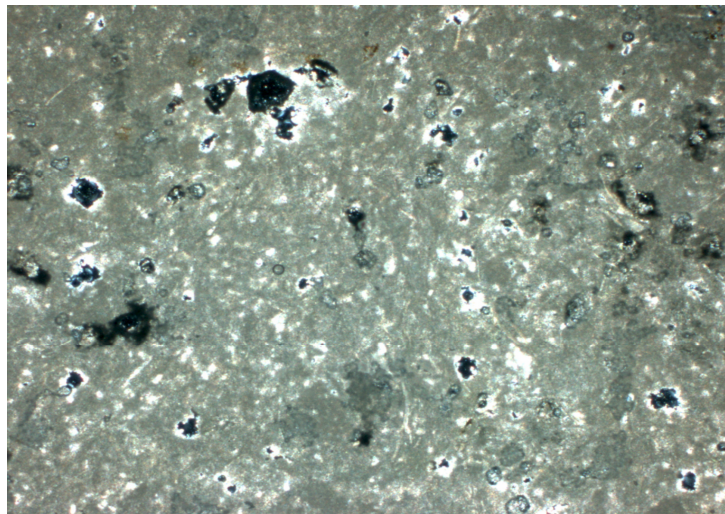
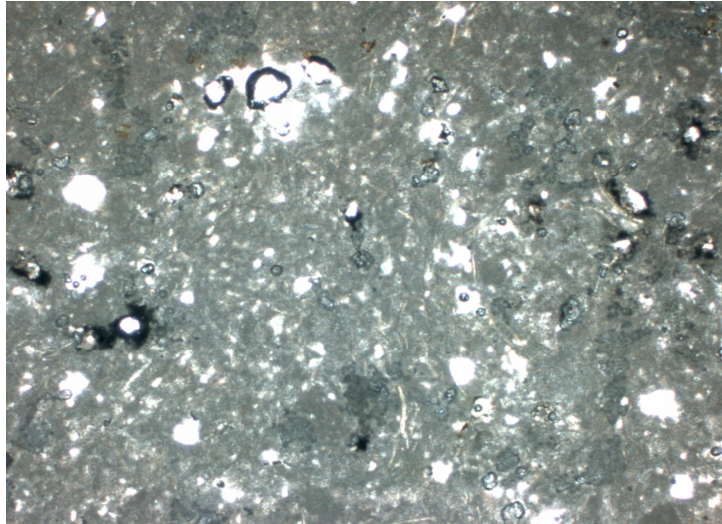


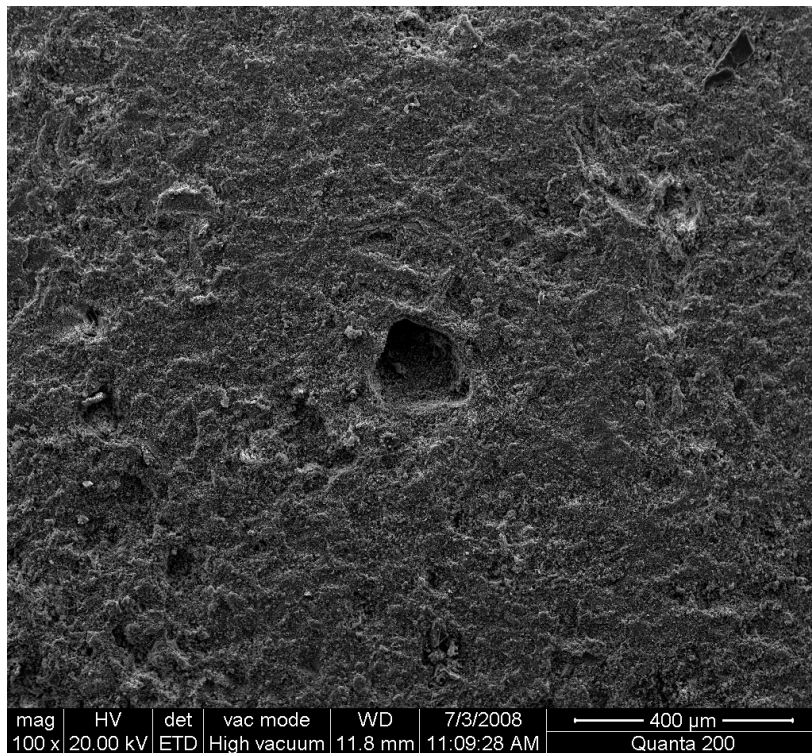
*Fig. 20. Laspra – micrographs (POL)
(NPx25) and (NCx25)*

The dolomite has a micritic character (grain size less than 4 micrometers), the crystals having idiomorphic tendency. The quartz grains have variable sizes, between 22 and 100 micrometers, sub-idiomorphic tendency. In the same micritic mass, very fine filosilicates of less than 4 micrometers can be observed, but they are very difficult to distinguish and identify. The voids within the stone are many and of variable geometry, regular or irregular, micropores being predominant within the stone (opening radius less than 7.5 micrometers); the macropores have the opening radius larger than 7.5 micrometers. The pores are spread all over the micritic mass, but the rock's degree of cohesion is considered to be high.

From the textural point of view, Laspra is a relatively isotropic rock, its behavior related to alteration being influenced by the fine grain size and by the multitude of micropores within the micritic mass, as well.

Small pieces of bioclasts and quartz grains are detectable in the microcrystalline mass. The bioclasts within the stone are fossils like mollusks (mainly bivalves and gastropods) and foraminifers.

As seen even macroscopically, iron oxides are present in Laspra's structure, these compounds being easy to identify due to their reddish color. The quartz grains can be characterized as having more or less spherical or ellipsoidal shapes, with the spherical index and roundness of approximately 0.3 – 0.5. The quartz grain size is of about 0.2 – 1.0 mm. From the porosity point of view, Laspra is a microporous stone, having moldic porosity.



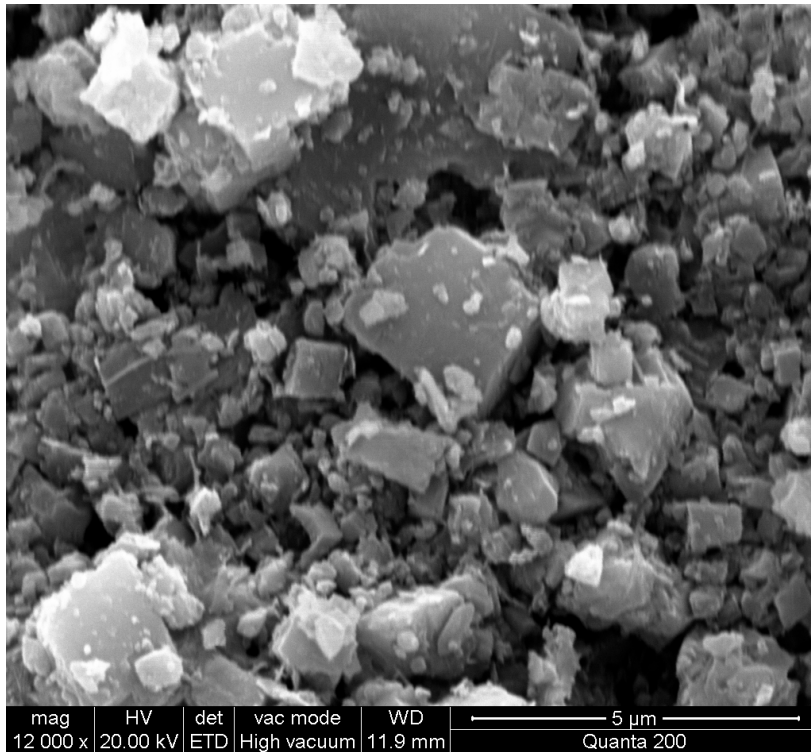
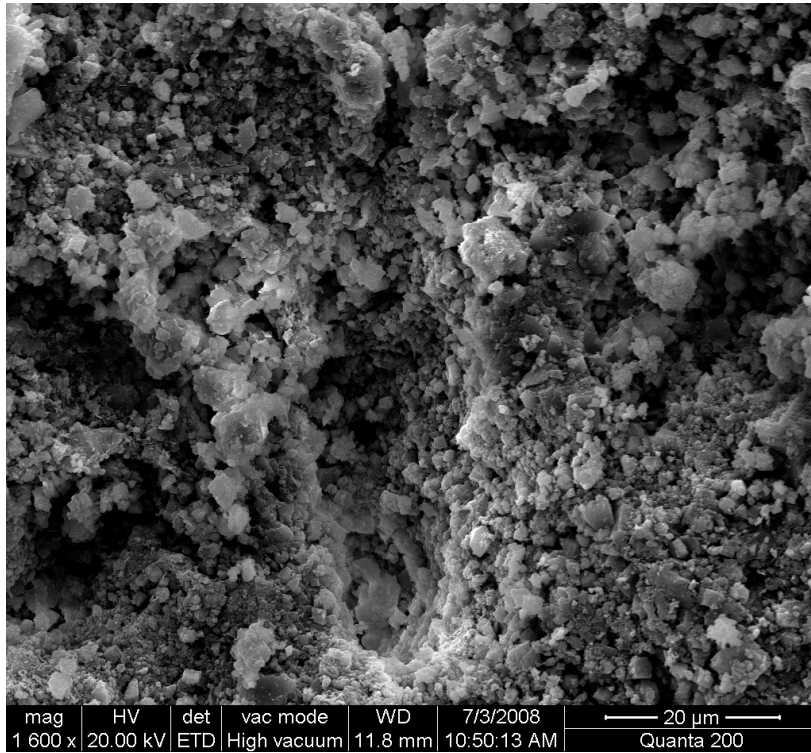


Fig. 21. Laspra – micrographs (ESEM)

V. 2. 2. Repedea

Macroscopic observation

Repedea's appearance is as a brownish stone, having a compact and coherent structure.

The stone's structure includes fossils, the visible remains having dimensions in between 2 mm and 2 cm.



Fig. 22. Macrographs of Repedea

The distribution of the fossils is heterogeneous, and the stone appears to be an anisotropic one, macroscopically speaking.

In some areas of the quarry, Repedea can be composed mainly of bioclasts, as seen in the next photo.



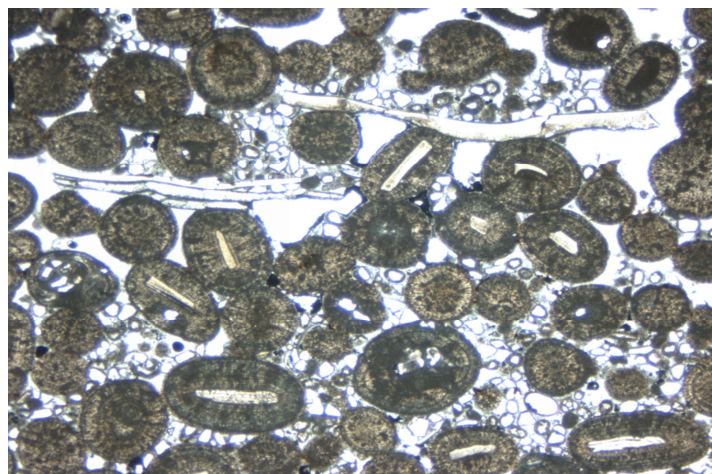
Fig. 23. Macrograph of Repedea

Microscopic observation

Repedea's texture can be described as an oolitic grainstone. The stone's matrix, between the oolites, as seen microscopically, is a micritic and microsparitic one.

The anisotropy of Repedea is determined by the difference in the oolites grain sizes and by the oolites distribution within the stone's structure.

From the homogeneity point of view, Repedea appears to be a more or less homogeneous material, the quartz grains being surrounded by cement of micritic (calcite) and microsparitic grain size.



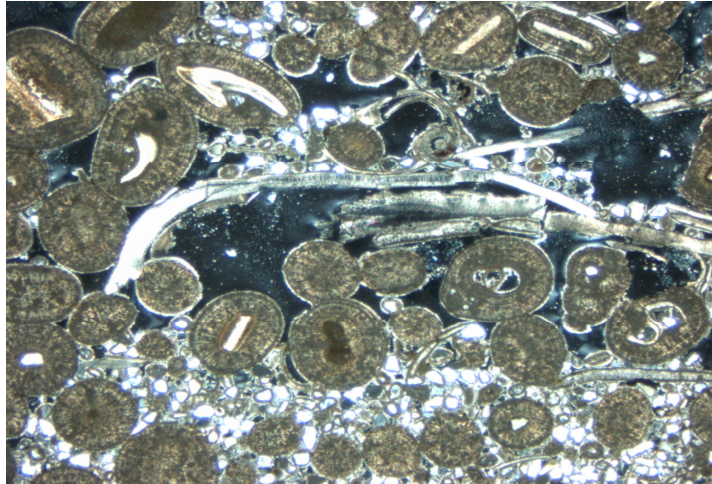


*Fig. 24. Repedeia – micrographs (POL)
(NPx10) and (NCx10)*

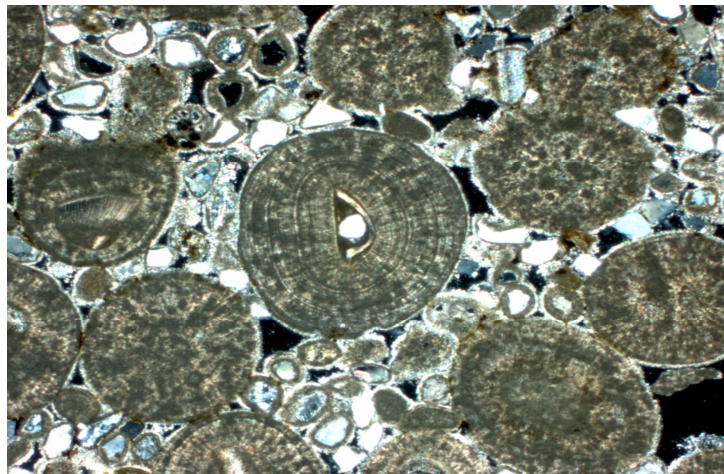
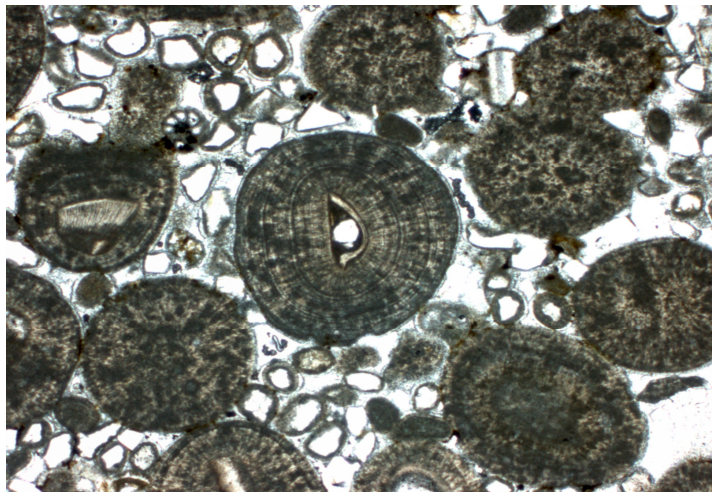
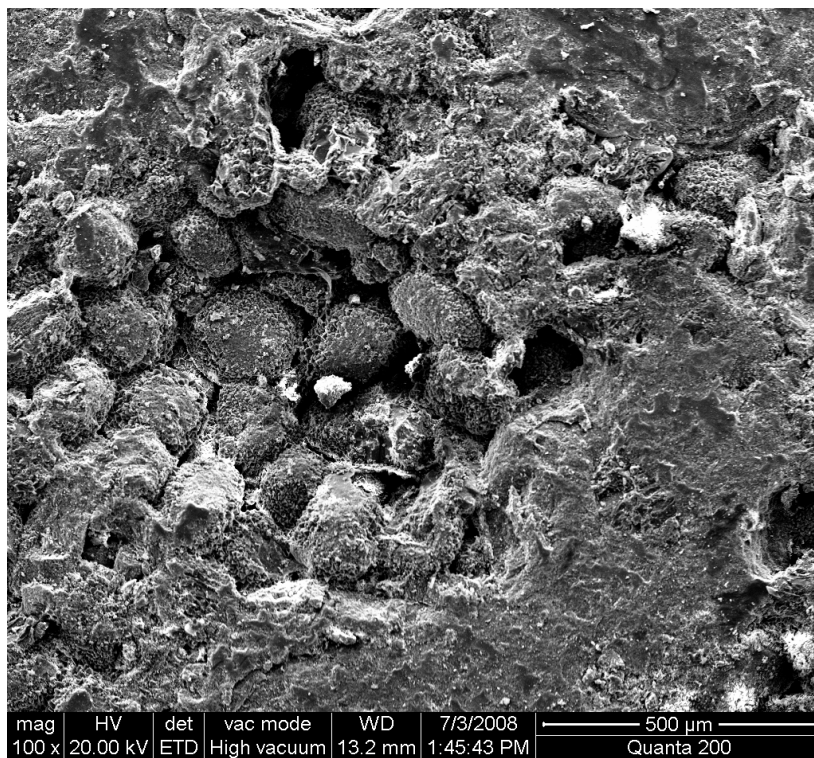


*Fig. 25. Repedeia – micrographs (POL)
(NCx25) and (NPx25)*

Most oolites have spherical or ellipsoidal shape, a diameter between 0.6 and 2.0 mm and present a quartz nucleus (one or more grains of quartz); a concentric lamina is developed around the nucleus (radial structure).

In some areas, one can observe between the oolites pieces of fossils like mollusks, brachiopods and gastropods, while in some other parts of the stone intraclasts can be identified.

This stone can be classified as a grainstone (according to Dunham, 1962) and as a oomicrite – oosparite (according to Folk, 1959 – 1962).



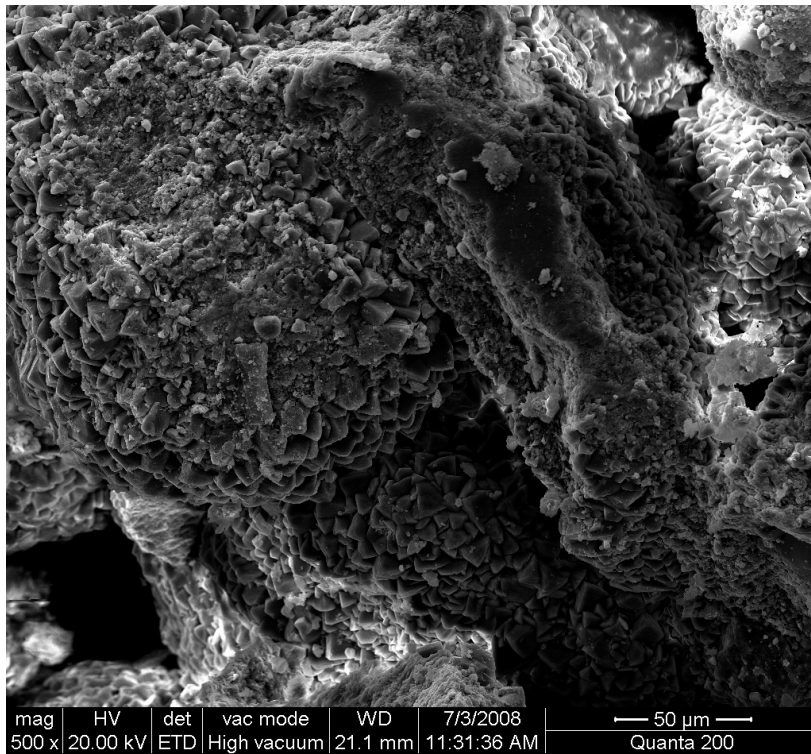
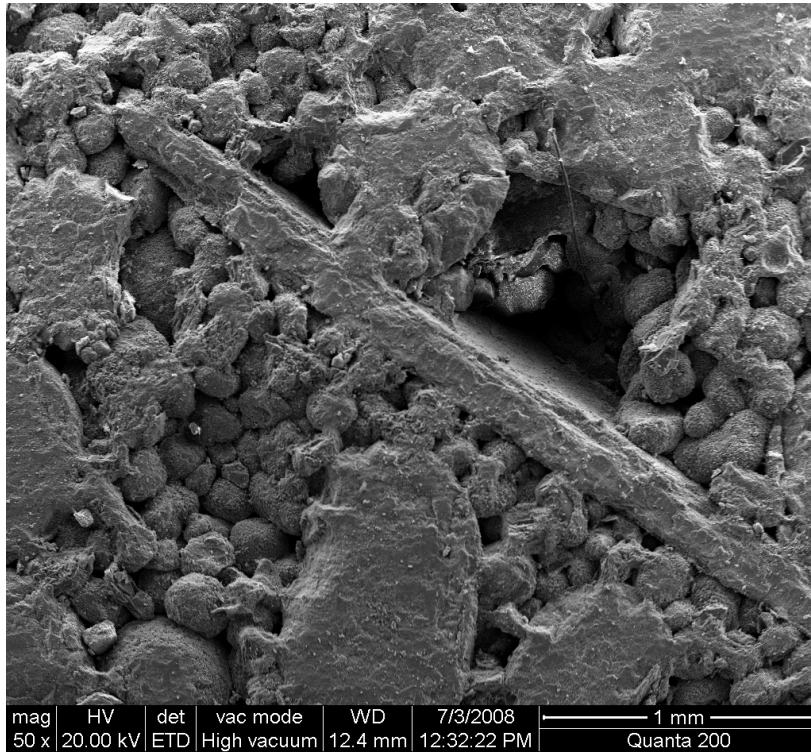


Fig. 26. Repedeia – micrographs (ESEM)

V. 3. Chemical composition

V. 3. 1. Laspra

Optical microscopy investigation of thin sections of the two types of studied stones was performed prior to the X-ray diffraction measurements, in order to establish the elemental analysis of the samples. Powder diffraction technique was applied in order to obtain the results.

The elemental analysis data were then compared to the results given by EVA's semi-quantitative analysis: EVA calculates the concentrations for every element from the concentrations of the compounds. The semi-quantitative analysis is performed based on the pattern's relative heights and on their I/I_{cor} values. The criteria used to compare the simulated and the measured scan is the weighted reliability R . R_0 represents the inevitable discrepancy due to the statistics of the X-ray diffraction (noise modelled by the Poisson's law). R/R_0 tends to 1 for an ideal fit. The calculated mass concentrations are displayed: for every pattern, for every element, calculated from the chemical formulas. Additionally, every element (except oxygen) is converted into its most common oxide, and the concentrations of the oxides are displayed. When the compounds are not the most common oxides, there is a difference between the concentration of oxygen computed from the pattern's formula and from the most common oxides. This difference, called Oxygen excess, is then displayed.

Scherrer formula gives a correspondence between the crystallite size and the full width at half maximum FWHM.

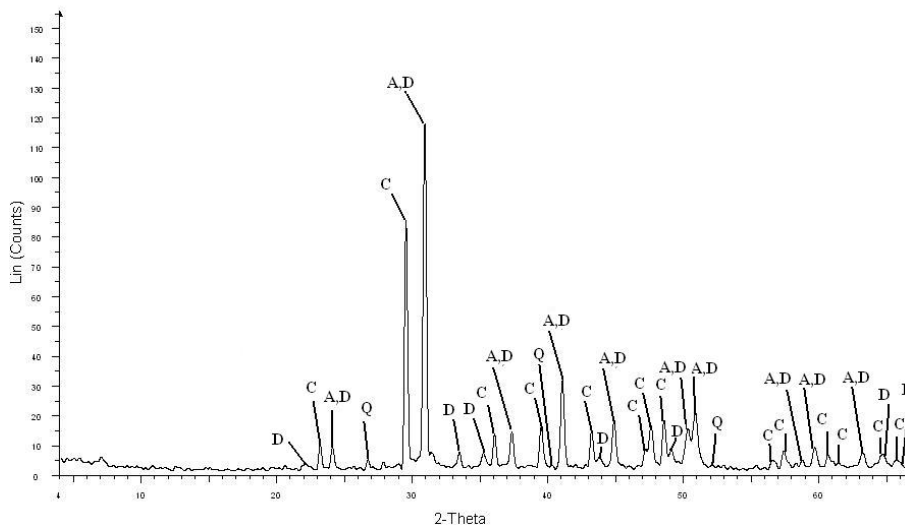


*Fig. 27.
XRD
patterns of
Laspra
sample:
C- calcite
A- ankerite
Q- quartz
D- dolomite*

The peaks of Laspra sample indicate the presence of ankerite, dolomite, calcite and quartz (Fig. 27). The intensity of ankerite is the highest, followed by calcite's intensity, quartz's intensity being very low. This is in agreement with the optical microscopy measurements of the thin sections of the sample.

Table 1 lists the XRD measurements results.

Table 1. XRD patterns for Laspra

Laspra	Ankerite Ca(Fe ₂ ,Mg)(CO ₃) ₂				Quartz SiO ₂		Calcite CaCO ₃			
Fitting parameter R/R ₀	1.02				1.4		1.16			
Concentrations (%)	C	10.5	CO ₂	38.6	O	53.3	C	12.0	CO ₂	44.0
	O	42.1	Excess	-7.0	Si	46.7	O	48.0	CaO	56.0
	Mg	5.3	MgO	8.8			Ca	40.0		
	Ca	17.6	CaO	24.6						
	Fe	24.5	Fe ₂ O ₃	35.0						
FWHM	0.183				0.437		0.152			
Crystallite size (X)	443.5				186.1		536.3			
I/I _{cor}	2.8				3		3.2			
System	Rhombo.H.axes				Hexagonal		Rhombo.H.axes			
Space group	R-3 (148)				P3221 (154)		R-3c (167)			
Cell param.	a = b = 4.82870 c = 16.15200				a = 4.91600 c = 5.40540		a = 4.98900 c = 17.06200			

Additionally, the peaks at $2\theta = 33.51, 35.25, 44$ and 49 suggest the presence of dolomite (CaMg(CO₃)₂).

Dolomite:

R/R₀: 0.991

Concentrations:

C 13.0% CO₂ 47.7%

O 52.1%

Mg 13.2% MgO 21.9%

Ca 21.7% CaO 30.4%

FWHM: 0.205

Crystallite size (Scherrer equation): 397.4 Å

I/Icor: 2.5

System: Rhombo.H.axes

Space group: R-3 (148)

Cell param.: a: 4.80690

c: 16.00200

The FT-IR spectra of the two stone samples were recorded in the 400 – 4000 cm^{-1} wavenumber region (64 scans). All FT-IR measurements were carried out at room temperature using the KBr pellet technique.

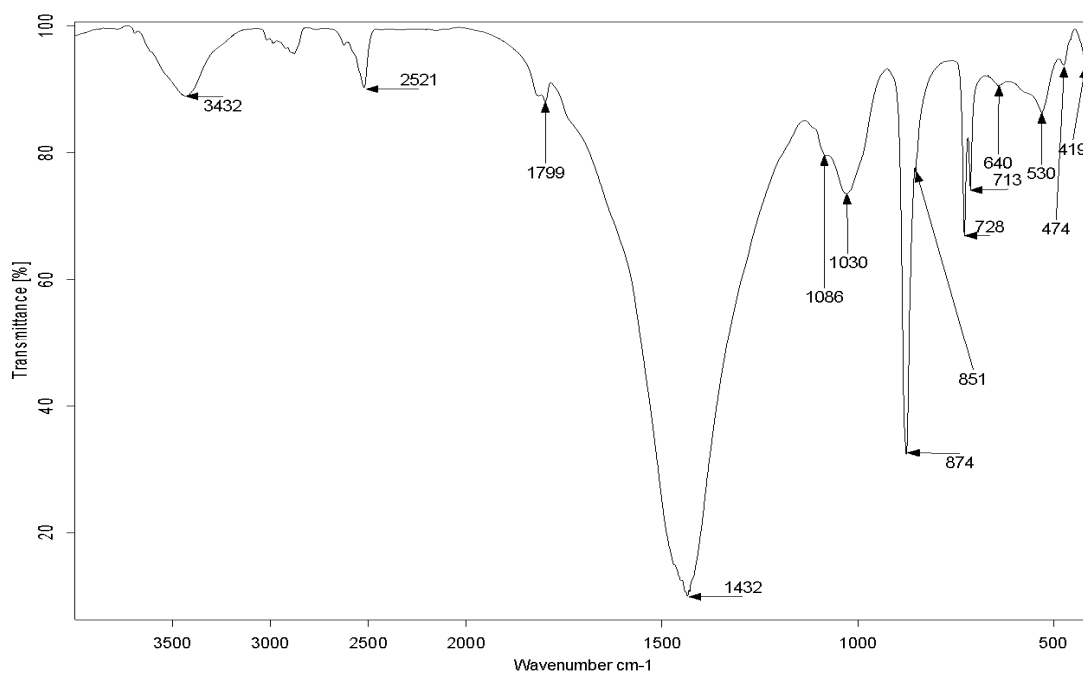


Fig. 28. FT-IR spectrum of Laspra

CaCO_3 : - 2520 cm^{-1}

Ca^{2+} - 713 cm^{-1}

CO_3^{2-} - 1799 cm^{-1}

-v asim stretching - 1432 cm^{-1}

- 1030 cm^{-1}

- 874 cm^{-1} out of plane

The mixture of aragonite and calcite which nucleated in the presence of the organic substrate can be observed in this spectrum. The characteristic peak of calcite is at 874 cm^{-1} ; those of aragonite are at 851 cm^{-1} and 1086 cm^{-1} .

The band at 1030 cm^{-1} corresponds to the CO_3^{2-} ions from the aragonite group. The appearance of the doubly degenerate band at 713 cm^{-1} and 728 cm^{-1} corresponds to Mg^{2+} (MgCO_3).

$$\begin{aligned} \text{O-Si-O: } \nu \text{ stretching} &= 530\text{ cm}^{-1} \\ &= 474\text{ cm}^{-1} \end{aligned}$$

The absorption band at 3432 cm^{-1} suggests the presence of water molecules (stretching vibration).

V. 3. 2. *Repedea*

Figure 29 shows that the peaks of Repedea sample indicate the presence of calcite, magnesian calcite, quartz and aragonite. This is in agreement with the optical microscopy data of the thin sections of the sample.

Table 2 lists the XRD measurement results.

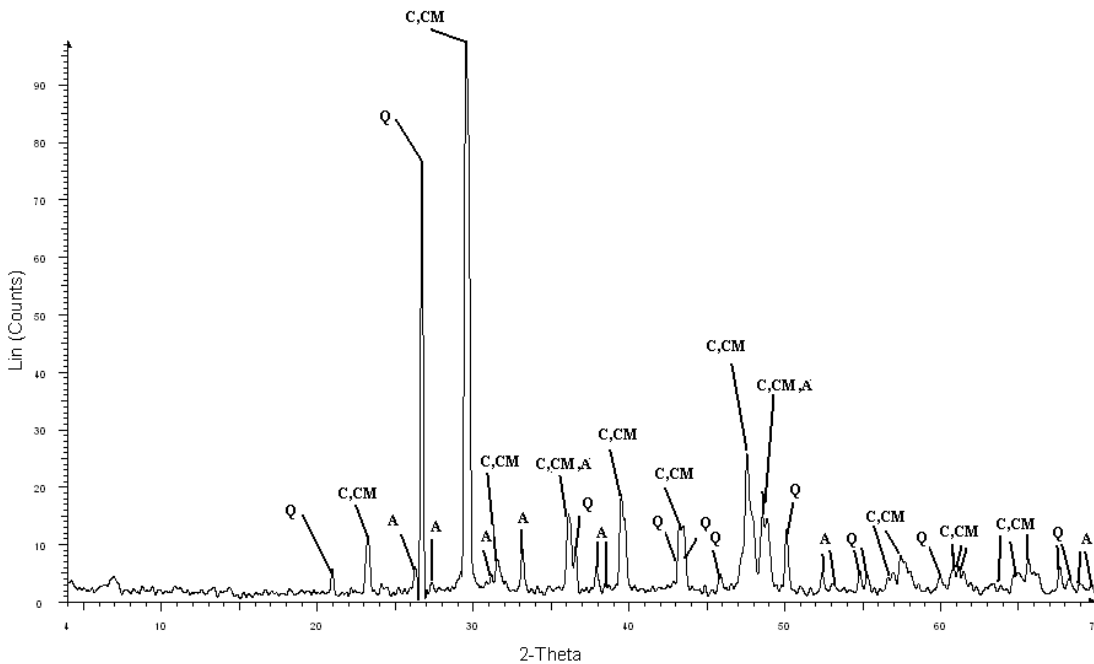


Fig. 29. XRD patterns of Repedea sample: C- calcite; A- aragonite; Q- quartz, CM- magnesian calcite

Table 2. XRD patterns for Repedea

Repedea	Calcite CaCO ₃		Quartz SiO ₂	Calcite, magnesian (Ca,Mg)CO ₃		Aragonite CaCO ₃	
Fitting parameter R/R ₀	0.812		1.25	0.901		1.32	
Concentrations (%)	C 12.0 O 48.0 Ca 40.0	CO ₂ 44.0 CaO 56.0	O 53.3 Si 46.7	C 13.0 O 52.1 Mg 13.2 Ca 21.7	CaO 30.4 MgO 21.9 CO ₂ 47.7	C 12.0 O 48.0 Ca 40.0	CO ₂ 44.0 CaO 56.0
FWHM	0.268		0.118	0.233		0.105	
Crystallite size (X)	303.6		686.9	349.7		776.9	
I/I _{cor}	2		3	1		1	
System	Rhombo.H.axes		Hexagonal	Rhombo.H.axes		Orthorhombic	
Space group	R-3c (167)		P3221 (154)	R-3c (167)		Pmcn (62)	
Cell param.	a = b = 4.98900 c = 17.06200		a = 4.91458 c = 5.40649	a = b = 4.94260 c = 16.85200		a = 4.96230 b = 7.96800 c = 5.74390	

The peak from $2\theta = 29$ is the highest, representing a superposition of calcite and magnesian calcite. Judging from the microscopic analyzes, calcite is the most abundant compound and magnesian calcite has a very low concentration, so the main contribution to the value of the intensity can be assigned to calcite.

The XRD results were complementary to those obtained from FT-IR spectroscopy.

Bending of the crystallization water - $\nu_{OH\ trans}$ - 3435 cm^{-1}

ν_{OH} - 1620 cm^{-1}

O-Si-O: ν asim stretching = 1083 cm^{-1}

= 803 cm^{-1}

ν rocking = 676 cm^{-1}

Si-O: ν stretching = 517 cm^{-1}

= 471 cm^{-1}

CaCO₃ - 2522 cm^{-1}

Ca²⁺ - 713 cm^{-1}

ν C=O ester - 1735 cm^{-1}

CO₃²⁻ - 1798 cm^{-1}

- ν asim stretching - 1426 cm^{-1}

- 875 cm^{-1} out of plane

SO_2 : v stretching - 415 cm^{-1}

- 571 cm^{-1}

CH-: v stretching bending (2923 + 2860 cm^{-1})

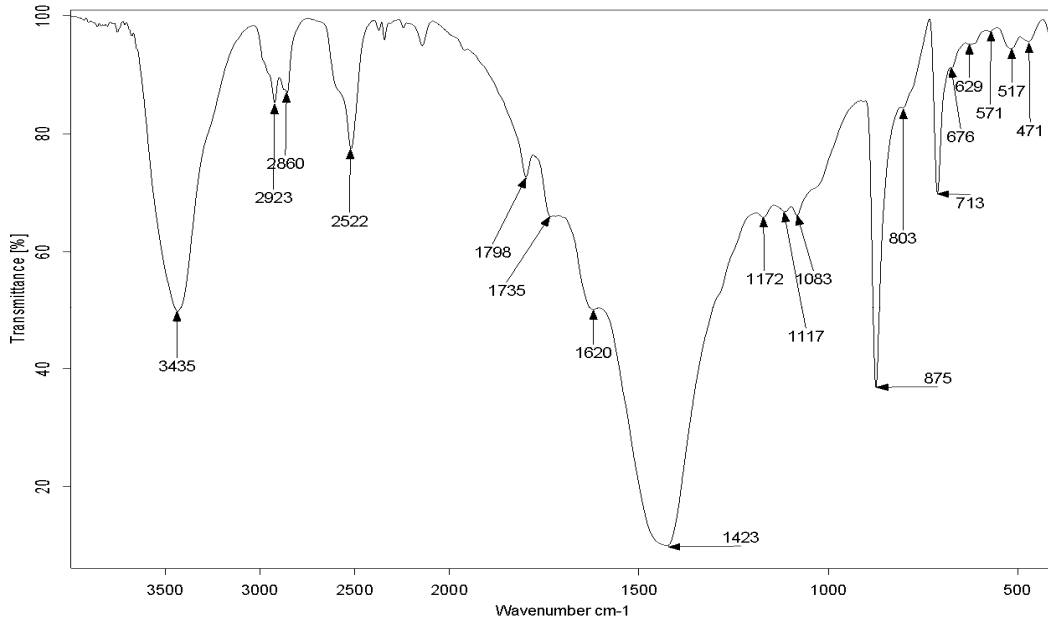


Fig. 30. FT-IR spectrum of Repedea

V. 4. Velocity of propagation of the ultrasonic waves

The use of the non-destructive techniques is well spread in the field of characterization of ornamental stones.

For this purpose, the ultrasonic test was performed in laboratory conditions – the variations of the velocities of propagation of ultrasonic waves in specimens of each selected stone. For this test, elastic waves – in particular the ultrasonic waves (20,000 Hz frequency) – were used to observe the changes in stone's characteristics and properties.

V. 4. 1. Laspra

To establish the level of anisotropy of the studied stones, the ultrasonic test was performed on six different specimens of Laspra, in all three directions. Figure 31 presents some of the results.

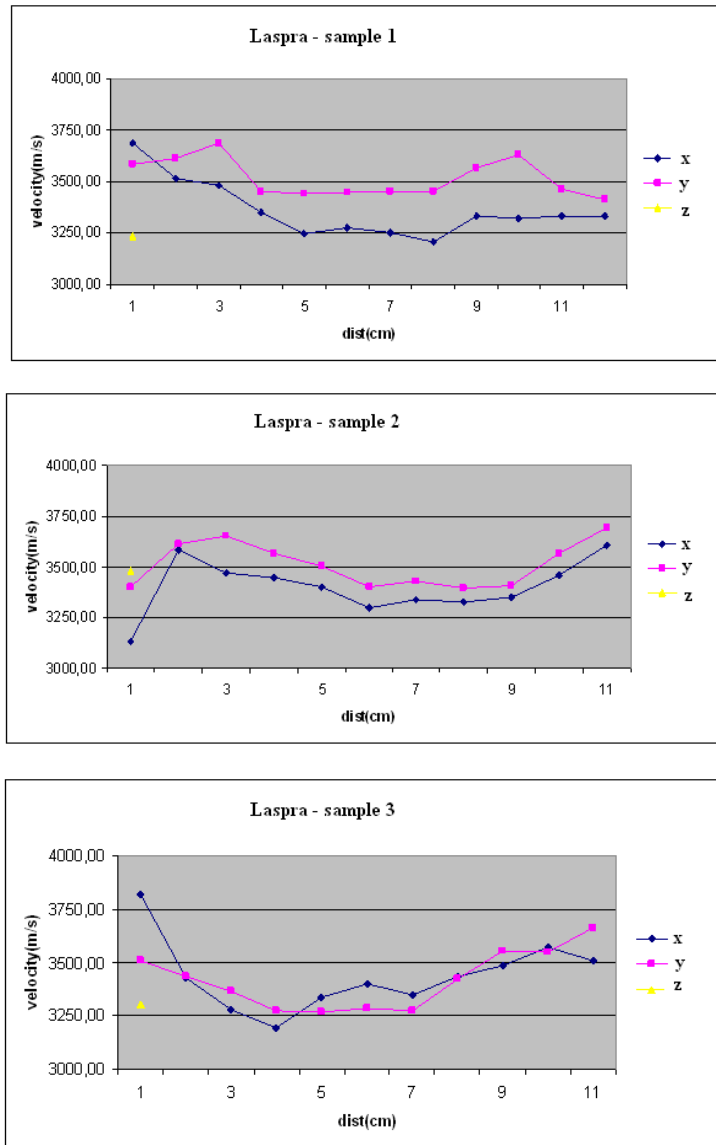


Fig. 31. Ultrasonic profiles of Laspra

In Laspra's case, the coefficient of anisotropy has values between 1.0 and 1.12.

Considering these values and interpreting the ultrasonic spectra, it appears that the studied stone is an isotropic and more or less heterogeneous one.

V. 4. 2. Repedea

To establish the level of anisotropy of the stone, the velocity of propagation of ultrasonic wave test was performed on six different specimens of Repedea, in all three directions. Figure 32 presents some of the experimental results.

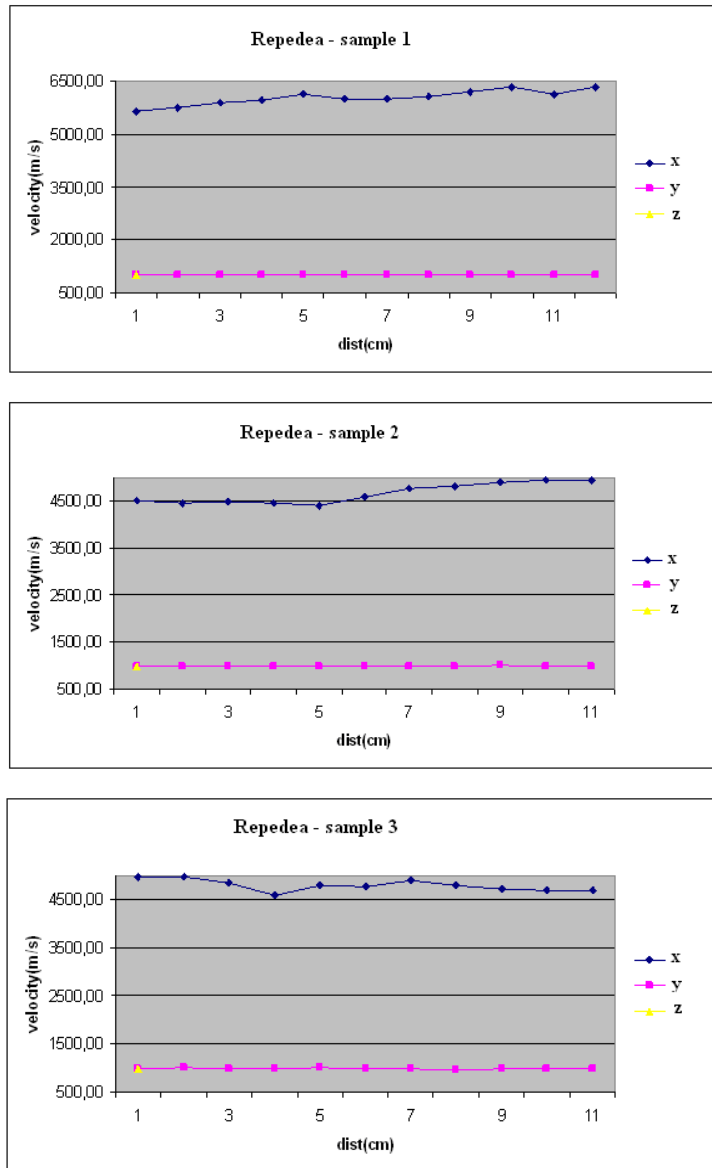


Fig. 32. Ultrasonic profiles of Repedea

From the point of view of the anisotropy coefficient, Repedea can be described as being very different from Laspra, as its coefficient of anisotropy exhibits important variations in value in two of the directions – x and y, z, as follows:

- x direction: the calculated values are between 4.52 and 6.08;
- y and z directions: the calculated values are between 0.99 and 1.03.

Judging from these values and interpreting the profiles obtained from the ultrasonic test, one can appreciate that Repedea is an anisotropic, but homogeneous material.

V. 5. Pore space structure

The porosity is considered to be one of the most important factors of the material properties for many rocks, and hardly exists a physical property of rocks that is not directly or indirectly influenced by porosity. Porosity can be defined as the ratio of pores (micro-voids) in the stone to its total solid volume. Pores and the capillary structure develop differently in each of the three stone groups.

From the alteration point of view, the porosity is one of the most significant physical properties of the rock – the amount of the voids and their connecting network conditioning the circulation of the fluids through the pores, this directly contributing to the alteration of the rock.

The voids within a rock structure can be classified into pores and fissures. Their different significance in cemented or in fissured rocks has been largely described in the literature. The values of porosity in rocks are extremely variable, therefore a generalization of the term is a very difficult task, the same rock being able to present high porosity values when weathered or, on the contrary, very low values when fresh. In sedimentary rocks, the pores develop as a result of compaction and cementing process. A large variety of pore sizes and shapes are characteristic of sedimentary stones.

The literature describes the following porosity values for the main rock types [59-61] (Table 3).

Table 3. Rock porosity values

Rock type	Porosity (%)
Cemented rocks	
Sandstone	5 – 30
Siltstone	21 – 41
Limestone, dolomite	5 – 40
Shale	0 – 10
Crystalline rocks	
Low fractured, dense rocks	0 – 5
Normally fractured rocks	0 – 10
Basalt	3 – 35

A common petrographic classification of pores in rocks, according to their sizes, (diameter in mm) is presented below [62].

Table 4. Classification of pores in rocks according to their diameter

Denomination	Diameter (mm)
Megapore	
large	256 – 32
small	32 – 4
Mesopore	
large	4 – 0.5
small	0.5 – 0.0625
Micropore	< 0.0625

To better describe the notion of porosity, a few terms related to the connection of the pores to each other must be added:

- isolated pores are pores presenting no connection to each other; they can also be called closed pores
- ink bottle pores are pores linked to the pore network by thin and narrow capillaries; usually, liquids like water can only penetrate such pores under pressure or vacuum
- dead end pores are connected to the pore network by only one side, the other one staying close to the network.

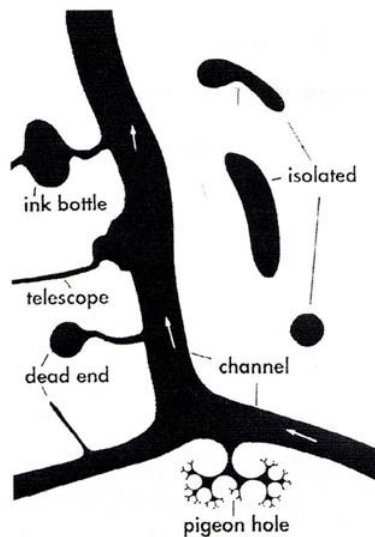


Fig. 33. Representation of pore types (according to Fitzner)

V. 5. 1. Hg intrusion porosimetry (MIP)

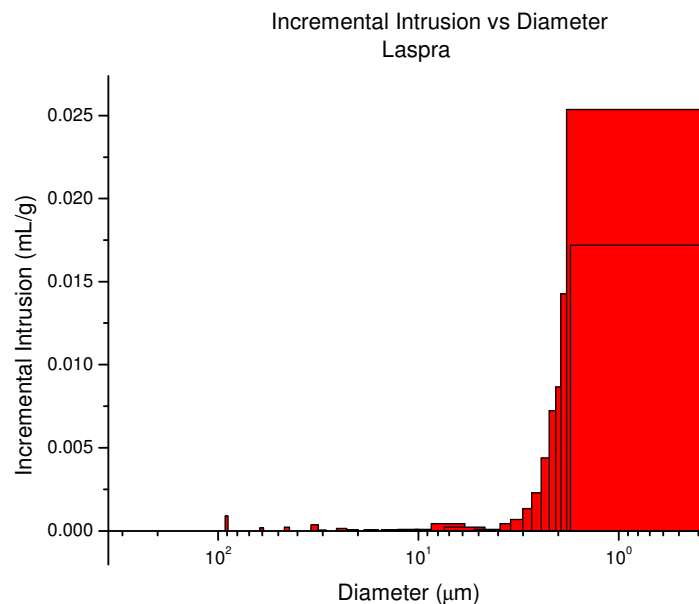
One of the most frequently used methods in the investigation of the porosity characterization of building stones, as well as for the assessment of their deterioration degree is mercury intrusion porosimetry (MIP).

The behavior of the porous media strongly depends on material's total porosity as well as on the pores thought size, shape and connection between the pores. The distribution given by MIP measurement reveals the pore throats as it is linked to the pressure necessary to the liquid to penetrate the pores. According to the literature [63], the throats control the transport properties, whereas the nodal pores command the storage capacity.

Mercury porosimetry can overestimate smaller pores and underestimate larger pores in the case of ink bottle pores. If a small radius pore is connected to a larger radius pore, the mercury can enter the large pore only when the pressure to enter the smaller pore is reached according to Laplace law. Both pores are invaded simultaneously and the volume considered is only the one of the smaller pore class. Therefore, large pore class can be underestimated and vice-versa, smaller pores class can be overestimated [64].

For each studied limestone, several experiments were performed, according to the previously described methodology.

Laspra presents a type of porosity which is difficult to detect, mainly due to the absence of the macropores and to the very small size of the micropores. The experiment revealed that Laspra contains exclusively connected micropores, presenting a very narrow access to the pores.



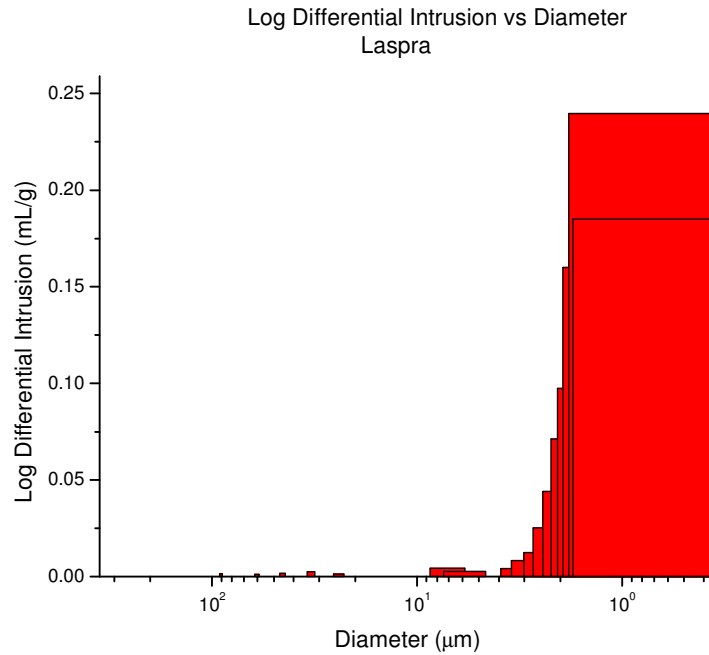


Fig. 34. Pore throat size distribution in Laspra sample

These figures reveal that Laspra presents an even pore size distribution, almost all pores having very small throat pore diameters. The data obtained from the mercury intrusion porosimetry are summarized in the table below.

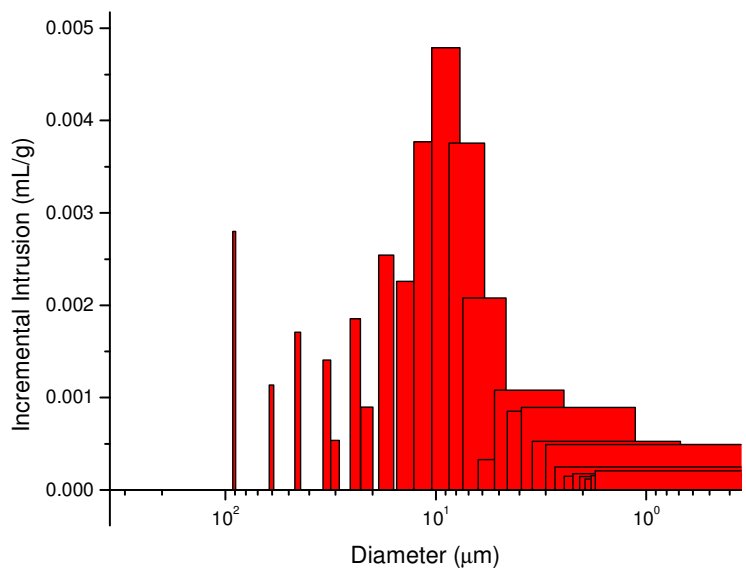
Table 5. Mercury intrusion porosimetry data for Laspra

Laspra	Open porosity (%)	Average pore throat diameter (μm)
	30	0.15

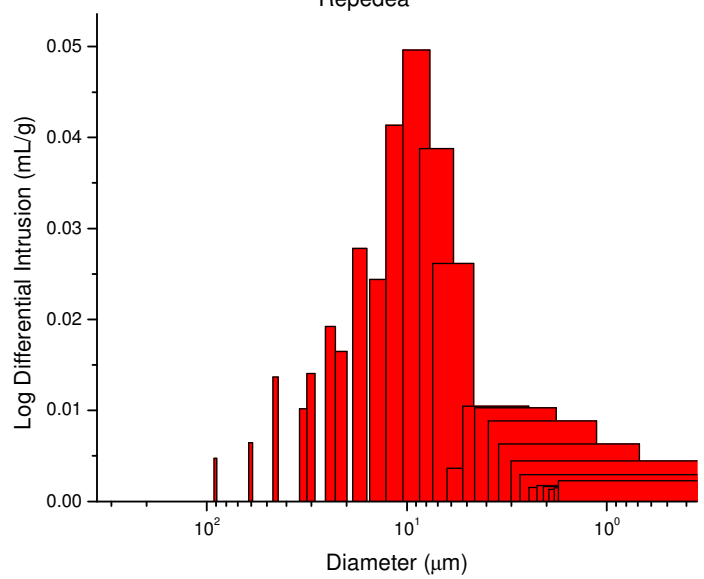
The mercury intrusion porosimetry test revealed for Repedea lower open porosity values and higher pore throat diameter sizes.

The data obtained using this technique are summarized in the figures below.

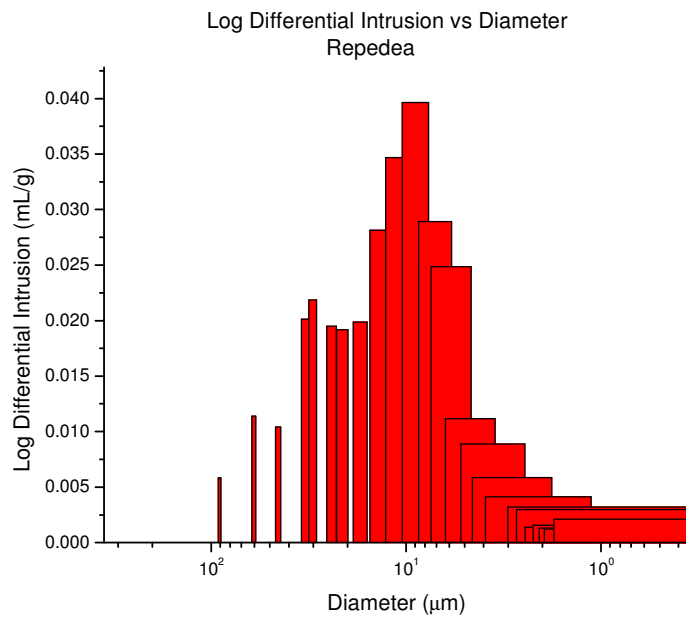
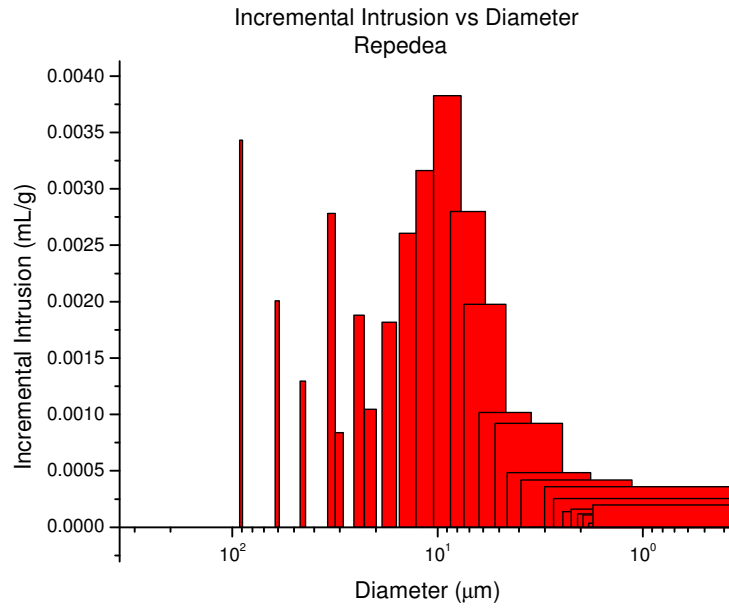
Incremental Intrusion vs Diameter
Repedea



Log Differential Intrusion vs Diameter
Repedea



(a)



(b)

Fig. 35. Pore throat size distribution in two Repedea samples

Table 6. Mercury intrusion porosimetry data for Repedea

Repedea	Open porosity (%)	Average pore throat diameter (μm)
	10	3.3

V. 5. 2. BET method

The pore size distribution, as well as specific surface area, can be estimated from nitrogen adsorption isotherms at liquid nitrogen temperature.

The Laspra sample presents a very small hysteresis at high pressure (in the range 0.5-0.995) that is assigned to small macropores combined to mesopores with a maximum at 39 Å.

The specific surface areas (S_{BET}) of the samples were calculated using the Brunauer – Emmett – Teller (BET) method in the 0.05 – 0.2 p/p° (Repedea) and 0.05 – 0.35 p/p° (Laspra) standard pressure range. The total pore volume V_p was evaluated on the basis of the amount adsorbed at the relative pressure of about 0.995 by converting the amount of nitrogen gas adsorbed at STP to the liquid volume at -196°C using the conversion factor, $c = 0.001547$.

The pore size distributions were obtained from the desorption branch of the isotherm using the corrected form of the Kelvin equation by means of the Barrett – Joyner – Halenda (BJH) method with a cylindrical pore model. Due to the fact that theoretically this method does not always fit to the pores of materials, the DFT (Density Functional Theory) method with slit pore and the NLDFT (Non-Local Density Functional Theory) equilibrium model were also applied. For Repedea sample, a very large distribution of pore size in the mesopores area is noticed when BJH is applied, with a maximum at 42 Å. The DFT method led to a narrow distribution of the pore size with a maximum at about 42 Å.

External surface (S_{ext}) and micropore volume (V_p) were assessed from t -plot method, considering the de Boer equation to estimate the thickness of a monolayer of nitrogen adsorbed at -196°C , t ($t = 0.354 \times n/n_m$).

The Repedea sample exhibits a large hysteresis at high relative pressure, which could be assigned to macropores. The hysteresis starts at the higher relative pressure (0.995), presents one inflexion point at $p/p_o = 0.5$ and closes at $p/p_o = 0.1$. It is supposed that this hysteresis is a combination of two hysteresis loops. Actually, it starts at high pressure as B shape and ends at very low pressure at D shape. The B shape is associated with slit-shaped pores while type D profile results from wedge-shaped pores with narrow

necks of one or both open ends. On the other side, the presence of hysteresis between $p/p_0 = 0.1 - 0.5$ could suggest the existence of some mesoporosity in this sample.

Table 7. BET summary data for Laspra and Repedea

Sample	S_{BET} ($m^2 \times g^{-1}$)	S_{ext} ($m^2 \times g^{-1}$)	S ($m^2 \times g^{-1}$)	V_p ($cm^3 \times g^{-1}$)	V_p ($cm^3 \times g^{-1}$)	Average pore size (\AA)
Laspra	4.2	4	5.05×10^{-1}	3.9×10^{-2}	2.9×10^{-4}	39
Repedea	0.6	1.3	-	4.6×10^{-3}	-	42

$1 \text{ \AA} = 10^{-4} \mu m$.

V. 6. Hydraulic properties

These properties involve a group of characteristics and experiments related to the behavior of the two selected limestones towards water, both in liquid and vapour state, taking into account the increasing or, on the contrary, the decreasing in the amount of water.

A close correlation has been reported in the literature between hydric properties of dolomite, limestone and sandstones and their textural features [65]. According to the authors, absorption, evaporation and capillarity processes are influenced by open porosity, but even more by the pore throat size. Also, larger pores may lead to accelerated hydric processes, and trapped porosity may slow down water circulation. The configuration of the pore system seems to condition the hydric properties.

This experimental work has as one of the objectives the investigation of the stone samples behavior regarding the evolution in time of water content within the stones in given experimental conditions. The hydric properties present a significant interest from several points of view, such as:

- the characterization of the porous system. The amount, size, shape and interconnection of pores are strongly related to the quantity of water taken or lost by the stone, as well as to the kinetic mechanisms. Therefore, new parameters related to water movement within the stone can be discovered, these ones being able to give valuable information on a general image of the stone porous system.

- the behavior of water inside the stone. Considering the facts that water represents a significant cause of stone decay and that water can be found in almost any environment, the study of the stones behavior towards water, in any of its forms, is

fundamental for the understanding and interpretation of many currently occurring phenomena. For example, hygroscopic water can facilitate the diffusion of salts inside a stone, and due to the capillary raising water some very elevated saturation degrees can be reached.

In summary, water transport is influenced by pore structure. The pore structure should integrate grain size, grain shape, and spatial organization of the grain as well as pore network connectivity (open porosity) and pore size distribution. The pore structure is very complex and contains many variables. The hypothesis that textural properties (grain size, grain contact, pore shape) control the pore structure and, therefore, the physical properties requires serious consideration.

A few standardised tests have been selected in order to investigate and evaluate the hydraulic properties of rocks.

Water characteristics

Water can be seen as a peculiar substance in the natural environment – at normal temperatures in the Earth, water is the only compound that can be found in all three states – liquid, solid and gas. When in solid state, water's density is lower than in liquid state. Its high specific heat index regulate the rate at which air changes temperature under the living conditions and this is why temperatures, especially in marine environments, are generally subjected to gradual changes. Water has a very high surface tension value. Surface tension is responsible for the capillary actions, allowing water to move through the tiny spaces of rocks porous system.

V. 6. 1. Water absorption / desorption

For carbonate stones, properties like absorption, desorption and capillarity are strongly influenced by the genesis of the rocks. The three above mentioned properties are related to the type of porosity of the stone, which can be primary or secondary.

When rocks are being immersed in water, they absorb a quantity of liquid that depends on the rocks petrographic characteristics and their pore space volume and structure [66]. The pore space structure (connectivity, tortuosity, sizes, throat, a.s.o.) controls the water kinetics within the rocks.

Water absorption is a very significant and practical parameter to be considered in building materials, its behavior, even in short-term, being studied for concrete, bricks, mortar, wood, ceramics, ornamental stones etc.

The opposite of water absorption process is water desorption. Generally speaking, the evolution of the drying process follows the next steps. First, water is transported to the rock surface, the evaporation phenomenon starting, then the drying rate remains constant for a while, and once the rock is no more able to maintain the initial water supply rate to its surface, the drying process follows the water linked to capillary forces, a new drying rate being registered, and the drying process becomes progressively slower.

To explain the difference in the behavior of the two types of carbonate stones, Laspra and Repedea, as far as water absorption, desorption and capillarity are concerned, one has to describe their main characteristics.

In the case of Laspra, the rock is consisting mainly in secondary ferroan dolomite and secondary ankerite and calcite. The presence of some preserved bioclasts is one of the arguments in favor of the secondary genesis of Laspra. The primary dolomite (or the dolomite coming from the chemical precipitation) is formed only from hypersalin media, having a $\text{pH} > 9$ and a lack of bioclasts. Secondary dolomites are formed through the substitution of the calcite with the dolomite, phenomenon known as dolomitization. This replacement process of calcite with dolomite gives birth to a secondary porosity which can reach sometimes 25% of the volume of the stone. This secondary porosity can be characterized by the presence of some random shape cavities which are communicating through very thin channels. These channels were mainly the circulation paths of the diagenetic solutions (rich in Mg and Fe). The distribution of these voids and tiny channels is random.

Repedea is a limestone consisting in ooids, bioclasts, as well as peloids and litoclasts in very small amounts. These are cemented by sparry calcite. In the case of Repedea, the porosity is a primary, intercrystalline one. Repedea has in its structure voids (small spaces) among the grains, these voids having dimensions of about 1 mm or less. The voids distribution within the structure of the stone is uniform. The pores are connected through tiny channels, although certain non-uniformity can be found as

concerns the connections among the pores; in some cases areas without any connections/links between the pores do exist. Nevertheless, the porosity can be considered as an isotropic one, the same degree of non-uniformity existing in the whole mass of the stone. The real (actual) porosity (determined by the volume of the pores which are connected both between themselves and with the exterior of the stone) is lower than the absolute porosity (the total volume of the pores).

Laspra and Repedea have, therefore, different characteristics in terms of porosity and therefore present a different behavior towards hydric properties. The most important difference is given by the relative porosity, which is smaller for Repedea and considerably higher for Laspra.

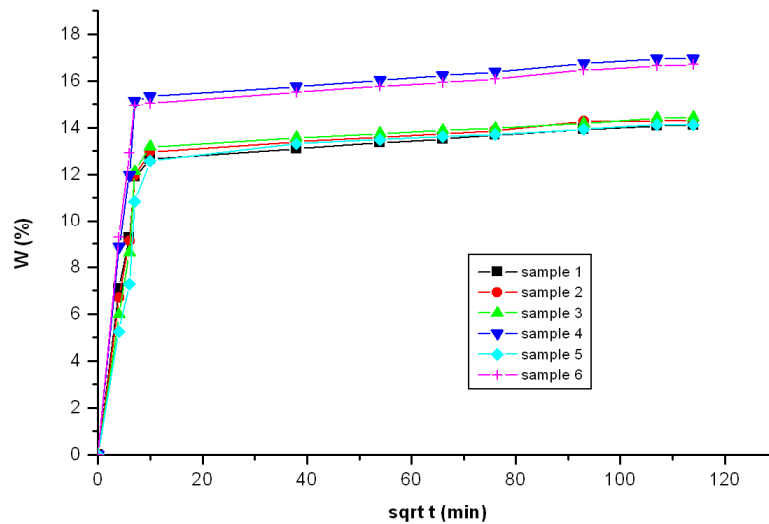


Fig. 36. Water content (%) for Laspra samples

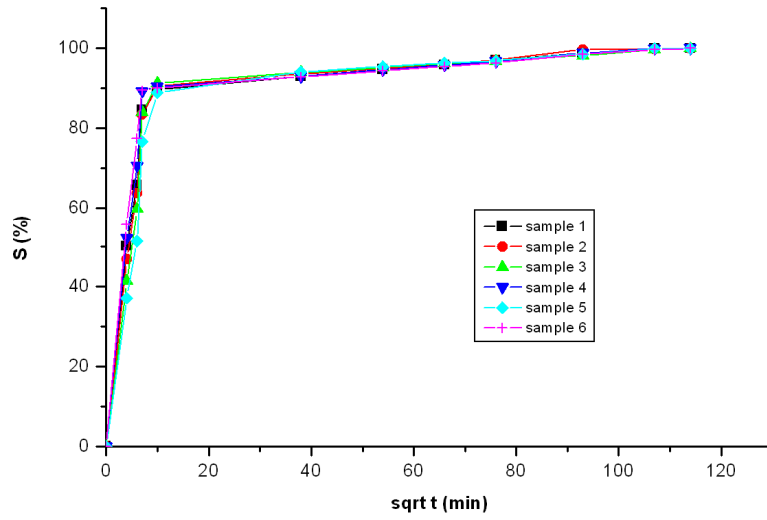


Fig. 37. Saturation degree (%) for Laspra samples

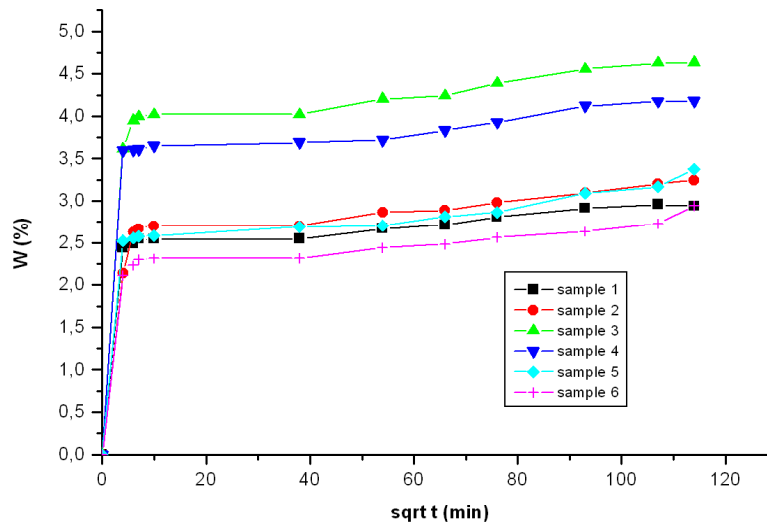


Fig. 38. Water content (%) for Repedea samples

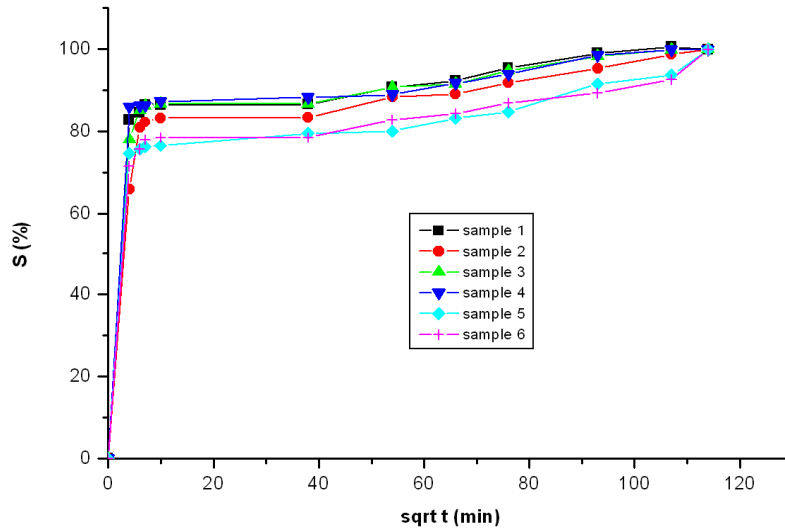


Fig. 39. Saturation degree (%) for Repedea samples

For both stones, water absorption should be similar at the beginning of the process, when water starts to enter into the stones and to fill their pores. The difference appears when the stone with lower relative porosity is completely filled with water. From that moment on, the water absorption takes place only in the case of Laspra, due to its high open porosity. For Laspra, the water absorption continues until the complete filling of the voids is attended.

Another notable difference between the two stones involves the water absorption rate. The rate of the absorption of water is higher for Laspra, where the slope during the first 4 minutes is higher. This is due to the system of communication between the pores and the surface of the stones. In the case of Laspra, these connections are achieved through channels. The channels allow the water to circulate at a higher scale than in the case of the connectivity between the pores of Repedea.

As for water desorption, from the same reasons, the same differences can be noticed.

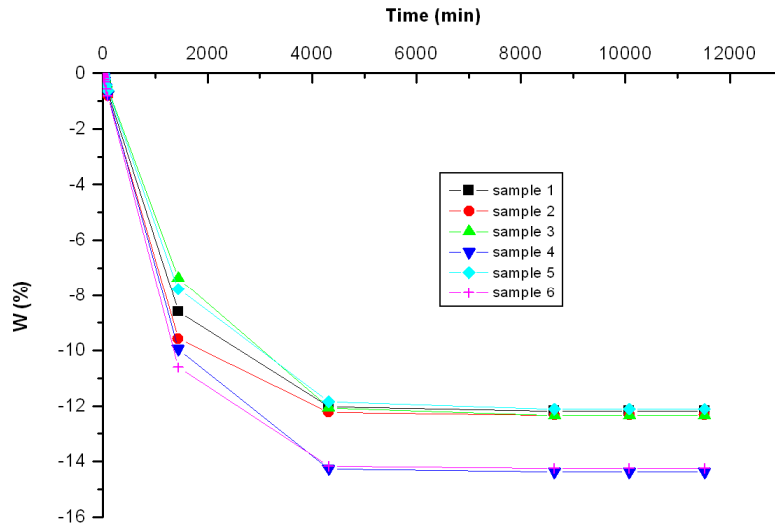


Fig. 40. Water content (%) for Laspra samples

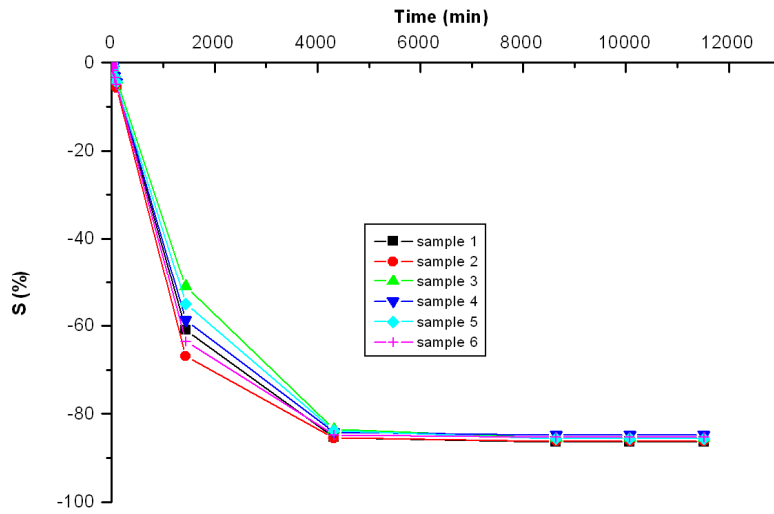


Fig. 41. Saturation degree (%) for Laspra samples

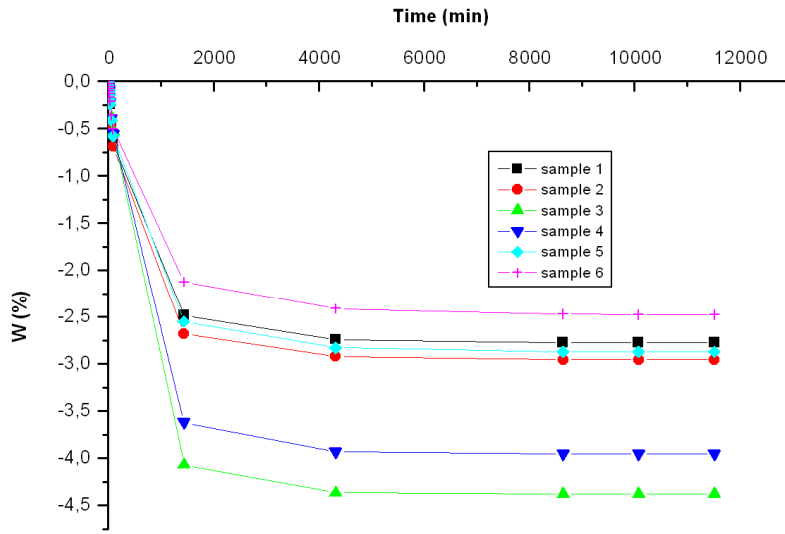


Fig. 42. Water content (%) for Repedea samples

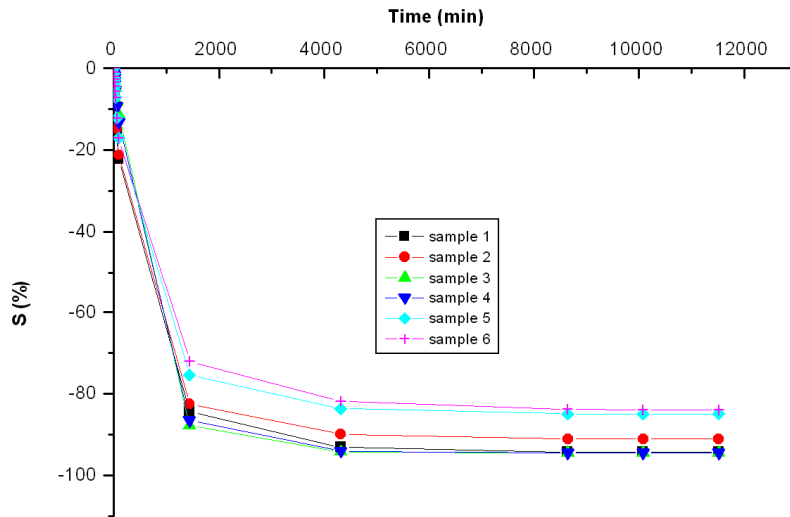


Fig. 43. Saturation degree (%) for Repedea samples

V. 6. 2. Water absorption by capillary suction

The capillarity represents a significant hydraulic property exhibited by some rocks, and provides information on the easiness to the vertical movement of water into rocks. These phenomena appear due to the hydrophilic character of the rocks, as well as to the configuration of their porous system [67]. The capillary suction is defined as the capacity that porous materials exhibit for suctioning some water above the level that presents the surface of liquids contained in them. The capillary pressure is the pressure difference across an interface separating two immiscible fluids, in the interior of a capillary, and depends on pore space and capillary structure [68].

The water absorption by capillarity consists in the quantification of the amount and velocity of water absorbed by the stone samples by capillarity suction. The capillary suction is quite rapid during the first minutes, and then increases slowly.

The capillarity is determined by the shape, the size, the distribution of the connecting channels, as well as by the size of the pores.

As far as Laspra is concerned, the channels having the same dimensions as the capillars are fewer, and as a result the amount of absorbed water through capillarity is increasing slowly. In addition, the non-uniform spatial distribution of the channels in Laspra will provide non-uniformity in the detection of the capillarity on different surfaces of the same sample (this phenomenon being practically undetectable in the case of Repedea).

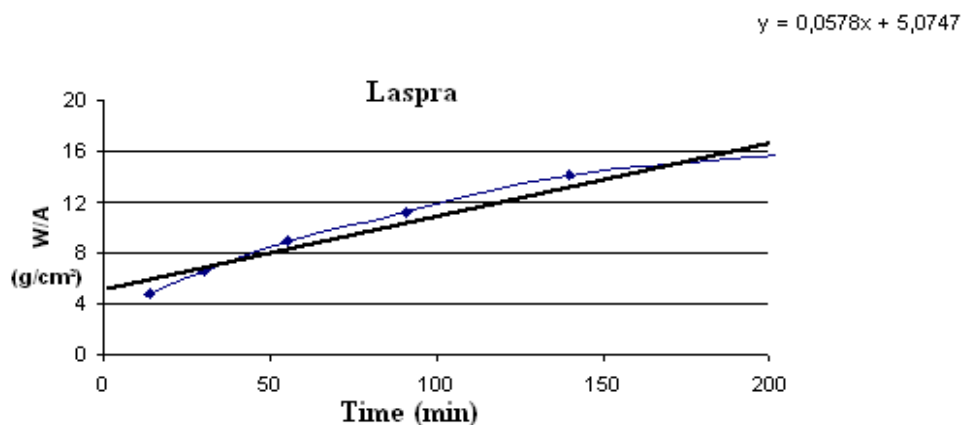


Fig. 44. Capillary suction in Laspra

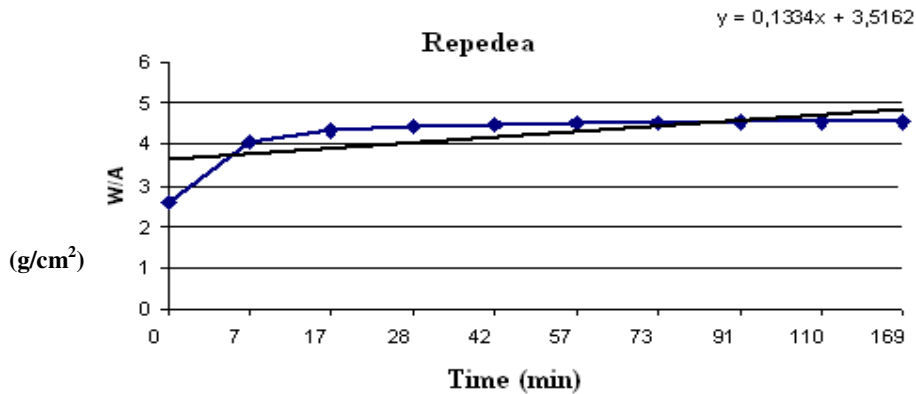


Fig. 45. Capillary suction in Repedeia

On the contrary, for Repedeia, water intrusion through capillarity is very rapid, due to the fact that the pores connecting channels and the pores themselves have generally the same size as the capillaries.

Quite rapidly, these pores and channels are filled with water, and the amount of further absorbed water (through capillarity) is extremely reduced (the slope being practically constant).

V. 6. 3. Water vapor permeability

Among other notions, permeability is associated with stones porosity. This is the extent to which the pores and capillary structures are interconnected throughout the stone. These networks, their size, structure and orientation affect the degree and depth to which moisture, vapors and liquids can be absorbed into the interior of the stone or migrate from the substrate by capillary action through the stone. Permeability may be higher in some directions than in others based upon pore size, shape and the distribution of the interconnectedness of the system. Stones permeability values can increase when the stone is highly fractured, soft or grainy. A particular variety of stone may be highly permeable (presenting a well defined interconnected network of pores), although its porosity is low (low percentage of voids).

LASPRA

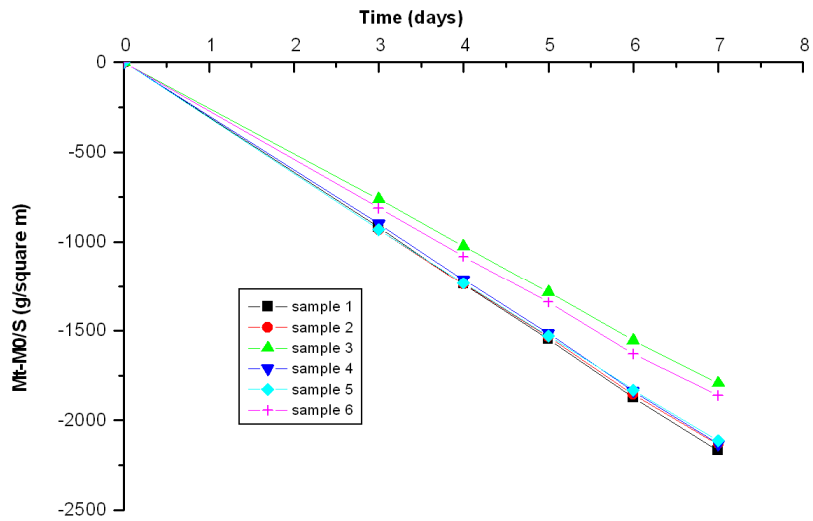


Fig. 46. Water vapor permeability for Laspra samples

REPEDEA

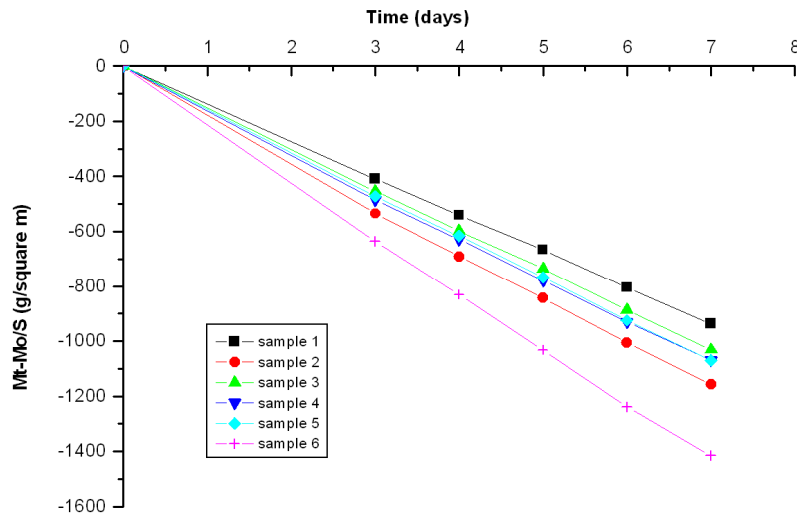


Fig. 47. Water vapor permeability for Repedea samples

Water vapor permeability may be linked to grain size and, according to some authors, is directly correlated to grain size where the higher the grain size the higher the permeability [69, 70]. The same authors pointed out the influence of the shape of the

grains in the packing and its effect on permeability and porosity. Spherical grains tend to have a higher porosity and permeability than disc-shaped grains. Once again, the contact between these grains is likely one way to evaluate the grain packing.

Generally, permeability is linked to open pathways in the rock sample – open pore throats as connections between pores, open cracks, and networks of open pores and cracks [71].

The water vapor permeability coefficients values for the two types of limestones are listed in the table below.

Table 8. Water vapor permeability coefficient values for Laspra and Repedea

	$-K_v (25^\circ)$ (g/m ² x 24 h)
Laspra	292.14
Repedea	180.45

As it can be seen in the table, Laspra registers higher water permeability coefficient values as compared to Repedea. This is mainly due to a higher open porosity of Laspra (30%) as opposite to Repedea, which exhibits an open porosity value of about 10%, as well as to the higher porous network connectivity in case of Laspra.

V. 7. Color measurements

The color of building stones, and particularly of geologic marble and limestones, is one of the most significant characteristics that define their aesthetic properties and value. Stone has been widely used from ancient times to the present not only in monuments but also in the decoration of buildings. Its main uses are in sculpture, pavement and cladding, and its ornamental value depends on its mechanical properties, durability, color, and conservation of color. Many forms of deterioration, from the aesthetic point of view, are caused by environmental conditions and urban pollution, and thus stone color stability is an essential parameter that must be mentioned, understood and monitored.

Color changes in building materials are usually attributed to the degree of oxidation of the chromophores in the chromogen minerals and to their concentration [72]. For example, one of the most powerful chromophores in these types of materials is

iron. Thus, mineral phases with oxidized ferric material produce a red-brown color in the stone, whereas reduced phases produce a blue-black color. When the building stones are exposed to atmosphere, oxidation reactions occur. For this reason, reduced phases change color quickly, whereas oxidized phases remain generally stable during exposure to weathering. The color parameters of the two studied limestones are listed below.

Table 9. Color parameters for (a) Laspra and (b) Repedea

Laspra	L*	a*	b*	C*	h
	86.28	-0.14	8.97	8.99	90.94

(a)

Repedea	L*	a*	b*	C*	h
	60.58	0.08	10.68	10.74	89.64

(b)

As mentioned in the previous chapters, Laspra can be described as having a bright white color ($L^* = 86.28$) and showing, from place to place, the presence of iron oxides traces, which appear as small reddish stains. Repedea exhibits a brownish color except when the presence of the organic fragments (pieces of sea shells, molluscs) can be observed, these fragments showing a white color.



(a)



(b)

Fig. 48. Macrographs of (a) Laspra and (b) Repedea

VI. Water repellent treatments

VI.1. Introduction

The increasing interest in the conservation/consolidation of historic structures and the accelerated deterioration of the environmentally exposed stone sculptures and buildings require the understanding of the mechanisms responsible for stone decay to develop the possibilities of optimum stone protection.

As is the case of some other materials, stone experiences change upon exposure to natural weathering. As long as the stone is in contact with any kind of environment, it undergoes chemical, mechanical, physical and/or biological weathering processes. Weathering is the natural disintegration and erosion of stone caused by the action of water, wind, and atmospheric gases. When used in building construction or for outdoor sculpture, stone is subject to other decay processes in addition to natural weathering due to its interaction with polluted urban-industrial environments, to improper selection or positioning of stone material, a.s.o.

Water is the most aggressive agent which acts as a vehicle for weathering processes. Water dissolves and transports soluble salts within the stone causing efflorescence on the surface and salt-induced spalling. The combination of water with gaseous pollutants results in acidic precipitation. Water is also responsible for frost damage in climates where freezing temperatures may occur. It is also water which favors the growth of microorganisms. Disintegration, surface erosion, cracking and crust formation are the most commonly observed symptoms of stone decay.

Last years, among a large variety of chemical products, alkoxy silanes have received an increased attention due to their successful performance as stone consolidants/water repellents. The use of alkoxy silanes for stone consolidation is not a recent development, the usage of tetraethoxy silane (TEOS) or ethyl silicate for stone

conservation being first suggested in 1861 by A. W. Hoffman. TEOS was produced as an industrial chemical around 1924 and A. P. Laurie received a patent for its use as a stone preservative in 1925. During the 1960's, massive laboratory research and field tests using ethyl silicate were carried out and yielded good results in Germany. Ethyl silicate and its combination with organosilicon hydrophobic agents have been commercially available in Western Europe since 1972 and thereafter in the United States and Canada. These developments have brought a large interest to the use of tetraethoxysilane and related compounds such as alkylalkoxysilanes in stone conservation [73].

Alkoxysilanes are a family of low molecular weight molecules able to hydrolyze with water to produce either silica or chains of alkylpolysiloxanes. The types of alkoxysilanes usually used in stone conservation are tetraethoxysilane (ethyl silicate or silicic acid ester), triethoxymethylsilane and trimethoxymethylsilane. When alkoxysilanes are deposited within the stone, the polymerization proceeds in two steps, through hydrolysis and condensation. At the end of the process siloxane ($-Si-O-Si-$) linkages are formed providing the strengthening effect. Nevertheless, there are several factors that control the rate of polycondensation and the structure of the forming products, such as the amount of water used in the reaction, the type of catalysts, and the type of solvents. Alkoxysilanes with methyl ($-CH_3$) groups provide water repellency as well as consolidation.

Even though alkoxysilanes have been usually applied to the consolidation / hydrophobization of sandstones, there have been attempts of using them on marble and limestone as well. Since 1969, ethyl silicate found its place in the consolidation of exposed surfaces and predominantly satisfactory results have been observed to date. Besides forming a binder similar to that in siliceous sandstone, alkoxysilanes have the ability to deeply penetrate within porous stone due to their low molecular weight. Their relatively high cost, their tendency to darken the color of the stone and their possible evaporation from the surface before hydrolysis are some of the problems encountered in their use [74].

One of the most significant properties of alkoxysilanes is their ability to penetrate deeply into porous stone. This advantageous property differentiates alkoxysilanes from their many predecessors. Their low viscosity and small constituent monomeric molecules give the alkoxysilanes a substantial penetrating power. They can penetrate certain porous

stones to a depth of 20 to 25 – 30 mm, thus eliminating the problems of shallow treatments. When alkoxy silane monomers are polymerized, the structure of the cured polymers provides chemical stability through strong silicon – oxygen – silicon bonds and produces a significantly high strengthening effect, alkoxy silanes being able to cure at normal outdoor temperatures. Hydrolysis of alkoxy silanes produces alcohols as by-products, but alcohols are not damaging to stone and evaporate as soon as they are generated, thus leaving the solid polymer in the stone. It has been reported that solidified material does not fill the entire pore space, but instead coats the pores, therefore permitting moisture transmission. Nevertheless, alkoxy silanes do have disadvantages. They have been reported to cause some slight changes in the color of treated stone, such as an initial darkening, and also the development of whitish spots on the stone. Additionally, alkoxy silanes are considered to be relatively expensive materials and the consumption of material is high in order to achieve deep penetration [75].

Alkoxy silanes are monomeric organosilicon compounds containing silicon, oxygen, carbon and hydrogen atoms. Most of these compounds are colorless and exhibit low viscosity, relatively low toxicity and moderate to low volatility. They react with water giving a solid polymer varying in nature from silicone resin to fine powder or glassy silica. The physical properties and chemical composition of the resulting product depend on the specific conditions during the total process.

The application of alkoxy silanes in stone consolidation / hydrophobization is based on the fact that the starting liquid compound can be converted into a consolidating solid deposit within the stone through interaction with either liquid water or water vapor. When the alkoxy silane is applied to stone as a monomeric molecule, its polymerization is initiated by a hydrolysis reaction.

Hydrolysis is the chemical reaction of an alkoxy silane with water or with the hydroxyl (– OH) groups on the surface of a mineral grain. Several types of stone, brick and clay have reactive hydroxyl groups on their surface. The alkoxy (– OR) groups of alkoxy silanes are capable of reacting with hydroxyl groups.

The hydrolysis reaction gives birth to a silanol and an alcohol as a by-product. During polymerization, this partially hydrolyzed molecule can then undergo either further hydrolysis or condensation reactions. Two silanol molecules, which are the products of the hydrolysis reactions, can react with each other and condense to form a dimer molecule, water being produced as well. Further hydrolysis and condensation proceed

simultaneously and beyond the dimer stage trimers, tetramers and eventually a network of polymers having a – Si – O – Si – O – Si – backbone, called siloxanes, is formed. The – Si – O – Si – O – linkages induce the conservation and strengthening effect.

If the alkoxy groups react with the hydroxyl groups present on the surface of the stone grains, they become molecularly (chemically) bonded to the substrate. One end of the siloxane chain is bonded to the surface of one mineral grain, while the other end is attached to an adjacent grain. If the reaction takes place with the hydroxyl groups of water molecules, the resulting network of polymers is not bonded to stone grains, but fills the intergranular spaces of the stone.

When alkoxy silanes with alkyl groups [alkyl(trialkoxy)silanes] polymerize, unlike the Si – O – C link (ester link), the Si – C link (silane link) resists hydrolysis and the final product retains alkyl groups attached to the siloxane backbone. The alkyl groups are non-polar and therefore provide water repellency.

For the effective application of alkoxy silanes in conservation, in addition to providing appropriate conditions for the reaction, application of the chemical treatment on an appropriate type of stone is important. The physical and chemical nature of the substrate also influences the polymerization process. Alkoxy silanes do not give the same results with all types of stone; the presence of reactive – OH groups on the mineral grains of the stone can lead to a molecular attachment of the siloxane chains to the mineral grains. Thus, it has been claimed that the alkoxy silanes are most effective for porous, fine-grained, weak stones with surface hydroxyl groups, such as many types of sandstone and clay rich stones. However, the conservation of calcareous stones such as limestone and marble with alkoxy silanes has been also achieved. Although the chemical affinity of silanes for calcareous stones is minimal, a network of polymer may fill the intergranular spaces of the stone and induce a consolidating effect without forming a chemical bridge between the grains.

The mechanism of alkoxy silane polymerization is quite complex and is still not completely understood.

An alkoxy silane-based treatment is usually sprayed with low pressure or brushed onto the substrate in repeated applications referred to as "cycles" by some manufacturers. The number of applications and the waiting time between cycles or applications can vary for different products; therefore, each product should be applied in accordance with manufacturer's recommendations. In the early stages, applications are absorbed very

rapidly. Further applications should normally take place until no more treatment is taken up.

Among the products applied over the years, alkoxy silanes and related compounds are still one of the most promising conservation agents. After decades of experience, alkoxy silanes have proved to be effective for the conservation of sandstones, limestones and earthen building materials. Considering the chemical structure, their most important advantage is their ability to polymerize and produce a chemically stable end-product similar to the minerals composing the stone (e.g. sandstone and earth) itself. Their deep penetration into porous stone, which derives at least in part from the extremely low viscosity of the monomers, also makes alkoxy silanes attractive conservation agents.

While these properties favor the choice of alkoxy silanes where such treatment is necessary, there are various factors which have not been fully explored. The mechanism of polymerization and the effect the rates of hydrolysis and condensation reactions have on the structure and stability of the resulting polymer are some of the aspects still open to debate.

While current literature includes an increasing number of case studies where alkoxy silanes have been used as treatments, information on the long-term effectiveness of the reported applications is rarely well documented. Although the long-term performance of a treatment can only be proved in time, it is not always possible to wait for years in order to evaluate a particular type of treatment.

VI. 2. Characterization of three selected worldwide used water repellent products (Lotexan-N, Silres® BS 290, Tegosivin HL 100)

Three worldwide used siloxane based water repellent products, namely Lotexan-N (KEIM), Silres® BS 290 (WACKER) and Tegosivin HL 100 (DEGUSSA GOLDSCHMIDT) were selected and analyzed by NMR (Figs. 49, 51 and 53) and IR spectroscopy (Figs. 50, 52 and 54) in order to determine their chemical structure.

VI. 2. 1. Chemical characterization

VI. 2. 1. 1. NMR spectroscopy and FT-IR spectroscopy

Structural analysis of Lotexan-N (KEIM), Silres® BS 290 (WACKER) and Tegosivin HL 100 (GOLDSCHMIDT)

The NMR analyses were performed on a Bruker Avance DRX 400 MHz spectrometer. The attribution of the signals was based on unidimensional and bidimensional experiments.

The FT-IR spectra were registered on a Bruker Vertex 70 instrument. The three siloxane based water repellents are very much alike, the common feature being the intense absorption between 1200 – 1000 cm^{-1} , a characteristic to siloxane based compounds.

Structural characterization of Lotexan-N

According to the producer, Lotexan-N (Keim) is a siloxane based, colorless, waterproofing protective product especially designed for unpainted, porous natural stone. All forms of natural stones, neutral or alkaline, can be protected against water, acid rain and atmospheric pollution. Lotexan-N penetrates into the pores of the natural stone and, after solvent evaporation, the main reactive substance is deposited in the pores and forms its waterproofing characteristic by chemical reaction with the normal building material and air humidity.

The application of Lotexan-N does not seal the pores of the natural stone, i.e. the water vapor permeability of the natural stone is maintained.

The ^1H -NMR spectrum of this product (Fig. 49a) indicates the presence of the resonance peaks at 0.9 and 1.3 ppm, characteristic to an aliphatic hydrocarbon solvent. Other resonance peaks, around 7.0 and 2.4 ppm, indicate an aromatic solvent (substituted benzene).

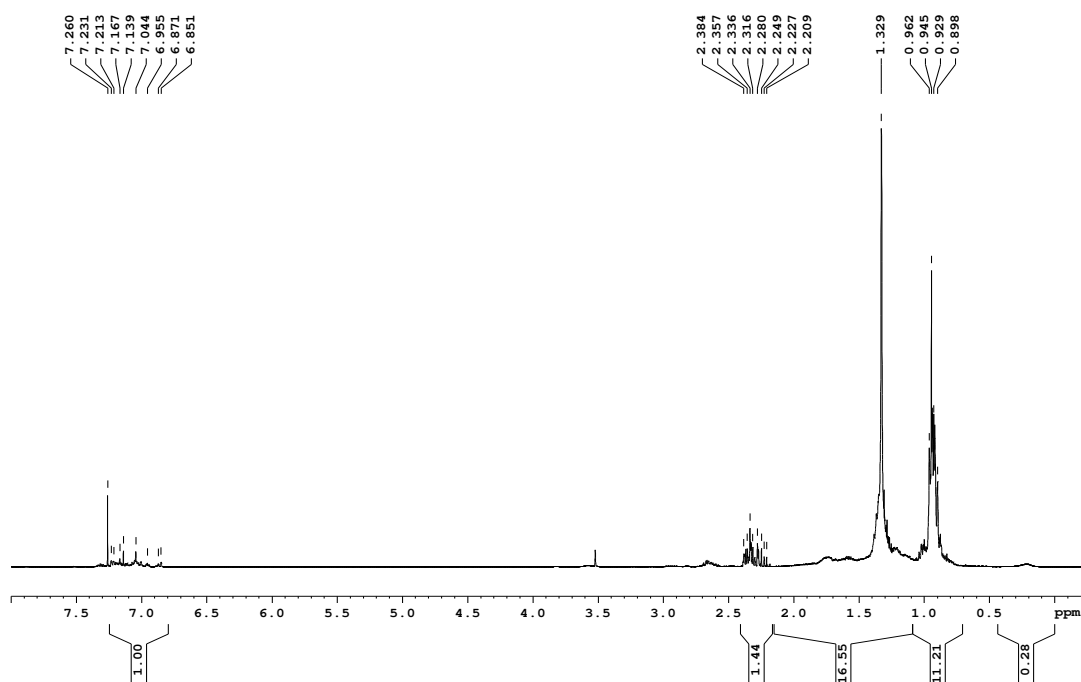


Fig. 49 (a). $^1\text{H-NMR}$ spectrum of Lotexan-N

The ratio between the aliphatic and aromatic solvents, calculated from the integral ratios of the corresponding resonance peaks, is about 7:1.

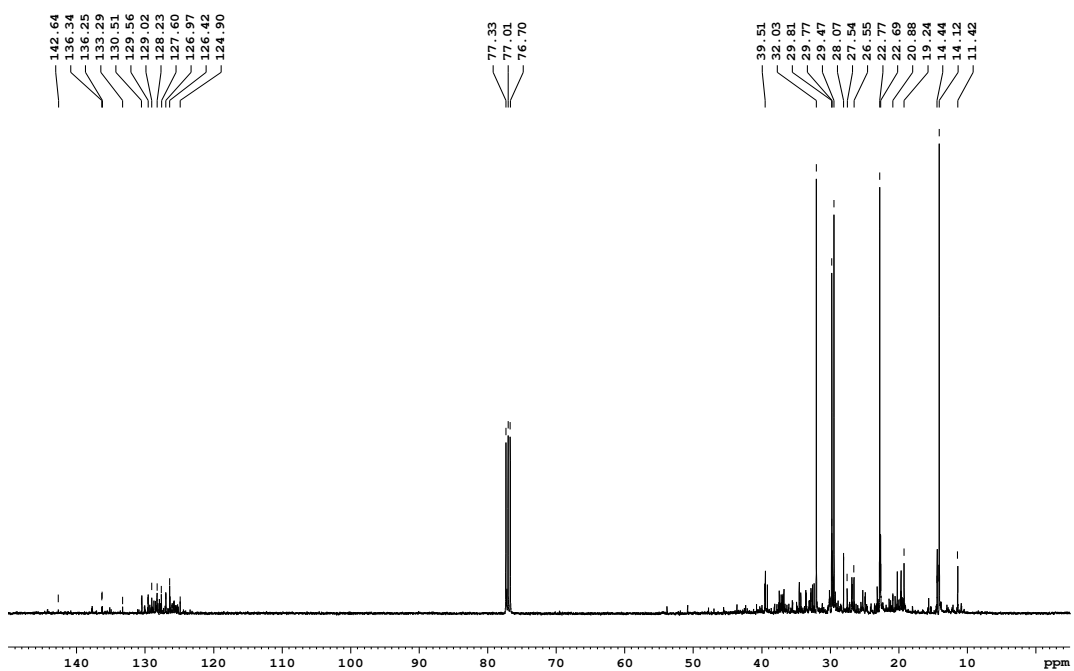


Fig. 49 (b). $^{13}\text{C-NMR}$ spectrum of Lotexan-N

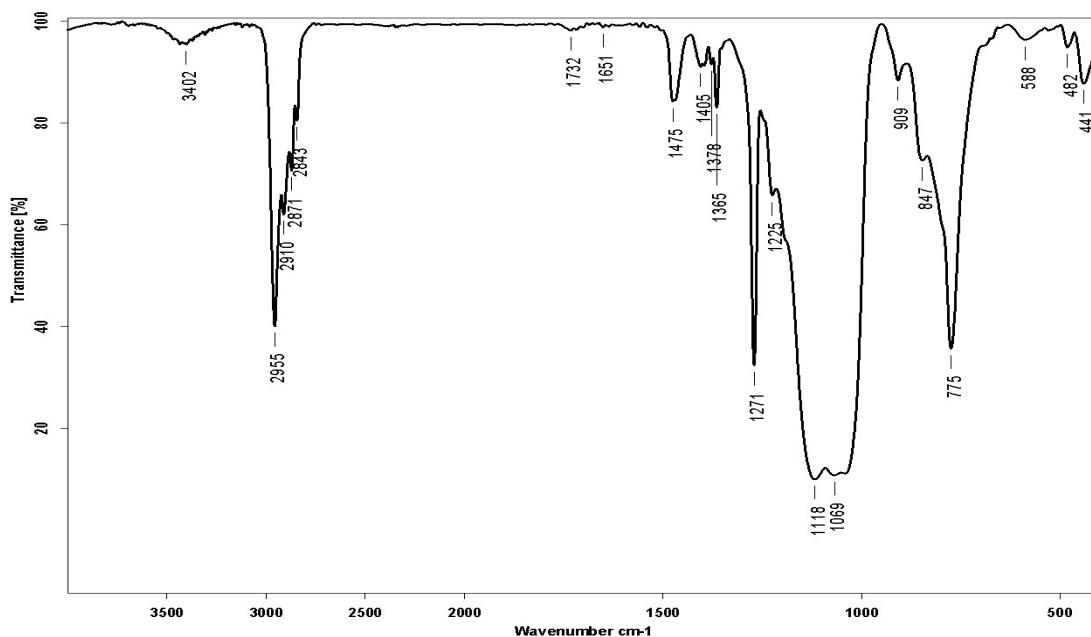


Fig. 50. FT-IR spectrum of Lotexan-N

The FT-IR analysis of the residue obtained after solvent evaporation (Fig. 50) indicates a crosslinked polysiloxane, as evidenced by the large Si – O – Si absorption band between 1000 and 1118 cm^{-1} .

The polysiloxane contains methyl substituents linked to the silicone atoms (absorption bands at 1271 and 847 cm^{-1}). The product is a siloxane prepolymer dissolved in an aliphatic / aromatic solvent mixture. Si – O – Si bands at 775 and 909 cm^{-1} , belonging to the Si – O – Si groups, are also visible in the IR spectrum. Thus, comparing the IR spectrum of the dry compound with the $^1\text{H-NMR}$ spectrum of the solution, one can conclude that the product is a siloxane prepolymer substituted with methoxy, methyl and alkyl groups dissolved in a mixture of aromatic / aliphatic hydrocarbon solvents.

Structural characterization of Silres® BS 290

According to the producer, Silres® BS 290 (WACKER) is a solventless silicone concentrate based on silane / siloxane and can be diluted with organic solvents. Dilute solutions of Silres® BS 290 in organic solvents serve as high-quality general-purpose water repellents for impregnating and priming mineral and highly alkaline substrates.

After application, Silres® BS 290 reacts with the atmospheric moisture or pore water in the substrate, thereby generating the active ingredient while liberating alcohol. The active ingredient greatly lowers the water absorbency of the substrate. Since neither

pores nor capillaries are clogged, the substrate retains a very high degree of water vapor permeability.

Silres® BS 290 is a mixture of silane and siloxane reactive compounds containing methoxy groups and methyl or alkyl substituents linked to the silicone atoms. In the $^1\text{H-NMR}$ spectrum (Fig. 51), these chemical entities are evidenced by the peaks appearing at around 3.5 ppm, 0 ppm and between 0.5 and 1.8 ppm, respectively.

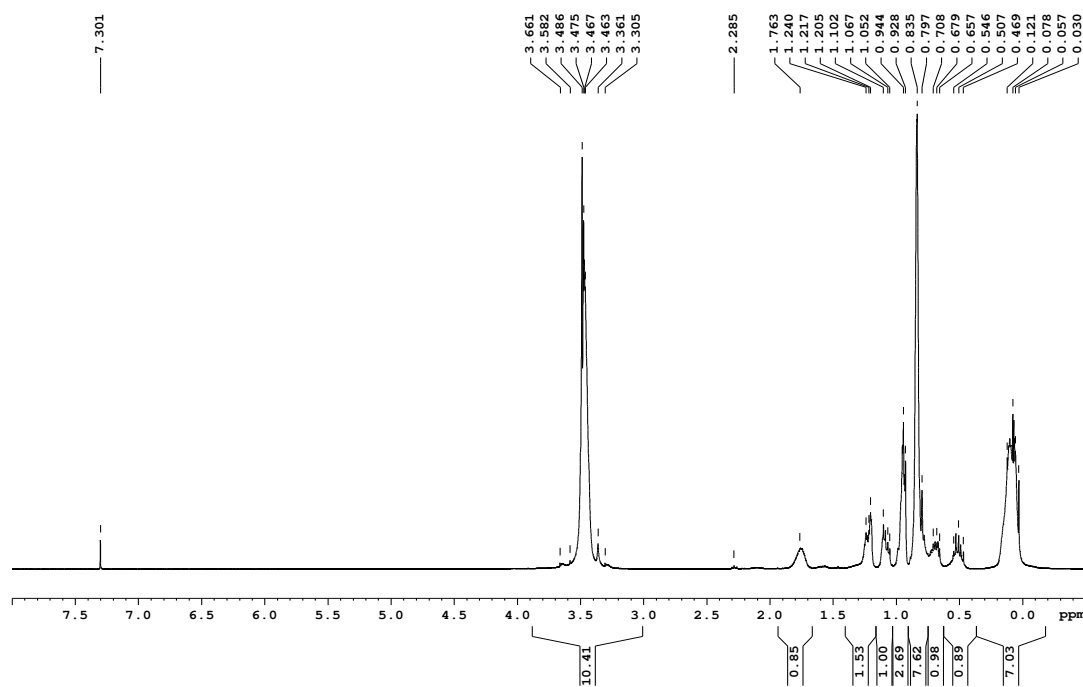


Fig. 51 (a). $^1\text{H-NMR}$ spectrum of Silres® BS 290

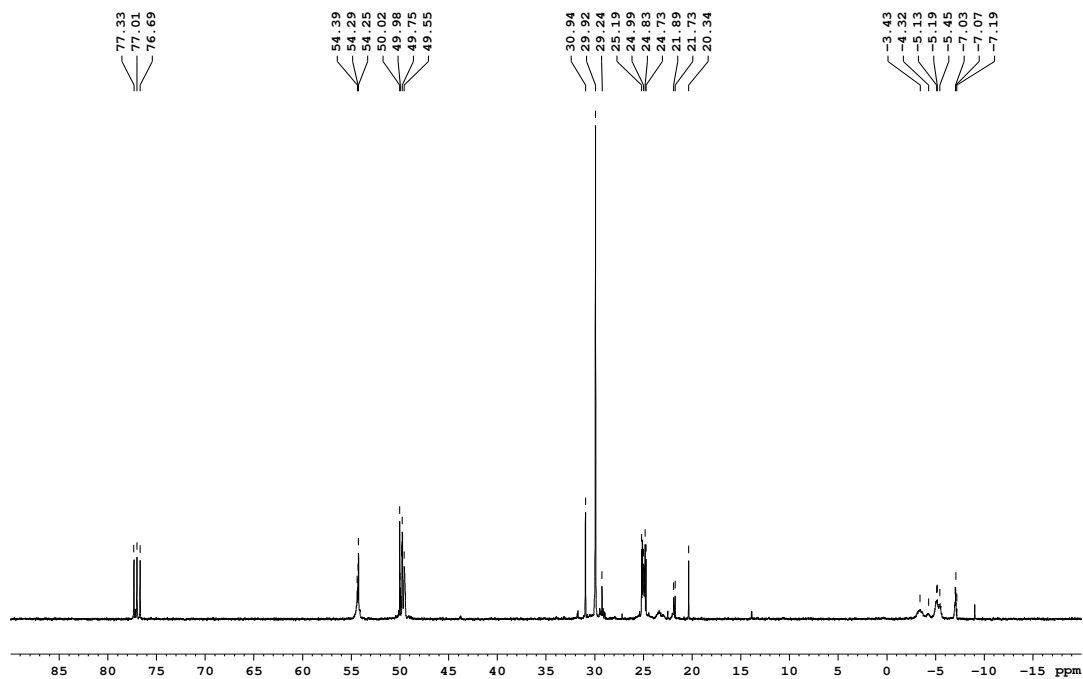


Fig. 51 (b). ^{13}C -NMR spectrum of Silres® BS 290

The chemical structure was confirmed by the FT-IR spectrum (Fig. 52), which shows the siloxane Si – O – Si band superposed on a Si – O – C band at 1020 and 1120 cm^{-1} , and methyl groups linked to the silicone atoms – the 1270 cm^{-1} band.

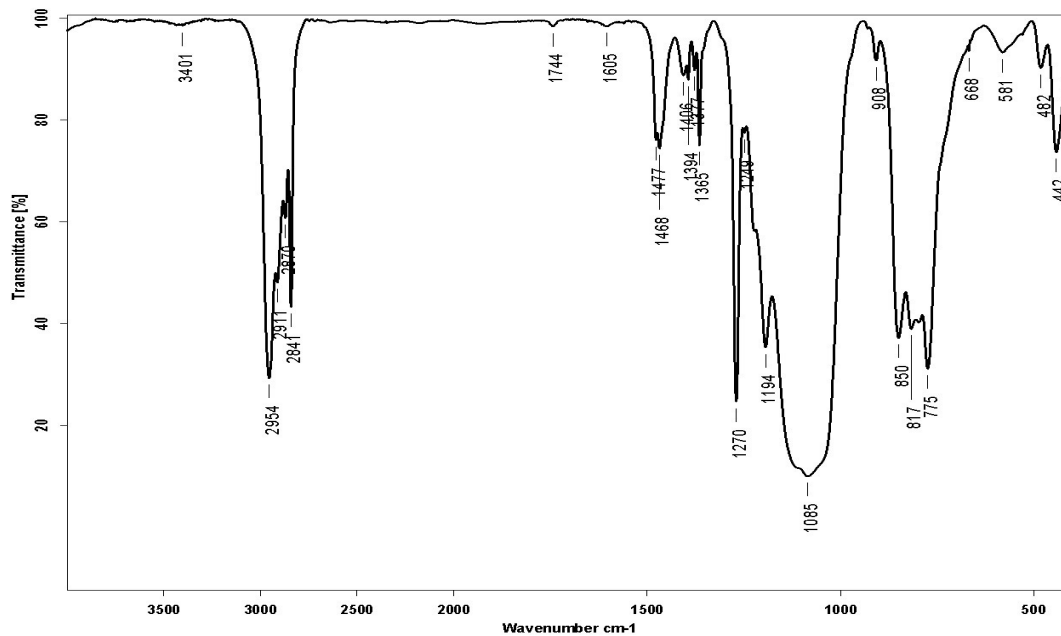


Fig. 52. FT-IR spectrum of Silres® BS 290

Si – O – C bands are also evidenced at 1294 cm^{-1} and 908 cm^{-1} . In the $775 - 850\text{ cm}^{-1}$ region, bands characteristic to Si – CH₃ and Si – O – C groups are also visible.

Structural characterization of Tegosivin HL 100

According to the producer, Tegosivin HL 100 (Goldschmidt) is a low molecular weight modified polysiloxane resin (methyl-ethoxy-polysiloxane); its application requires the dissolution in white spirit.

As revealed from the NMR spectrum (Fig. 53), this chemical product is a typical methyl ethoxy siloxane resin having ethoxy and methyl substituents attached to the silicone atoms; the ratio between the non-functional methyl groups and the reactive ethoxy groups was found to be about 3.3:1 from the ratio of the corresponding peaks integrals at 0.1 ppm (Si – CH₃) and one of the peaks from the ethoxy group at 1.2 ppm (– CH₃) or 3.8 ppm (– CH₂ –).

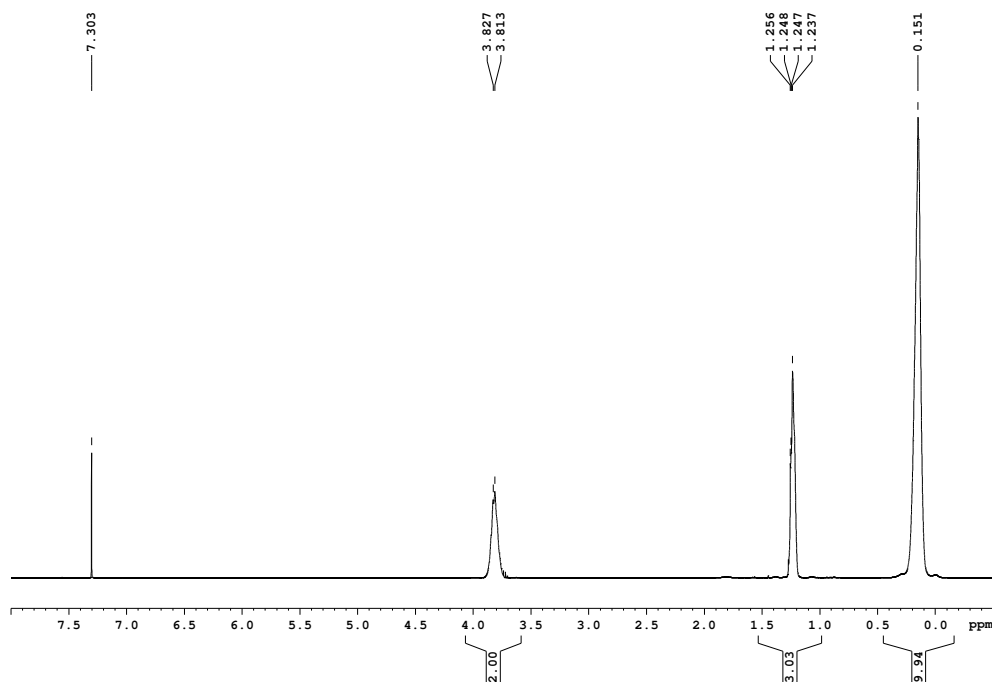


Fig. 53 (a). ¹H-NMR spectrum of Tegosivin HL 100

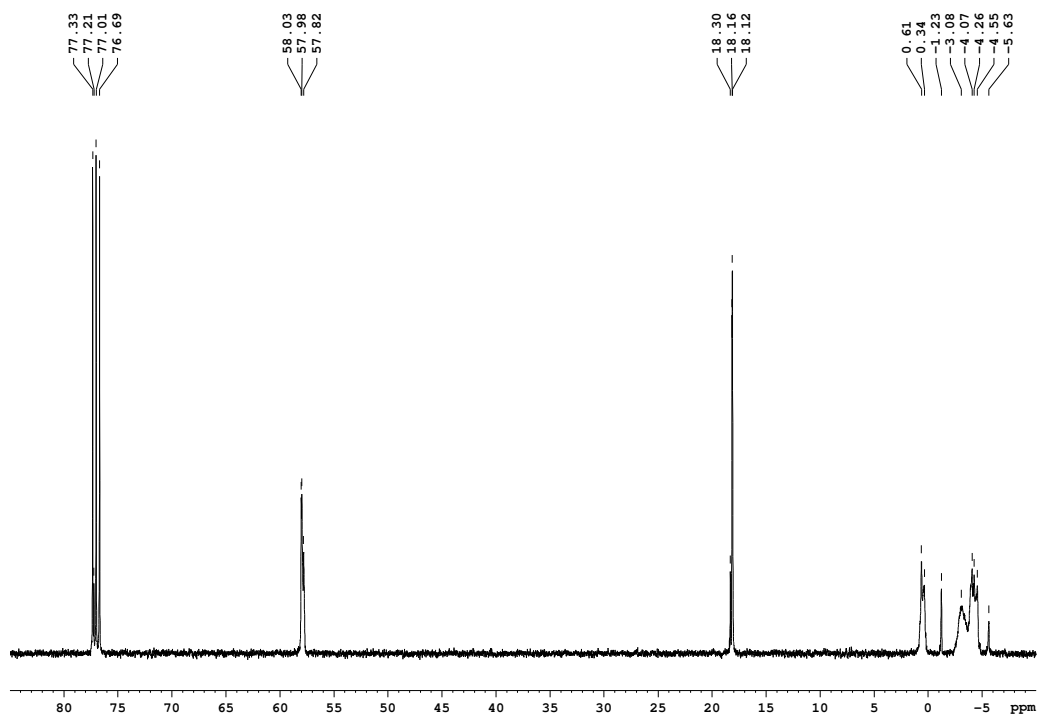


Fig. 53 (b). ¹³C-NMR spectrum of Tegosivin HL 100

The FT-IR spectrum of Tegosivin HL 100 (Fig. 54) contains typical absorption bands at 1270 cm⁻¹ (Si – CH₃) and at 961 cm⁻¹ (Si – OCH₃).

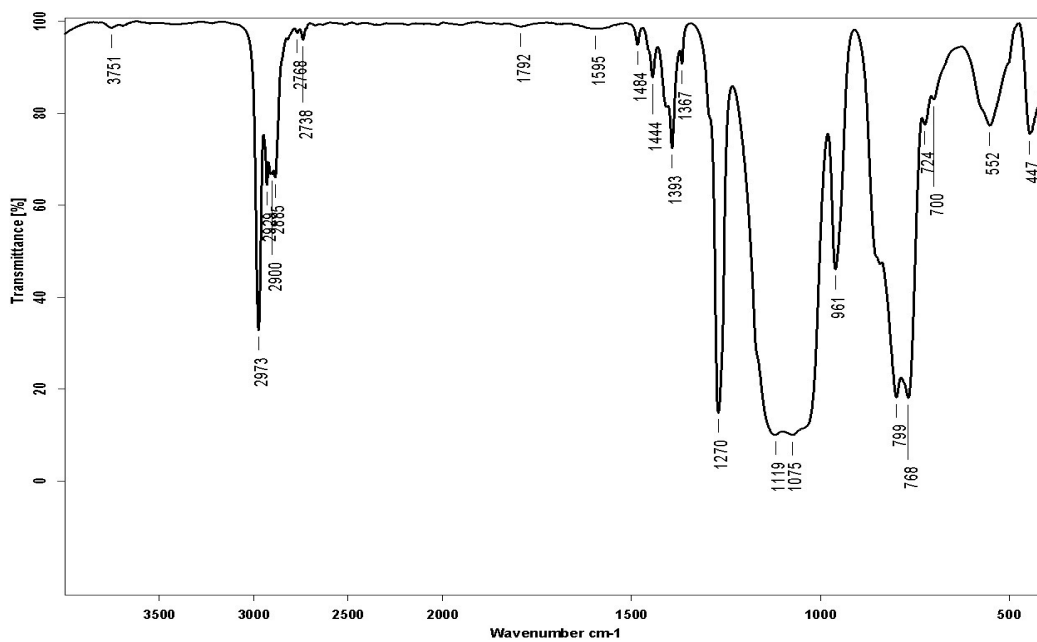


Fig. 54. FTIR spectrum of Tegosivin HL 100

The regions between 1000 and 1120 cm^{-1} and between 768 and 860 cm^{-1} indicate superposed absorptions of Si – O – Si and Si – O – C groups and of Si – CH₃ and Si – O – C groups, respectively.

NMR and FT-IR analyses of the three commercial products yield the following general chemical formula:

Lotexan-N: $-\text{Si}(\text{CH}_3)(\text{OCH}_3) - \text{O} -] - [- \text{Si}(\text{R}_1)(\text{R}_2) - \text{O} -]$
+ CH₃ – (CH₂)_n – CH₃ + C₆H₄(CH₃)₂ (aliphatic / aromatic solvent mixture as major constituent of the product), R₁, R₂ = alkyl radicals

Silres® BS 290: $[- \text{Si}(\text{CH}_3)(\text{OCH}_3) - \text{O} -] - [- \text{Si}(\text{R}_1)(\text{R}_2) - \text{O} -]$, solventless

Tegosivin HL 100: $[- \text{Si}(\text{CH}_3)_2 - \text{O} -] - [- \text{Si}(\text{CH}_3)(\text{OCH}_2\text{CH}_3) - \text{O} -]$, solventless.

VI. 2. 2. Thermal stability and properties

VI. 2. 2. 1. Thermogravimetric (TGA) and differential scanning calorimetry (DSC) analysis

Thermogravimetric investigation of Lotexan-N (KEIM), Silres® BS 290 (WACKER) and Tegosivin HL 100 (GOLDSCHMIDT)

The thermal properties are among the most important properties of any material. Thermal stability and thermal degradation kinetics may be significant to both production and application of the studied product.

The thermogravimetric analysis (TGA) was performed using a Mettler Toledo model TGA/SDTA 851 instrument, under nitrogen flow (20 $\text{cm}^3 \text{min}^{-1}$), at a heating rate of 10° C/min, from 25 to 900° C. The initial mass of the samples was 4-6 mg.

The thermal stability of the samples was evaluated by dynamic thermogravimetric analysis. Figures 55-57 show the TG, the differential weight loss DTG and DTA curves of the samples.

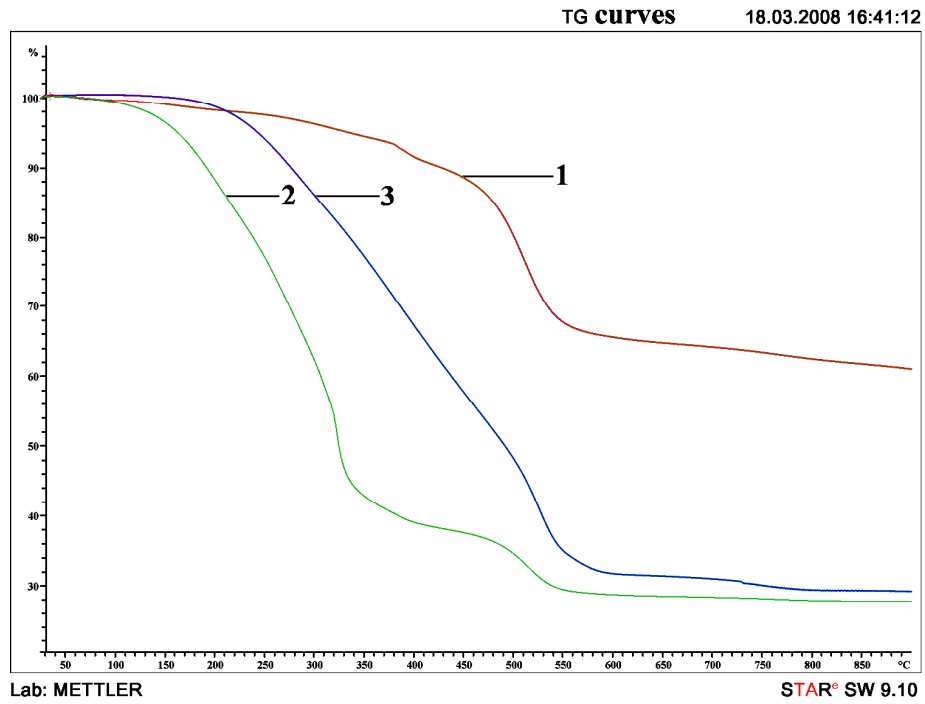


Fig. 55. TG curves of 1 – Lotexan-N, 2 – Silres® BS 290, 3 – Tegosivin HL 100

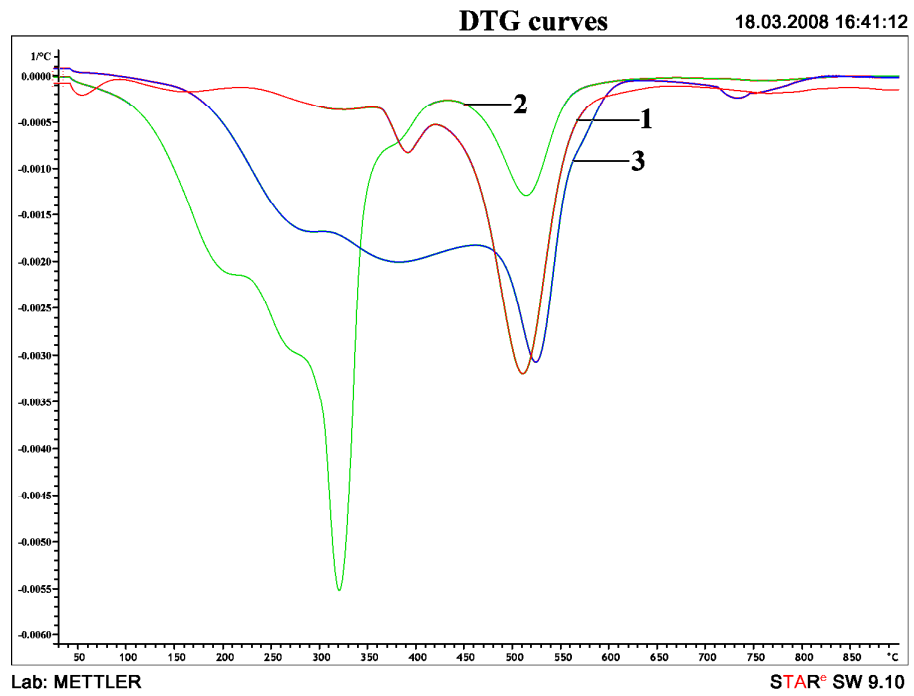


Fig. 56. DTG curves of 1 – Lotexan-N, 2 – Silres BS® 290, 3 – Tegosivin HL 100

Table 10 summarizes the most important thermogravimetric characteristics obtained from the thermograms.

Table 10. Thermogravimetric parameters

Sample	Stage of the thermal degradation	T _i	T _m	T _f	W%	DTA data
Lotexan-N	I	149	152	227	2.14	endo
	II	227	302	379	3.98	endo
	III	379	386	462	4.00	exo
	IV	462	512	900	28.60	exo
Silres® BS 290	I	141	193	242	22.02	endo
	II	242	262	303	16.53	endo
	III	303	321	341	19.15	exo
	IV	341	384	397	4.05	exo
	V	486	520	542	10.26	exo
Tegosivin HL 100	I	208	262	352	22.05	endo
	II	352	374	491	26.50	exo
	III	491	524	555	22.69	exo

W% - weight loss of the polymer after the end of each stage of decomposition

The temperature parameters are the initial temperature of decomposition (T_i), the temperature at the maximum rate of weight loss (T_m) and the final temperature of sample decomposition (T_f). These parameters are defined and obtained from the measured TG and DTG curves, useful for the analysis of the thermal degradation dynamics in order to determine the activation energy (E_a) of the studied samples.

The percentage loss of weight, W%, is equal to $[(m_0 - m) \times 100] / m$, where m₀ and m represent the weight of the sample at the starting point and during the scanning, respectively. For all samples, the degradation processes are not complete, a residue being left in each case.

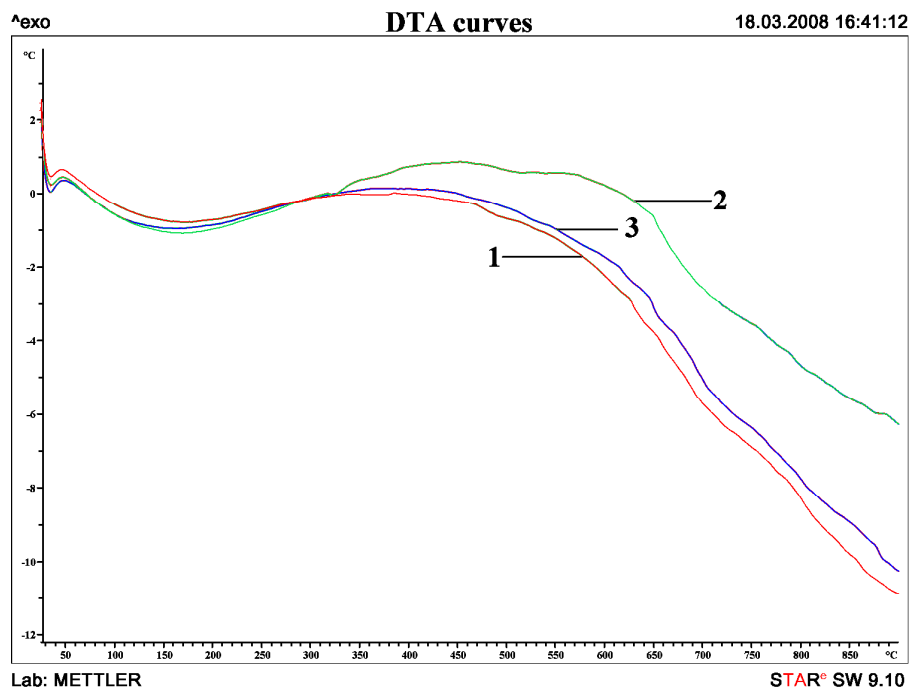


Fig. 57. DTA curves of 1 – Lotexan-N, 2 – Silres® BS 290, 3 – Tegosivin HL 100

The degradation process exhibits three, four or five maxima of decomposition. For all investigated samples, the last two degradation steps have the value close to the temperature of the maximum rate of weight loss. For this stage, the thermogravimetric values were processed by the Freeman – Carroll differential method. The results are presented in Table 11.

The Freeman – Carroll method assumes $F(\alpha) = (1 - \alpha)^n$ and considers incremental differences in $(d\alpha / dT)$, $(1 - \alpha)$ and $1 / T$ which leads to the expression:

$$\Delta \ln \left(\frac{d\alpha}{dT} \right) = n \Delta \ln(1 - \alpha) - \left(\frac{E_a}{RT} \right) \Delta \left(\frac{1}{T} \right) \quad (1)$$

where α is equal to $(m_0 - m) / m$.

This expression can be used to determine the value of the activation energy E_a by plotting

$$\left[\frac{\Delta \ln(d\alpha / dT)}{\Delta \ln(1 - \alpha)} \right] \text{ against } \left[\frac{\Delta(1/T)}{\Delta \ln(1 - \alpha)} \right].$$

The intercept gives the reaction order, n . E_a can be calculated from the slope.

Table 11. Kinetic characteristics corresponding to the last two degradation steps

Sample	Stage	n	Ea (kJ/mol)	lnA
Lotexan-N	III	1.22±0.086	150.11±16.31	22.36±3.00
	IV	1.42±0.016	215.60±1.74	28.11±0.28
Silres® BS 290	IV	1.18±0.031	130.36±4.79	19.09±0.90
	V	1.42±0.014	242.50±1.88	32.12±0.30
Tegosivin HL 100	II	0.35±0.001	17.74±0.52	3.35±0.10
	III	0.48±0.063	185.11±0.063	22.95±0.02

n – reaction order, Ea – activation energy, A – pre-exponential factor

The thermal degradation of the samples in nitrogen atmosphere is a three, four or five steps reaction. The peak width of DTG curves of the last two degradation steps has a value close to the temperature corresponding to the maximum rate of weight loss.

The TG curves clearly indicate that from the three investigated products, the highest thermal stability is shown by Lotexan-N, followed by Tegosivin HL 100 and Silres® BS 290. At the same time, the amount of the remaining residue at the highest temperature the samples have been heated is the most significant for Lotexan-N.

VI. 2. 2. 2. Rheological properties

Rheological measurements of the three water repellents (Lotexan-N, Silres® BS 290 and Tegosivin HL 100, using white spirit as solvent) were carried out on a Physica MCR 501 rheometer (Anton Paar) equipped with a Peltier device for the temperature control. The measurements were performed using a plate-plate geometry with a diameter of 50 mm. Due to the reduced viscosity of the samples, the gap was fixed at 0.300 mm.

Anton Paar rheometers may be used to measure both Newtonian and non-Newtonian fluids. A Newtonian fluid is one in which the viscosity does not depend on shear rate. Regardless of the level of applied shear, the viscosity remains the same.

For all samples both rotational (flow and viscosity curves) and oscillatory tests (amplitude sweep and frequency sweep) were performed. An oscillatory temperature sweep was also carried out for all solutions.

All flow curves were measured under isothermal conditions (20° C). The shear rate was preset between 1 and 1,000 s⁻¹. The flow curves for the three samples and a comparison of all viscosity profiles and dependencies of the shear stress on shear rate are presented in Fig. 58.

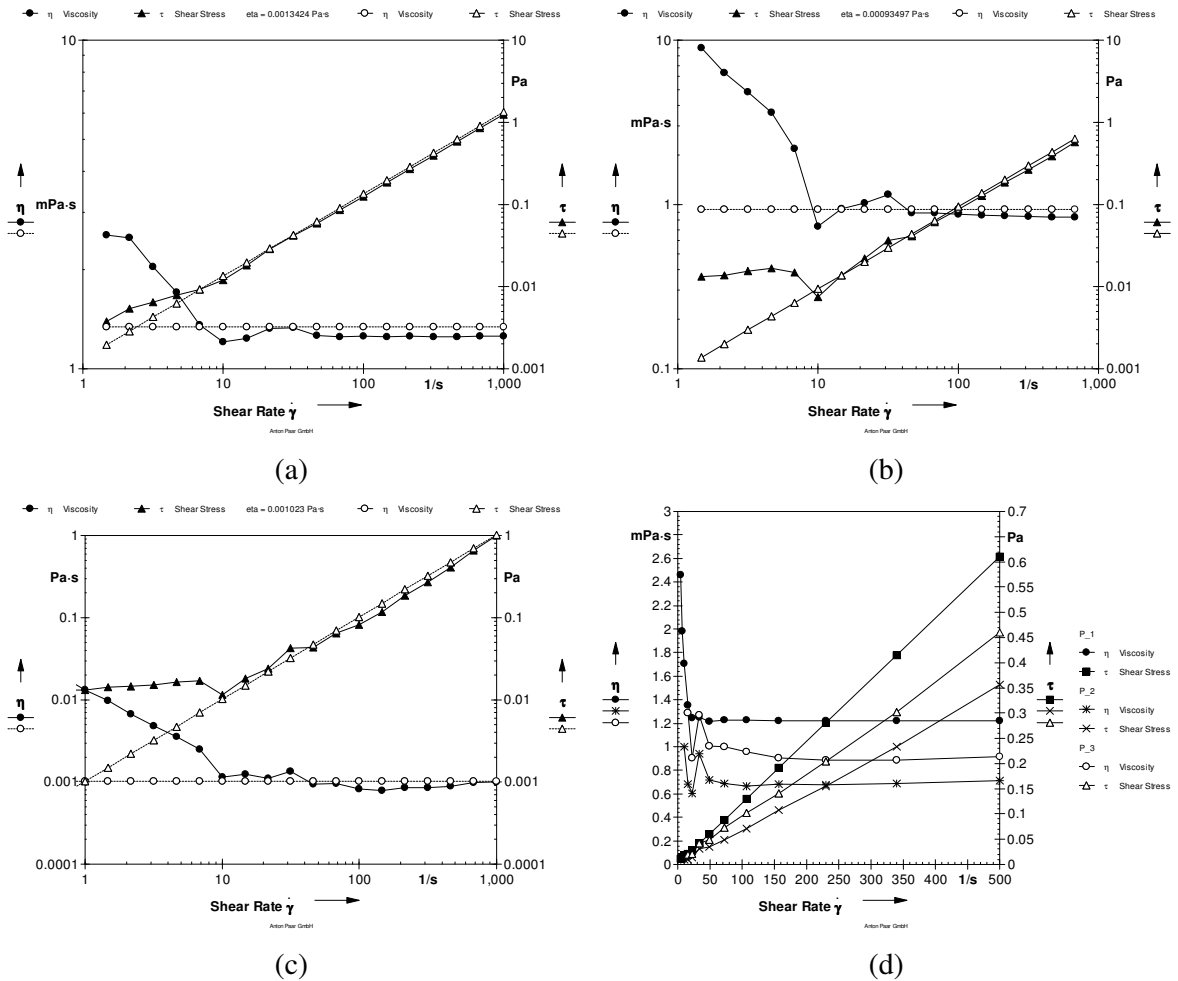


Fig. 58. Flow curves for the analyzed samples: (a) Lotexan-N; (b) Silres® BS 290; (c) Tegosivin HL 100; (d) comparison of all samples (linear scale)

A fluid is defined as a substance that undergoes irreversible deformation when subjected to a steady state shear or tensile stress. The viscosity is a key parameter to characterize this deformation and is a measure of the resistance of the solution to flow under mechanical stress. Two units characterize the viscosity value – the original CGS units and the (relatively) new SI units. The usual units of viscosity used in the US are centiPoise, cP. One cP is equal to one milliPascal second, mPas.

High viscosity solutions require a high level of stress to flow rapidly, while a low viscosity solution will deform and flow rapidly with a minimum of force. For example, water presents a low viscosity and will flow readily out of a glass under normal gravity forces, whereas molasses (a high viscosity material) will take a long time to flow from a glass. The viscosity of a coating fluid is an important rheological property which needs to be accurately measured and controlled during the development of the product and

during its manufacturing to insure optimum quality and a reproducible cost effective manufacturing process.

The flow properties of the three samples are related to spreading or coating of the material on the substrate. The depth of penetration into the stone is also dependent on the viscosity, in other words on the ability to flow. The slope of the curve represents the viscosity. When the curve is a straight line (as for the analyzed samples), the slope is constant and the viscosity is independent on the shear rate. All samples behave as Newtonian fluids with the viscosity independent on the shear rate, but to have a fully developed Newtonian structure it is recommended to use a shear rate higher than 10 s^{-1} (these shear rates are the most suitable for the application procedure).

The characteristic viscosities for the three samples are as follows: η Lotexan-N = 1.3424 mPas, η Silres® BS 290 = 0.93497 mPas, η Tegosivin HL 100 = 1.023 mPas, very close to the characteristic value of water (1.00 mPas). This is a clear indication that their penetration in the stone is easy to obtain and the time needed for the product to penetrate the stone is not too long. The dotted lines represent the Newtonian model applied to experimental data.

The fluid viscosity is a key variable in the following properties:

- Determining the best coating method to be used
- Coating weight control in roll coating methods
- Coating quality level and reproducibility from applicator
- Coating quality in dryer
- Leveling of coating after application.

Routine measurements of viscosity prior to coating should be part of the normal quality control system for the coater. Often a problem is detected after the solutions are all consumed in the application process. It may be very difficult to determine the source of the problem if rheological data are not available.

Until the liquid coatings dry and become immobile, their flow behavior needs to be predicted. Basic questions involve the wetting and spreading of thin liquid layers as they flow on geometrically-complex surfaces. At the same time, the important physical properties of the liquid (such as viscosity and surface tension) are continually changing as it dries.

To prove once more the Newtonian character of the analyzed samples, oscillatory tests were performed. The first test was the amplitude sweep in which the amplitude of deformation was varied between 0 and 100% and loss modulus (G'') and complex viscosity (η^*) were recorded (Fig. 59). Four different angular frequencies (ω) were used for each sample: 10, 30, 50 and 100 rad/s. As it can be seen from Fig. 59, loss modulus is independent on strain amplitude and increases with the angular frequency. Lotexan-N and Tegosivin HL 100 samples have almost similar G'' values, while Silres® BS 290 sample is characterized by a lower value.

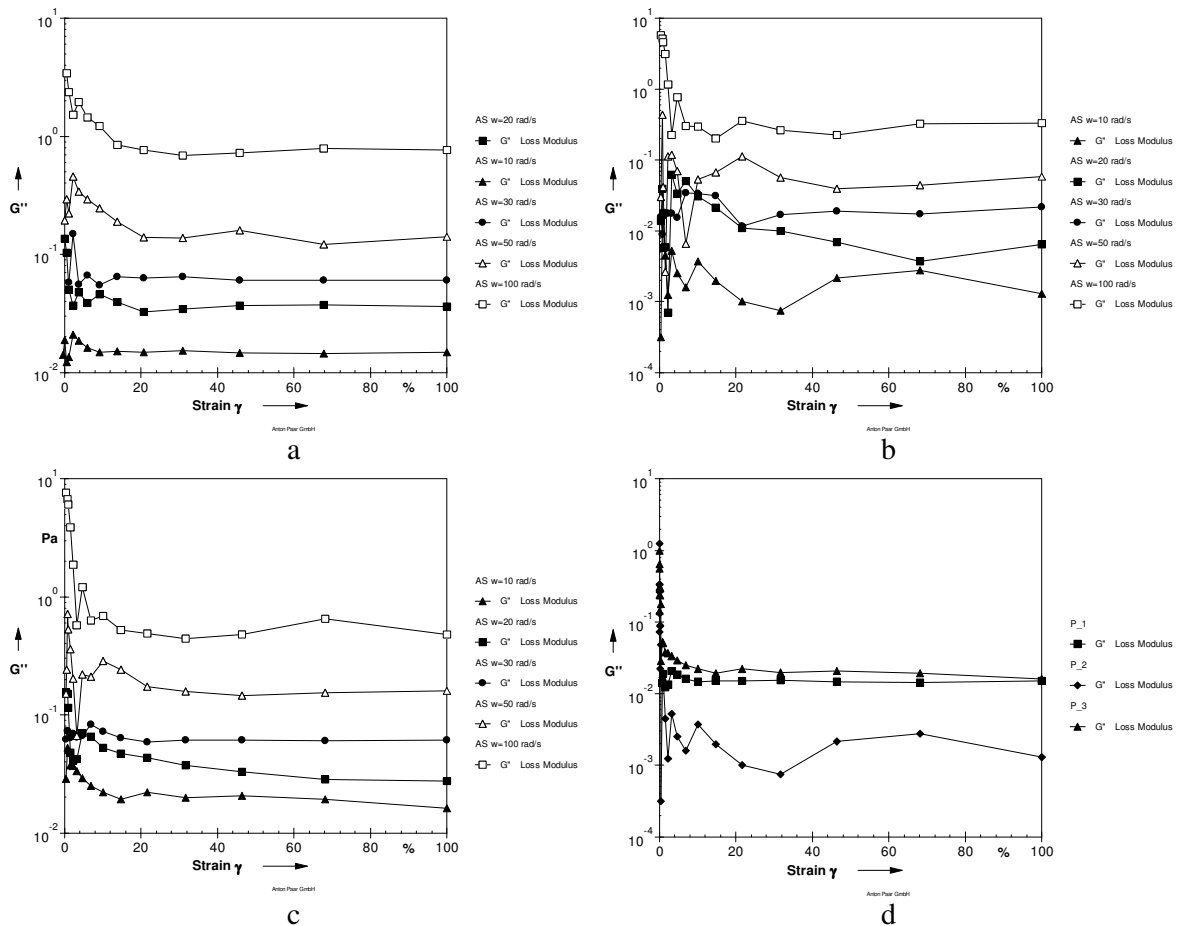


Fig. 59. Amplitude sweep for the analyzed samples: (a) Lotexan-N; (b) Silres® BS 290; (c) Tegosivin HL 100; (d) comparison of G'' for all samples

G'' – loss modulus, is a measure of the deformation energy used by the sample during the shear process. This energy is spent during the process of changing the material's structure. There is motion between molecules, particles, a.s.o. causing frictional forces between these components, and therefore frictional heat occurs. Energy losing materials are showing an irreversible deformation behavior. Thus, G'' represents the viscous behavior of the tested material.

The increase of the loss modulus with three orders of magnitude when the angular frequency is increased suggests the necessity to use an intense movement for a better quality of the surface during application.

For the frequency sweeps (Fig. 60) the amplitude of deformation (γ) was kept constant while the angular frequency (ω) was varied between 1 and 100 rad/s. For all samples the effect of the amplitude of deformation on loss modulus and complex viscosity was taken into consideration. As seen in Fig. 60, Lotexan-N and Tegosivin HL 100 samples have again a similar behavior with a slight decrease of G'' up to 10 1/s followed by an increase (more evident for Tegosivin HL 100 sample) for lower values. The Silres® BS 290 sample has a loss modulus almost independent on frequency. A higher stability of Silres® BS 290 could be supposed for a large range of application conditions.

The increase of complex viscosity for higher values of frequency suggests some modifications in the arrangements of the particles in solution.

An oscillatory temperature sweep was also carried out for all solutions. As expected, the viscosity of all solutions decreased when temperature increased (Fig. 60). The activation energy was calculated applying the Arrhenius equation

$$\eta = A \cdot e^{E_a / RT}$$

where E_a is the activation energy of viscosity, T is the temperature, R is the molar gas constant and A is approximately a constant.

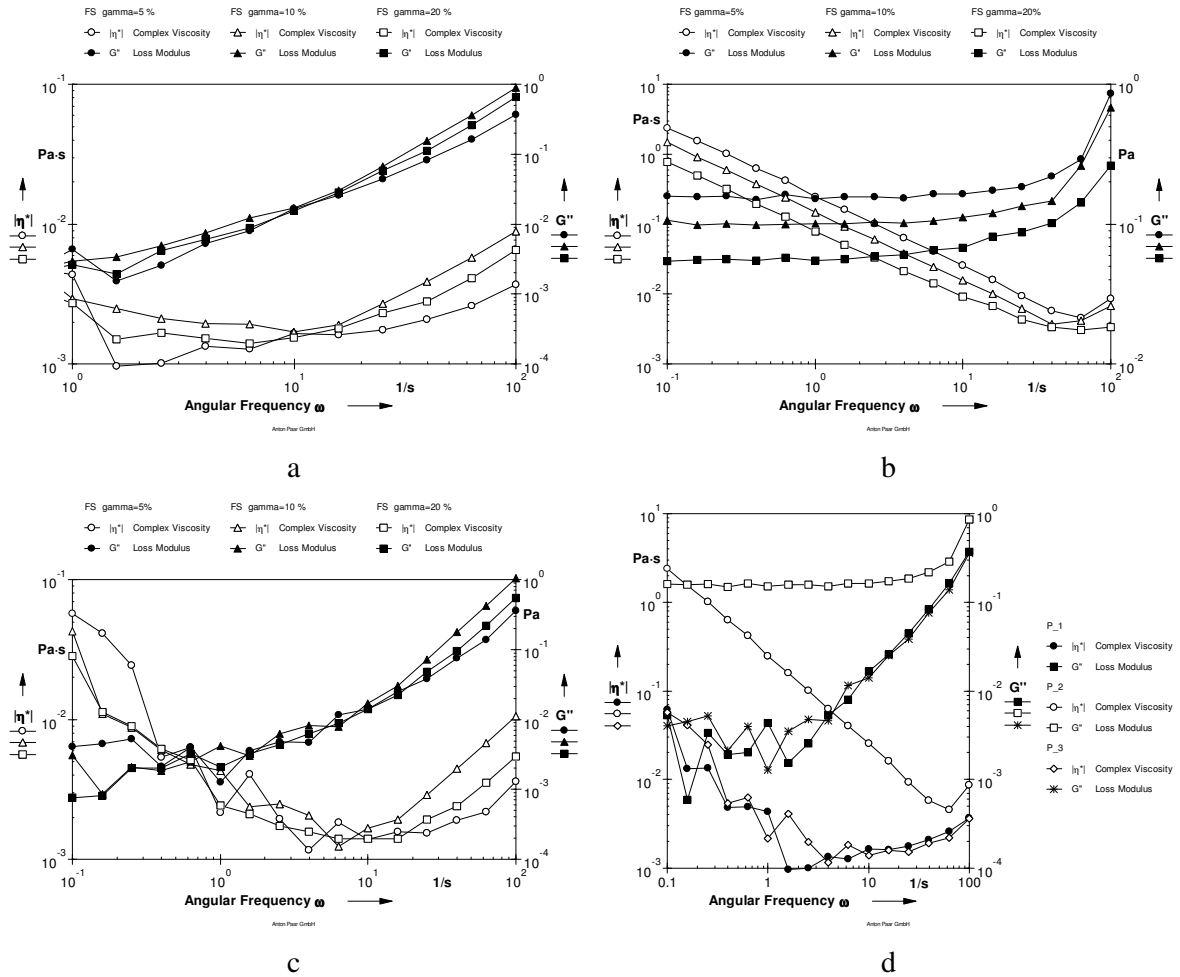


Fig. 60. Amplitude sweep for the analyzed samples: (a) Lotexan-N; (b) Silres® BS 290; (c) Tegosivin HL 100; (d) comparison of loss modulus and complex viscosity for all samples

The activation energies for the three samples are the following ones:

Lotexan-N	$E_a = 0.31060$ KJ/mol
Silres® BS 290	$E_a = 0.27881$ KJ/mol
Tegosivin HL 100	$E_a = 0.22436$ KJ/mol.

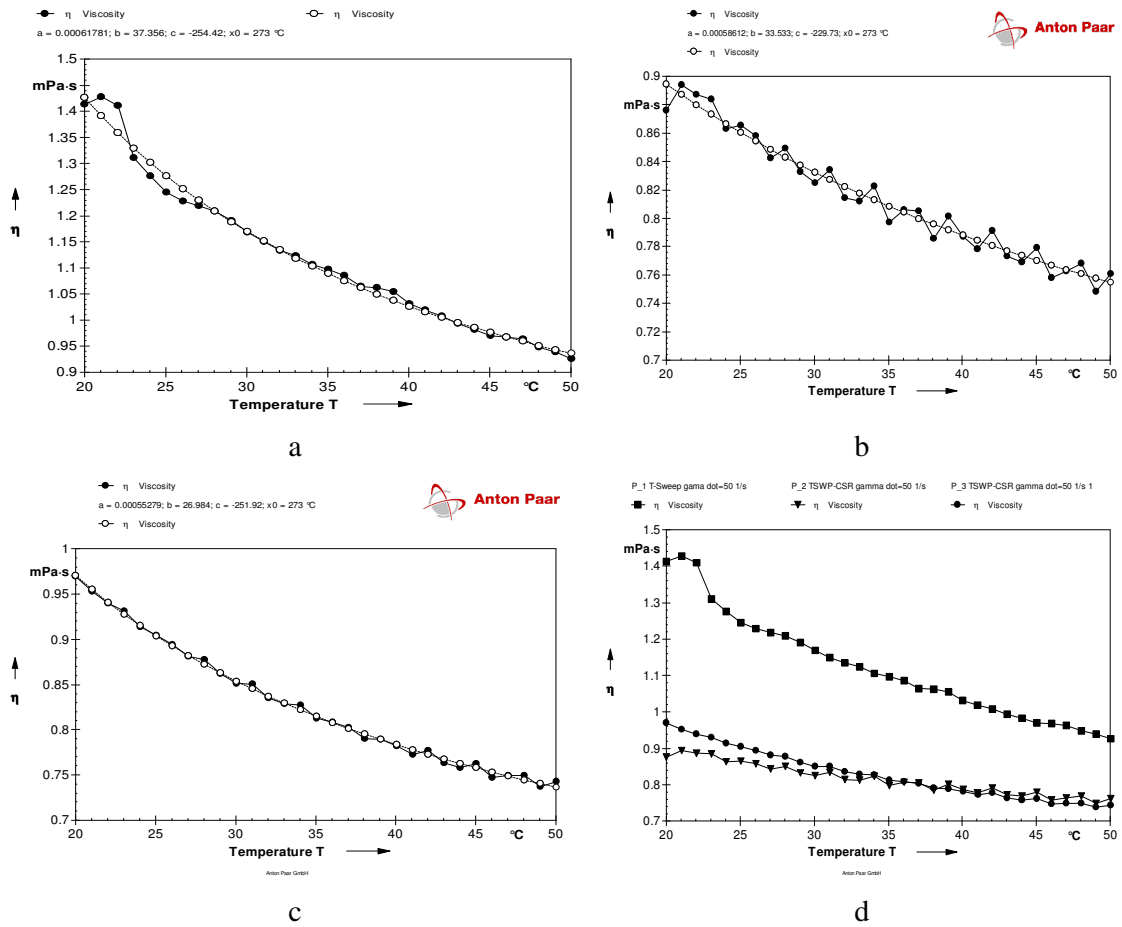


Fig. 61. Temperature sweep for the analyzed samples: (a) Lotexan-N; (b) Silres® BS 290; (c) Tegosivin HL 100; (d) comparison for all samples (the dotted lines and open symbols represent the theoretical Arrhenius model)

All the determinations suggest a Newtonian behavior of the samples. The viscosity decreases in the order: η Lotexan-N $>$ η Tegosivin HL 100 $>$ η Silres® BS 290.

The oscillatory tests indicate a more stable structure of the Silres® BS 290 solution. This one also has the lowest viscosity, very close and even lower than water, thus preventing some unwanted effects in application: an undulated wetting surface, entrapping air bubbles at all rates of application, a small depth of penetration.

VI. 3. Synthesis and characterization of a new water repellent product

VI. 3. 1. Introduction

For the present study, a new compound, based on 3-(trimethoxysilyl)propyl methacrylate (TMSPMA), was synthesized and characterized using various methods.

The sol-gel process has been found to be successful in applications in the stone conservation field. The products obtained through this process polymerize within the pores of the stone by means of a classic sol-gel process, thereby strengthening the material. Their advantages are known: the low viscosity of some products allow them to deeply penetrate into porous stone; after polymerization, which occurs upon the contact with the environmental moisture, a stable gel with a silicon-oxygen backbone is formed.

Hybrid inorganic-organic composites derived by sol-gel processing are materials that can be potentially designed for a wide range of applications. Structural diversity is achieved by controlling the relative ratio of organic *vs.* inorganic content, the level of structural complexity of the organic component and its nature, the chemical composition of the inorganic precursor molecule, and the reaction conditions used to synthesize the composites. Thus, this synthetic framework offers the promise of engineered multicomponent composite materials designed for specific and targeted applications, for instance in waveguides [76-78], optical biosensors [79] or thermally stable non-linear optical materials [80].

Among the sol-gel precursors, 3-(trimethoxysilyl)propyl methacrylate (TMSPMA) is one of the most important compounds with dual-network forming capability, widely used in the preparation of organic/inorganic hybrid nanomaterials [81, 82]. It has a polymerizable methacrylate group at one end and the alkoxy silane groups able to form inorganic networks *via* sol-gel route at the other end.

Synthetic polymeric materials, having water repellent properties, are being used as protective materials for stone. A class of water dispersed polymers widely used in restoration of cultural heritage is represented by polyacrylates, thermoplastic materials derived from the polymerization of different esters of acrylic acid. Polyacrylates and methacrylates are among those more frequently used: superficial treatments which include them are meant to have both protective and consolidating properties. Polyacrylates are also characterized by good physico-chemical properties like flexibility, transparency, lack of color and long-term durability. Due to their characteristics of

reduced drying time, optical clarity, mechanical properties, adhesion and chemical stability, and stability against oxygen and UV radiation, one of their most important uses is in the formulation of paints and surface coatings. Numerous restoration works confirm the large scale employment of polyacrylates due to their excellent properties of flexibility, transparency and ease of application.

These materials can form a transparent, dense, uniform thin films on various substrates. The hybrid materials can combine the flexibility, density, toughness and easy processability of the organic component with the hardness, chemical and weather resistance of the inorganic component, thereby exhibiting a multifunctional behavior. The $-\text{Si}(\text{OR})_3$ groups are readily hydrolyzed into $-\text{Si}(\text{OH})_3$ groups, which can subsequently be turned into crosslinked polysilsesquioxane by polycondensation.

Silsesquioxanes are a family of compounds characterized by a ratio of 1.5 between the silicon and oxygen atoms [83] and their structures can be expressed in the general formula $(\text{R} - \text{SiO}_{1.5})_n$ ($n = \text{even number}$) [84]. The silsesquioxane family is now recognized to have enormous potential as a building block for various advanced materials, and its applications as organic-inorganic nanocomposites can be found in catalysis, coordination chemistry and material science. The hydrolysis and condensation of substituted alkoxy silanes, $\text{R} - \text{Si}(\text{OR}')_3$, containing a nonhydrolyzable $\text{Si} - \text{C}$ bond, are known to give a variety of silsesquioxanes with various substituent groups and cage structures [83, 85]. If the polymer self-assemblies contain the $-\text{Si}(\text{OR})_3$ groups, organic/inorganic hybrid materials may be produced after the gelation of the preformed self-assemblies [86]. Through self-assembly of TMSPMA-based block copolymers in solution, various organic/inorganic hybrid morphologies, including spheres [87], vesicles [88, 89] and compound vesicles [90] with silica oxide network have been obtained by a gelation process occurring only in the TMSPMA domains of the preformed aggregates.

This subchapter reports the synthesis of a hybrid (nano/micro) composite with organized domains (spherical, tubular or lamellar) obtained through radical polymerization of 3-(trimethoxysilyl)propyl methacrylate in the presence of a surfactant (dodecylamine) with a primary amine group, able to form hydrogen bonds.

The discovery of the surfactant-templated synthesis in the early 1990's permitted the obtention of ordered mesoporous silica gels. The surfactant, added in a concentration below its critical micellar concentration (cmc), acts as a structure-directing agent during the polymerization process. The main advantage of these new materials, called *molecular*

sieves, is their ordered mesopores with uniform size, which is determined by the size of the surfactant aggregate.

This type of synthesis prevents the cracking of the gel during the drying phase for two reasons:

(1) the surfactant creates a coarsening of the gel network thus reducing the capillarity pressure;

(2) the decrease of the surface tension provided by the surfactant also reduces the capillarity pressure.

Therefore, the purpose was to obtain a crack-free gel by using a surfactant as a template for the pores of the gel.

The selected materials represent a unique combination of three different components namely methacrylate, hydroxyl functionality and silicon-alkoxy groups. The hydrolyzable silicon alkoxyde at one end can be condensed to form an inorganic Si – O – Si network and simultaneous polymerization of the methacrylate group at the other end can conduct to a highly crosslinked, dense networked structure [91].

VI. 3. 2. Synthesis

Synthesis of the hybrid composite with silsesquioxane units

The nanocomposite samples were obtained through radical polymerization of TMSPMA in the presence of the surfactant (dodecylamine) and 2,2'-azobis(2-methylpropionitrile) (AIBN). The surfactant was added in a concentration above its critical micellar concentration (cmc) in order to act as a structure-directing agent during the polymerization. The matrix undergoes a free radical polymerization and the silica phase polymerizes in a sol-gel process. The reaction was acid catalyzed in a water / hydrochloric acid solution by keeping the HCl / TMSPMA molar ratios equal to $1.85 \cdot 10^{-2}$ and the H₂O / TMSPMA ratio smaller than 2 (stoichiometrically deficient amount of water). AIBN (2 wt% of TMSPMA mass) was used as thermal initiator of the organic monomer polymerization.

The mole ratios of the mixture were: 1 TMSPMA : 2 H₂O : 11 ethanol : 0.004 HCl : 0.003 dodecylamine.

TMSPMA containing dodecylamine in an ethanol solution was mixed with AIBN and mechanically stirred for 30 minutes and then added to a hydrochloric acid solution (HCl 37%, Aldrich) and distilled water, and stirred for other 30 minutes. The

polymerization process was carried out at 60° C for 48 h. After solvent evaporation in vacuum, the product was obtained as a transparent solid at room temperature and dried in vacuo at 60° C for three days.

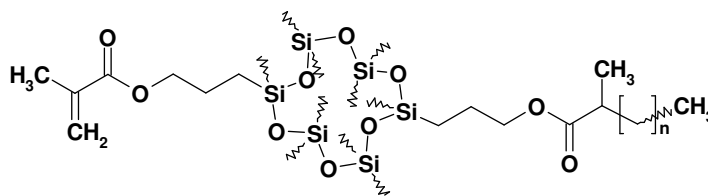


Fig. 62. Schematic structure of TMSPMA hybrid composites

VI. 3. 3. Chemical characterization

The crystallographic structure of the TMSPMA compound and of the TMSPMA polymer mixed with stone powder was studied using X-ray diffraction and FT-IR spectroscopy.

The X-ray diffraction diagram of TMSPMA compound is shown in Figure 63. The X-ray diffraction diagram evidences the presence of a narrow crystalline peak at 26.640 (3.343 Å), attributed to polyhedral silsesquioxanes that are normally crystallizable, as opposite to the ladder amorphous ones. At the same time, the broadening of the diffraction peak is probably due to the fact that the crystallite size is in nanometer scale. The reflection from 26.640 (3.343 Å) is associated with the hexagonal crystalline structure from 101 diffraction plane, with a hexagonal unit cell of $a = 4.91$ and $c = 5.4$ Å, besides a value of 8.14 nm of the crystallite size.

Quartz

R/R0: 1.35

FWHM(30) : 0.999

Crystallite size (Scherrer): 81.4 Å

I/Icor: 2.9

System: Hexagonal

Space group: P3121 (152)

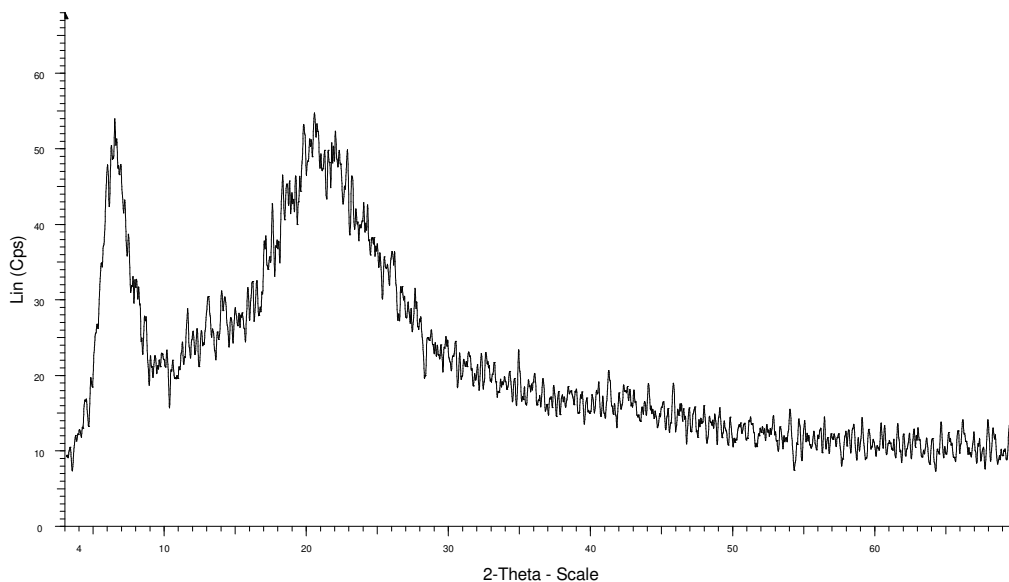


Fig. 63. The X-ray diffraction diagram of the TMSPMA compound

The FT-IR spectrum of the TMSPMA is shown in Figure 64. A characteristic band corresponding to O – H stretching vibrations of the hydroxyl groups due the strong hydrogen bond of intramolecular and intermolecular type appears at around 3485 cm^{-1} . The hydrogen bonds are playing a crucial role in such conformational arrangements, creating hydrophobic associated domains. Two small peaks at 3750 and 3106 cm^{-1} , attributed to silanols (isolated and geminal) and hydrogen-bonded silanol groups, respectively, can be also distinguished, while the vicinal ones and the physical adsorbed water are characterized by adsorption bands in the $3000 - 3750\text{ cm}^{-1}$ range. The presence of these peaks support Sommer's hypothesis that silane bonds are converted to silanol bonds during gelation. The silanol bonds are very reactive and subsequent condensation of adjacent silanol bonds increases the area of the siloxane network peak in the FT-IR spectra. The C – H alkyl stretching band can be observed in the $2894 - 2956\text{ cm}^{-1}$ range. The absorption peak from 1719 cm^{-1} may be attributed to the stretching vibration of carbonyl groups, while the one around 1637 cm^{-1} can be assigned to acrylic double bonds (C = C), indicating that not all of these have reacted.

The vibrational spectra of the silicates can be divided into two regions. The first region covers the $4000 - 1600\text{ cm}^{-1}$ frequency range, where stretching and bending vibrations of water molecules appear. The second region (below 1300 cm^{-1}) includes the vibrations due to the silicate layer and charge-balancing cations. Generally, the $\gamma_{\text{as}}(\text{Si} - \text{O} - \text{Si})$ modes appear in the $1200 - 1000\text{ cm}^{-1}$ region, whereas $\gamma_{\text{s}}(\text{Si} - \text{O} - \text{Si})$ appears in

the 700 – 400 cm^{-1} region. With increasing silica contents of the hybrid composites there is an intensity increase of some characteristic peaks of the silica phase such as the Si – O – Si stretching, the presence of such type of bonds confirming the existence of covalent linkages between the organic groups and the silica, which leads to a better compatibility and to a crosslinking network between the organic and inorganic components. For TMSPMA compound, Si – O – Si bands can be observed at 1169 cm^{-1} and 1120 cm^{-1} . The peak from 940 cm^{-1} is associated to the Si – OH asymmetric stretching due to incomplete condensation of the Si – OH bonds. These silanol groups are able to continue reactions with other molecules and produce new siloxane bridges. Additional peaks at around 698 – 785 cm^{-1} (for symmetric Si – O – Si stretching vibration) can be also seen.

Due to the trimethoxysilane groups, TMSPMA exhibits self-assembling properties. Generally, the trialkoxysilyl end groups of various alkyltrialkoxysilanes ($\text{R} - \text{Si}(\text{OR})_3$), when hydrolyzed, enable polycondensation into crystalline or amorphous silsesquioxanes with complex (T cube-like or ladder-like) structures. Such type of silsesquioxane structures generated during the polycondensation, either polyhedra or ladders, may be inferred from FT-IR spectroscopy observing the location of bands characterizing the antisymmetric Si – O – Si stretching vibrations. The appearance of a single band centered near 1120 – 1130 cm^{-1} may be taken as good evidence for the presence of a polyhedral structure, while the presence of two bands centered near 1040 cm^{-1} and 1120 – 1130 cm^{-1} is characteristic of a cis-syndiotactic ladder configuration. The cage or ladder-like silsesquioxane configurations are largely influenced by the type of organic group bonded to the silicon atom, taking into account a steric effect promoting intramolecular condensation. Some authors suggest that the ladder-like structure is easy to form if the group R is a simple group such as – H, – CH_3 , – Cl etc. owing to difficult interactions with each other, while the presence of bulky organic groups such as – $\text{CH}_2\text{CH}_2\text{CH}_2\text{OCOC}(\text{CH}_3) = \text{CH}_2$, – $\text{CH}_2\text{CH}_2\text{CH}_2\text{OCH}_2\text{CH}[\text{O}]\text{CH}_2$, – $\text{CH}_2\text{CH}_2\text{CH}_2\text{NH}_2$ etc. favor a cage structure leading to a narrow distribution of polyhedra due to the presence of a bulky organic substituent and the higher interactions with each other. At the same time, other different structures are frequently proposed such as randomly connected three-dimensional networks of trifunctional monomers, ladder structures, and a combination of linear, ladder, and cage-like fragments. In the present study, the presence of one band in both FT-IR spectra, centered near 1120 – 1130 cm^{-1} , marks out the polyhedral structures formed by Si – O – Si bonds. The intensities of these bands in

the case of hybrid composites are increasing with oligomeric silsesquioxane content and narrowing of this band indicates that silsesquioxane environment for hybrid composites is more homogeneous.

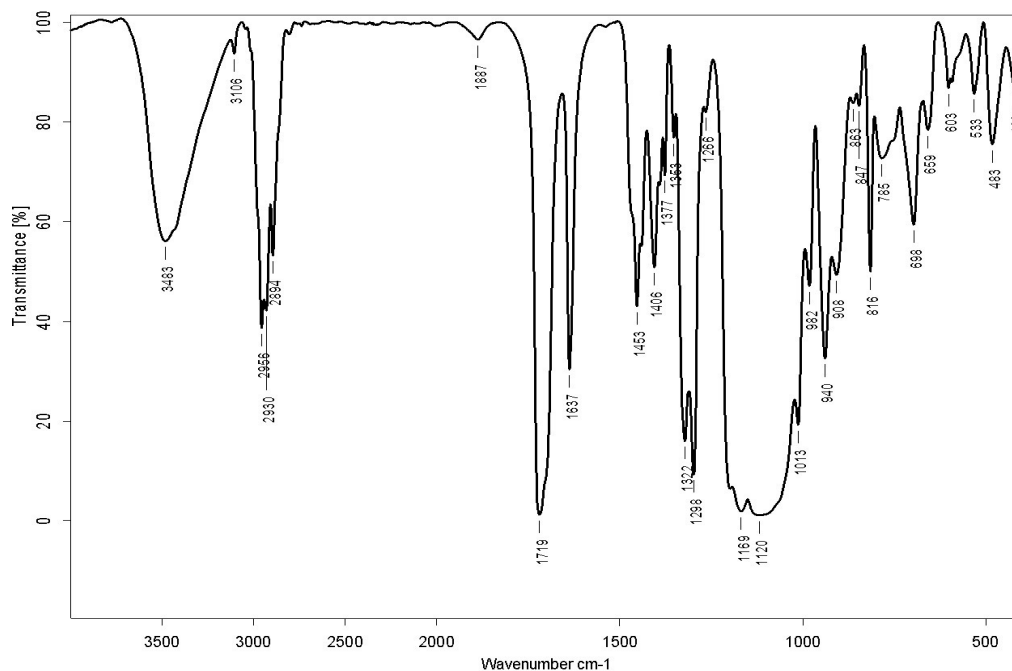


Fig. 64. FT-IR spectrum of TMSPMA compound

Silica has a complex morphology that lies down from nanometer to micron size scale. Manipulation of the morphology at each structural level determines the properties of the product. The physical properties of silica essentially depend on the synthesis procedure, the most important ones being represented by the specific surface, the dimensions of the primary particles and aggregates, as well as by the porosity. The differences between these physical characteristics are correlated with the organization form of the silica particles (aggregates or agglomerates). In the silica structure, three types of particles organization can be distinguished. At the smallest size scale, quasi-spherical primary particles ranging from 3 to 500 nm in diameter are found, these ones controlling the specific surface area of the powder. Under the effect of colloidal forces, the primary particles are clustered to form disordered aggregates at the 0.1 μm size scale. Typically, aggregates are further linked to form agglomerates that extend up to hundreds of μm in size. The dimension of the primary particles, as well as the density and the aggregation and agglomeration degrees influence the porosity and the specific surface of

the silica. SEM characterization was conducted in order to evaluate the morphology of the hybrid composites (Figure 65).

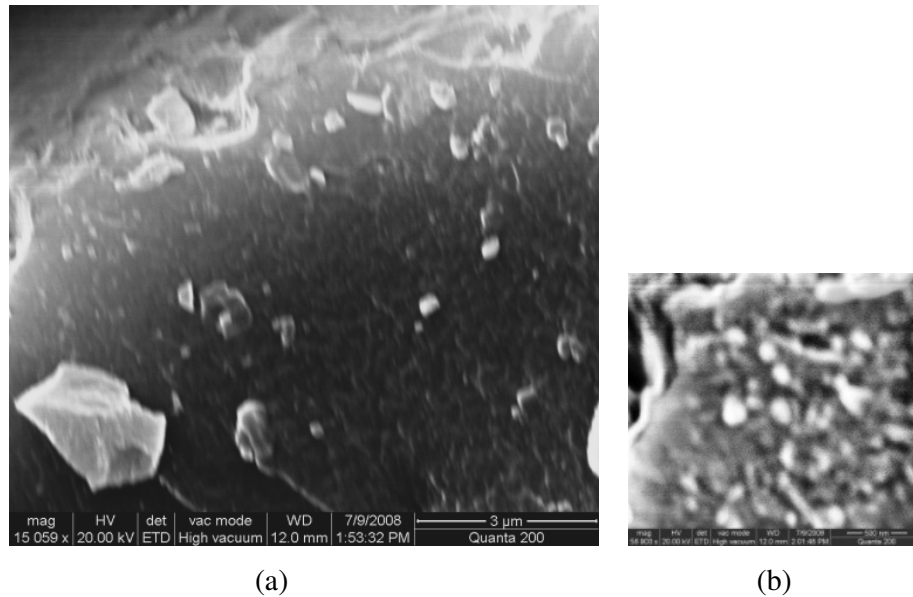


Fig. 65. SEM photographs for TMSPMA (a) 3 μm, (b) 500 nm

The SEM examination of the hybrid compounds revealed the presence of small silsesquioxane aggregates ranging from 100 – 800 nm. As can be seen, the surfactant directed the silsesquioxanes into 3-D spherical arrangements that, at a certain scale, are connected together into tubular and continuous structures while, in the polymeric matrix, some ordered regions consisting of a self-assembly of semi-cylindrical shells can be observed.

Polymer-stone mixture

The samples were prepared by casting the same amount of TMSPMA polymer onto powder stones and drying in vacuum at 30° C. Due to the different composition of the stones, the deposited polymer has different behaviors. In the case of Laspra, the polymer maintains its crystalline polyhedral structure while in the case of Repedea it adopts a different amorphous configuration (ladder). In both cases, a decrease of the signal corresponding to calcite is evidenced as a consequence of the acid environment.

TMSPMA cast on Laspra sample

The peaks of Laspra powder sample mixed with TMSPMA polymer is presented in Figure 66.

The intensities of ankerite and dolomite peaks are the highest, followed by calcite's intensities; the quartz is very low represented.

By adding the polymer, the intensity of all peaks drastically decreases, indicating a decrease in the crystallinity degree. The stone structure, in terms of order, is affected, and the resulted compound presents a wide halo at angles $< 30^\circ$, which is characteristic of polymers, with the peaks of ankerite, calcite and dolomite.

From Table 12, one can see that the crystallite size of ankerite and calcite is increasing, for quartz it remains practically the same and for dolomite it decreases.

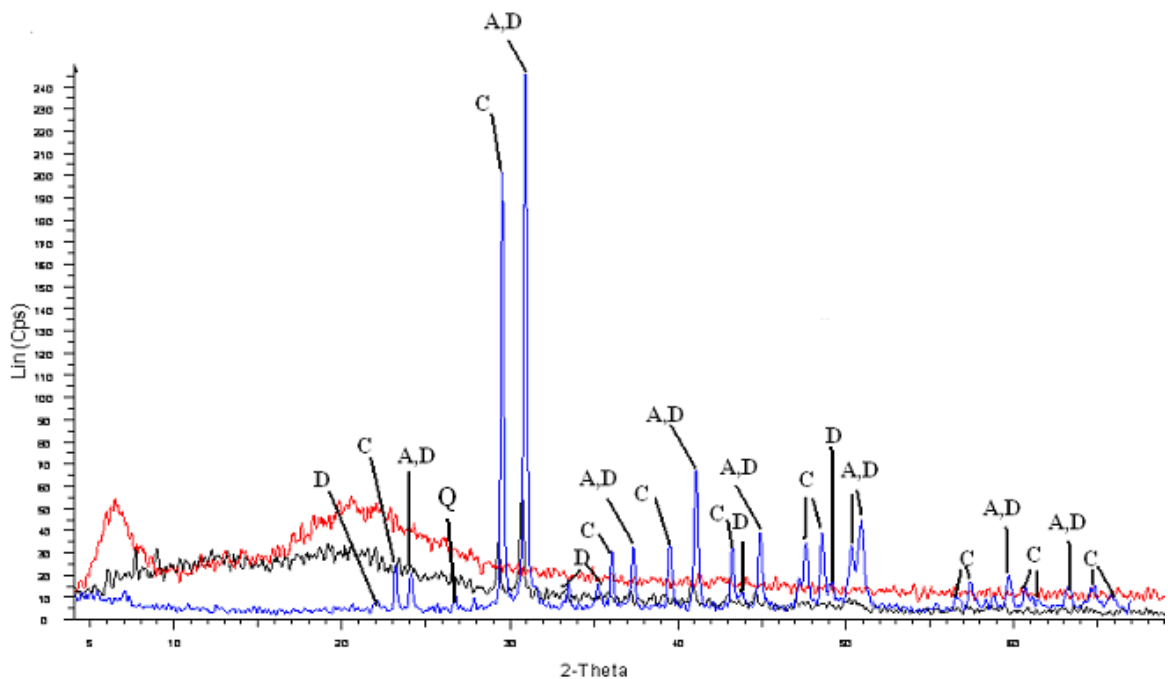


Fig. 66. XRD patterns of Laspra (blue), polymer (red), stone and polymer mixture (black)

Table 12

Laspra	Ankerite Ca(Fe ₊₂ ,Mg)(CO ₃) ₂		Quartz SiO ₂	Calcite CaCO ₃	
Fitting parameter R/R ₀	1.18		1.21	1.2	
Concentrations (%)	C 10.5 O 42.1 Mg 5.3 Ca 17.6 Fe 24.5	CO ₂ 38.6 Excess -7.0 MgO 8.8 CaO 24.6 Fe ₂ O ₃ 35.0	O 53.3 Si 46.7	C 12.0 O 48.0 Ca 40.0	CO ₂ 44.0 CaO 56.0
FWHM	0.159		0.443	0.0956	
Crystallite size (X)	511.7		183.5	850.8	
I/I _{cor}	2.8		3.4	3.2	
System	Rhombo.H.axes		Hexagonal	Rhombo.H.axes	
Space group	R-3 (148)		P3221 (154)	R-3c (167)	
Cell param.	a = b = 4.82870 c = 16.15200		a = 4.91344 c = 5.40524	a = 4.99100 c = 17.06200	

Dolomite CaMg(CO₃)₂

C 13.0% CO₂ 47.7%

O 52.1%

Mg 13.2% MgO 21.9%

Ca 21.7% CaO 30.4%

FWHM(30): 0.247°

Crystallite size (Scherrer): 329.1 Å

I/I_{cor}: 2.5

System: Rhombo.H.axes

Space group: R-3 (148)

a: 4.80690

c: 16.00200

TMSPMA cast on Repedea sample

The peaks of Repedea sample mixed with TMSPMA polymer (Figure 67) indicate no change in the composition and the presence of calcite, magnesian calcite, quartz and aragonite. The intensity of quartz peaks at 20.860 (4.25 Å) and 26.640 (3.343 Å) associated with the hexagonal crystalline structure from 100 and respectively 101 diffraction plane are drastically increasing in the mixture. The intensities of calcite and magnesian calcite peaks at 23.049 (3.855 Å) and 29.395 (3.036 Å) are decreasing in the mixture as compared to the pure stone.

One can see, in Table 13, that the crystallite size is decreasing for all compounds.

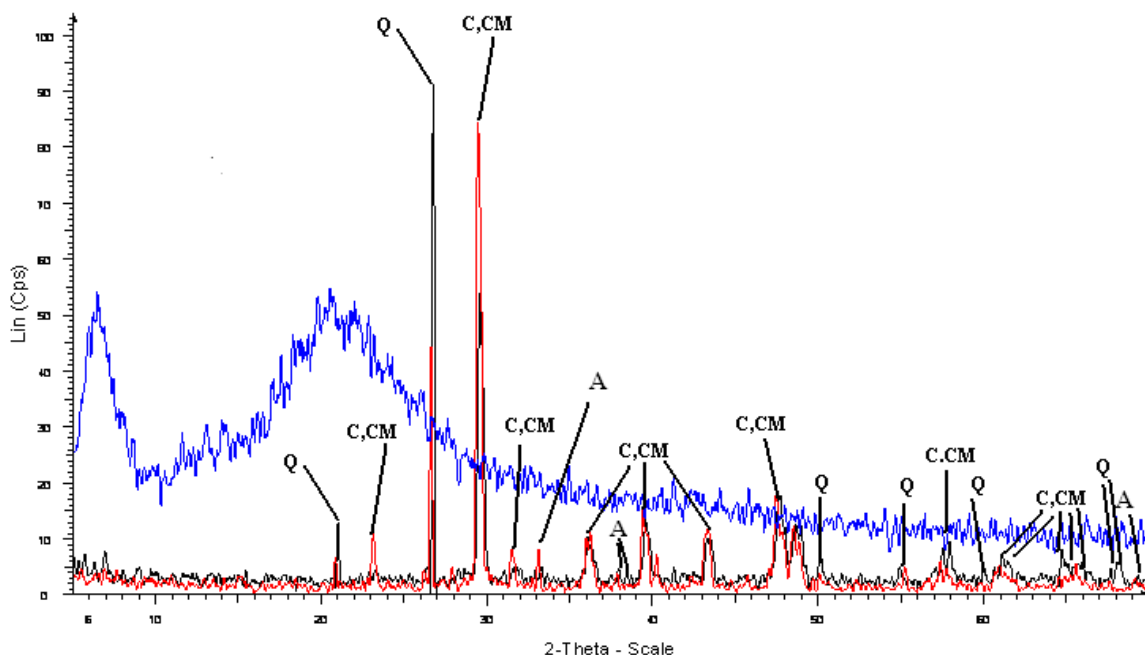


Fig. 67. XRD patterns of Repedea (red), polymer (blue), stone and polymer mixture (black)

Table 13

Repedea	Calcite CaCO ₃		Quartz SiO ₂	Calcite, magnesian (Ca,Mg)CO ₃		Aragonite CaCO ₃	
Fitting parameter R/R ₀	0.962		0.996	0.894		1.01	
Concentrations (%)	C 12.0 O 48.0 Ca 40.0	CO ₂ 44.0 CaO 56.0	O 53.3 Si 46.7	C 13.0 O 52.1 Mg 13.2 Ca 21.7	CaO 30.4 MgO 21.9 CO ₂ 47.7	C 12.0 O 48.0 Ca 40.0	CO ₂ 44.0 CaO 56.0
FWHM	0.464		0.16	0.264		0.446	
Crystallite size (X)	175.1		509.9	308.6		182.5	
I/I _{cor}	3.2		3.1	1.9		1.1	
System	Rhombo.H.axes		Hexagonal	Rhombo.H.axes		Orthorhombic	
Space group	R-3c (167)		P321 (154)	R-3c (167)		Pmcn (62)	
Cell param.	a = b = 4.99100 c = 17.06200		a = 4.91400 c = 5.40600	a = b = 4.94260 c = 16.85200		a = 4.96110 b = 7.96720 c = 5.74070	

The FT-IR study provides details about the reaction between TMSPMA and the two stone samples (Figure 68). For Repedea, as the reaction progresses, the 3375 cm⁻¹ band corresponding to O – H stretching vibrations of the hydroxyl groups decreases and a redistribution of the intensities in the 3100 – 3750 cm⁻¹ region can be noticed. At the same time, an intense broad band with a complex structure at around 1100 – 1000 cm⁻¹ argues for the formation of siloxane species (Si – O) on the surface and can be evidenced for both samples, the bands being assigned to a silsesquioxane network formed through condensation and self-assembling of silanols. The concentration of silsesquioxane units is of approximately 40% higher in the case of Repedea stone. It is to be noted that this condensation did not go to completion. The appearance of two bands for Repedea, at 3135 cm⁻¹ (H-bonded silanols) and 3745 cm⁻¹ (isolated and geminal Si – OH) indicates the presence of non-coupled silanols (Si – OH), these small peaks hence supporting Sommer's hypothesis that silane bonds are converted to silanol bonds during gelation. Silanol bonds are very reactive and subsequent condensation of adjacent silanol bonds increases the area of the siloxane network peak in the FT-IR spectra.

As opposite to Repedea, Laspra behaves differently: being isotropic and relatively homogeneous, in parallel with the hydrolysis and polycondensation reaction, the adsorption of water becomes competitive and the increase of the band from 3432 cm⁻¹ is

registered. The C – H alkyl stretching band can be observed at 2850 – 2956 cm^{-1} . The absorption peak from 1720 cm^{-1} may be attributed to the stretching vibration of carbonyl groups, while the one around 1637 cm^{-1} can be assigned to acrylic double bonds (C = C), indicating that not all these groups have reacted, as well as an overlapping with the deformation mode of adsorbed molecular water in the pores of the stone. As a consequence of the presence of an acid medium (pH = 4), the CO_3^{2-} asymmetric stretching from calcite is registering a small decrease in case of Repedea, while in the case of Laspra, a dramatic reduction can be evidenced, this behavior being attributed to the reaction between calcium carbonate and hydrochloric acid, with the formation of calcium chloride. Other carbonates such as dolomite do not react as easily with these acids as calcite does and this differentiates these somewhat similar minerals more readily. Since no dolomite is present in the structure of Repedea, one can conclude that this type of stone is acid-resistant, a valuable information as far as the stone is to be used in conditions favorable for acid rains.

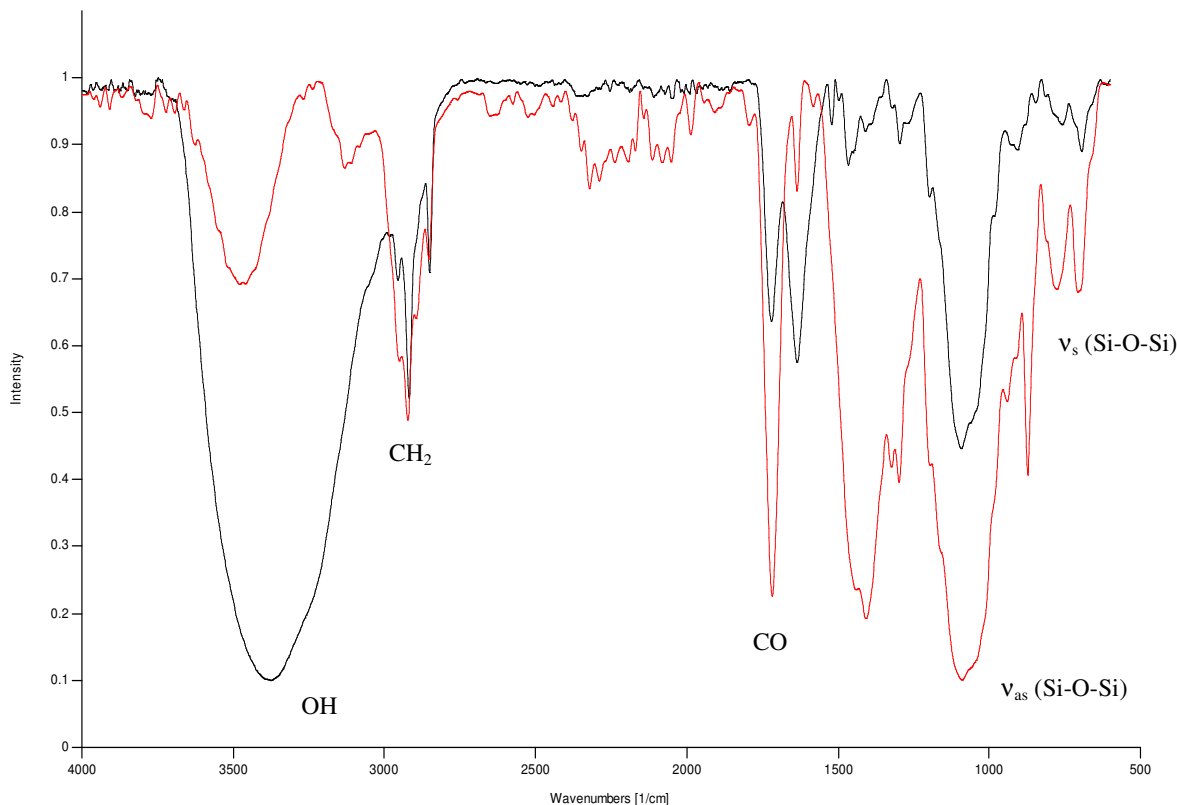


Fig. 68. FT-IR spectra of TMSPPMA compound cast on both stone samples (— Laspra, — Repedea)

The present investigation represents an attempt to design and propose a water repellent product able to assure, on stone surface, functional groups providing both water repellency and strengthening properties.

VI. 3. 4. Thermal stability

Thermogravimetric analysis of TMSPMA

The thermogravimetric analysis (TGA) was performed under nitrogen flow ($20 \text{ cm}^3 \text{ min}^{-1}$) at a heating rate of $10^\circ \text{ C min}^{-1}$ from 25 to 900° C with a Mettler Toledo model TGA/SDTA 851 instrument. The initial mass of the samples was of 4 – 5 mg of TMSPMA.

Differential scanning calorimetry (DSC) analysis was performed using a Mettler Toledo DSC 1 instrument (Mettler Toledo, Switzerland) operating with version 9.1 of Stare software. The samples (2 – 4 mg of TMSPMA) were encapsulated in aluminum pans having pierced lids to allow escape of volatiles. A heating rate of $10^\circ \text{ C min}^{-1}$ and nitrogen purge at 120 mL min^{-1} were employed.

Figures 69 and 70 present the TG and the DTG curves of the TMSPMA sample. Detailed TGA data are reported in Table 14.

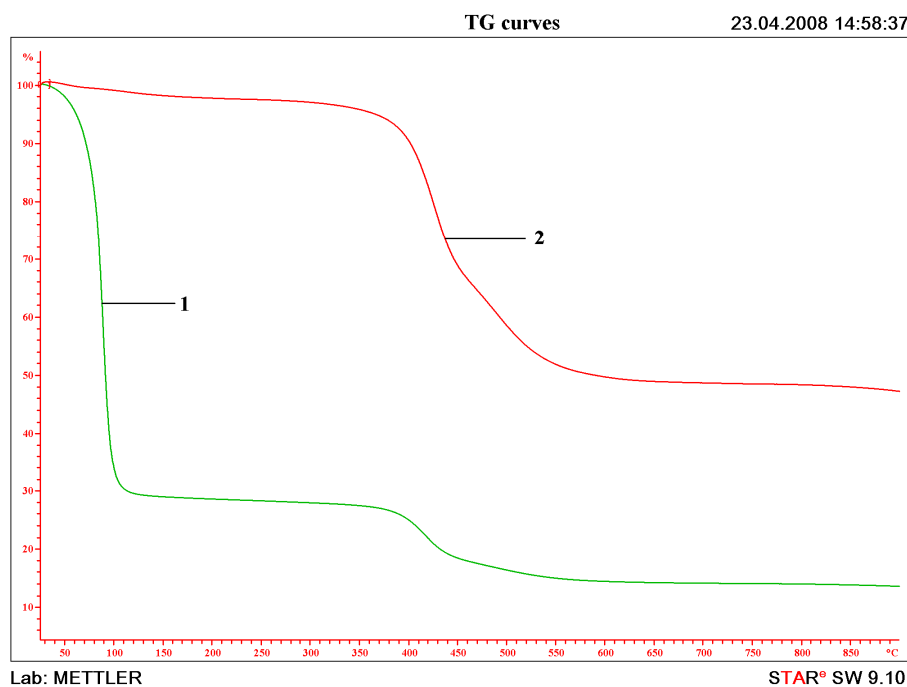


Fig. 69. TG curves of TMSPMA samples (1 – with solvent; 2 – solid form)

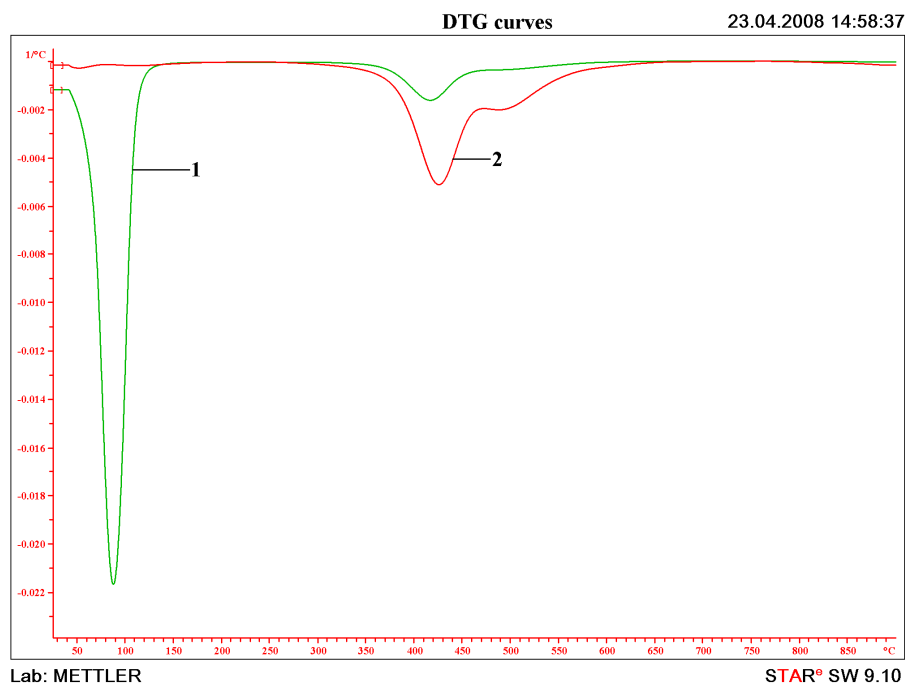


Fig. 70. DTG curves of TMSPPMA samples (1 – with solvent; 2 – solid form)

For both samples, the degradation processes are not complete, in each case a residue being left. Table 14 reveals the TG data such as T_i – the initial thermal degradation temperature, T_m – the temperature corresponding to the maximum degradation rate, T_f – the final temperature at which the degradation process for each stage ends, mass loss (W%), corresponding to each stage, and DTA characteristics (endo or exo).

Table 14. Thermogravimetical parameters (sample numbering as in Figs. 69 and 70)

Sample	Stage of thermal degradation	T_i	T_m	T_f	W%	DTA characteristic data
1	I	54	80	98	71.41	endo
	II	384	416	533	14.59	exo
2	I	67	85	143	3.03	endo
	II	380	428	447	28.46	exo
	III	447	501	570	21.70	exo

The degradation process exhibited two and three maxima of decomposition. The TG and DTG curves of the polymer samples, obtained under inert atmosphere, indicate a

complex degradation pathway. The comparison between the thermogravimetric curves shows that the positions of the DTG maxima in stage II are similar for both samples.

The thermogravimetric values for the last stage were processed by the Freeman – Carroll differential method and the results are presented in Table 15.

Table 15. Kinetic characteristics corresponding to the last degradation step (sample numbering as in Figs. 69 and 70)

Sample	Stage	n	Ea (kJ/mol)	lnA
1	II	1.60±0.009	258.77±1.42	40.51±0.25
2	II	1.20±0.007	216.77±0.79	32.41±0.14

n = reaction order; Ea = activation energy; A = pre-exponential factor

The kinetic characteristics suggest the complexity of the thermal degradation that takes place through successive reactions accompanied by exothermal processes.

The DSC measurements were performed on samples of 2 – 4 mg in the range of – 80 to 200° C at a heating rate of 10° C min⁻¹ (N₂ atmosphere: 120 L min⁻¹). The glass transition temperature (Tg) was evaluated with the Stare-software version 9.10 (Mettler Toledo, Switzerland; calibration with indium and zinc). The DSC curve (Fig. 71) reveals the Tg values for sample 2 (Tg = – 49.24° C).

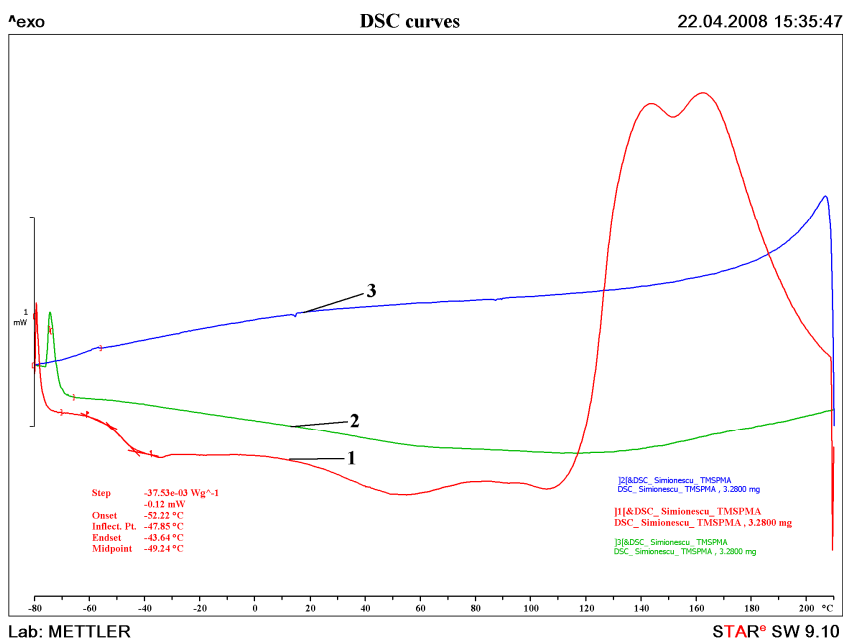


Fig. 71. DSC curve of TMSPMA sample (solid form) (1- first heating -80→200° C; 3- cooling 200→ -80° C; 2- second heating -80→200° C)

In the experimental temperature range (-80° to 200° C) the DSC thermogram of TMSPMA displayed a single glass transition temperature value at -49.24° C, attributed to the oligomeric silsesquioxane moieties. Such a low Tg value for a highly crosslinked silsesquioxane polymer demonstrates that the polymer network possesses a substantial molecular freedom, which is inconsistent with a ladder-like structure composed by small cycles. Therefore, this type of composite consists primarily of a combination of linear, ladder and cage-like silsesquioxane fragments. This structure is leading to the formation of nanocavities within the TMSPMA compound.

The two competitive factors affecting the Tg value in silsesquioxane-containing composites are the restriction effect of silsesquioxane cages on polymer chain motion (that enhance the glass transition temperature) and the inclusion of the bulky silsesquioxane group that can give rise to the increase of the free volume of the system and results in the depression of the Tg [92].

Depending on the nature of the interactions of the silsesquioxane cages with the polymer matrix (functionalities of silsesquioxane, type of polymer matrix and organic groups in silsesquioxanes), the silsesquioxane-containing (nano/micro) composites can display higher [93] or lower [94] Tg values as compared to the parent polymers. In the TMSPMA hybrid composite the incorporation of nanosized silsesquioxane crosslinkers increased the Tg value as compared to pure silsesquioxanes (-55° C). This increase is due to the separation of polymeric chains caused by the bulkiness of the silsesquioxane fragment cages.

The thermal degradation of the samples in nitrogen atmosphere is a two and three steps reaction. The peak width of DTG curve of the two degradation steps has a value of the temperature near the maximum rate of weight loss. One can conclude that TMSPMA is a very resistant compound as far as the thermal degradation is concerned, its thermal degradation beginning at around 380° C.

VI. 3. 5. Rheological properties

Rheological analysis of TMSPMA

Rheological measurements were carried out on a Physica MCR 501 rheometer (Anton Paar) equipped with a Peltier device for temperature control. The measurements were performed using a plate-plate geometry with a diameter of 50 mm. The gap was fixed at 0.300 mm due to the reduced viscosity of the samples.

Both rotational (flow and viscosity curves) and oscillatory tests (amplitude sweep and frequency sweep) were performed. An oscillatory temperature sweep was also carried out for the solutions.

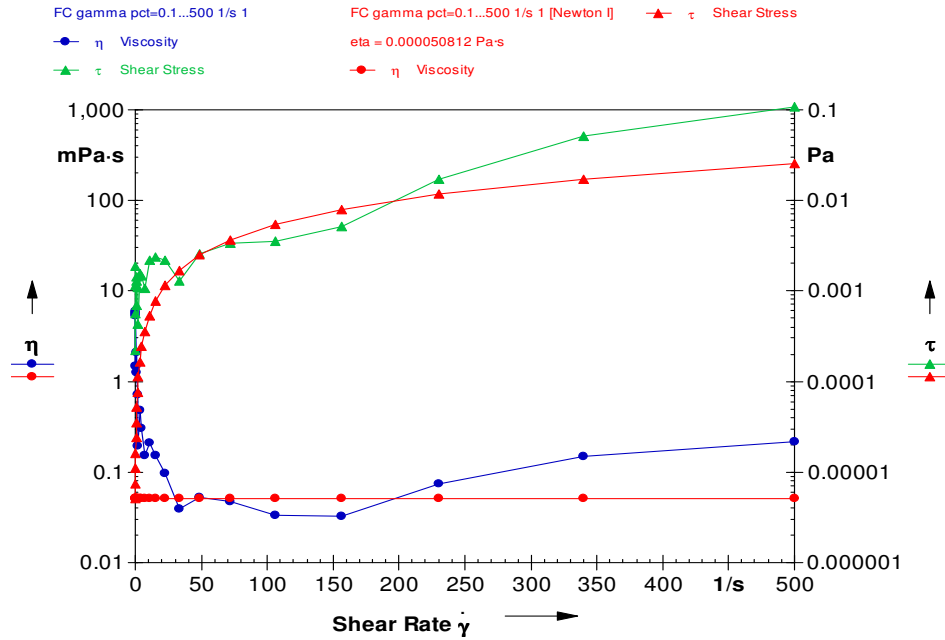


Fig. 72. Flow curves for TMSPMA

The flow curve was measured under isothermal conditions ($20^{\circ}C$). In this range the sensitivity of the instrument is surpassed. The flow curve for the sample and the dependency of the shear stress on the shear rate are presented in Fig. 72.

TMSPMA sample behaves as a Newtonian fluid with the viscosity independent of the shear rate, but to have a fully developed Newtonian structure it is recommended to use a shear rate higher than $10 s^{-1}$. This shear rates are the most suitable for the application procedure. The characteristic viscosity of the investigated sample is $\eta = 0.5 mPa \cdot s$.

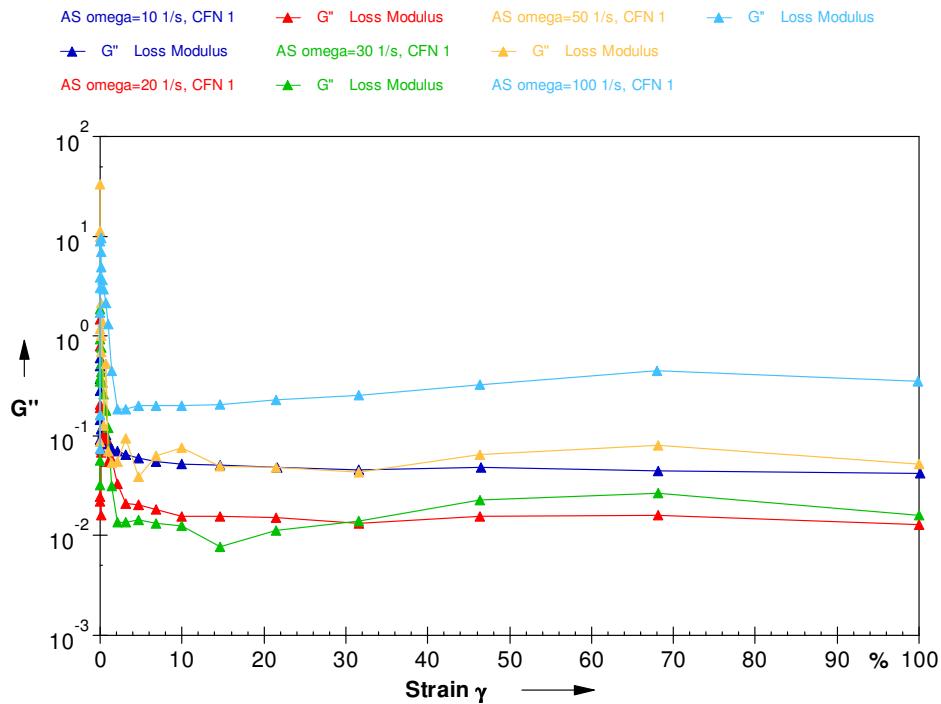


Fig. 73. Amplitude sweep of TMSPPMA

To prove once more the Newtonian character of the analyzed samples, oscillatory tests were performed. As can be seen from Figure 73, loss modulus is independent on strain amplitude and increases with the angular frequency. The increase of the loss modulus with two orders of magnitude when the angular frequency increases suggests the necessity to use a intense movement for a better quality of the surface during application.

For the frequency sweeps (Fig. 74) the amplitude of deformation (γ) was kept constant while the angular frequency (ω) was varied between 1 and 100 rad/s. The effect of the amplitude of deformation on loss modulus and complex viscosity was taken into consideration. The sample has a loss modulus almost independent on the frequency for more than two decades.

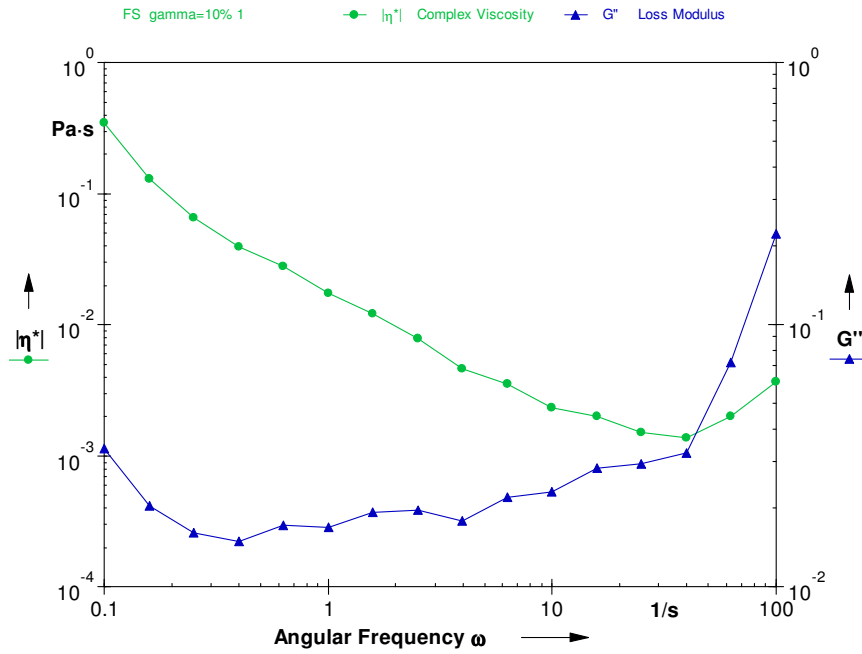


Fig. 74. Frequency sweep for TMSPMA

An oscillatory temperature sweep was also carried out and showed the viscosity decrease with increasing temperature (Fig. 75). The activation energy was calculated as being 1.9706 kJ/mol.

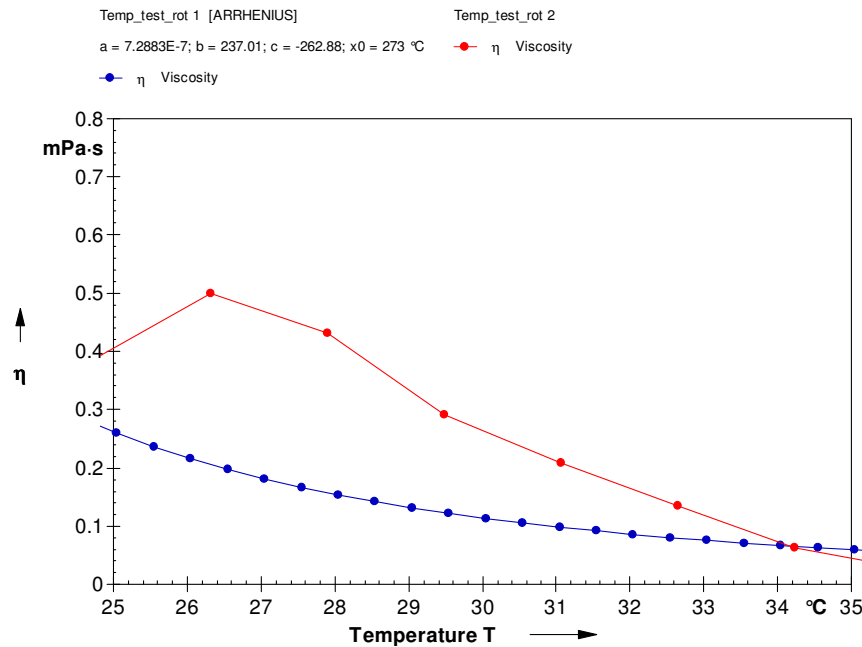


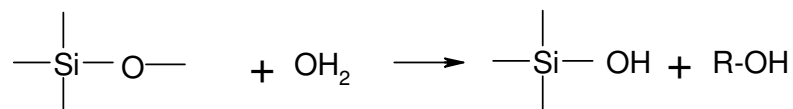
Fig. 75. Temperature sweep for TMSPMA

All experimental results suggest a Newtonian behavior of the sample, with a viscosity lower than water – an indication of good penetration ability within the porous structure of the stones.

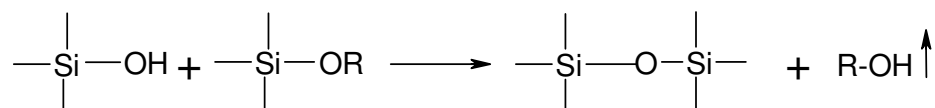
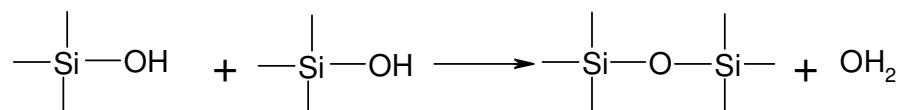
VI. 4. Conclusions

Chemistry of silicone based water repellents – their adhesion to carbonate stone

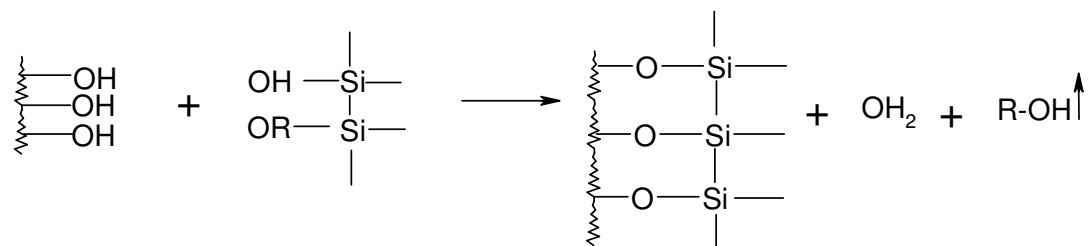
The commercial silicone-based water repellents (Lotexan-N, Silres® BS 290 and Tegosivin HL 100) contain reactive alkoxy groups (methoxy and ethoxy) attached to the silicon atoms. The following reactions are possible during the formation of the water repellent film, reactions that involve water coming from the surrounding atmosphere or from inside the stone:



The formed silanol groups are able to further interact to each other or with the alkoxy silanes, giving rise to polysiloxanes with increased molecular weight:



The adherence of the siloxane repellents to stone surface is based on the reaction of the residual OH groups present on the surface with either silanol or alkoxy silane units.



The water repellency of the products is based on the known orientation of the siloxane chains towards polar surfaces with the oxygen atoms close to the surface and the alkyl groups oriented towards the air – film interface.

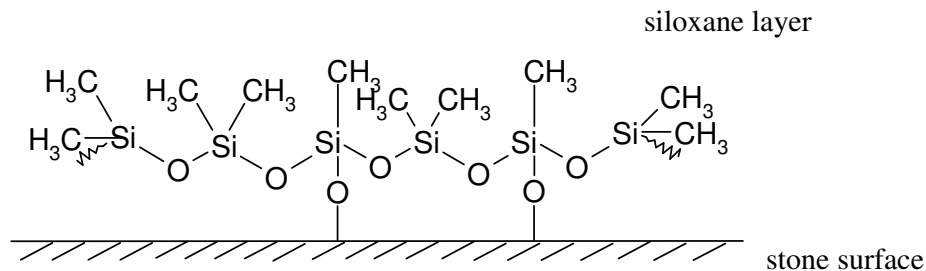
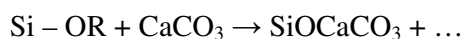
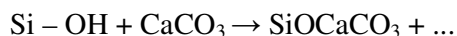
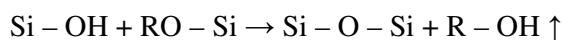
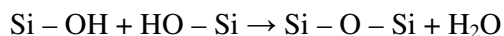
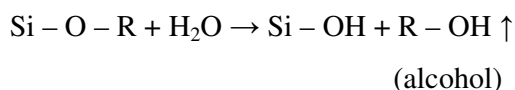


Fig. 76. Orientation of the polysiloxane chain on stone surface

The Si – O / stone linkages are sensitive to hydrolysis, especially in basic or acidic media. Halogenated salts are also known to increase the rate of hydrolysis of such linkages. Thus, the water contained within the stone, which migrates towards the stone surface, or the water coming from the environment and penetrating the repellent film through cracks will break both the linkages of the siloxane chains and the linkages between the siloxane chain and the stone, causing, in the end, the damage of the polymeric film.

Si – O – CH₃ groups appear in the composition of Lotexan-N and Silres® BS 290, while Si – O – CH₂ – CH₃ groups appear in the composition of the third studied water repellent, Tegosivin HL 100. These groups are alkoxy silane reactive groups.



R = alkyl groups.

To improve the water repellency characteristics of the products to be used for the deposition as films on stone surfaces, the following approach has been considered:

An entirely new chemical product, *viz.* a silsesquioxane-based hybrid nanocomposite with self-assembling properties, was designed and synthesized through radical polymerization of 3-(trimethoxysilyl)propyl methacrylate as polymeric matrix in the presence of a primary amine surfactant. The starting compound contains both methacrylate and silica phases. A new class of hybrid nanocomposites were obtained through this approach. In these nanocomposites, silica is dispersed in the form of domains with typical sizes in the nanometer range. The self-assembling properties of the synthesized composites are ascribed to the existence of supramolecular assemblies of surfactants, as well as to the combination of linear, ladder, and cage-like fragments of silsesquioxane type. The incorporation of the surfactant within the sol-gel derived matrix leads to compounds that avoid the cracking of the gel while drying inside the stone.

Among the various techniques used so far for the preparation of hybrid composites, the sol-gel technique is one of the most versatile and widely used. 3-(trimethoxysilyl)propyl methacrylate (TMSPMA) is a sol-gel precursor and, at the same time, a compound with dual network forming capability, *i.e.* through the trimethoxy groups and through the methacrylate double bonds.



In acid pH environment (the used experimental conditions), this compound undergoes the transformation of $\text{H}_3\text{C-O-Si}$ groups into HO-Si groups. The resulting compound will thus contain three -O-H groups (able to undergo condensation reactions) and a methacrylic group -C=C- (able to undergo thermal/photo-induced polymerization reactions) per molecule. As a result, a TMSPMA hybrid composite is obtained.

Cast on stones surfaces, this compound undergoes (a) crosslinking reactions through the polymerization of the methacrylate bonds, and (b) the formation of Si-OH-stone (silica component) bonds. The chemical structure of the compound is a hydrophobic one, and the hydrophobicity increases with ageing, as well as the mechanical properties and film resistance. This hybrid composite material should act both as a water repellent product and as a strengthener of the polymer-stone matrix

the product (~ Si – O – Si – O – moieties) and the structure of the stone that contains O=Si=O crystals; the high number of – OH groups existing on both stone surface and polymeric network determines a better compatibilization between the two materials

- due to the presence of the dodecylamine surfactant, the nanocomposite yields the formation of crack-free gels, this leading to an improved durability of the polymeric protective layer (this aspect will be detailed in Chapter VIII)

- the used synthetic approach yields nano-sized hybrid particles, able to easier and deeper penetrate into porous stones and, once inside, to self-assemble (due to the trimethoxysilane groups), further improving the treated stone durability.

VII. Treated stones characterization

VII. 1. Introduction

The property that has been most searched in surface coatings is water repellency. The logic behind the approach is based on the idea that since water is involved in most forms of stone decay, a treatment that prevents the ingress of water should help to reduce decay. It has also been argued that water repellents should help to prevent resoling, although this claim has not been adequately substantiated.

Water repellency has been provided largely by alkoxysilanes, silicones, and fluoropolymers. The development of the fluoropolymers provides an interesting, but also rare, instance of "tailor-made" products. They are close relatives of polytetrafluoroethene (PTFE, or Teflon), renowned for its nonstick properties.

There are some properties that are helpful in building up an overall picture of the treated stone, even though they may not give any direct indication on the treatment's effectiveness. These include the stone's appearance, the treatment's depth of penetration, the stone's granular disintegration, a.s.o.

Sample preparation

The stone samples were cut in blocks (5 x 5 x 1 cm and 5 x 5 x 5 cm) and stored in desiccators at 25° C and 50% relative humidity (RH) for at least 24 h prior to coating application. The products were applied by brushing the stone surfaces with polymer solution, according to each manufacturer recommendation. After coating application, the stone samples were kept in desiccators at room temperature and 50% RH. Solvent evaporation was followed gravimetrically until the treated stone specimens reached a steady weight. The contact angles were measured using an automatic Kruss Easydrop Standard Goniometer. Capillary water absorption measurements were performed using

the gravimetric sorption technique [95, 96] – the weighted stone blocks were placed for 24 h on a filter paper pad partially immersed in distilled water and then weighted again to determine the amount of water absorbed by capillary forces. The degree of protection against water absorption by capillarity, PC, was calculated for 24 h of samples exposure to water [97] with the relation $PC = (A_1 - A_2) / A_1$, where A_1 is the mass of water absorbed by the uncoated substrate and A_2 is the mass of water absorbed by the treated substrate [72]. Both A_1 and A_2 were determined by gravimetric measurements.

Water vapor permeability measurements were performed according to the protocol described in Chapter IV. Color alteration measurements (optical characteristics) were investigated following the procedure detailed in Chapter IV.

VII. 2. Characterization of the treated stones

VII. 2. 1. Microscopic investigation

The microscopic investigation was performed with a Quanta 200 Environmental Scanning Electron Microscope (ESEM). The instrument produces enlarged images of a variety of specimens, achieving magnifications of over 100,000x and providing high resolution imaging in a digital format. This important and widely used analytical tool provides exceptional field of view, minimal specimen preparation, and the ability to combine the technique with X-ray microanalysis.

A few ESEM micrographs of Laspra and Repedea treated with Lotexan-N, Silres® BS 290, Tegosivin HL 100, as well as with the TMSPMA nanocomposite material are shown below, as examples. All the micrographs performed on the treated limestones samples are given in Annex 1.

The ESEM micrographs were performed at many different magnification orders, but for a better comparison, Fig. 78 and Fig. 79 present micrographs taken at x1000 magnification.

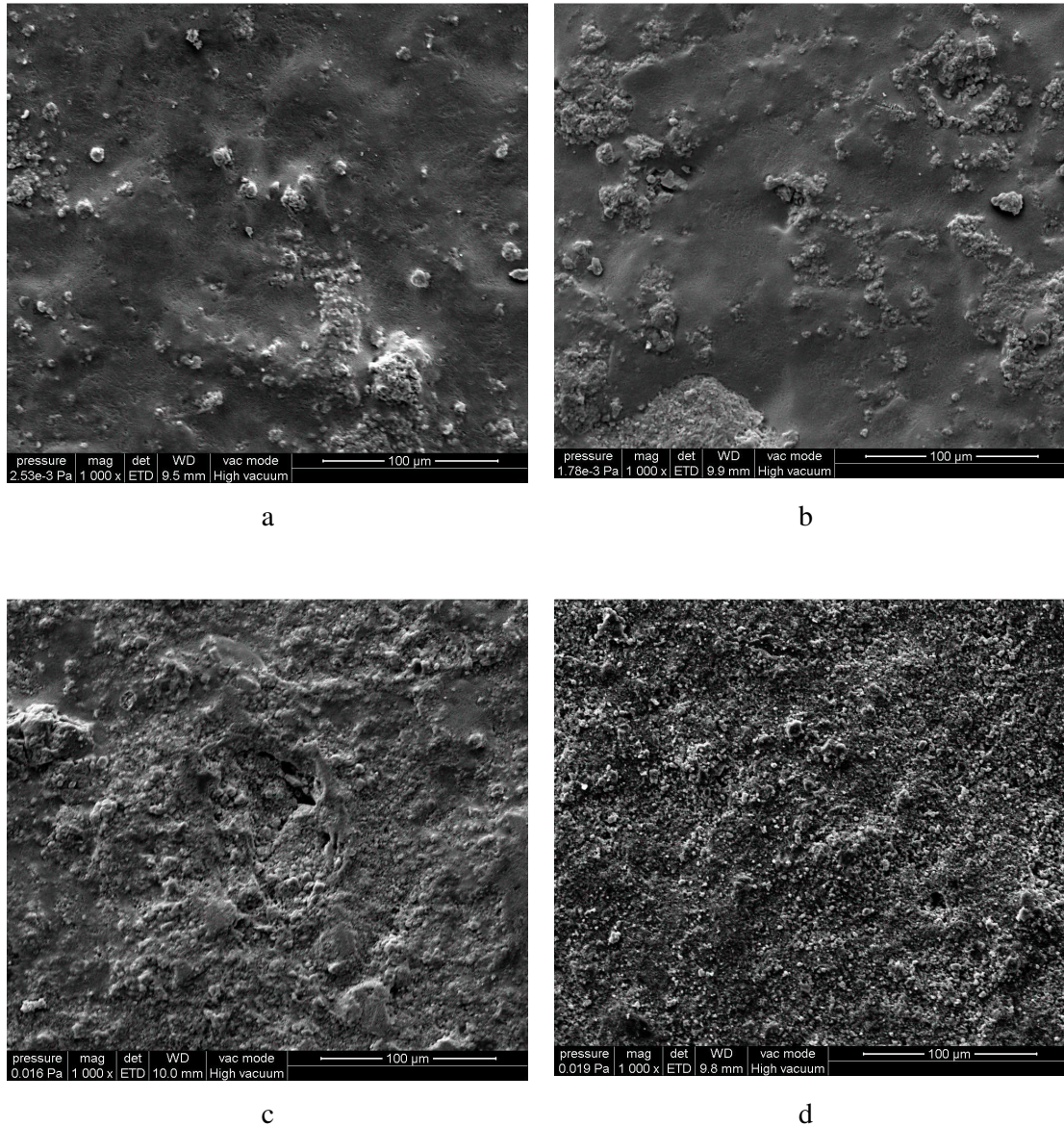
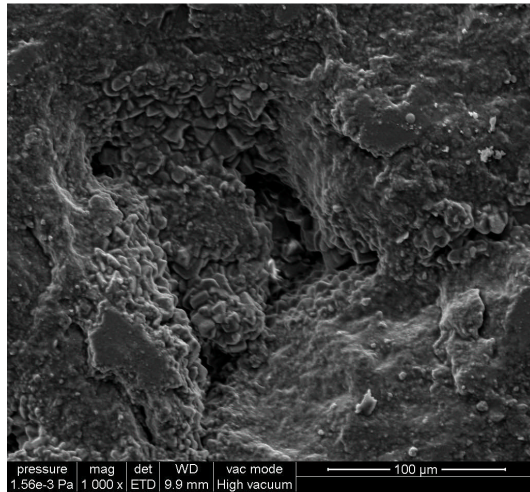
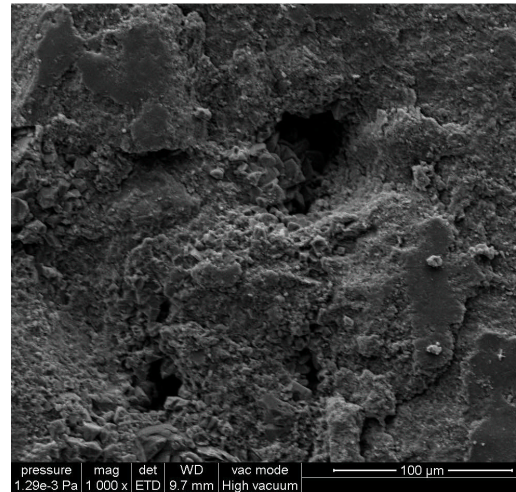


Fig. 78. ESEM micrographs of Laspra treated with (a) Lotexan-N; (b) Silres® BS 290; (c) Tegosivin HL 100 and (d) TMSPMA (x 1000)

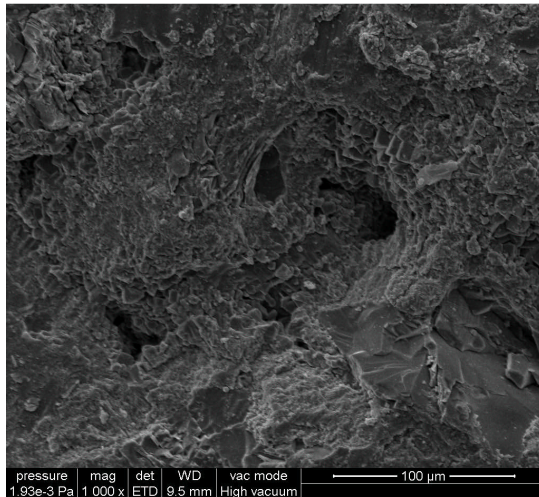
The ESEM observation of limestone samples brushed with different water repellents allowed the determination of parameters referring to treatment impregnation such as the type of coating, film-forming capacity, adherence to material, continuity of treatments, spalling or cracking etc.



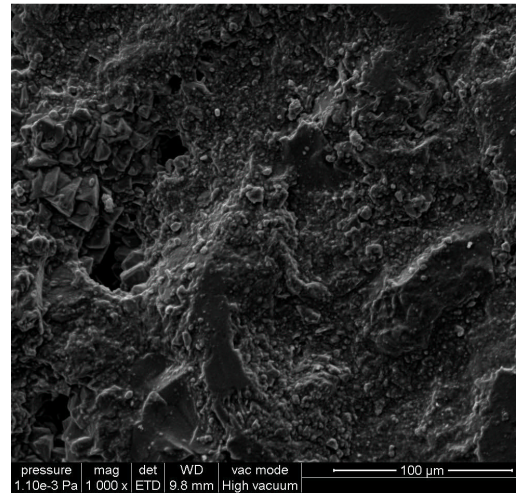
a



b



c



d

Fig. 79. ESEM micrographs of Repedea treated with (a) Lotexan-N; (b) Silres® BS 290; (c) Tegosivin HL 100 and (d) TMSPPMA (x 1000)

From Fig. 78 and Fig. 79 one can notice the different behavior of the commercially available products and the new synthesized nanocomposite material when applied onto the limestone surfaces. These differences seem to be more evident in Laspra's case, where one can observe the formation of a more or less compact and continuous polymeric film on the stone samples surfaces treated with Lotexan-N, Silres® BS 290 and Tegosivin HL 100, film that show no visible cracks at x1000 order of magnification (in fact, even for higher orders of magnification, no cracks or fissures have been detected).

For the stones treated with TMSPMA, the samples don't show the same surface morphology. More visible in the case of Laspra, the stone surface doesn't seem to be covered with a compact film, TMSPMA polymerizing through a sol-gel process. Due to its nanosized particles, the nanocomposite material is able to penetrate the stones substrates deeper than the commercial ones, not leading to the formation of a compact polymeric film on top of limestone surfaces. This particular coating behavior of TMSPMA will be further related to other parameters, such as contact angle or water vapor permeability values.

VII. 2. 2. Contact angle measurements

To investigate the hydrophobicity induced by treating the two stones, i.e. Laspra and Repedea, with water repellent products, the treated stones were submitted to contact angle measurements using a Kruss Easydrop Standard Goniometer. The stones were treated with the four siloxane-based water repellent products (Lotexan-N, Silres® BS 290, Tegosivin HL 100 and TMSPMA) and submitted to contact angle measurements after solvent evaporation and complete drying. As examples, the images of Laspra treated with Lotexan-N and Repedea treated with Tegosivin HL 100 are shown below.

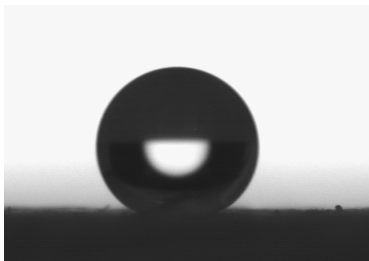


Fig. 80. Laspra treated with Lotexan-N – image of a water drop on stone surface

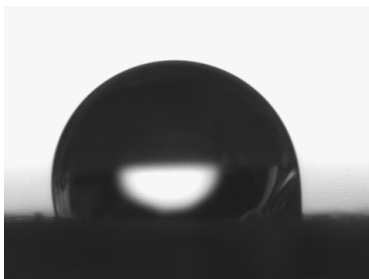


Fig. 81. Repedea treated with Tegosivin HL 100 – image of a water drop on stone surface

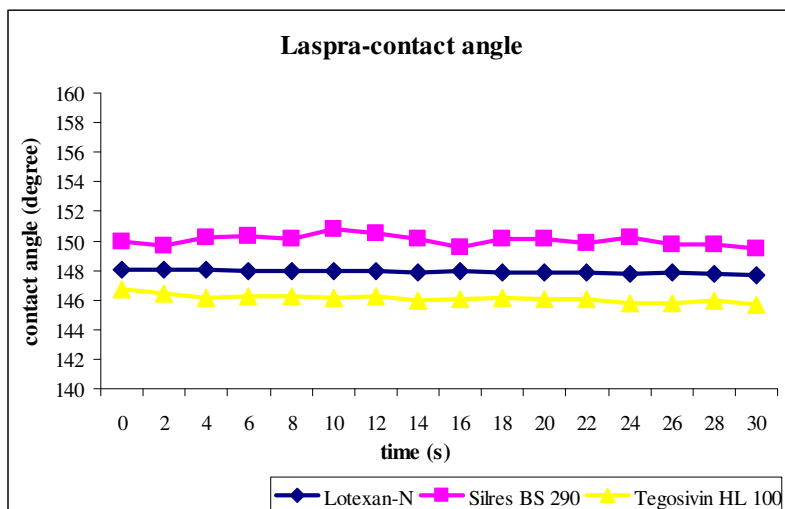


Fig. 82. Laspra – contact angle values

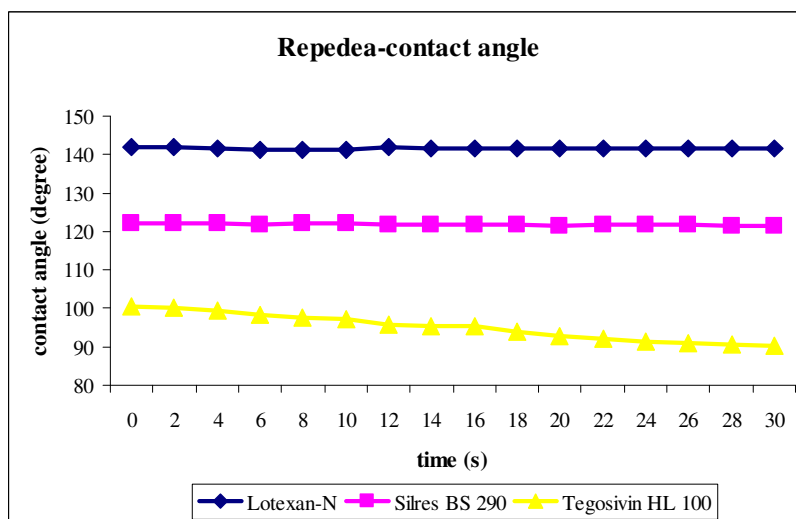


Fig. 83. Repedea – contact angle values

As can be seen from both the photos and the graphs, a first observation is that the two treated stones exhibit a different behavior.

Laspra shows contact angle values between 147° and 151° when treated with Lotexan-N, Silres® BS 290 and Tegosivin HL 100. These high values clearly show that all treatments are highly hydrophobic. Moreover, practically no variation in contact angle is observed for all these products during the 30 seconds of measurement.

As for Repedea, the curves showing the variation of the contact angles in time for the different treatments are, in some cases, shifted downwards as compared to the curves recorded for Laspra. The best results, i.e. 142° and 141°, are recorded for Lotexan-N followed by Silres® BS 290 (123°). For these two products, the variation of the contact angle in time is insignificant. TMSPMA and Tegosivin HL 100 recorded, from the beginning, lower values of the contact angle, the other products also showing a slight decrease of the contact angle in time.

The photos taken during the 30 seconds of measurement also confirm these comments. With increasing the hydrophobicity of the treated surface, the contact angle increases, the water drop presents an almost perfect spherical shape, and even the deposition of the drop on the surface is difficult – for example, the deposition of the water drop was extremely difficult on Laspra when treated, e. g., with Silres® BS 290. In this particular case, three to five attempts have been made in order to successfully release the water drop on the treated surfaces. On the other hand, for Repedea quite different behaviors of the water drops were obtained, i.e. with decreasing the hydrophobicity / the contact angle of the treated stones, the shape of the drops changed from a spherical one to ellipsoidal shapes and for some treatments part of the drops was seen to penetrate inside the superficial layers of the material.

TMSPMA behaves in a different way, for Laspra exhibiting values between 120°- 104°, a slight decrease of the contact angle being observed during the 30 seconds after water drop deposition. This product can be considered less adequate from the contact angle point of view. In the case of Repedea treated with TMSPMA a constant 105° contact angle value was registered.

Table 16. Laspra and Repedea – contact angle values (degrees)

	Lotexan-N	Silres® BS 290	Tegosivin HL 100	TMSPMA
Laspra	148	151	147	120 ↓
Repedea	142	123	100 ↓	105

VII. 2. 3. Water vapor permeability measurements

One of the most significant attributes that a water repellent polymeric product has to prove after application to a stone surface is the ability to allow the stone to “breathe”,

making the stone surface water repellent, but not water proof. The majority of researchers believe that stone needs to "breathe." In other words, stone should remain permeable to water vapor, in order to avoid any buildup of moisture (and consequent shear stresses) at the interface between the treated zone and the untreated stone below.

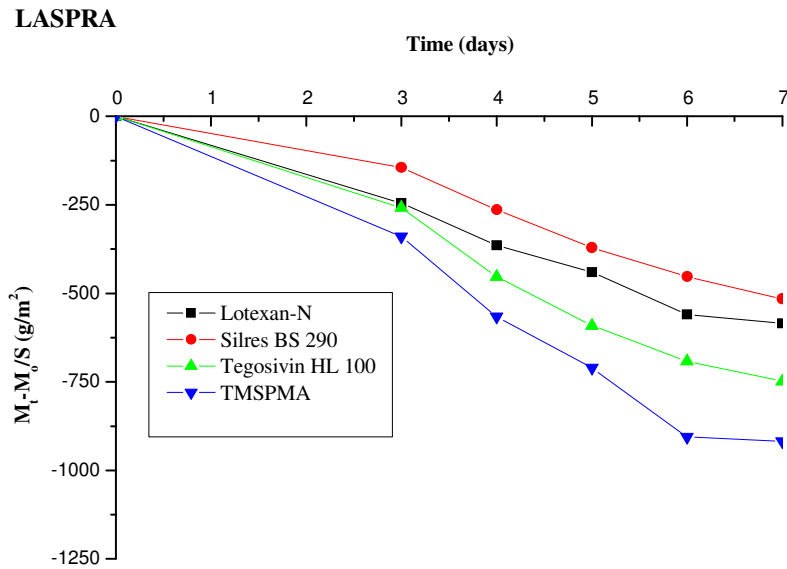


Fig. 84. Laspra – water vapor permeability graphs

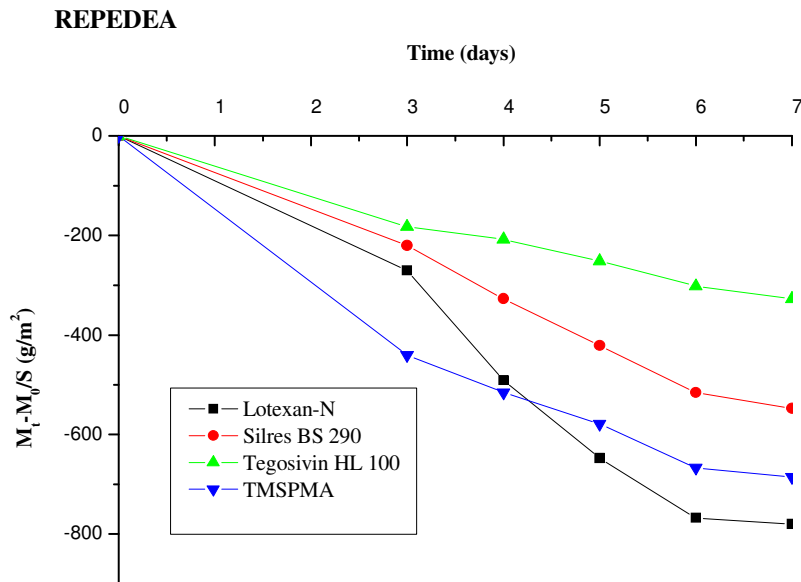


Fig. 85. Repedea – water vapor permeability graphs

Another manner to express the water vapor permeability values is through the water vapor permeability coefficient, K_v ($\text{g}/\text{m}^2 \times 24\text{h}$).

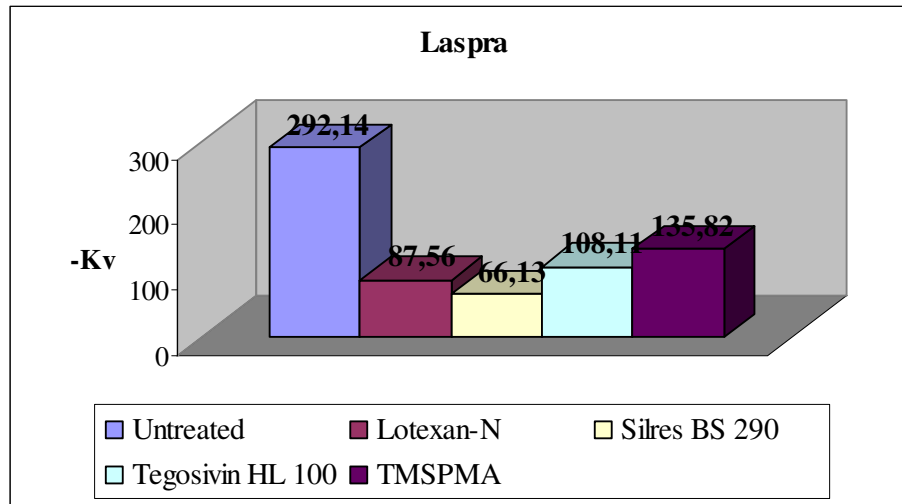


Fig. 86. Laspra – water vapor permeability coefficient values

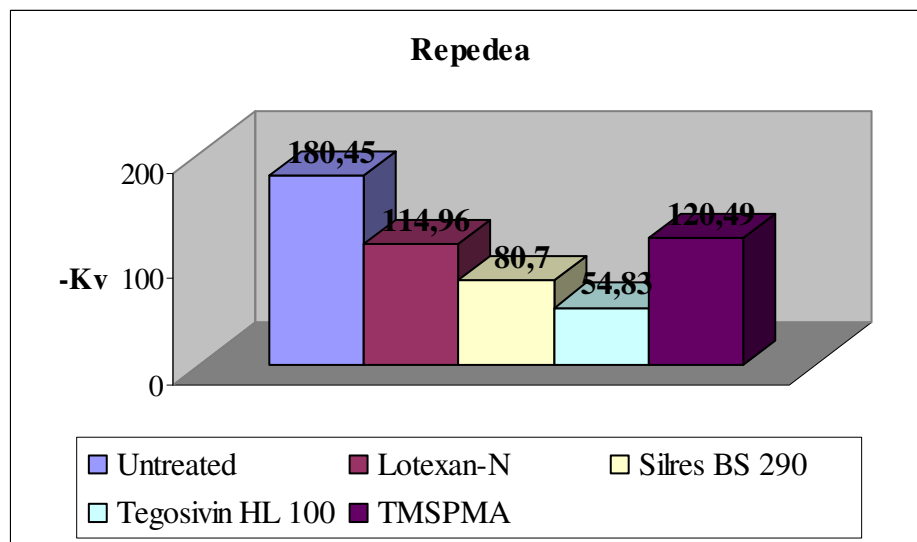


Fig. 87. Repedea – water vapor permeability coefficient values

As expected, the untreated stone registers, for both Laspra and Repedea, the highest water vapor permeability values. Following the application of the siloxane-based water repellents, the values of water vapor permeability coefficient are exhibiting a decrease. The lower the decrease in the values of water vapor permeability coefficient after stones treatment – as compared to the untreated stone samples – the better the result.

As evident from Fig. 86 and Fig. 87, the lowest decrease in water vapor permeability coefficient values is registered for Laspra and Repedea treated with TMSPMA. Due to the self-assembling properties, the nano builder introduces particular atoms or molecules onto the limestones surfaces. The molecules are aligning into particular positions, leading to the formation of a variety of intermolecular forces to achieve large scale, hierarchical and functional structures, in order to minimize the total energy. Over the curing period, TMSPMA nanoparticles self-assemble and bond to the surface; this nano-coating doesn't form only as a coverage on the surface, since nanoparticles are able to penetrate deeply inside porous stones without blocking the small pores, therefore allowing the stone substrate to "breathe" and leading to a better water vapor permeability coefficient value. The worldwide used siloxane-based water repellents present, as shown in previous chapters, large molecules in their structures, therefore leading to their uneven distribution within the stones structure and to a possible blocking of some of stone pores – these concluding in a dramatic decrease of the values of water vapor permeability coefficients.

The most significant decrease in the values of the water vapor permeability coefficient is registered for the samples treated with Silres® BS 290 in case of Laspra and for the samples treated with Tegosivin HL 100 in case of Repedea.

VII. 2. 4. Color measurements

Aesthetics is one of the most important aspects in heritage conservation. The color changes that might intervene following the treatment of stones with chemical products (water repellents, consolidants, strengtheners, pollution deterrents, a.s.o.) have to be reduced to a maximum extend in order to alter as little as possible as compared to the untreated sample.

The color measurements were taken on samples of Laspra and Repedea, before and after the treatment with each siloxane-based water repellent product and were evaluated using CIE L* a* b* and CIE L* C* h systems, where L* is the variable lightness which can vary from 0 (black) to 100 (white), a* and b* are the chromatic coordinates, i.e., + a is red, – a is green, + b is yellow and – b is blue. The attributes of chroma are C* – saturation or color purity, and hue h – color wheel. The global color variation (ΔE^*) was evaluated using the formula $\Delta E^* = (\Delta L^{*2} + \Delta a^{*2} + \Delta b^{*2})^{1/2}$.

The total color change exhibited by Laspra and Repedea samples, treated with the three commercially available siloxane-based water repellents and the new synthesized nanocomposite are presented below.

Table 17. Laspra – total color change after treatment application

Laspra	Lotexan-N	Silres BS 290	Tegosivin HL 100	TMSPMA
ΔE^*	1.14	1.91	0.75	2.87

Table 18. Repedea – total color change after treatment application

Repedea	Lotexan-N	Silres BS 290	Tegosivin HL 100	TMSPMA
ΔE^*	10.38	12.18	11.92	12.15

Some authors consider that in order to have a generally acceptable ΔE^* , its value has to be lower than 5; other authors state that this threshold value should be 10 [97, 98].

Several categories can be established in accordance with the chromatic variations induced by the applied treatments, considering the ΔE^* parameter:

- $\Delta E^* < 1$: Tegosivin HL100 applied on Laspra;
- $1 < \Delta E^* < 10$: Lotexan-N, Silres® BS 290 and TMSPMA applied on Laspra;
- $\Delta E^* > 10$: Lotexan-N, Silres® BS 290, Tegosivin HL 100 and TMSPMA applied on Repedea.

It is to be mentioned that even if the acceptable chromatic variation is considered to be $\Delta E^* < 10$, some monumental stones are not fitting in these limits no matter the applied treatment, depending on their composing minerals. This appears to be the case of Repedea, which registers total color change values higher than 10 no matter the applied water repellent chemical product.

VII. 2. 5. Mapping of treatments distribution

MicroFT-IR analyses were performed in order to chemically monitor the distribution of the chemical treatments within the treated stones by obtaining a chemical map of the siloxane-based water repellent treatments within the treated limestone's cross-sections.

After embedding the stone samples in polyester resin (Fig. 88) and polishing in cross-section, the investigation of the water repellents distribution within the cross-sectioned samples was performed.

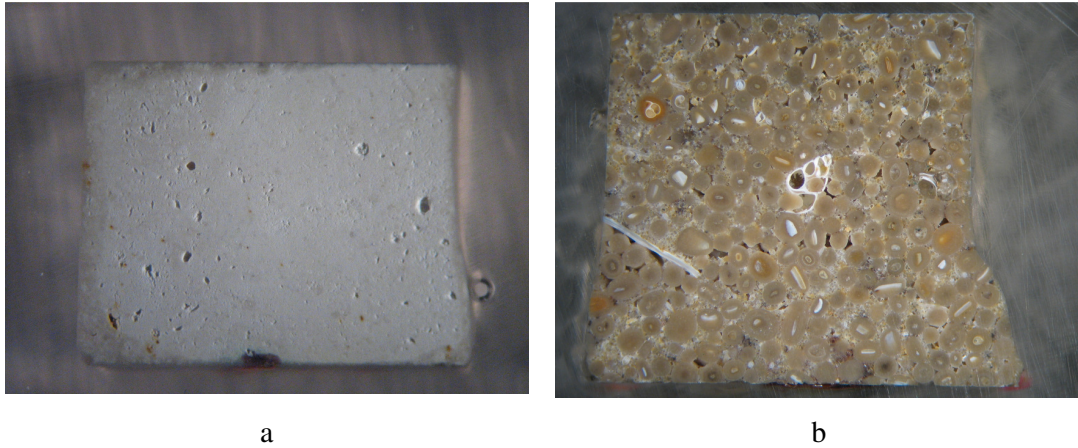


Fig. 88. Samples embedded in resin: (a) Laspra and (b) Repedea

The obtained maps showed, from a chemical point of view, the localization of the water repellent treatments within the 1 cm in depth cross-sectioned limestone samples, a few images being presented below.

Fig. 89 shows, as an example, a micrograph of a Laspra sample which was treated with Tegosivin HL 100, embedded in resin, polished and then submitted to the experiment.

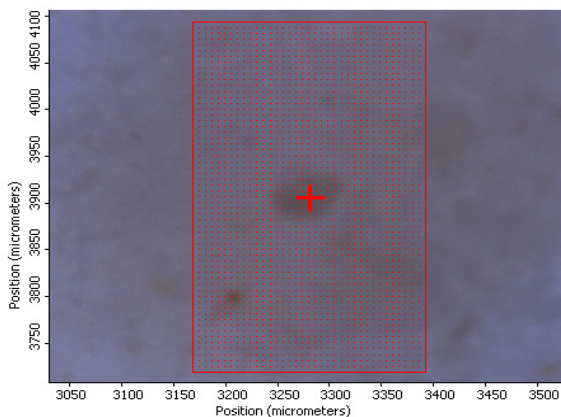


Fig. 89. Micrograph of an area of a cross-sectioned Laspra sample treated with Tegosivin HL 100

The micrograph illustrates the presence of a huge pore (pore size of about 65 x 34 micrometers) roughly situated in the middle of the selected area. In the additional

chemical map (Fig. 90) one can distinguish the intensities of the silicate band, corresponding to the siloxane-based product (Tegosivin HL 100). The signal of the band corresponding to the silicate is gradually decreasing from red (high intensity of the silicate band) to yellow, green and blue (very low to no intensity of the silicate band).

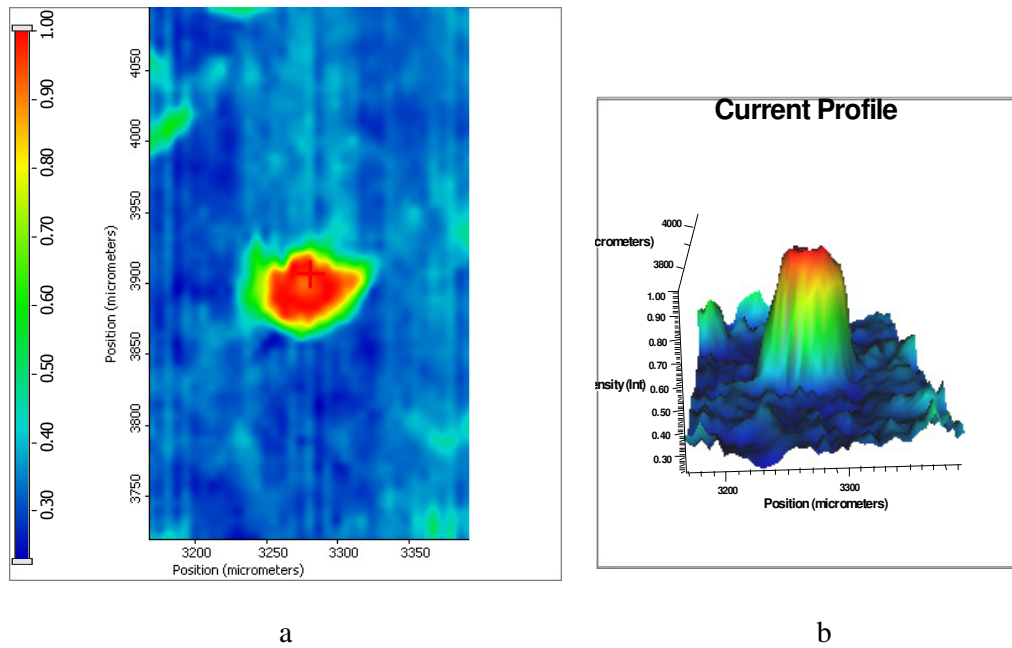


Fig. 90. Chemical map of an area of a cross-sectioned Laspra sample treated with Tegosivin HL 100. (a) 2D map; (b) 3D map showing the intensity of the silicate treatment

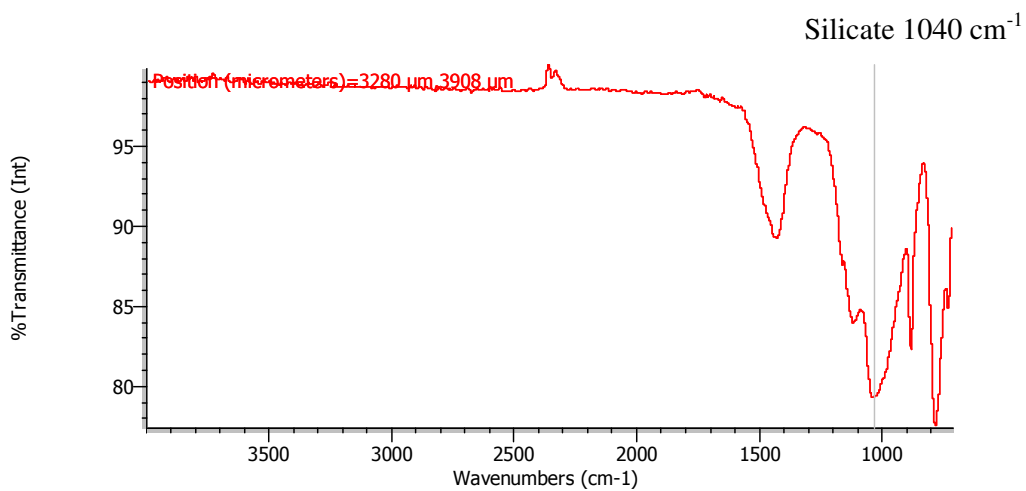
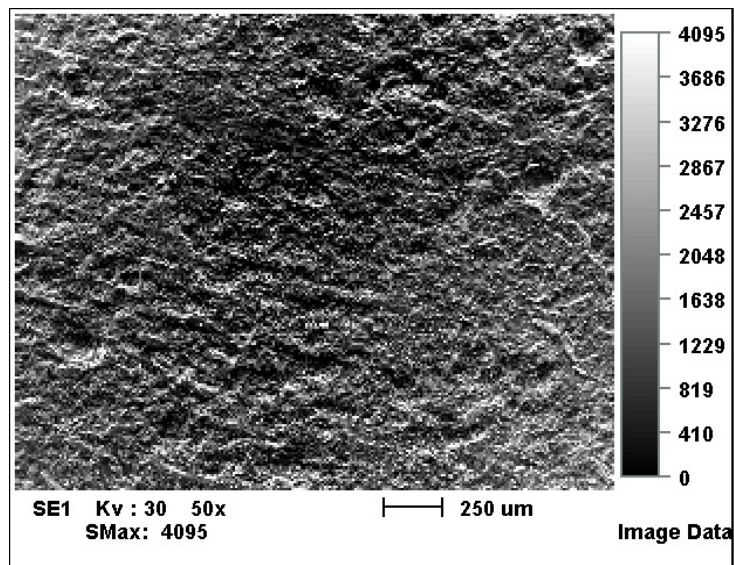
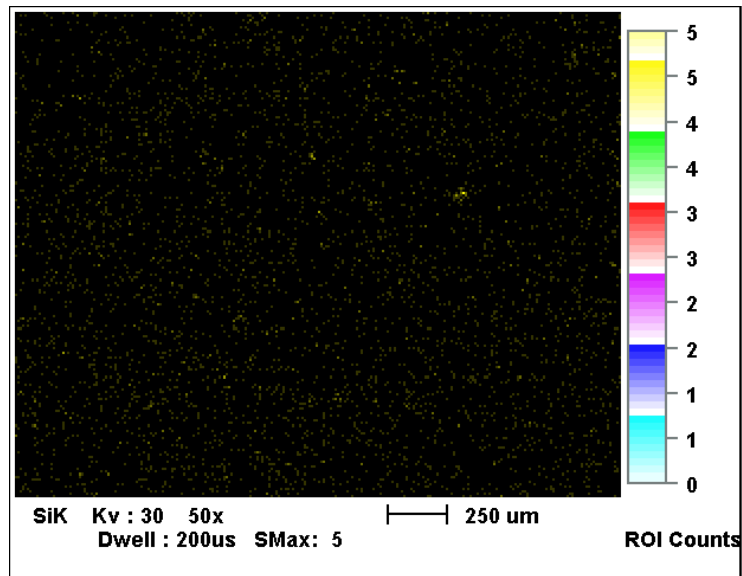


Fig. 91. Silicate FT-IR spectrum of an area of a cross-sectioned Laspra sample treated with Tegosivin HL 100

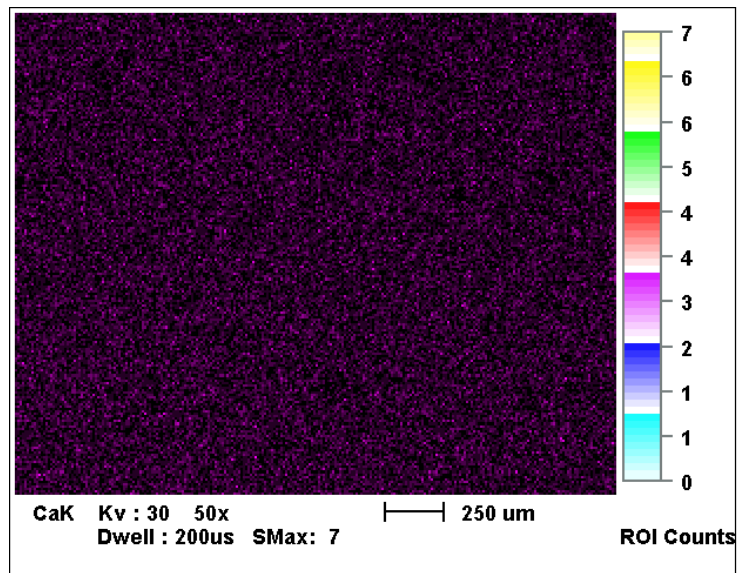
Fig. 90 shows that the highest intensity of the band corresponding to the water repellent silicate can be found within the pore, gradually decreasing towards pore's rims. This is a clear indication of the fact that the siloxane-based treatments are concentrated, even after solvent's evaporation, in stone's larger pores, coating and filling them and, as it will be further demonstrated, blocking them and disabling these stone areas to "breathe".

To obtain additional information on the distribution of the siloxane-based water repellent treatments within the two porous stones, this technique was correlated with the mapping which can be achieved through SEM-EDAX technique. An example is shown in Fig. 92.





b



c

Fig. 92. Mapping of an area of a Lapra sample treated with Tegosivin HL 100. (a) SEM micrograph; (b) EDAX mapping showing in yellow Si distribution; (c) EDAX mapping showing in purple Ca distribution

It has to be mentioned that using the EDAX mapping technique one can obtain a map corresponding to the localization of different chemical elements on a certain sample, but not a chemical map – through this technique being impossible to distinguish if the detected chemical element (e. g., Si) belongs to stone's minerals or to the applied chemical treatment.

The same techniques were applied for all Repedea treated samples. A few examples are shown below.

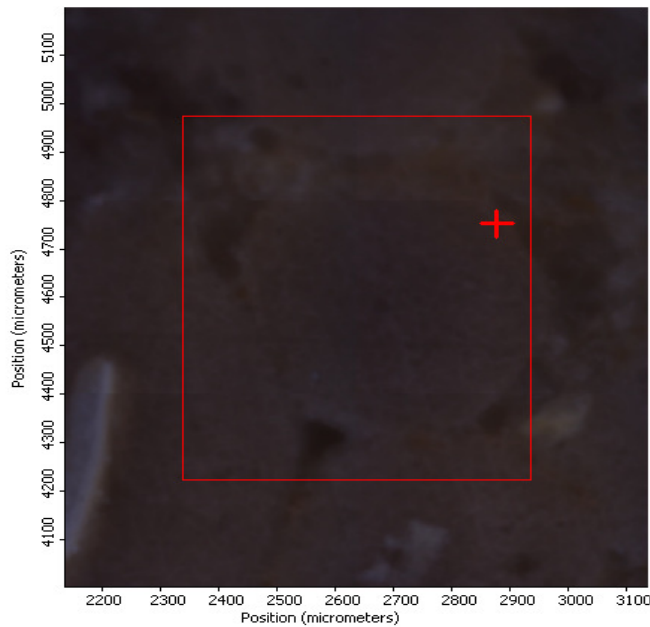


Fig. 93. Micrograph of an area of a cross-sectioned Repedea sample treated with Lotexan-N

Fig. 93 illustrates a micrograph representing a small part of a Repedea treated with Lotexan-N cross-sectioned sample. In the center of the image one can observe the presence of an almost perfectly rounded oolite surrounded by voids. The corresponding chemical maps are shown in Fig. 94 and Fig. 95.

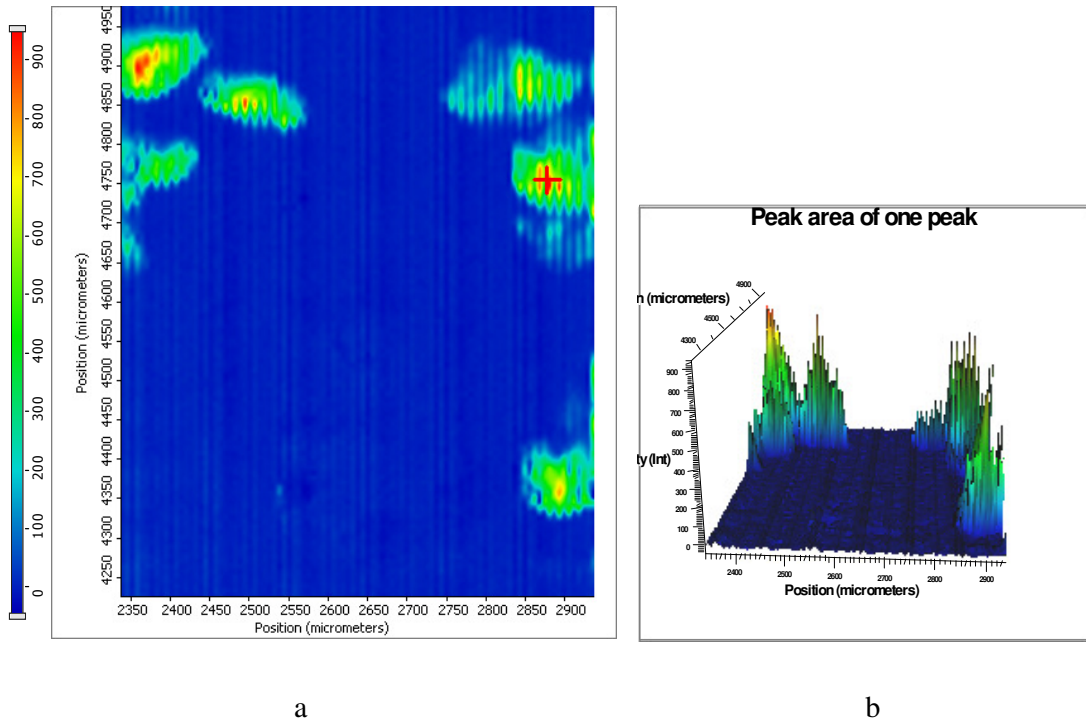


Fig. 94. Chemical map of an area of a Repedea sample treated with Lotexan-N. (a) 2D map; (b) 3D map showing the intensity of the silicate treatment

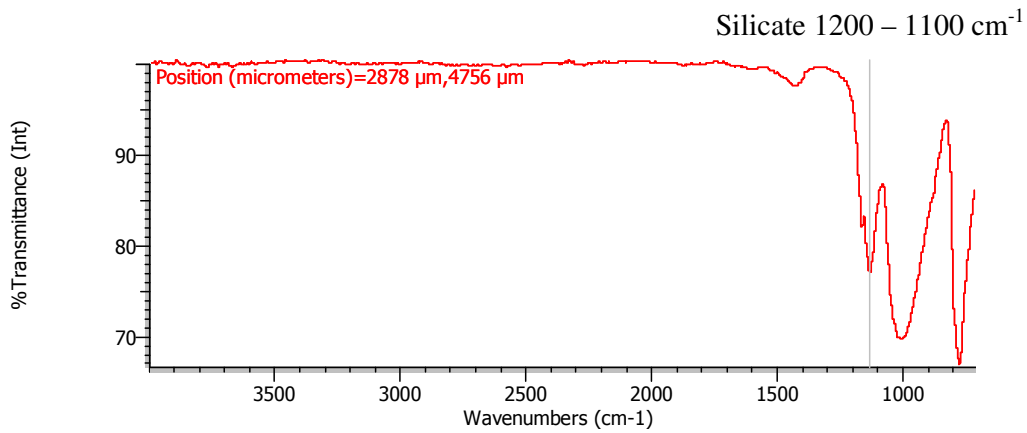


Fig. 95. Silicate FT-IR spectrum of an area of a cross-sectioned Repedea sample treated with Lotexan-N

Complementary to the chemical map related to the monitorization of the silicate treatment, Fig. 96 shows the chemical map corresponding to the localization of the limestone's carbonate.

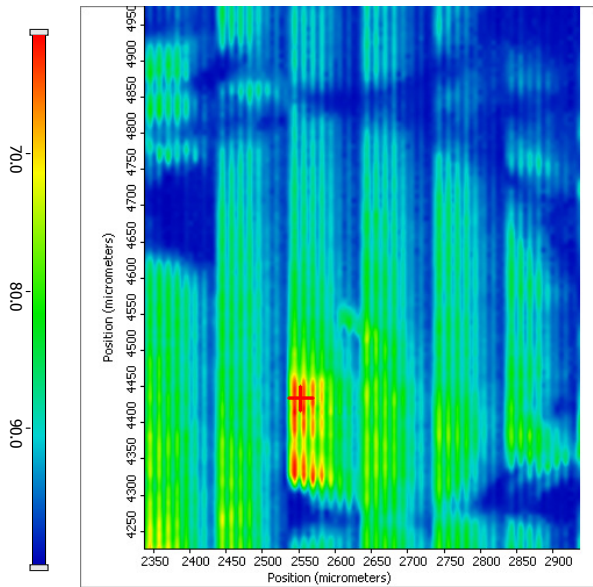


Fig. 96. Chemical map of an area of a Repedea sample treated with Lotexan-N

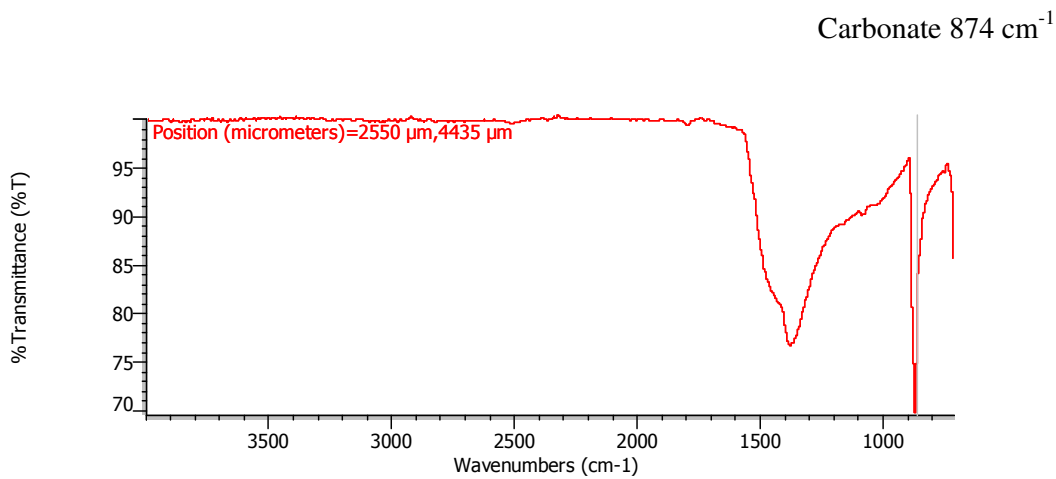
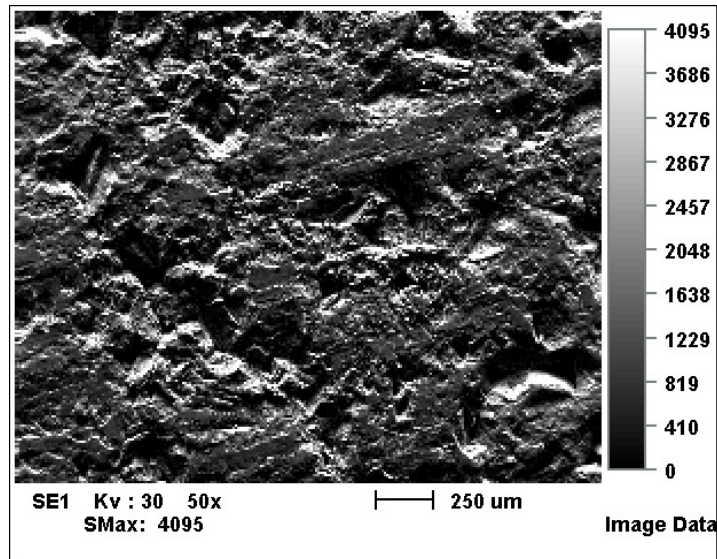


Fig. 97. Carbonate FT-IR spectrum of an area of a cross-sectioned Repedea sample treated with Lotexan-N

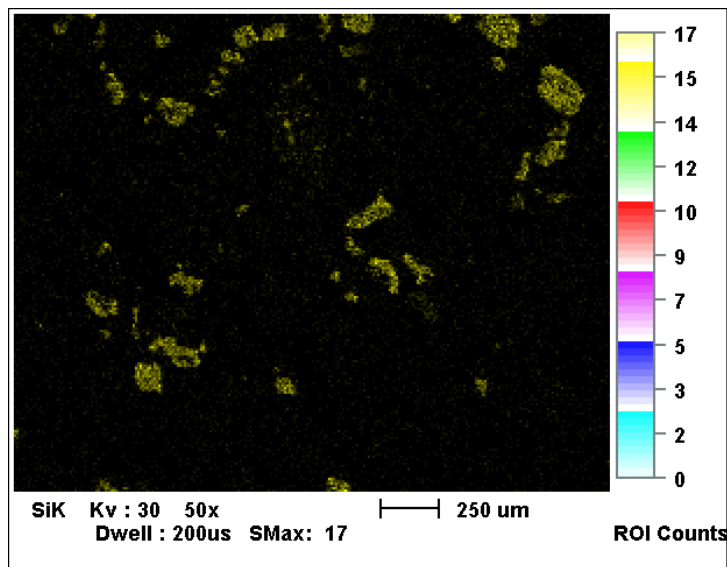
As in the case of Laspra cross-sectioned sample treated with Tegosivin HL 100, the chemical maps are clearly illustrating that the silicate belonging to the siloxane-based water repellent product registers a higher intensity of the band localized in stone's voids surrounding the oolite, the intensity decreasing from red to yellow, green and blue. From this chemical map it again appears that the silicate treatment is coating and filling Repedea's voids – the absence of any intensity corresponding to the treatment's silicate band in the oolite area being explained by the fact that the intensities of the carbonate

band are extremely strong, shadowing or overpowering the lower intensities corresponding to the silicate band.

The EDAX mapping of a Repedea sample treated with Lotexan-N is shown in Figure 98.



a



b

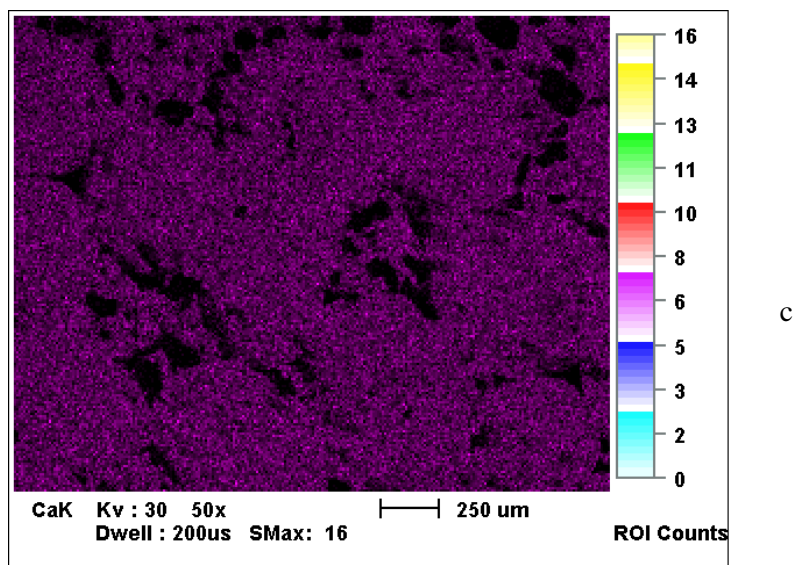


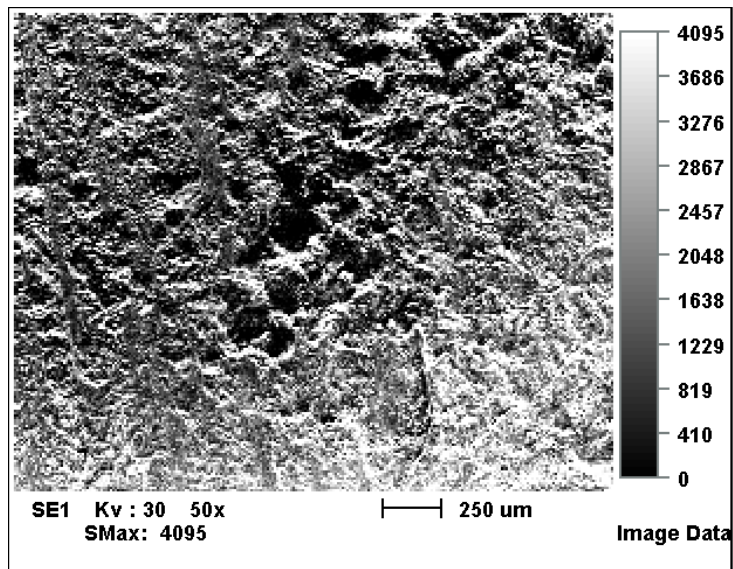
Fig. 98. Mapping of an area of a Repedea sample treated with Lotexan-N. (a) SEM micrograph; (b) EDAX mapping showing in yellow Si distribution; (c) EDAX mapping showing in purple Ca distribution

The monitorization of the distribution of the commercially available products within the treated limestone samples demonstrated that all three products manifest the same behavior in relation to stone's substrates, no significant difference being registered among the distribution of Lotexan-N, Silres® BS 290 and Tegosivin HL 100 within Laspra or Repedea samples.

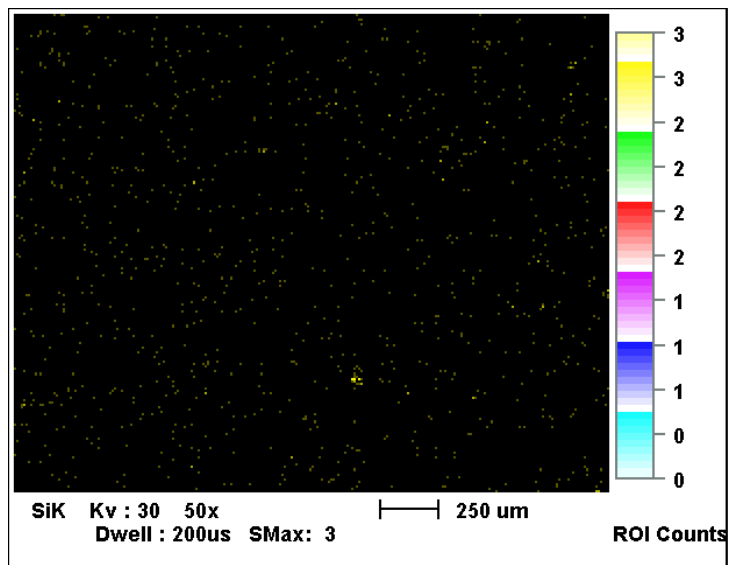
The same techniques were used in order to monitor the localization of the newly synthesized water repellent nanocomposite within Laspra and Repedea cross-sectioned samples.

The performance of ATR technique on TMSPMA treated Laspra and Repedea samples (cross-section) yielded no results – the chemical maps, performed repeatedly, illustrating the complete absence of the intensities corresponding to the TMSPMA's silicate bands. Since both limestone samples were treated with the nanocomposite material before their processing for the ATR μ FT-IR investigation, one can conclude that the nano-dimensioned silicate particles of the treatment determined a localization and distribution of TMSPMA impossible to be monitorized using this technique, which can

function within the micrometer and not nanometer range. However, distribution maps corresponding to the nanocomposite product's localization in Laspra and Repedea samples were obtained using EDAX mapping (Fig. 99) (these being distribution and not chemical maps).



a



b

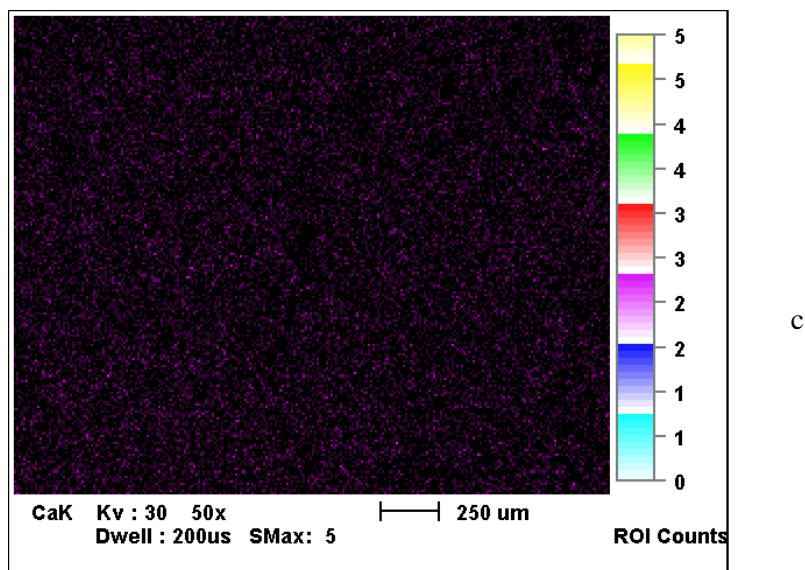


Fig. 99. Mapping of an area of a Laspra sample treated with TMSPMA. (a) SEM micrograph; (b) EDAX mapping showing in yellow Si distribution; (c) EDAX mapping showing in purple Ca distribution

Fig. 99 (b) shows the even distribution of the Si particles all over the selected area, which comes as opposite to the same maps performed on both Laspra and Repedea samples when treated with any of the worldwide used products. This can be also explained through the difference in composition, particle size, polymeric network arrangement and properties which are evident for the commercial compounds as compared to the nanocomposite material.

VII. 3. Conclusions

A summary of the protective efficiency parameters of the studied water repellent treatments applied onto Laspra and Repedea is given in Table 19.

Table 19. Summary of protective efficiency parameters for the selected stone substrates and treatments

	Q _c , degree	PC	K _v (25° C) (g/m ² x 24 h)	ΔE*
Laspra			292.14	
Lotexan-N	148	0.57	87.56	1.14
Silres® BS 290	151	0.53	66.13	1.91
Tegosivin HL 100	147	0.93	108.11	0.75
TMSPMA	120	0.65	135.82	2.87
Repedea			161.89	
Lotexan-N	142	0.85	114.96	10.38
Silres® BS 290	123	0.95	80.7	12.18
Tegosivin HL 100	100	0.75	54.83	11.92
TMSPMA	105	0.50	120.49	12.15

The table presents the effect of the protective coatings applied onto the limestones in terms of static contact angle (Q_c), protection against water absorption by capillarity (PC), permeability coefficient (K_v) and global color variation (ΔE*).

Contact angle measurements are a significant index of treated stone surface water repellency. For stone protection, the minimum acceptable value for Q_c is 90° [98] and, as can be seen from the experimental data given in Table 19, a good surface hydrophobicity was attained for all investigated coating / substrate combinations. An interesting conclusion can be drawn, i.e., the degree of hydrophobicity, expressed by the measured contact angles, is different for the same polymeric coating applied on different stone substrates. This behavior is expected since Young's equation is valid only for passive, atomically flat and chemically homogeneous surfaces.

The petrophysical variations of the limestones after the application of water repellents (water-stone contact angle, water-vapor permeability and color) allow the assessing of the performance of the tested treatments. Considering the water-stone contact angle results (Table 19), one can establish the following hierarchy:

- 100° – 120°: Tegosivin HL 100 and TMSPMA applied on Repedea;
- 120° – 140°: Silres® BS 290 and TMSPMA cast on Repedea and Laspra, respectively;
- > 140°: Lotexan-N, Silres® BS 290 and Tegosivin HL 100 applied on Repedea and Laspra, respectively.

In contrast to the instant water repellency represented by the contact angle measurements, the long-term water resistance is given by the differences in water absorption by capillarity for untreated and coated stone substrates. As expected, the polymer coatings are decreasing, to a higher or lower extent, the amount of water absorbed by the stone sample. Similar measurements were performed for all investigated coating / substrate combinations and the results are summarized in Table 19. The higher is the PC value, the higher protection against water absorption by capillarity is achieved. The impermeability of polymeric coating film to water vapor can lead to water condensation just underneath the film. In time, this can determine the loss of film adhesion and, eventually, film detachment [99].

The reduction in water vapor permeability is inevitable, as a consequence of the water repellent properties of the polymeric film, but the lowest possible decrease is pursued [96]. The less the reduction in water vapor permeability as compared to the untreated stone, the higher is the efficiency of the chemical treatment. The water vapor permeability values of the specimens impregnated with the treatments yield to the following conclusions:

- reduction < 30 %: Lotexan-N and TMSPMA applied on Repedea;
- reduction ranging between 30 and 70 %: Silres® BS 290 and Tegosivin HL 100 applied on Repedea and Tegosivin HL 100 and TMSPMA applied on Laspra;
- reduction > 70%: Silres® BS 290 and Lotexan-N cast on Laspra.

The optical changes determined by the coatings are usually attributed to the degree of oxidation of the chromophores in the chromogen minerals, as well as to their concentration [100]. The chromatic parameters of the limestones before and after treatment (Table 19) were determined to analyze the effect of the protective coating on optical stone properties: the smaller the differences between the measured values before and after coating, the better the obtained results.

According to the chromatic changes induced by the applied treatments (considering the ΔE^* parameter) the following classification can be made:

- $\Delta E^* < 1$: Tegosivin HL 100 applied on Laspra;
- $1 < \Delta E^* < 10$: Lotexan-N, Silres® BS 290 and TMSPMA applied on Laspra;
- $\Delta E^* > 10$: Lotexan-N, Silres® BS 290, Tegosivin HL 100 and TMSPMA on Repedea.

To conclude, the efficiency of the three worldwide used siloxane-based water repellents (Lotexan-N, Silres® BS 290 and Tegosivin HL 100) and of the newly synthesized nanocomposite material (TMSPMA), applied onto two limestones – Laspra and Repedea – was investigated. The advantages of coatings obtained from siloxane-containing polymer matrices are the consequence of their ability to crosslink *in situ* following substrate treatment. The best option for a siloxane-based water repellent used for the protection of the selected limestones should yield the best results in terms of water / stone contact angle, water absorption by capillarity, water vapor permeability and optical properties (color alteration). For the assessment of siloxane-based water repellent coatings, one has to take into consideration the highest attained liquid water-repellency values – as evidenced by an increase in water-stone contact angle, the lowest induced decrease in water vapor permeability, the lowest water absorption by capillarity as well as the lowest induced chromatic variations. From the obtained results, it can be pointed out that the same siloxane-based polymeric treatment yields different results and performances when applied to distinct carbonate stones.

VIII. Artificially accelerated ageing

VIII. 1. Introduction

During the last decades, many attempts have been made to understand the nature of degradation factors and their impact on monumental buildings in a more systematic and scientific manner.

The term “atmospheric pollution” usually refers to the element of the atmosphere which has been altered by human activities. Changes in natural and polluted atmospheres can be highly variable both across space and time. In coastal environments, for example, there is naturally more salt in the atmosphere than in inland environments.

Some of the major pollutants that affect stonework are carbon dioxide, sulphur dioxide, nitrogen oxides and particulates such as smoke. Carbon dioxide is probably more familiar as a “greenhouse gas”, contributing to global warming, but it also combines with water in the atmosphere to produce carbonic acid, meaning that the natural rainfall is actually a weak solution of carbonic acid with a pH of about 5.6 (pH = 7 being neutral and pH = 1 being the most acidic one). The reactions of other pollutant gases, such as sulphur dioxide and nitrogen oxides, produce more acidic rainfall. Nitrogen oxides can produce a similar reduction in pH by the formation of nitric acid, but these oxides are harder to detect, especially in terms of their impact on stonework. The above mentioned gases are produced by industrial, commercial and residential activities in urban and increasingly in rural areas.

In any particular part of an urban area, depending on the local industries, other pollutant sources, topography and climate, a great deal of variation in the amount of pollution found should be taken into account.

Pollutants such as carbon dioxide are also having an impact on the general climate. Although a 2 – 5° C rise in temperature and a rise in sea-level are predicted over the next 50 years, these general figures hide a great deal of regional variation in climate change.

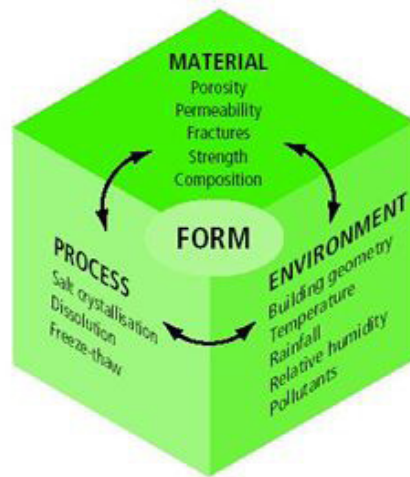


Fig. 100. Example of factors influencing the interactions between pollutants and materials

This chapter deals with the evaluation of the durability of the two selected limestones, Laspra and Repedea, against three of the most aggressive stone decay factors: UV irradiation, salt mist action and SO₂ action in the presence of humidity. To understand and evaluate what happens with the two limestones when exposed to the action of these factors, artificially accelerated ageing tests were performed. These tests have the purpose of simulating the corresponding natural agents' actions on the untreated and treated limestones, using special climatic chambers. In laboratory tests, these climatic chambers are used in order to accelerate, in an obvious artificial manner, the stones deterioration phenomena, yielding in a matter of weeks or months an image of what might happen to the stones after a much longer exposure to the corresponding natural environment. The artificially accelerated ageing tests have proved their importance in understanding a certain material's deterioration process, even if not always the results obtained through these tests are 100% similar to those attained in a natural environment.

In order to evaluate and compare the behavior of Laspra and Repedea – untreated samples / treated with the three worldwide known water repellents and the newly

synthesized nanocomposite material / treated and artificially aged – several evaluation methods were applied using standardized tests.

For a better understanding and comparison of the obtained results, the same evaluation tests were performed for two of the three artificially accelerated ageing tests included in this study. The treated stones resistance against salt mist action and SO₂ action was evaluated through visual investigation, contact angle measurements, water vapor permeability measurements, color and weight measurements. As for their resistance against UV action, this study focused on the treated stone samples, as well as on the characterization of the polymeric films used to protect the stones, different evaluation methods being used.

VIII. 2. Artificially accelerated ageing under UV irradiation

VIII. 2. 1. Artificially accelerated ageing under UV irradiation – polymeric films

VIII. 2. 1. 1. FT-IR spectroscopy

The three worldwide used water repellent products (Lotexan-N, Silres® BS 290 and Tegosivin HL 100), as well as the newly synthesized nanocomposite material, TMSPMA, were cast as films and analyzed through FT-IR spectroscopy.

As expected, the FT-IR spectra of the three siloxane-based water repellent products (Lotexan-N, Silres® BS 290 and Tegosivin HL 100), performed in liquid form were identical with the spectra of the same products cast as films, these spectra being analyzed in Chapter VI. The same films were submitted to artificially accelerated ageing tests – the films were aged for 500 and 1000 hours in an Angelantoni CH250 climatic chamber, at 40° C, under UV irradiation and studied after each ageing cycle. The FT-IR spectra of all products, cast as films, were recorded after the first accelerated ageing cycle (500 hours) and after the second ageing cycle (1000 hours of exposure to UV irradiation). The results are described below.

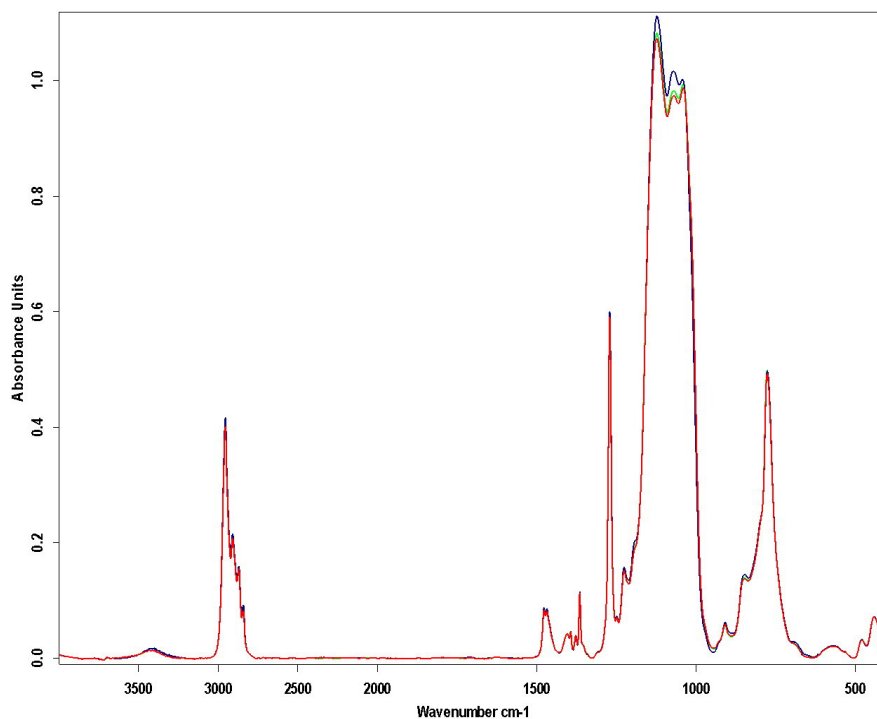


*Fig. 101. FT-IR spectrum of Lotexan-N, cast as film;
 — FT-IR spectrum of Lotexan-N, unaged; — FT-IR spectrum of Lotexan-N, aged for 500 hours; — FT-IR spectrum of Lotexan-N, aged for 1000 hours*

The FT-IR spectra of Lotexan-N, cast as a film, unaged and aged for 500 and 1000 hours, respectively, show that no degradation/modification of the polymeric film occurs during the accelerated UV ageing process. The three FT-IR spectra are superposed, the intensity of the bands being practically the same except for the 1000 – 1220 cm^{-1} region, where a slight modification of the intensity of the bands attributed to Si – O – Si bonds is observed. However, even in this region, the modification of the spectra during the second ageing cycle is almost negligible.

As a conclusion, it appears that the UV ageing process, performed at 40° C during 1000 hours, doesn't affect the protective polymeric film, which remains, for Lotexan-N, practically unchanged, i.e., maintains its properties for a long period of exposure to UV irradiation.

Almost the same comments are valid for Silres® BS 290 (Fig. 102).

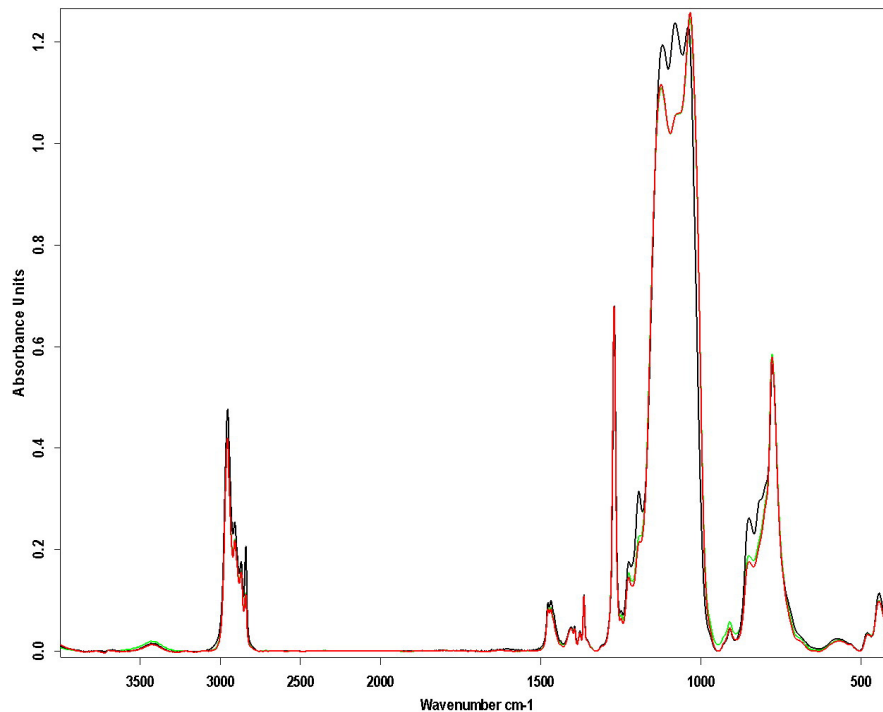


*Fig. 102. FT-IR spectrum of Silres® BS 290, cast as film;
 — FT-IR spectrum of Silres® BS 290, unaged; — FT-IR spectrum of Silres® BS 290,
 aged for 500 hours; — FT-IR spectrum of Silres® BS 290, aged for 1000 hours*

The only slightly modified area is the $1000 - 1200 \text{ cm}^{-1}$ one, where a small decrease of the signals of the peaks attributed to the Si – O – Si bond is observed. This slight loss of siloxane takes place only during the first cycle (500 hours) of UV irradiation accelerated ageing, the spectrum registered after 1000 hours being identical to that recorded after the first ageing cycle.

Again, these observations argue for a good environmental behavior of the water repellent product.

For Tegosivin HL 100, the first accelerated ageing cycle (500 hours of UV irradiation) determines a pronounced modification of the FT-IR spectrum (Fig. 103), i.e. the loss of part of the siloxane product (for instance through photo-induced degradation of the main siloxane network accompanied by the elimination of low molecular weight components).

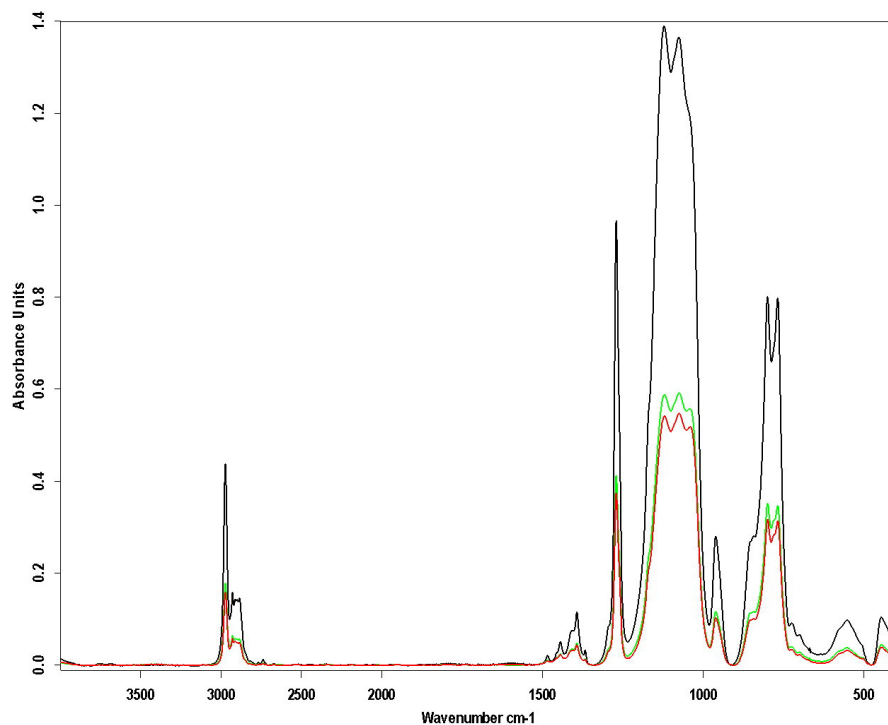


Fig. 103. FT-IR spectrum of Tegosivin HL 100, cast as film;
 — FT-IR spectrum of Tegosivin HL 100, unaged; — FT-IR spectrum of Tegosivin HL 100, aged for 500 hours; — FT-IR spectrum of Tegosivin HL 100, aged for 1000 hours

Practically all major signals decrease almost 50% in intensity during the first degradation cycle, while the second cycle is basically of no further consequence.

Considering the attribution of the typical absorption bands and their variation during degradation it appears that the major chemical groups Si – CH₃ (1270 cm⁻¹), Si – OCH₃ (961 cm⁻¹), Si – O – Si, Si – O – C, Si – CH₃ (1000 – 1200 cm⁻¹) are affected by the UV irradiation. As a consequence, one can conclude that the environmental stability of Tegosivin HL 100 is somewhat lower as compared to those of Lotexan-N and Silres® BS 290 – at least for the first accelerated ageing cycle –, so that the protective ability of Tegosivin HL 100 films is less efficient.

The FT-IR spectrum of unaged TMSPPMA film presents the peaks characteristic to the chemical structure of the product. According to the spectrum recorded after 500 hours of UV ageing, the UV accelerated ageing of the polymeric film determines a strong attenuation of the spectrum. The ageing promotes different chemical reactions, i.e.

the hydrolysis and further condensation of the methoxy groups and the polymerization of the unpolymerized methacrylic double bonds (Fig. 104).

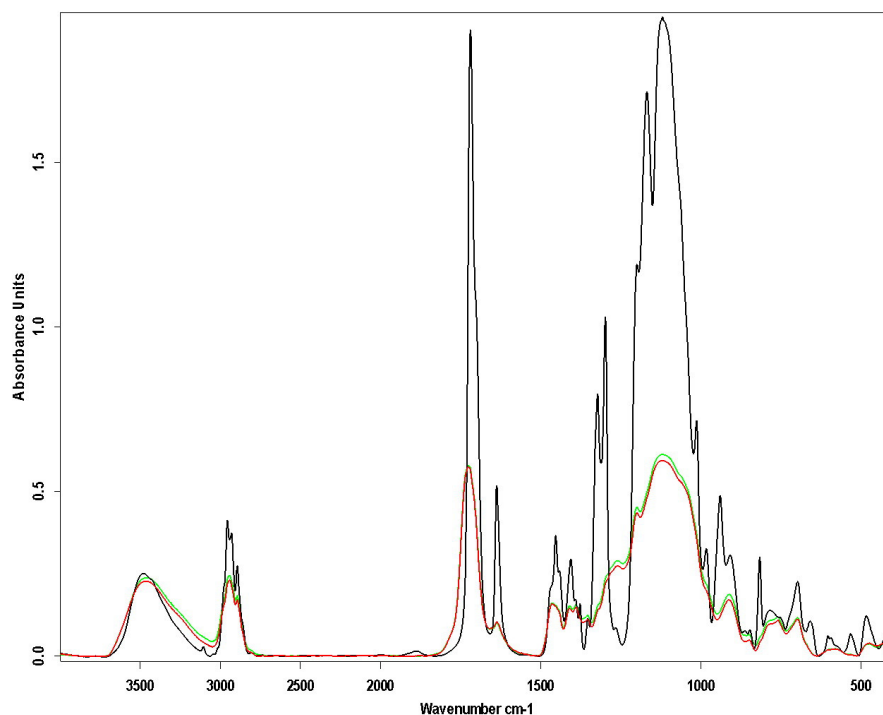


*Fig. 104. FT-IR spectrum of TMSPMA, cast as film;
 — FT-IR spectrum of TMSPMA, unaged; — FT-IR spectrum of TMSPMA, aged for 500 hours; — FT-IR spectrum of TMSPMA, aged for 1000 hours*

These changes appear in the FT-IR spectrum through the diminishing of the Si – O – C signals (1013 – 1180, 1298, 908, 940, 982 cm^{-1}) and the appearance of a large signal centered at 1180 cm^{-1} , band that overlaps different signals.

The C = C unsaturated bonds, evidenced by the absorption at around 1640 cm^{-1} , disappear in the FT-IR spectrum of the polymeric film aged for 500 hours, as a consequence of the polymerization of the unsaturated bonds under UV.

A second consequence of the polymerization process consists in the shifting and the broadening of the absorption band specific to the C = O bond from 1719 to 1730 cm^{-1} . The spectrum recorded after the second accelerated ageing cycle (1000 hours of UV irradiation) is identical to the one registered after the first cycle. Therefore, all chemical transformations induced by the first ageing cycle lead to the formation of a very stable polymeric film, highly crosslinked, able to resist without any changes to longer ageing periods.

VIII. 2. 1. 2. Swelling and solubility tests

The polymeric materials / films have been tested in terms of durability by means of swelling and solubility tests. These ones were carried out on unaged and aged films (500 and 1000 hours, respectively, 40° C, UV irradiation). Due to their film forming capacity, Lotexan-N, Silres® BS 290, Tegosivin HL 100 and TMSPMA have been tested through swelling and solubility tests. These products have the ability to form films on glass plates. The unaged and aged films were immersed in neutral and modified pH (i.e., pH = 7.2; pH = 5.5; pH = 8.5) water for 24 hours. Good resistance to water, widely present in the environment, is a significant proof of product's durability.

Table 1. Swelling / solubility values (%) – film water resistance in (a) neutral pH; (b) acid pH; (c) basic pH

pH = 7.2 unaged samples	Time (h)	Lotexan-N	Silres® BS 290	Tegosivin HL 100	TMSPMA
	1	1.77	0.15	- 1.22	2.35
	2	1.77	0.15	- 0.82	2.61
	6	1.92	0.53	- 0.60	3.26
	24	1.53	0.15	- 0.08	2.61

(a)

pH=5.5 ^a unaged samples	Time (h)	Lotexan-N	Silres® BS 290	Tegosivin HL 100	TMSPMA
	1	2.11	0.15	0.22	0.18
	2	2.52	0.69	0.31	0.18
	6	2.52	0.69	0.42	0.18
	24	4.25	40.97	0.88	- 0.25

(b)

pH=8.5 ^b unaged samples	Time (h)	Lotexan-N	Silres® BS 290	Tegosivin HL 100	TMSPMA
	1	1.35	0.35	0.89	2.33
	2	1.32	0.35	0.77	2.33
	6	1.12	0.35	0.49	2.33
	24	0.91	0.53	0.14	2.5

(c)

^a – for hydrochloric acid; ^b – for sodium hydroxide

Swelling (%) = $100 (W_s - W_0) / W_0$, where W_s is the weight of the film after immersion in water solution and W_0 is the weight of the dry film before the immersion. Negative values indicate partial solubilization.

All four tested polymeric films showed a very good water stability behavior at pH = 7.2. Silres® BS 290 film reached, after 24 hours immersion in water, a swelling degree of 0.15%, while TMSPMA film reached a slightly higher value of 2.61%. Tegosivin HL 100 showed a slight weight loss (dissolution of small amounts of the original film), but the value attained after 24 hours indicates a very low film solubility.

As for the results obtained for pH = 5.5, the experimental data show that all films present a very good water resistance / stability, except for Silres® BS 290 which proves a somewhat different behavior, i.e., the swelling degree attains 40.97% after 24 hours of immersion. However, considering that the films were introduced in an acidic medium, the stability towards acid water is acceptable.

At pH = 8.5, all films present a very good water resistance / stability, the higher swelling degree being registered for TMSPMA – 2.33 – 2.50% for 24 hours of immersion.

A literature survey shows that many polymeric materials used in stone conservation (e. g., the polyacrylates) attain very high swelling degrees (up to 200%) or, by the contrary, high dissolution rates (up to – 75%) when submitted to swelling and solubility tests in water of different pH values. Therefore, it is obvious that the three polymeric films under investigation show very good results, being appropriate as water repellent products.

After a first 500 hours ageing cycle in a UV climatic chamber, at 40° C, the polymeric films of Lotexan-N, Silres® BS 290, Tegosivin HL 100 and TMSPMA were taken out of the climatic chamber in order to test their swelling and solubility behavior. The polymeric films have been immersed in neutral and modified pH (i.e., pH = 7.2; pH = 5.5; pH = 8.5) water for 24 hours. The results are given in Table 21.

Table 21. Swelling / solubility values (%) after 500 hours of UV irradiation – film water resistance (a) neutral pH; (b) acidic pH; (c) basic pH

pH = 7.2 500 h aged samples	Time (h)	Lotexan-N	Silres® BS 290	Tegosivin HL 100	TMSPMA
	1	0.48	0.23	0.22	1.35
	2	0.59	0.34	0.22	1.48
	6	0.59	0.34	0.41	1.85
	24	1.28	1.84	0.37	1.48

(a)

pH=5.5 ^a 500 h aged samples	Time (h)	Lotexan-N	Silres® BS 290	Tegosivin HL 100	TMSPMA
	1	0.33	- 0.46	0.12	1.01
	2	0.41	- 0.30	0.12	1.34
	6	0.60	1.22	0.18	2.02
	24	0.80	0.30	0.69	1.85

(b)

pH=8.5 ^b 500 h aged samples	Time (h)	Lotexan-N	Silres® BS 290	Tegosivin HL 100	TMSPMA
	1	0.33	0	0.2	1.46
	2	0.41	0.48	0.4	1.55
	6	0.60	0.48	0.6	1.73
	24	0.80	- 0.16	1.07	1.82

(c)

^a – for hydrochloric acid; ^b – for sodium hydroxide

The data given in Table 21 show that the 500 hours of ageing has no significant influence on the swelling / solubility behavior of the films. The highest recorded swelling values, no matter the pH, amount to 2.02%, a perfectly acceptable value. At the same time, while Tegosivin HL 100 unaged film shows a slight dissolution at pH = 7.2, no dissolution was registered for the aged (500 hours) film.

The 1000 hours aged samples results are given in the Table 22. The same ageing and swelling / solubility conditions were applied.

Table 22. Swelling / solubility values (%) after 500 hours of UV irradiation – film water resistance (a) neutral pH; (b) acidic pH; (c) basic pH

pH=7.2 1000 h aged samples	Time (h)	Lotexan-N	Silres® BS 290	Tegosivin HL 100	TMSPMA
	1	0.18	0	0	0.36
	2	0.18	0	0	0.36
	6	2.90	3.02	0.25	0.62
	24	1.80	0.48	0.40	1.48

(a)

pH=5.5 ^a 1000 h aged samples	Time (h)	Lotexan-N	Silres® BS 290	Tegosivin HL 100	TMSPMA
	1	0.28	0.34	0	1.02
	2	0.30	0.34	0	1.93
	6	1.90	1.18	0	2.50
	24	1.60	0.20	0	2.50

(b)

pH=8.5 ^b 1000 h aged samples	Time (h)	Lotexan-N	Silres® BS 290	Tegosivin HL 100	TMSPMA
	1	0.32	0.26	0.13	1.28
	2	0.80	1.77	0.22	1.66
	6	1.80	0.75	0.30	1.88
	24	1.80	0.75	0.48	1.88

(c)

^a – for hydrochloric acid; ^b – for sodium hydroxide

Again, it appears that prolonged accelerated ageing doesn't diminish film water resistance of the four investigated samples in neutral, acid and basic aqueous environment. On the contrary, some of the samples (e.g., Tegosivin HL 100 in acidic medium) show a very high stability – during 24 hours of swelling measurements, the swelling degree remains zero (no swelling or polymer dissolution occurs). Very good swelling values are also obtained for TMSPMA films.

As a general conclusion, the four films under investigation (Lotexan-N, Silres® BS 290, Tegosivin HL 100 and TMSPMA), both unaged and aged (500 and 1000 hours, respectively) show a remarkable stability in water. This highly recommends the products for water repellent applications in stone conservation.

It is to be underlined that other commercial products, described in the literature, show significantly higher swelling degrees (sometimes up to 200%) or lose part of their substance by solubility in water (up to 50%).

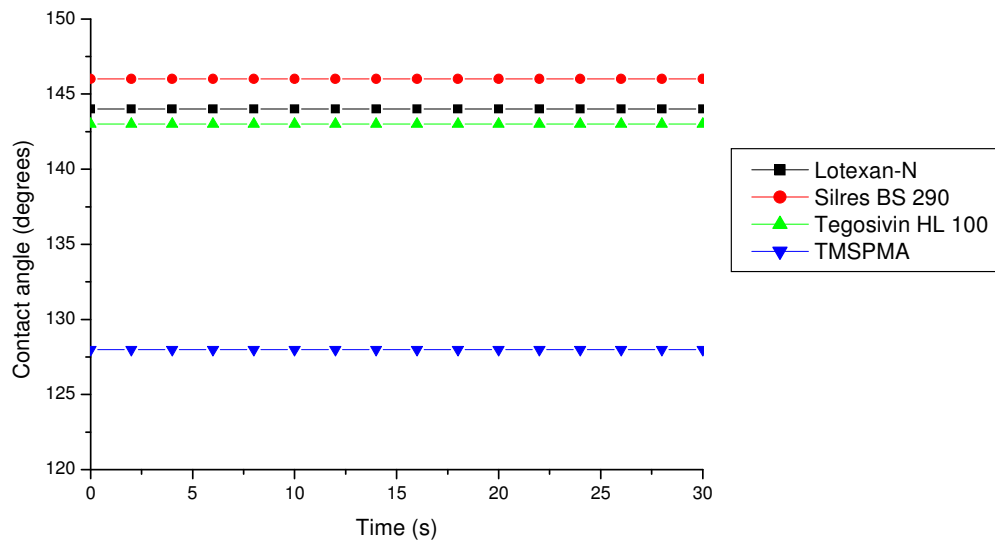
VIII. 2. 2. Characterization of the treated stones after the artificially accelerated ageing under UV irradiation

VIII. 2. 2. 1. Contact angle measurements

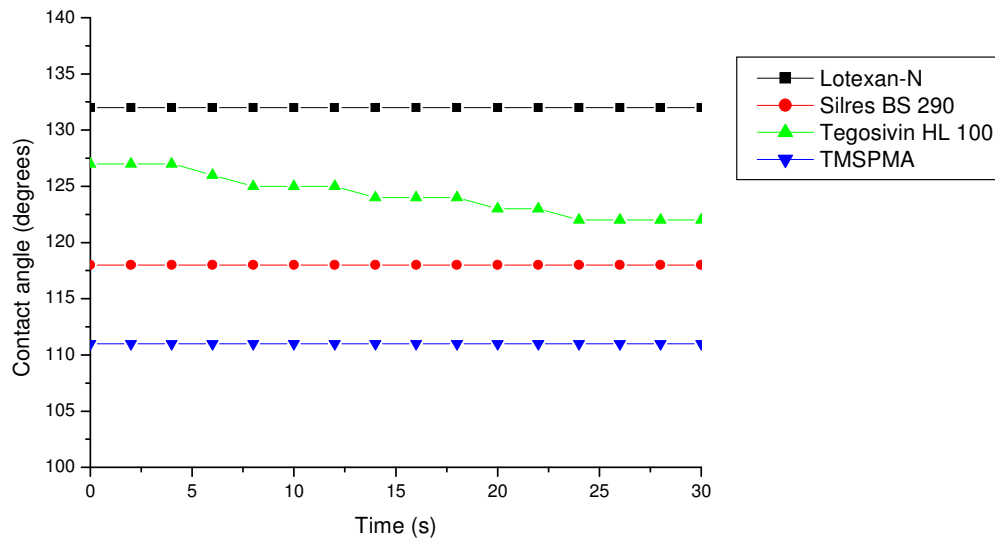
Since the study involves water repellent chemical products, the contact angle is one of the most significant elements in the evaluation of the two limestones treated with the three selected worldwide used siloxane-based products and with the newly synthesized nanocomposite material. Contact angle measurements were performed on the treated, but unaged Laspra and Repedea (Chapter VII), these ones being repeated, using the same technique and instrument, on the treated, but aged under different ageing agents, stone samples.

In this chapter, the purpose was to evaluate the behavior of Laspra and Repedea, treated with Lotexan-N, Silres® BS 290, Tegosivin HL 100 and TMSPMA in terms of their contact angle value after the exposure of the treated limestones for 1000 hours to UV irradiation.

The contact angle values registered by the treated and aged Laspra and Repedea samples are presented in Fig. 105.



(a)



(b)

Fig. 105. Contact angle values after 1000 hours of artificially accelerated ageing under UV irradiation. (a) – Laspra, (b) – Repedea

Table 23 (a) and (b) lists the contact angle values of Laspra and Repedea, treated with Lotexan-N, Silres® BS 290, Tegosivin HL 100 and TMSPMA, before and after 1000 hours of artificially accelerated ageing under UV irradiation.

Table 23. Contact angle values of Laspra and Repedea;
(a) treated; (b) treated / aged for 1000 hours under UV irradiation

	Lotexan-N	Silres® BS 290	Tegosivin HL 100	TMSPMA
Laspra	148	151	147	120 ↓
Repedea	142	123	100 ↓	105

(a)

	Lotexan-N	Silres® BS 290	Tegosivin HL 100	TMSPMA
Laspra	144	146	143	126
Repedea	132	116	127 ↓	111

(b)

Considering that the artificially accelerated ageing tests are simulating, in an artificial and, most significantly, accelerated manner what happens in nature, one must interpret the obtained results from this perspective. The data in Table 23 clearly indicate that no significant degradation / change in the contact angle values registered by the treated vs. treated / aged stone samples occurs.

In case of Laspra, the three commercial siloxane-based water repellents (Lotexan-N, Silres® BS 290 and Tegosivin HL 100) are exhibiting the same behavior in terms of contact angle, the samples showing a slight decrease in the contact angle value. However, if one takes into consideration that the stone samples were exposed to 1000 hours of continuous UV irradiation, their behavior may be considered to be very good – their water repellency being not affected by the exposure to UV irradiation at 40° C.

For Repedea, the samples treated with Lotexan-N and Silres® BS 290 show, as in the case of Laspra, a decrease in the contact angle values; this decrease must not be considered significant considering the experimental conditions of the artificially accelerated ageing test. Repedea treated with Tegosivin HL 100 registers an increase in the contact angle value after the exposure to 1000 hours of UV irradiation, probably due to the finalization of the polymerization due either to UV irradiation or to the elevated temperature conditions (40° C).

Prior to the artificially accelerated ageing under UV irradiation at 40° C, both Laspra and Repedea treated with TMSPMA registered a slight decrease in contact angle values (more pronounced for Laspra and barely noticeable for Repedea) during the 30

seconds of measurement. After 1000 hours of UV irradiation at 40° C, Laspra treated with the nanocomposite material exhibited contact angle values of either 126° or 132° (two stone samples, treated with each of the four water repellents, were introduced in the UV climatic chambers and then analyzed through every evaluation method), with either 6° or 12° degrees higher than the treated, but unaged samples. These values are higher than the ones of the treated / unaged stone samples and, as it can be observed from Fig. 105 (a), remain constant during the 30 seconds of measurement.

A better behavior after 1000 hours of UV irradiation was registered for Repedea treated with TMSPMA, as well, the contact angle value increasing with about 6° and showing a constant value during the 30 seconds of measurement.

During the artificially accelerated ageing, TMSPMA polymeric layers became more hydrophobic, increasing the water repellency. The 40° C temperature used in the experiment determines the networking of the polymeric structure through the polymerization of the remaining free methacrylate units, thus increasing system's hydrophobicity. At the same time, the additional formation of the cage-like fragments of silsesquioxane type also increases system's water repellency.

VIII. 2. 2. 2. Water absorption by capillary suction

Another significant parameter to be studied when discussing stone's durability is water absorption by capillary suction. Laspra and Repedea, untreated and treated with Lotexan-N, Silres® BS 290, Tegosivin HL 100 and TMSPMA, were tested in terms of water absorption by capillarity (g H₂O / 100 g stone) according to the standard procedures.

The curves describing the water absorption by capillarity of Laspra, both untreated and treated with the studied water repellent products, are given in the next figure (for all figures in this sub-chapter, the program used for the representation links the experimental data through a point by point technique).

Figures 106 – 111 reveal the experimental results of the untreated stones, of the same stones treated with the four different siloxane-based water repellents, but unaged, and of the stones treated and aged for 1000 hours under UV irradiation at 40° C.

Laspra – Lotexan-N curves (Fig. 106) show that the treatment decreases the water absorption by capillarity (24 hours) from about 12.5 grams of water / 100 grams of stone to about 5.5 grams of water / 100 grams of stone and the accelerated ageing further

strongly decreases the water absorption by capillarity that reaches a maximum value of 0.5 grams of water / 100 grams of stone.

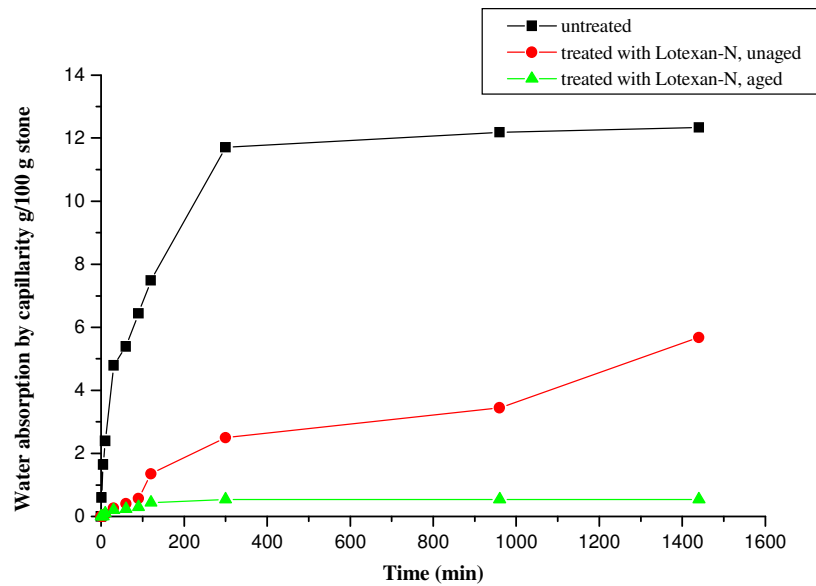


Fig. 106. Water absorption by capillarity – Laspra – Lotexan-N system

These experimental data are interesting – they show that, by ageing, the treated stone becomes more and more water impermeable. It thus appears that ageing of the polymeric film deposited on stone surface (and partially penetrating into the superficial layers of the stone) results in a hydrophobization of the film (disappearance / transformation of the hydrophilic groups) and in the crosslinking of the polymeric chains.

The same observations are valid for the Laspra – Silres® BS 290 system (Fig. 107) – the chemical treatment and the accelerated ageing yield a strong decrease of water absorption by capillarity.

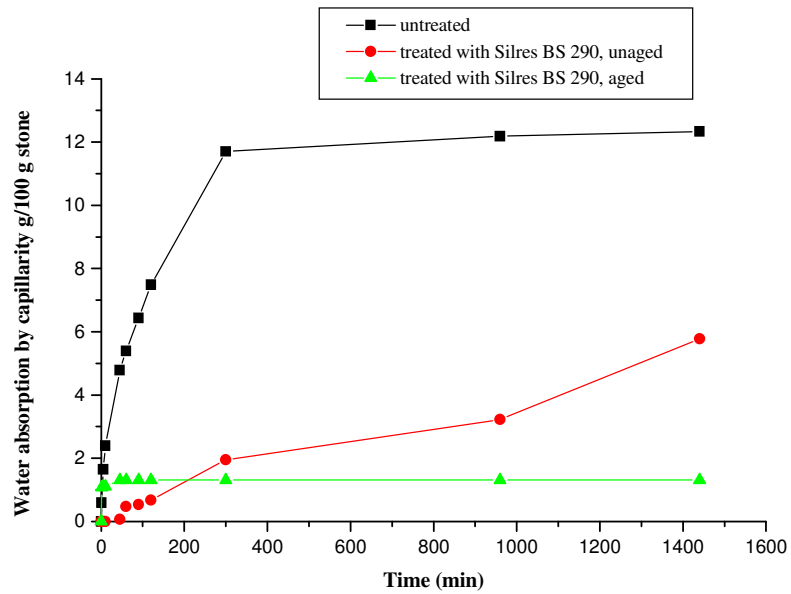


Fig. 107. Water absorption by capillarity – Laspra – Silres® BS 290 system

The hydrophobization of Laspra is even more significant for the Laspra – Tegosivin HL 100 system (Fig. 108) – a maximum water absorption of 0.7 grams of water / 100 grams of stone being attained for the treated and unaged stone, while the treated and aged one remains at about 0 grams of water / 100 grams of stone.

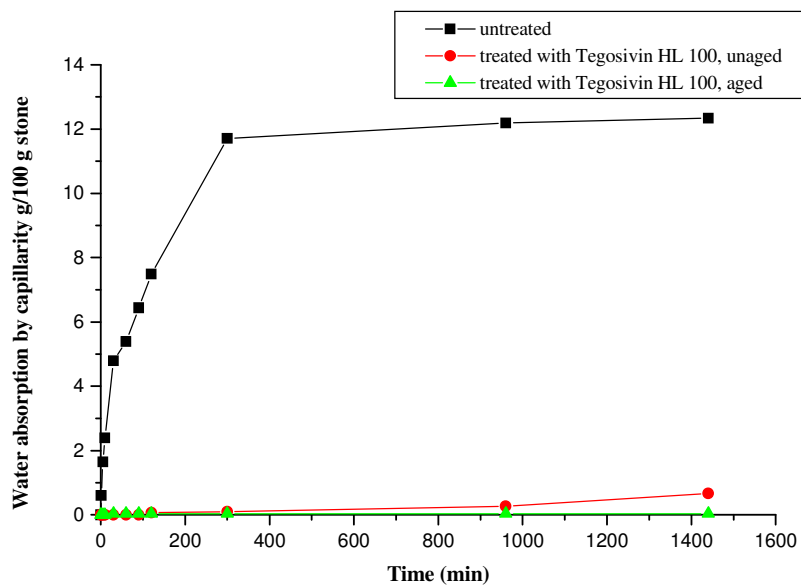


Fig. 108. Water absorption by capillarity – Laspra – Tegosivin HL 100 system

In the case of Repedea, the best results from this perspective proved to be provided by Silres® BS 290 (Fig. 109) – the water absorption by capillarity reaches 0.2 grams of water / 100 grams of stone for both treated and treated and aged samples (superposed curves).

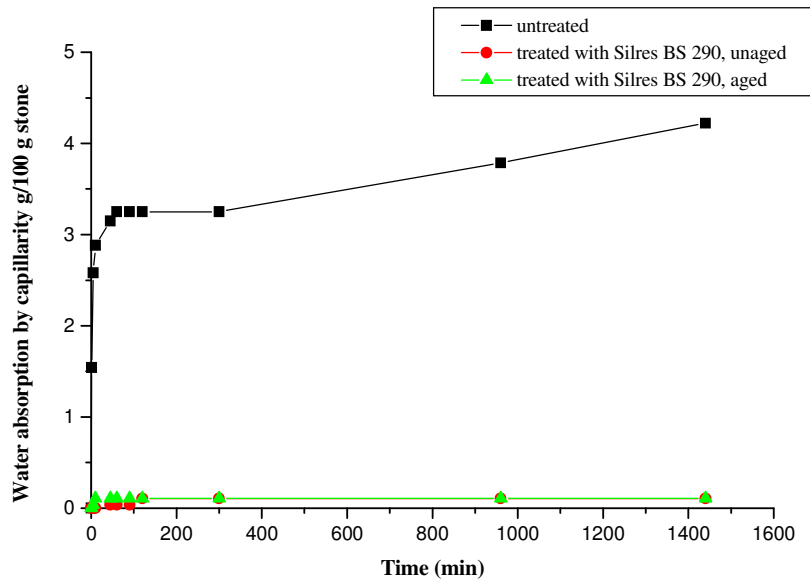


Fig. 109. Water absorption by capillarity – Repedea – Silres® BS 290 system

Lotexan-N (Fig. 110) and Tegosivin HL 100 (Fig. 111) induce practically the same effect – the treatment strongly diminishes the water absorption of the stone, but ageing slightly increases the water absorption of the treated stones. No explanation – apart from a partial slight degradation of the polymeric film under the UV irradiation – can be given for this behavior.

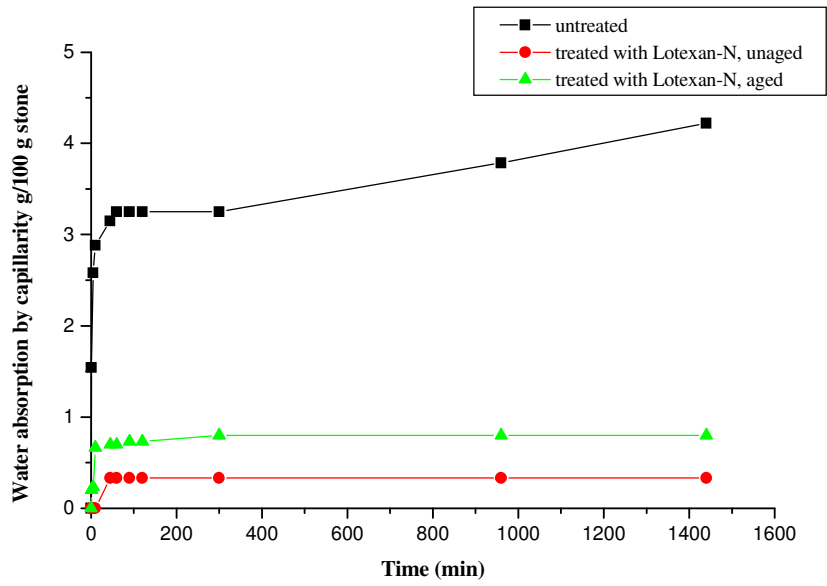


Fig. 110. Water absorption by capillarity – Repedea – Lotexan-N system

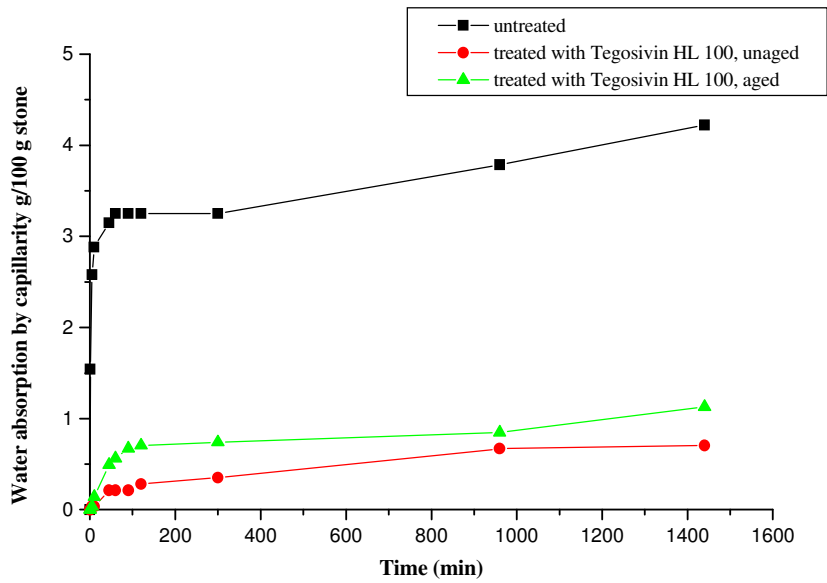


Fig. 111. Water absorption by capillarity – Repedea – Tegosivin HL 100 system

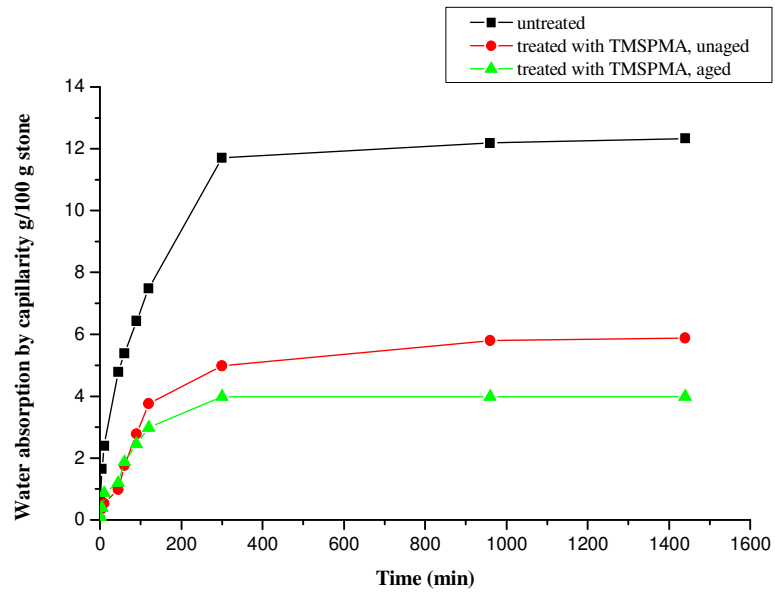


Fig. 112. Water absorption by capillarity – Laspra – TMSPMA system

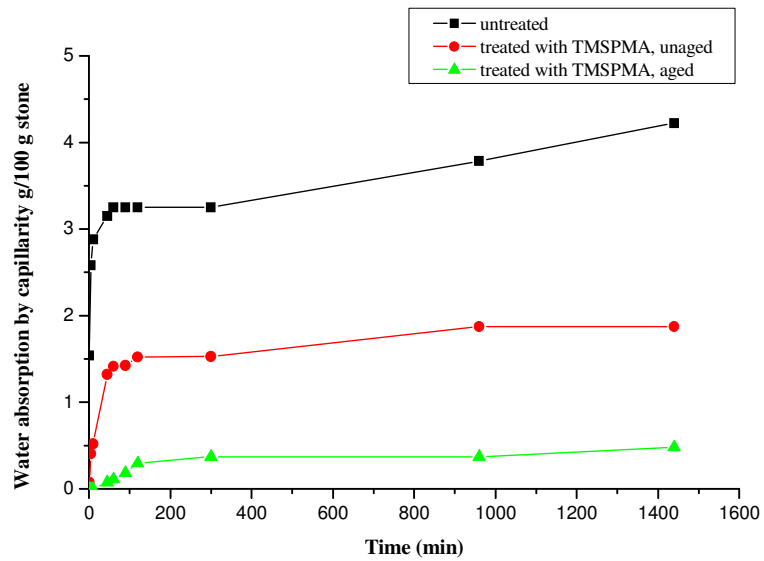


Fig. 113. Water absorption by capillarity – Repedea – TMSPMA system

The nanocomposite material proved to behave better, from the water absorption by capillarity’s perspective, after the exposure to UV irradiation at 40° C. Nevertheless, considering the graphs scale, TMSPMA afforded better results when applied on Repedea than on Laspra.

For Repedea, Tegosivin HL 100 and Lotexan-N prove to be the less efficient products, but this statement has a relative value since the water absorption by capillarity of the Repedea – Tegosivin HL 100 aged sample amounts to only 1.11 grams of water / 100 grams of stone, and Lotexan-N behaves quite similarly. TMSPMA ranges in a good position.

As for Laspra, the less efficient treatment is TMSPMA, while the best results are obtained through the treatment with Tegosivin HL 100. This unusual behavior (as compared to the effect of the simple treatment) will be discussed later.

VIII. 2. 3. Conclusions

The specialized literature states that siloxane-based chemical products used in stones conservation exhibit a very good stability towards UV irradiation. This is in agreement with the data presented in this chapter. However, the investigation, from the resistance to UV irradiation perspective, revealed interesting aspects, such as the difference in the behavior of both limestone samples treated with the commercially available products *vs.* the behavior of the ones treated with the new nanocomposite material.

The water repellent polymeric films proved, in almost all cases, a very good stability towards swelling and solubility – film water resistance being a significant aspect in the evaluation of a certain product's durability. The FT-IR spectra, performed on every polymeric film before and after each 500 hours of UV irradiation at 40° C, demonstrated that changes in the macromolecular structure of the products occur only during the first ageing cycle, a more or less constant behavior following afterwards.

When evaluating the treated limestones performance after their exposure to artificially accelerated ageing under UV irradiation at 40° C, one must point out the slight decrease in the contact angle values registered by both Laspra and Repedea for the samples treated with Lotexan-N, Silres® BS 290 and Tegosivin HL 100, unlike the samples treated with TMSPMA, which exhibit an increase in these values. The obtained contact angle data are in concordance with the water absorption by capillarity results, except in the case of the stones treated with TMSPMA – these results will be discussed further in this chapter.

VIII. 3. Resistance to salt mist action

VIII. 3. 1. Introduction

Along with air pollution, soluble salts represent one of the main causes of cultural heritage building stone decay. Generally, the growth of salt crystals within the pores of a stone may generate stresses able to overcome stone's tensile strength and, in time, transform the stone into powder. It is widely recognized that salt crystals also greatly limit the durability of porous building materials. Salt weathering is a process of rock disintegration that takes place in a variety of environments and affects many types of rocks [101]. Salt deterioration can be as well described as a known and widespread geomorphic process [102, 103] responsible for the degradation of stonework and masonry used in architectural heritage all over the world [104]. Natural and artificial porous media become contaminated with salts in many different ways, in this context moisture and ground water rising from foundations being the responsible sources. Some materials may even contain salts inherently, while in other cases, salt deposition in buildings and stone monuments at coastal sites is mainly caused by marine aerosol [105, 106].

A number of mechanisms have been proposed to explain the damage caused by soluble salts to porous materials. They include generation of crystallization pressure, hydration pressure, thermal expansion, osmotic pressure and chemical weathering [107]. Besides hydration pressure, which appears to be a non-existing phenomenon (it just seems to be crystallization pressure due to formation of a hydrated phase following dissolution of an anhydrous one [108-110]), all other mechanisms may to some degree contribute to the overall damage process. However, crystallization pressure appears to be the most relevant [108, 109, 111-115].

Most commonly, evaporation may induce salt crystallization [115], the highly concentrated saline solutions yielding to a large volume of precipitates [116]. The growth of a crystal in a confined space (pore) can exert a pressure sufficient to exceed the rupture modulus of most ornamental materials, including natural stone, mortars and bricks, causing their breakage [117, 118]. It is generally accepted that the damage to porous stones arises from repeated cycles of crystallization / dissolution of soluble salts within the porous matrix of the stone [115]. These processes can alter both porosity and

pore size distribution of the stones, changing also their mechanical properties (compression strength, sclerometric resistance, microhardness) [119].

Under room conditions, the sodium chloride – water system has one stable phase: halite (NaCl). Halite crystallization takes place over pore surface due to heterogeneous nucleation (i.e., pore – solution – air interface) and tends to grow on the stone surface, producing efflorescence. The role of pore size distribution in stone decay caused by salt crystallization is of great consequence due to its influence on both crystallization pressure and mineral distribution in the stone. In materials with small pores, the crystallization pressure will be higher than in materials with large pores [109, 111, 120-124], and mineral precipitation tends to occur preferably within the inner part of the stone (forming subflorescences). Both phenomena increase the risk of stone decay and, therefore, reduce its resistance against crystallization.

To prevent or reduce water intrusion, water repellent products are applied on architectural stone surfaces in order to create an impermeable barrier to water, without limiting the water vapour permeability of the material, therefore allowing the passage of water vapour through the stone out of the walls [125]. A minimal reduction in water vapour permeability values through coated limestones reduces the possibility of deterioration due to freeze-thaw cycles or salt crystallization by ensuring that natural evaporation can occur. Otherwise, water-soluble salts, which may be normally deposited on the surface of the limestones as efflorescence, can be trapped beneath the coating, at a depth of a few micrometers, producing a granular disintegration and powdering, and therefore leading to mass loss and spalling [7].

The application of water repellent treatments is expected to slow down the deterioration process and to increase the durability of the monumental stones. This subchapter describes the resistance of Laspra and Repedea, coated with the three selected siloxane-based chemical products and with the newly synthesized hybrid nanocomposite with silsesquioxane units [37, 126] against salt mist action.

Saline minerals are frequently used in salt crystallization laboratory tests to mimic the crystallization of the soluble salts in porous materials [127, 128]. The salt mist accelerated ageing test was performed according to UNE-EN 14147 European Standard. After stone cutting and treatment, the stone samples were kept in desiccators at room temperature. When reaching constant weights, the samples treated with the three siloxane-based commercially available water repellents and with the nanocomposite

material were introduced in a salt mist climatic chamber. The chamber was covered in order to avoid the evaporation process. The salt mist artificial ageing was performed by alternating wetting by spraying (with 5% saline solution) and drying cycles. A spraying cycle took place for 4 hours and then was followed by a drying cycle of 20 hours.

The experiment was performed for 30 cycles, until one of the selected limestones (Laspra) became extremely deteriorated, and then continued for another 30 cycles for Repedea (Fig. 114).



(a)



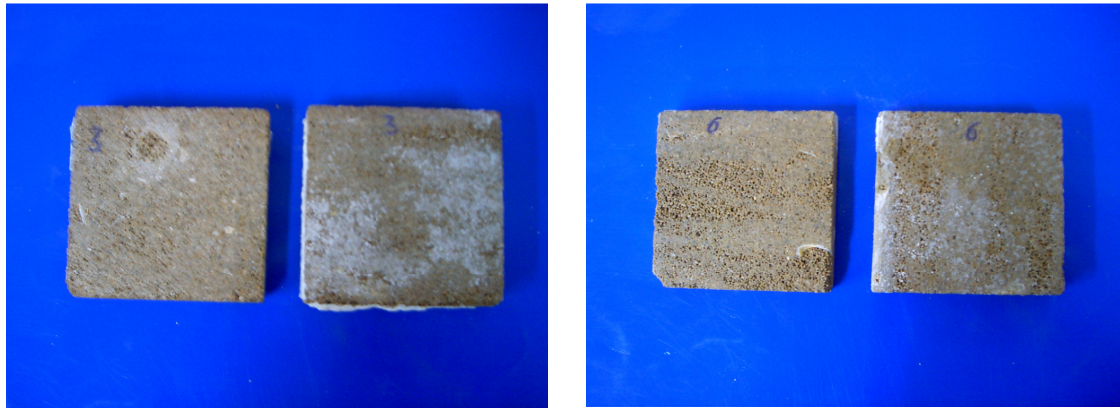
(b)



(c)



(d)



(e)

(f)

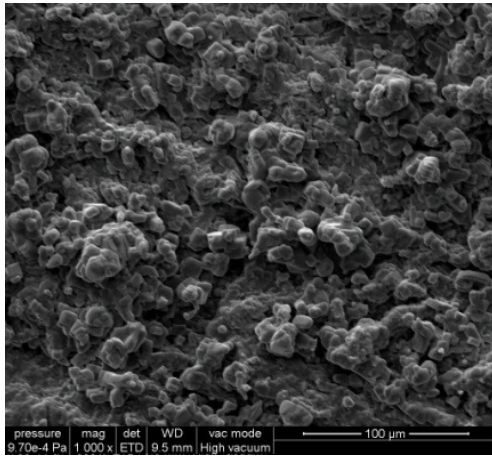
Fig. 114. Laspra treated with (a) Lotexan-N: before and after 30 artificial accelerated ageing cycles; (b) – (c) Tegosivin HL 100 after 30 artificial accelerated ageing cycles; (d) TMSPMA before and after 30 artificial accelerated ageing cycles; (e) Repedea treated with Tegosivin HL 100 before and after 60 artificial accelerated ageing cycles; (f) Repedea treated with TMSPMA before and after 60 artificial accelerated ageing cycles

VIII. 3. 2. Characterization of the treated stones after salt mist action

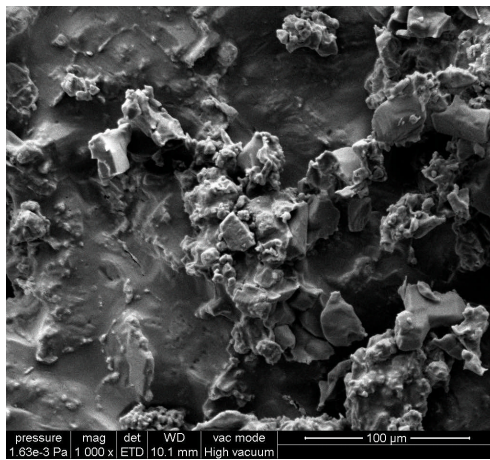
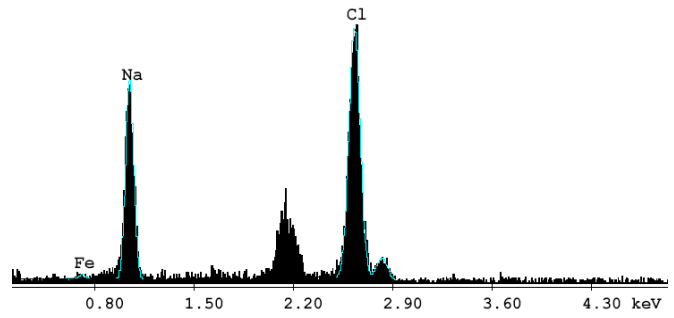
VIII. 3. 2. 1. Visual investigation

The salt and mineral identification was performed studying the mineral habit using high vacuum scanning electron microscopy (ESEM). The measurements were taken using a Quanta 200 instrument equipped with an energy dispersive X-ray device, EDX.

The behavior of the water repellent treatments towards the two selected limestones in this artificially accelerated ageing test was first evaluated by identifying through ESEM analysis the granular disintegration and surface morphology. A few ESEM micrograph examples of Laspra and Repedea, both untreated (Figure 115) and coated with the polymeric films (Figures 116, 117) are shown here, the other performed ESEM micrographs being listed in Annex 1.



(a)



(b)

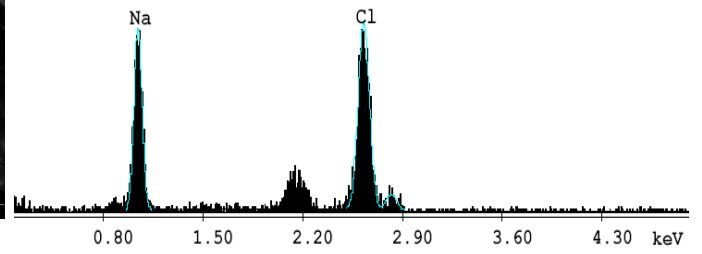
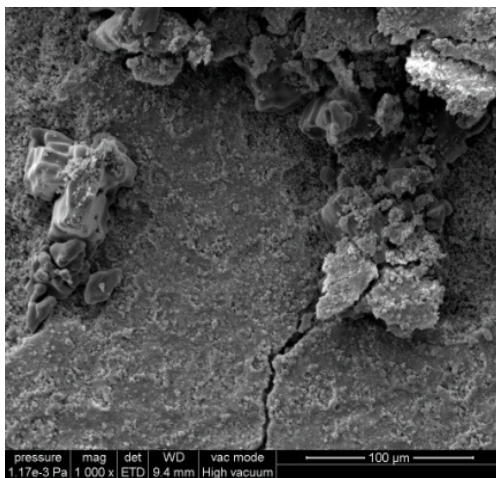
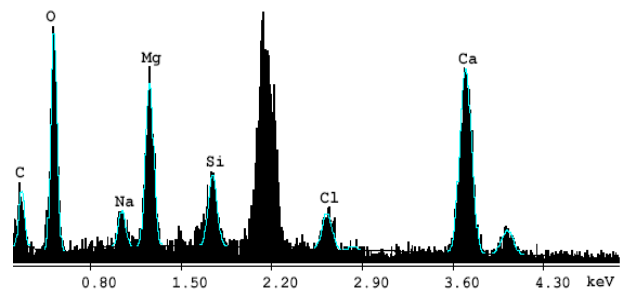
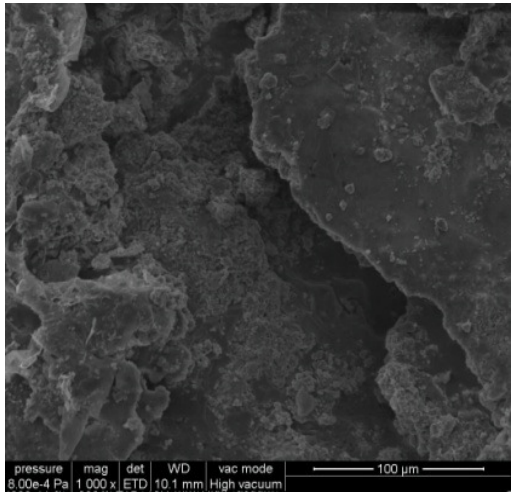


Fig. 115. ESEM micrographs, EDX diagrams and elemental composition of (a) Laspra after 30 ageing cycles and (b) Repedea, after 60 ageing cycles

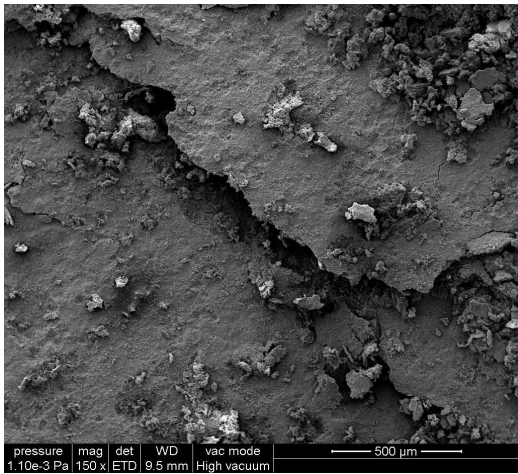
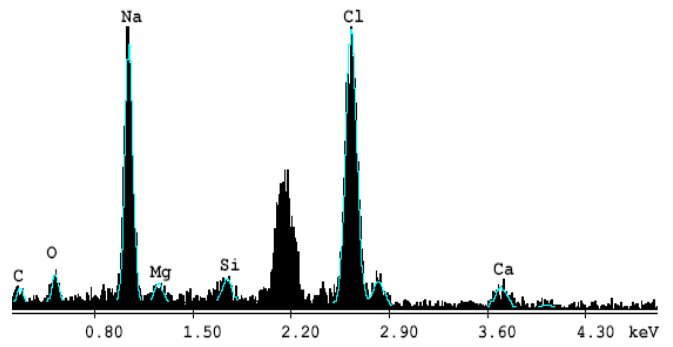


(a)

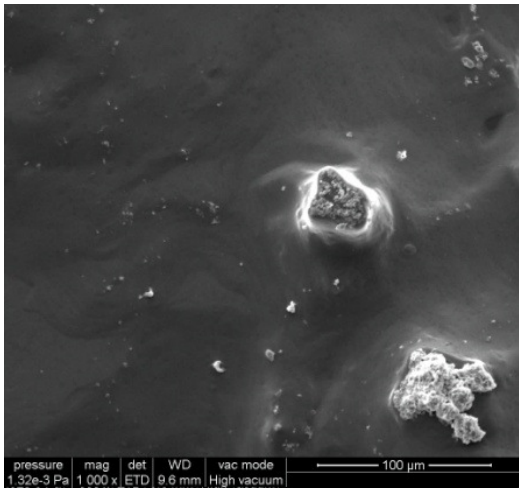
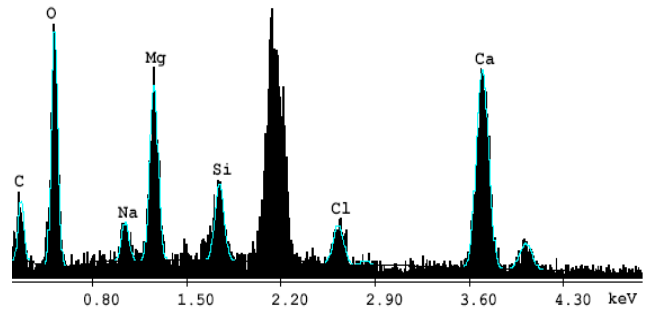




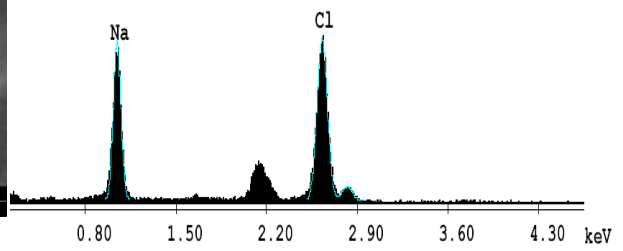
(b)



(c)



(d)



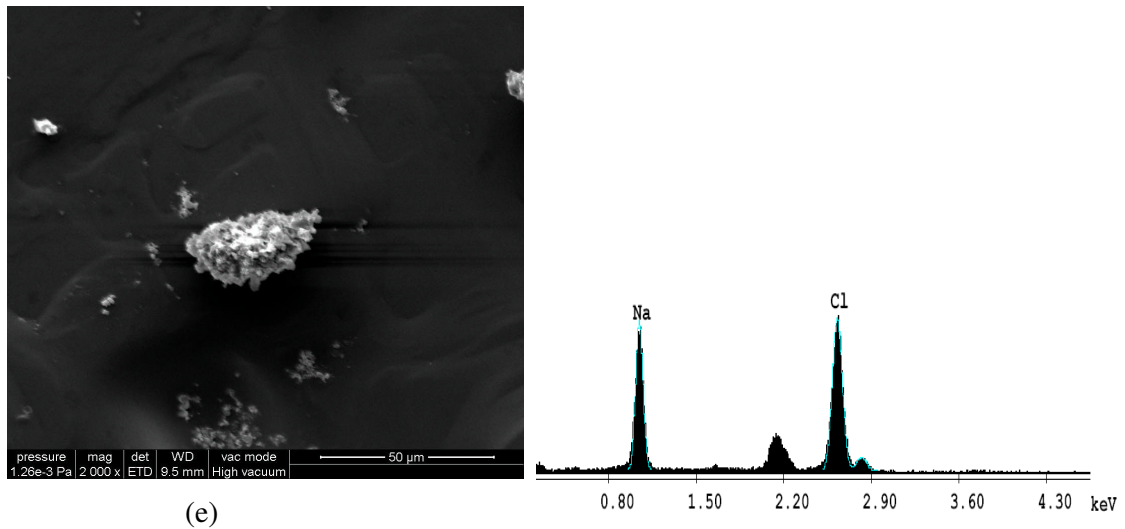
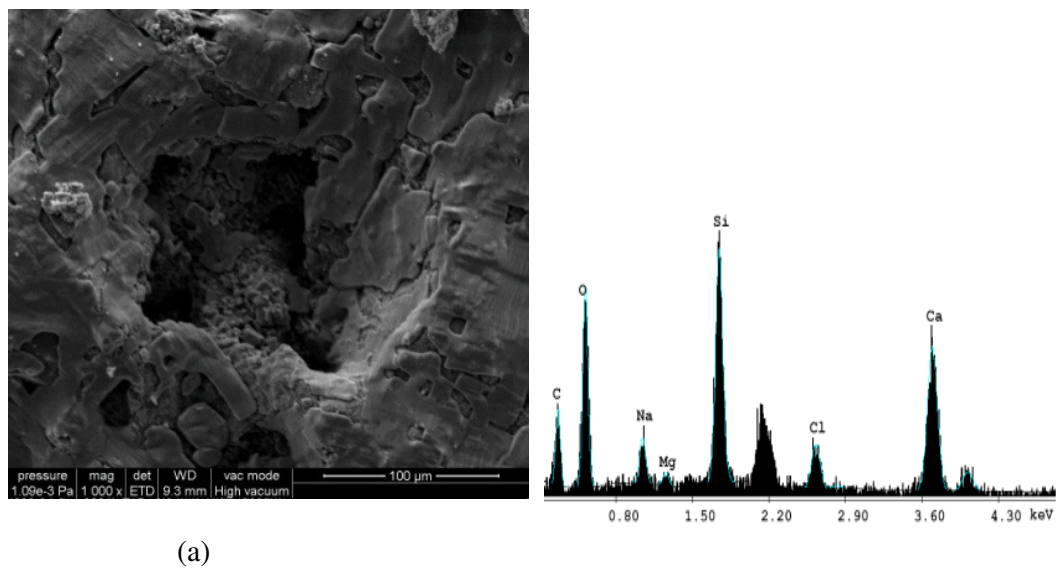
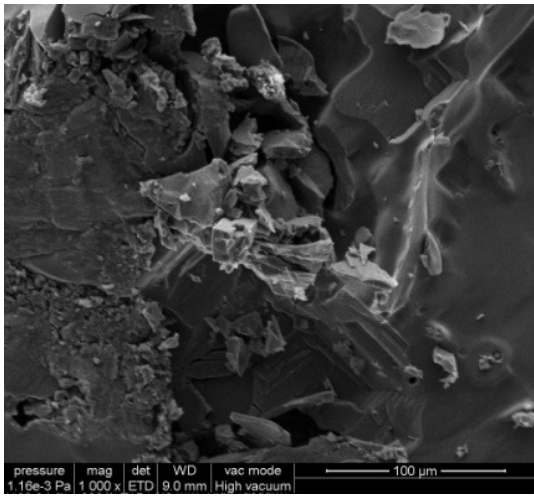
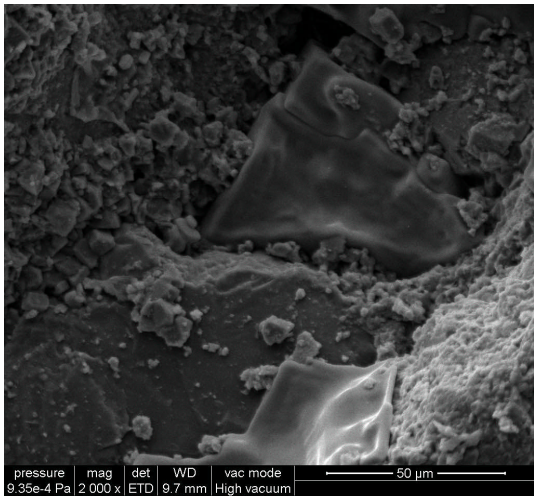
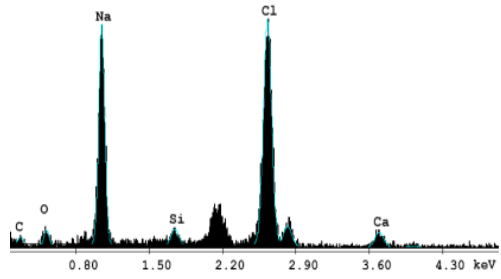


Fig. 116. ESEM micrographs and corresponding EDX diagrams of Laspra coated with (a) Lotexan-N, (b) Silres® BS 290, (c) Tegosivin HL 100, (d), (e) hybrid nanocomposite with silsesquioxane units – after 30 cycles of salt mist artificial accelerated ageing

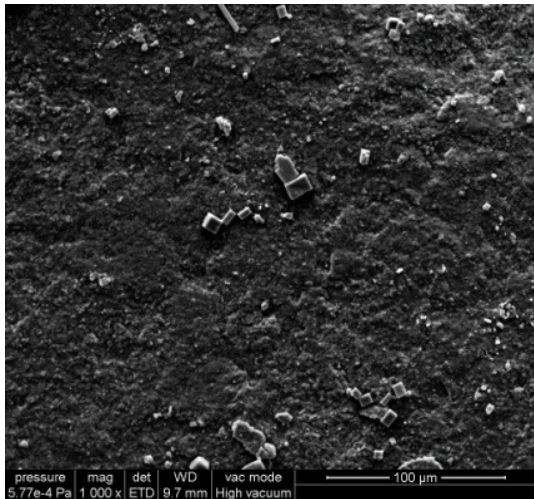
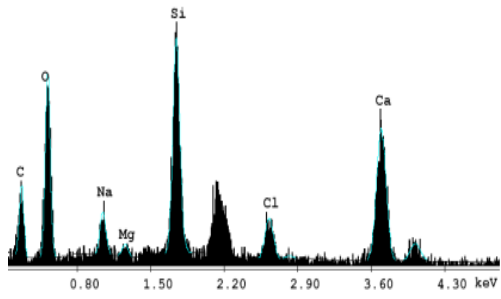




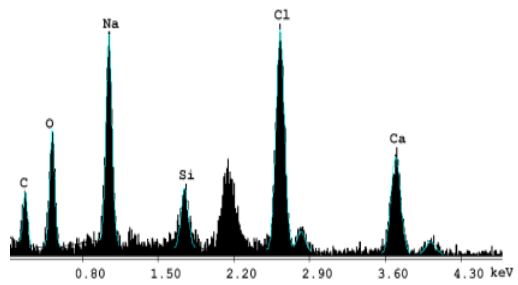
(b)



(c)



(d)



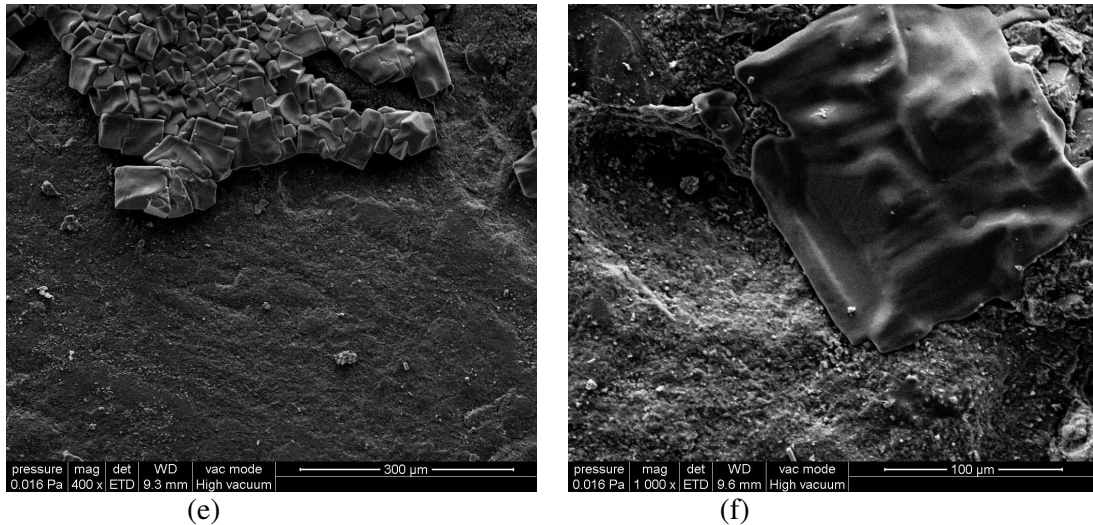


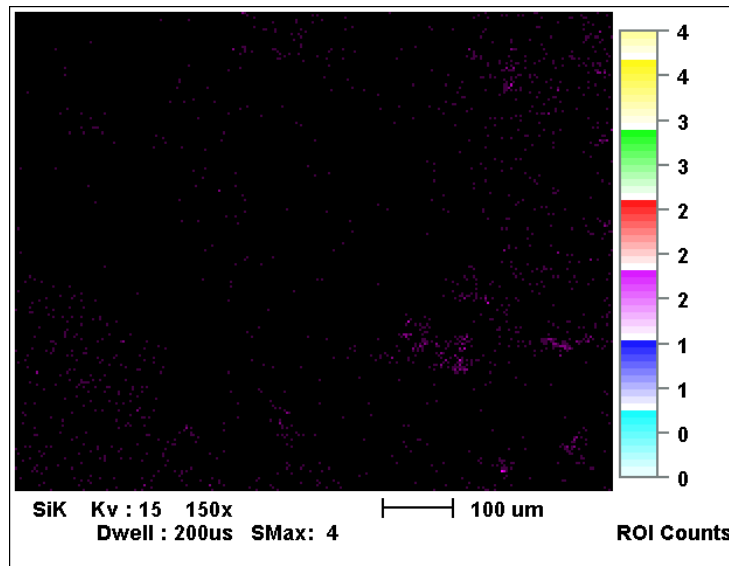
Fig. 117. ESEM micrographs and corresponding EDX diagrams of Repedea coated with (a) Lotexan-N, (b) Silres® BS 290, (c) Tegosivin HL 100, (d), (e), (f) hybrid nanocomposite with silsesquioxane units after 60 cycles of salt mist artificial accelerated ageing

These images show that NaCl crystals tend to nucleate heterogeneously, revealing a strong interaction between the crystals in different zones. The ESEM images illustrate a higher amount of NaCl crystals deposited onto the surfaces of the untreated stones. For those treated with TMSPMA, during evaporation, NaCl crystallizes as small efflorescences on stone surface (Figures 116d, 117d). As for the commercial products, this process is extended to a depth of micrometers (sometimes reaching 1 mm), the outermost polymeric layer showing large fractures and being severely deteriorated. This produces a visible granular disintegration and powdering, therefore leading to stone mass loss (Figures 116a-116c, 117a-117c).

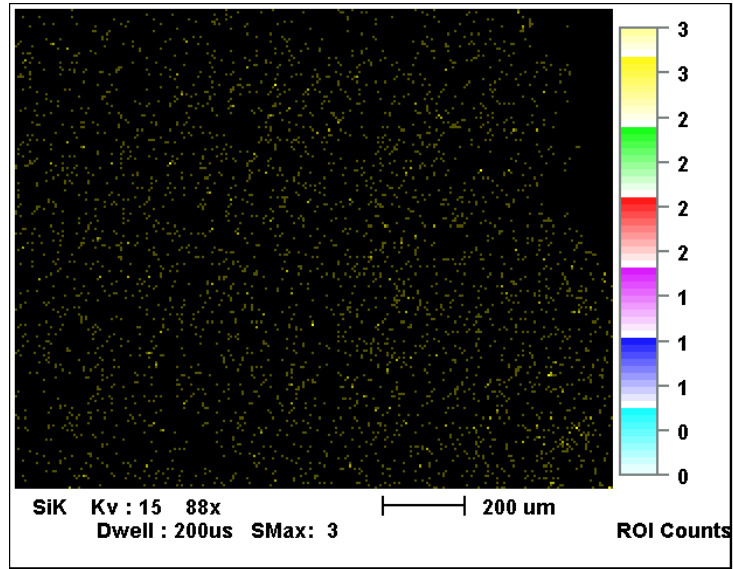
Moreover, the salts crystallize in depth, showing more often cracks parallel to the evaporation surface. It is interesting to note that in ESEM micrographs salt crystals are observed both underneath and above the cracks, but hardly in the cracks themselves (Figures 116a, 116c, 117a, 117c). The absence of salt filling the cracks yields to a mechanism supporting the differential dilation of zones with high and low salt content that may have a major role in stones damage [129, 130]. The shape of the salt crystallizing in material's depth is more difficult to be interpreted. In depth, NaCl has been observed to crystallize mainly as an agglomeration of crystals (Figure 117a, 117c) or as smooth layers on pore walls (Figure 117b). This may be related to the wetting properties of the NaCl solution [131, 132] and may explain why in depth precipitation of halite often occurs as a smooth layer instead of elongated crystals. The stone degradation

can be attributed to different mechanisms [133, 134] which involve the hygroscopic attack of salt aqueous solutions, the later crystallization of the salts inside the rock, as well as the microorganisms and plants action and also the acidic atmospheric contaminants like the SO₂ and the NO₂ that bring the process to stone dissolution. These degradation mechanisms underline the imperative to protect the stone, particularly against water action, this one facilitating the entrance of contaminants and the growth of microorganisms.

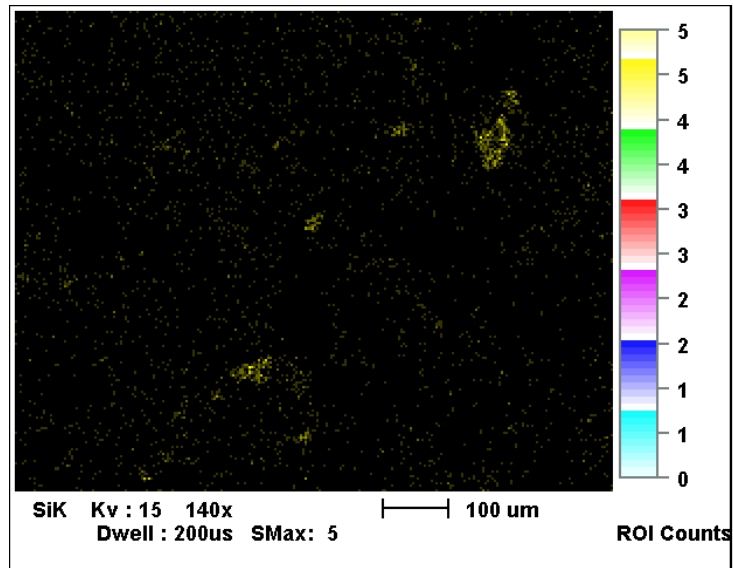
The sealing capacity of these products and the depth of penetration were analyzed by scanning electron microscopy and X-ray mapping of silicium. ESEM micrographs show surface texture variation of the samples with product application. On the samples brushed with siloxane-based products square base polyhedrons have been visualized, that denoting product's presence around and within the pores.



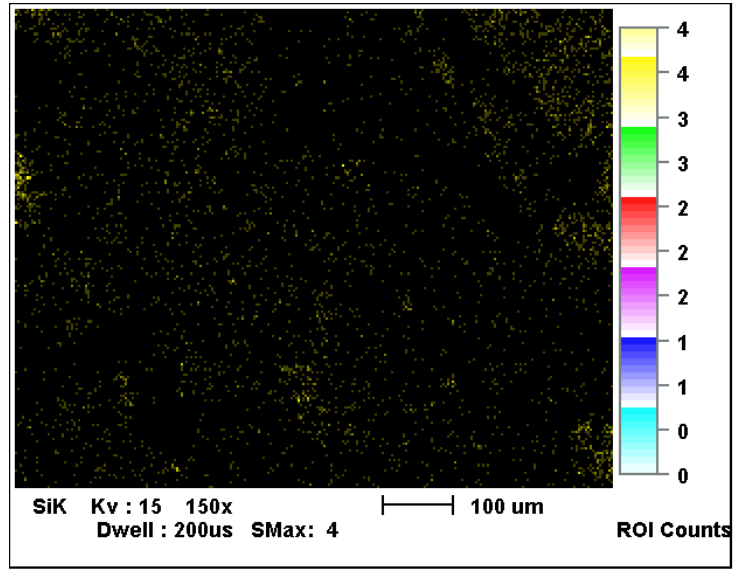
(a)



(b)



(c)



(d)

Fig. 118. EDX – Si mapping of (a) Laspra treated with Lotexan-N after 30 ageing cycles; (b) Laspra treated with TMSPMA after 30 ageing cycles; (c) Repedea treated with Tegosivin HL 100 after 60 ageing cycles; (d) Repedea treated with TMSPMA after 60 ageing cycles

VIII. 3. 2. 2. Contact angle measurements

As previously mentioned, contact angle measurements, water vapor permeability measurements, color and weight measurements were performed, as evaluation methods, following the resistance against salt mist action and, further, against SO₂ action in the presence of humidity artificially accelerated ageing. The results were then compared to the ones obtained for the treated, but unaged limestone samples.

Table 24. Contact angle values of Laspra and Repedea treated, but unaged

	Lotexan-N	Silres® BS 290	Tegosivin HL 100	TMSPMA
Laspra	148	151	147	120 ↓
Repedea	142	123	100 ↓	105

As shown in VIII. 3. 1. and VIII. 3. 2. 1., Laspra became very deteriorated after only 25 – 30 artificially accelerated ageing cycles, some of the samples losing grains through the powdering effect or being completely broken when touched and moved (Fig. 114b and 114c), making a further investigation of these Laspra samples impossible. This

is the case of the samples of Laspra which had not been treated and of the ones treated with the three selected commercially available water repellents; the only ones that were still intact and afforded a complete investigation were the Laspra samples treated with the nanocomposite material (Fig. 114d).

The contact angle values exhibited by the limestones after performing the resistance against salt mist action artificially accelerated ageing test are given in Fig. 119 and Fig. 120.

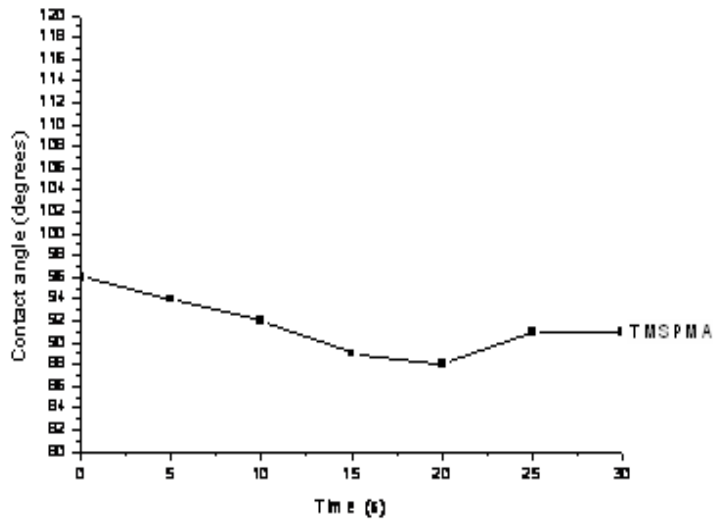


Fig. 119. Laspra treated with TMSPMA – contact angle values after 30 salt mist ageing cycles

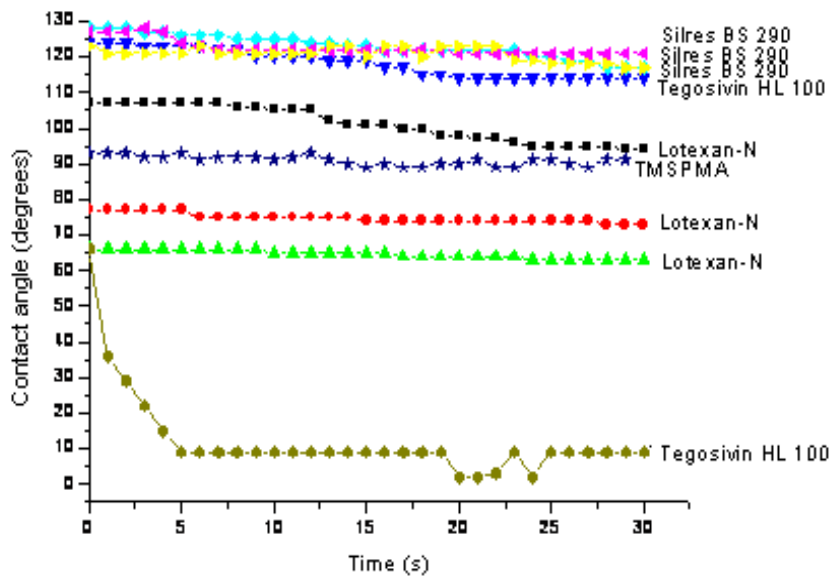


Fig. 120. Repedea – contact angle values after 60 salt mist ageing cycles

For Repedea, the samples proved to become less deteriorated, even after 60 artificially accelerated ageing cycles (Fig. 114e and 114f) and were submitted to the evaluation methods.

The samples of Laspra treated with the nanocomposite hybrid material registered a 96° contact angle value during the first seconds of measurement, a slight decrease in the values being exhibited during the 30 seconds of measurements. This may be considered to be a very good result, especially taking into consideration that the other Laspra samples, treated with the worldwide used siloxane-based water repellents, showed no contact angle at all – the water drop being instantly sucked by Laspra's surface.

After performing 60 artificially accelerated salt mist cycles, Repedea samples registered the contact angle values shown in Fig. 120. More than one contact angle curve corresponding to the same treated sample may be observed in this figure, depending on the level of deterioration of the polymeric film on the particular spot where the water drop was placed. Fig. 120 presents the most representative contact angle curves registered by the treated / aged Repedea samples, no generalization being possible. This demonstrates that the water repellent polymeric film is damaged in a random manner (Fig. 116 and Fig. 117), the registered contact angle values depending on the location the measurement was made.

VIII. 3. 2. 3. Water vapor permeability measurements

To gain an insight into the resistance of limestones to salt decay phenomena, some of the most important parameters controlling the uptake and transport of liquids within the stone, namely the water vapor permeability and porosity are to be taken into account. Considering the water vapor permeability, the lower the reduction in water vapor permeability as compared to the untreated stone the higher the efficiency of the chemical treatment. Due to the powdering and high mass loss of Laspra samples (untreated and treated with Lotexan-N, Silres® BS 290 and Tegosivin HL 100) the only one that afforded this experiment was Laspra treated with TMSPMA (Fig. 121).

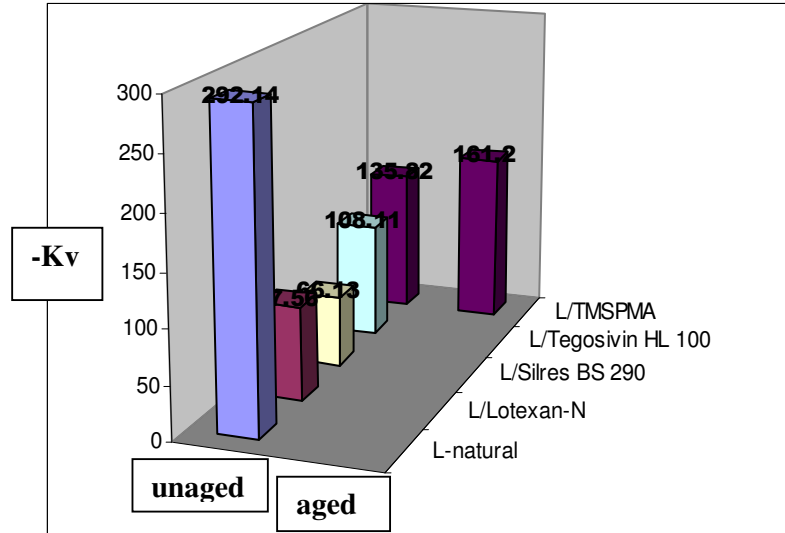


Fig. 121. Laspra – water vapor permeability values – before and after the salt mist artificially accelerated ageing

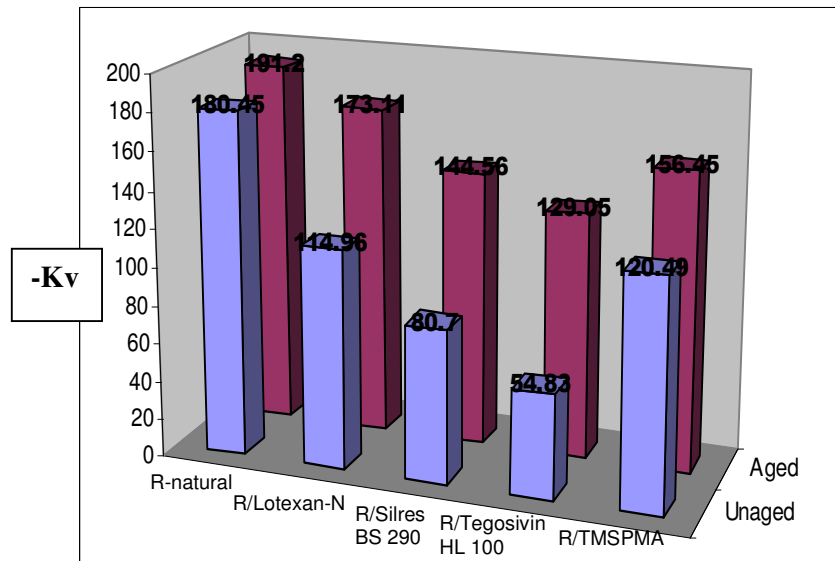


Fig. 122. Repedea – water vapor permeability values – before and after the salt mist artificially accelerated ageing

For TMSPMA, the water vapor permeability values of the specimens impregnated with the selected siloxane-based products evidence the lowest decrease and, therefore, a reduced possibility of deterioration due to salt crystallization. Due to the self-assembling properties, the nano builder (TMSPMA precursor) introduces particular atoms or molecules onto limestone surface. The molecules then align themselves into particular positions, involving the orchestration of a variety of weak, intermolecular

forces to achieve large scale, hierarchical and functional structures, in order to minimize the total energy. Over the curing period, TMSPMA nanoparticles self-assemble and bond to the surface; moreover, this nano-coating does not remain only as coverage on the surface, since nanoparticles are able to deeply penetrate inside porous stones without blocking the small pores. Usually, the growing salt crystals exert repulsive forces on pore walls, and the resulting stresses can exceed the strength of the stone. Due to the small dimensions and good water vapor permeability, TMSPMA reduces the repulsion and inhibits salt solution transport to the surface, thus avoiding the appearance of surface damage induced by salts.

Although Lotexan-N shows a water permeability value close to TMSPMA, the granular disintegration and powdering illustrated in ESEM images evidence that this product, together with the other two commercial products, doesn't induce a good durability towards salt mist action. The worldwide used product's polymeric films entrap the water-soluble salts beneath the coating and the accumulation is leading to spalling (evaporation and subsequent salt crystallization will take place at or just below stone surface). These treatments are actually blocking or sealing some of the pores and capillaries (as previously shown in VII. 2. 5), resulting in a lower water vapor permeability and loss of performance. However, the cracks and fractures appearing within stone surfaces allow these ones to "breathe" well up to a certain level and, therefore, an increase in the water vapor permeability values is registered.

When reaching saturation or usually supra-saturation, salts crystallize from the solution present in the building material porous system. The role of the porous system is significant, influencing both crystallization pressure and mineral distribution in the stone. Since crystallization pressure is inversely related to the radius of the pores, Laspra, with a high volume of small pores, will be submitted to very intense crystallization pressures, able to destroy the stone. Previous studies have demonstrated that chlorides preferentially crystallize into small pores in the 0.1 – 1 μm range [135]. Therefore, Laspra is more susceptible than Repedea to salt decay processes.

Table 25. Laspra and Repedea – open porosity and average pore throat diameters

	Porosity (%)	Average pore throat diameter (μm)
Laspra	30	0.15
Repedea	10	3.30

The porous system is not only responsible for the transport and thus location of salt crystallization; it also has a strong influence on the crystallization rate, as well as on the shape of the halite crystals. Repedea has large, isolated pores, less accessible to solution and, therefore, less subjected to salt accumulation, while Laspra presents a high porosity and interconnected small pores through which occurs the transport of the salt solution.

Whereas the shape of salt crystals crystallizing inside the stone is mainly related to the supra-saturation ratio at which crystallization occurs [136], the shape of salt crystallizing on a porous material depends on a larger number of factors. Material properties (thin crystals grow on a dense substrate, thicker crystals on a substrate having large pores), solution supply (very low solution supply gives place to whisker crystals, high supply to salt crust), evaporation rate and water content in the substrate (salt crusts are formed on wet substrates, whisker-like crystals on less humid materials), they all contribute to determine the shape of the crystals [137]. The observed type of stone damage can be related to the location of salt accumulation. Whisker crystals have been observed on the surface of Repedea, a coated substrate characterized by low moisture transport (Figures 117b, 117c), whereas salt crusts have been found on Laspra, substrate characterized by a relatively high moisture transport (Figures 116d, 116e).

VIII. 3. 2. 4. Color measurements

The color measurements were performed in order to assess the optical changes occurring after salt mist artificially accelerated ageing. The results of the color measurements are listed in Table 26 and Table 27.

Table 26. Laspra – total color change after 30 ageing cycles

	ΔE^*	ΔE^* after ageing
Laspra – untreated		-
Laspra – Lotexan-N	1.14	-
Laspra – Silres® BS 290	1.91	-
Laspra – Tegosivin HL 100	0.75	-
Laspra – TMSPMA	2.87	1.98

Table 27. Repedea – total color change after 60 ageing cycles

	ΔE^*	ΔE^* after ageing
Repedea – untreated		2.17
Repedea – Lotexan-N	10.38	9.11
Repedea – Silres® BS 290	12.18	11.26
Repedea – Tegosivin HL 100	11.92	2.86
Repedea – TMSPMA	12.15	10.95

For Laspra treated with TMSPMA and aged, the total color change ΔE^* registers only a slight difference as compared to the treated, but unaged samples. This comment is also valid for the samples of Repedea treated with Lotexan-N, Silres® BS 290 and TMSPMA; Repedea treated with Tegosivin HL 100 is the only one which shows a dramatic total color change. The parameters that exhibit the most significant color change are L^* and b^* , as presented in Fig. 123.

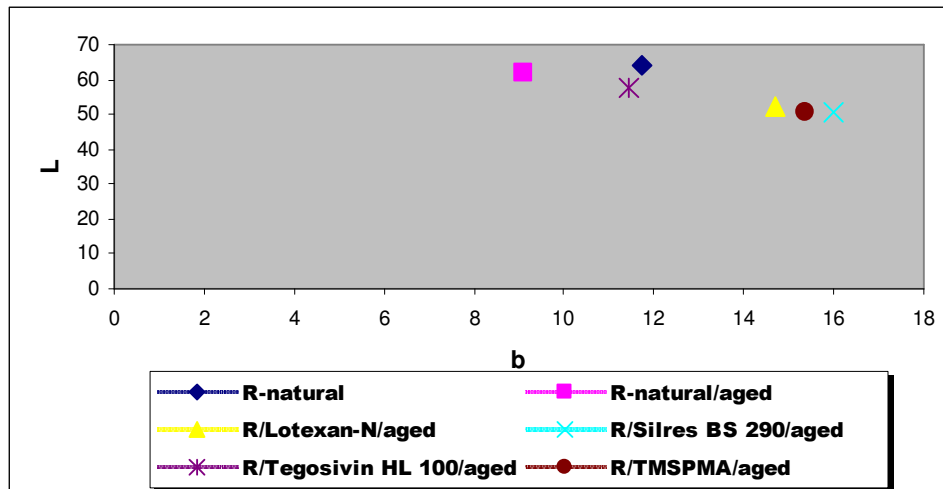


Fig. 123. Repedea – color change after the resistance to salt mist action test – L^* and b^* parameters

VIII. 3. 2. 5. Weight measurements

The weight loss registered by a stone sample after the exposure to the aggressive action of salt mist is an important evaluation parameter to be taken into consideration, as it clearly indicates a stone sample's level of degradation and its durability from a particular weathering agent's perspective.

Even if the samples of Laspra – untreated and treated with the commercial water repellents – were severely damaged and proved to be unfit for a further investigation (contact angle, water vapor permeability and color measurements) after their removal from the salt mist climatic chamber, a trial to quantify their mass loss was still made using the less deteriorated samples. Fig. 124 gives a rough idea of the mass loss registered by the less damaged Laspra samples; however, these values are not to be considered fully accurate.

Laspra and Repedea proved to have different behaviors from the mass loss point of view – the results are listed in Fig. 124 and Fig. 125.

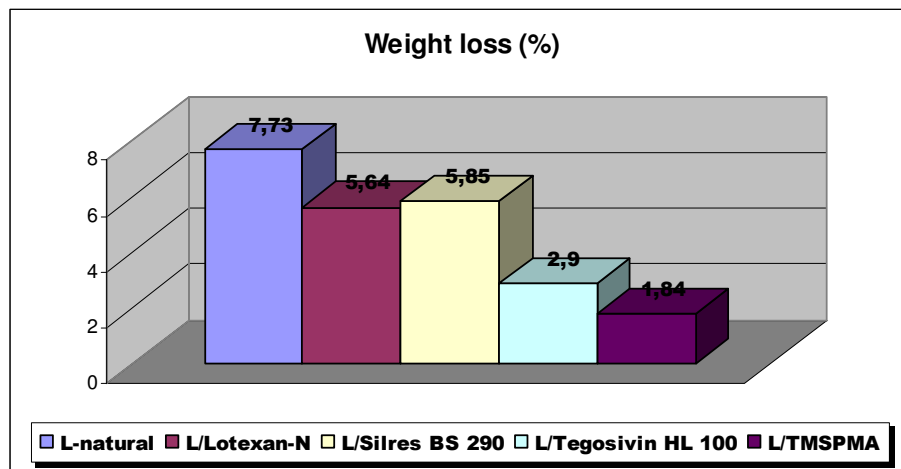


Fig. 124. Laspra – weight loss after 30 salt mist ageing cycles

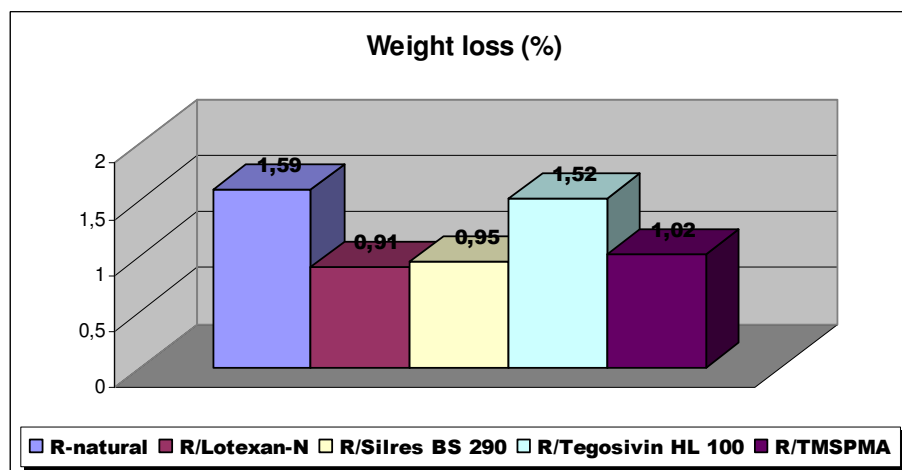


Fig. 125. Repedea – weight loss after 60 salt mist ageing cycles

The graphs clearly indicate a much higher mass loss in case of Laspra, due to the powdering, existing fractures and even breakage of some of the aged samples, the lowest mass loss being exhibited by Laspra treated with the new nanocomposite material – 1.04%.

Repedea samples show a significantly reduced mass loss, even after 60 artificially accelerated ageing cycles, with no important differences between the samples treated with one water repellent product or another. The best value, however, from the mass loss perspective is registered by Repedea treated with Lotexan-N.

VIII. 3. 3. Conclusions

The behavior of the two selected limestones – natural and treated – towards salt mist action was evaluated performing microscopic investigation (ESEM, EDX, EDX-mapping), contact angle, water vapor permeability, color and weight measurements. The salts, dissolved in solution, are transported to different locations through the pore system of the material, moisture transport properties of both the substrate and the water repellent product having a strong influence on the location of salt crystallization. The interconnection between different pore systems is also of crucial importance in determining the location of salt crystallization. Cracks are not located exactly at the place where salt accumulates but near the interface between areas with high and low salt contents. These observations suggest that a mechanism of differential dilation of zones with high and low salt contents may be in this case responsible for the damage.

From the comparative assessment of the data obtained in this study, a better protective coating of the two limestones treated with the hybrid nanocomposite can be proposed. For the commercially available products, the salt crystallization within constrained volumes (pores) exerts a great stress within the material, resulting in its cracking and breakdown.

For Laspra, the nanocomposite with silsesquioxane units represents the best choice in terms of durability of the treated limestone, since it shows a much higher water vapor permeability value, a slight total color change and the lowest mass loss. The only Laspra samples that afforded contact angle measurements were the ones treated with TMSPMA.

In Repedea's case, the difference in the behavior of the investigated water repellents is not that significant as for Laspra, but a better performance for the samples treated with the newly synthesized nanomaterial can be underlined, as proved especially by ESEM micrographs, the contact angle value and the total color change.

When treated with Lotexan-N, Silres® BS 290 and Tegosivin HL 100, both Laspra and Repedea exhibit no significant differences, the same degradation mechanism being valid.

VIII. 4. Resistance to SO₂ action in the presence of humidity

VIII. 4. 1. Introduction

The main atmospheric pollutant affecting the building materials is primarily SO₂ which is very reactive, corrosive and acidifies the rain. This compound is released into the environment's air and travels over long distances by overpowering winds before returning to earth as rain, fog, dust, or snow. Acid rain is a hazardous environmental issue, which can be broken down into two parts, has a detailed chemical make-up, causes health problems, and can be prevented. Sulphur dioxide reacts with atmospheric water to produce sulphurous acid (H₂SO₃). This is what is popularly referred to as „acid rain”. Acid deposition is a more precise term for acid rain, which has two main parts, dry and wet. Dry deposition refers to the deposition of pollutant gases and particles in the absence of rain. It can result from pollutant gases or from particulates falling and attaching themselves on the surface of the stone. The most important contribution to dry deposition is that of the gases and is generally due to nearby polluting sources. Wet deposition refers to the deposition of pollutants dissolved in moisture droplets and rain falling on to stone surfaces. Of these, rain is more efficient than moisture droplets in scavenging pollutants from the air. Rain is the main contributor to wet deposition and long range transport of pollutants. The latter can have a significant effect only in specific environmental conditions.

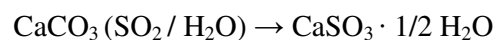
Dry deposition on a sheltered surface may lead to the formation of a deposition crust. It can also occur on a surface exposed to rainfall and runoff, but here the reaction products are removed once rainfall and runoff reach the surface and move across and into the material. In the case of limestone, both wet and dry depositions produce the

same alteration; limestone is converted to calcium sulphate (gypsum). The reaction through dry deposition (direct gas-to-solid reaction) is about five times slower in producing this decay product than the reaction *via* wet deposition (reaction in solution).

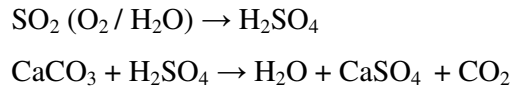
Dry deposition

Dry deposition, which is more important than wet deposition for highly polluted areas [138], results from the transfer of pollutant gases and / or particles, including aerosols, from the atmosphere to a surface in the absence of rain and are in general originated in nearby sources, and therefore called short range deposition. Gases are the most important contributors to dry deposition and their arrival at the surface in question is governed through molecular diffusion or atmospheric turbulence. Gases can react with both the surface of the stone or aerosol particles. Of these, larger particles (> 10 pm in diameter) can fall onto the surface through gravity, smaller particles can reach it through atmospheric turbulence, while Brownian movement is the most important motion for submicron particles (< 0.1 pm). For the latter, the smaller the particle, the faster its deposition rate since the surface acts as a sink and retains the particles by Van der Waals forces. These processes are strongly affected if the particles and / or the surface in question carry an electrostatic charge or if condensation or evaporation processes operate simultaneously.

Sulfur dioxide, in addition to atmospheric particulate matter and water (liquid or gaseous), is accepted as the main decay factor in urban and polluted environments [139, 140]. Almost all of the studies carried out are trying to establish the origin of gypsum detected on the surface of weathered materials, to elucidate the formation mechanism and to identify the weathering factors involved in the decay processes. The main effects of sulfur dioxide on limestones are the formation of crusts and the loss of material due to solubilization, which can represent 30 – 50% of material loss [141]. The loss of material can also be produced where weathering crusts reach certain thicknesses and then drop from the stone surface [142]. In case of dry deposition, the formation of gypsum from the reaction of calcium carbonate with sulfur dioxide could be schematized as



Another possibility is the absorption of sulfur dioxide in rain water, liquid atmospheric aerosols, or moist film supported on a stone surface (wet deposition), where it is oxidized to form a sulfuric acid solution that dissolves the calcium carbonate by gypsum formation:



The presence of at least a minimum water content is critical so that the processes involved can occur [143, 144], water – in a liquid or gaseous form – having a strong influence on the material or surface reactivity.

The acidic compounds within the stones structures affect in a particular manner the carbonate materials, giving birth to Ca and Mg sulphites and sulphates. The SO₂ attack takes place first and with preponderance on stone surface. The Ca and Mg sulphites and sulphates are characterized by a much higher solubility than CaCO₃. CaSO₃ is three times more soluble than CaCO₃ and gypsum (CaSO₄ · 2H₂O) is almost a hundred times more soluble than CaCO₃. These compounds are further dissolved in rainwater and therefore introduced, through the stones porous system and fractures, deeper within stones structure.

The deposition of gases and larger particles (which are the ones that deposit faster) occurs in the boundary layer over the surface and is influenced by the nature of the substrate, its surface conditions and its micro-environment. The concentration of gases and of particles affect their rate of deposition, while the deposition rate is enhanced by an increase in pollutants concentration, air turbulence, roughness and heterogeneity of the receiving surface, chemical affinity of the surface for the pollutants, as well as surface moisture.

The uptake of acidic gases depends on the amount of moisture within the stone, which is determined to a great extent by properties that affect the transfer of humidity. These properties are water absorption, water vapor permeability, hygroscopic moisture content and evaporation rate. However, these properties can be all related to porosity and specific surface area. Stone's porosity can be regarded as the principal characteristic of the stone as the rest of the properties are determined by open porosity and pore size distribution. Hygroscopic moisture content refers to the uptake of moisture from the

ambient air and is considered to be very important in the dry deposition of acidic gases. Hygroscopic adsorption depends on the relative humidity of the air, the nature of the material, the diameter of the pores and the specific surface area.

Several authors have indicated that SO₂ deposition is proportional to the surface area of the stone wetted by adsorbed water. Hygroscopic salts (including corrosion products such as nitrates, chlorides and previous deposits of SO₂) can influence the moisture content of porous materials. These salts attract moisture from the air and could be important in maintaining the moisture film on the surface of carbonate stones. Non or slightly hygroscopic materials can become strongly hygroscopic when such salts are entrapped in their pores. This can lead to increased absorption and oxidation rates of atmospheric SO₂ to form calcium sulphate. The presence of soluble impurities can also function as a catalyst in sulphation.

The oxidation of SO₂ can occur in a homogeneous process in the gas phase or heterogeneously in gas-liquid or gas-solid reactions. Of the several mechanisms that can oxidize SO₂ in the gas phase, the most relevant is the one involving free radicals in photochemical smog. For gas-liquid reactions, the absorption of the gas is more rapid than the desorption reaction. Smaller droplets (< 100 µm diameter) have a higher absorption rate (less than 1 s) than larger ones, and the rate-determining step is the oxidation of the SO₂. Several factors influence this oxidation rate: the presence of one or more heavy metals that can act as catalysts and the pH of the droplet / solution which is in turn affected by the presence of alkaline gases such as ammonia. For the gas-solid reaction, two possibilities have been postulated. One corresponds to an initial adsorption of the SO₂ on the surface, neutralization to sulfite and subsequent oxidation to sulfate. It has been found that sulfite constitutes a significant fraction of the sulphur of aerosols with diameter in the 1 to 4 µm range. The second corresponds to the oxidation of the adsorbed SO₂ catalyzed by surface impurities and subsequent sulfation reaction.

Deterioration mechanisms

Among the mechanisms contributing to stone deterioration and specific deposition phenomena, one can enumerate:

- Physical mechanisms. The presence of water at the surface is known to be a key factor in promoting the fracturing and erosion of stone. Water penetrates pores

and fissures and causes mechanical stresses both by freezing and by the hydration and subsequent crystallization of salts.

- Chemical mechanisms – some deposited chemical agents react with stone surface. Sulphur compounds have been indicated as the most critical factors in this regard, mainly because they are often acidic and reach high concentrations in city and suburban air, but nitrogen compounds should be considered as well. Fluxes of trace gases (e. g., sulphur dioxide) can be high, especially when promoted by biological activity. Dissolution by chemical reaction with contaminants contained in precipitation is one of the most familiar eroding processes, particularly in the case of carbonate stones.
- Biological mechanisms. Many different biological factors have been proved to be important. Growth lichens, algae, mold, fungi and bacteria are able to promote at least surface deterioration. Some bacteria can synthesize sulphuric (or nitric) acid from airborne sulphur dioxide (or nitrogen oxides). Guano contains phosphoric acid, which can also cause considerable damage.

VIII. 4. 2. Characterization of the treated stones after exposure to SO₂ contaminated atmosphere

VIII. 4. 2. 1. Visual investigation and salt crust characterization

The microscopic investigation was performed in order to assess limestone's surface morphology. The gypsum crystals produced during the SO₂ deposition experiments can occur basically in three types: (i) prismatic, (ii) sheet-like (or as rosettes when crystals are twinned) and (iii) needle-like. Different shapes of gypsum crystals are commonly found on the outer surface of many monuments as well [145]. The shape of the crystals is not only influenced by the environmental conditions, i.e. temperature, pH, organic matter content [146], but also by the presence of chemical impurities [147]. Generally speaking, on samples subjected to the SO₂-contaminated atmosphere for 24 h, the dominant morphology of the gypsum crystals is needle-like, becoming more equidimensional as the test continues until they are sheet-like after 7 days. With reference to cultural heritage buildings, this would indicate that crusts comprising sheet-like or rosette crystals correspond to advanced stages of deterioration, while needle-like crystals represent the first stages of weathering.

Crystals of different shapes were found in the present study. For natural Repedea subjected to SO_2 action, ESEM micrographs evidence the presence of prismatic crystals, as well as stellate crystalites (Fig. 126). The latter structures represent the calcium sulphite hemihydrate, which appears as a first step. These crystallites have distinct sites of nucleation, being separated from each other by unaltered calcite. With progression of the reaction, the crystallites grow larger and eventually become united, forming a continuous crust of $\text{CaSO}_3 \cdot \frac{1}{2} \text{H}_2\text{O}$. However, if some moisture is able to condense, calcium sulphite crystals are oxidized and hydrated and form gypsum crystals, having a prismatic and bladed appearance.

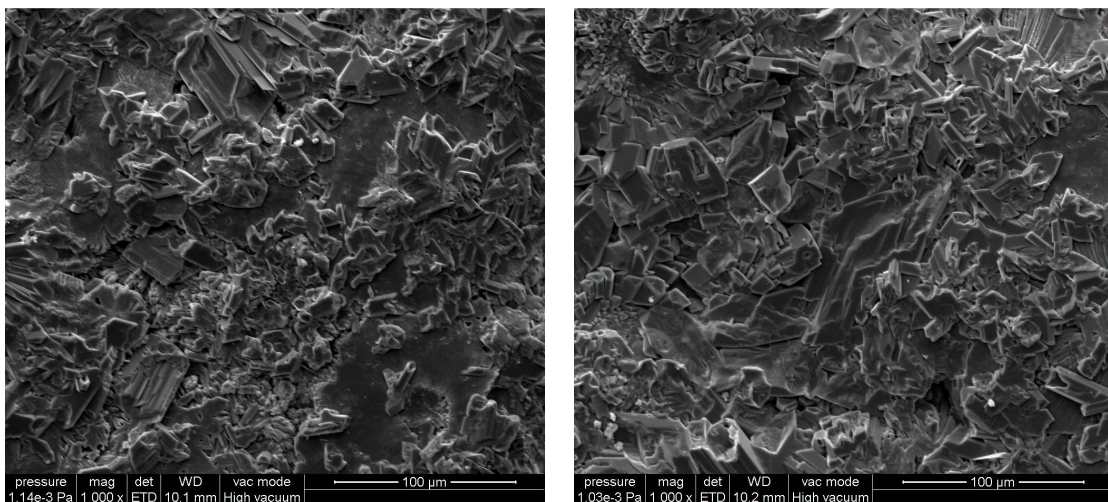


Fig. 126. Repedea – ESEM micrographs – after exposure to SO_2 contaminated atmosphere

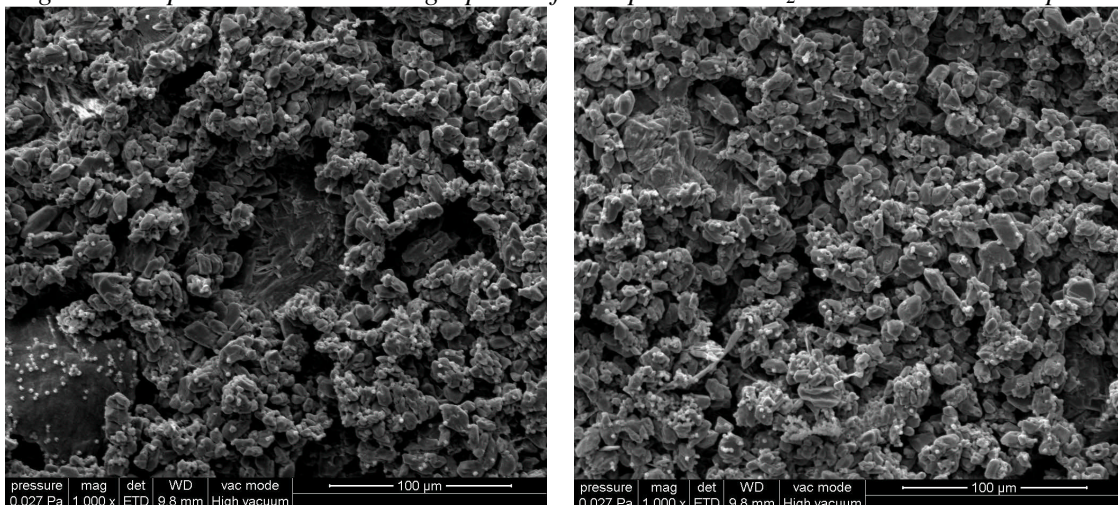


Fig. 127. Laspra – ESEM micrographs – after exposure to SO_2 contaminated atmosphere

In case of natural Laspra, an accelerated degradation and mass loss was evidenced (Fig. 127).

A few examples of the performed ESEM micrographs corresponding to Laspra and Repedea treated with the worldwide used water repellents and with the newly synthesized nanocomposite are shown below; a complete cover of the ESEM micrographs can be found in Annex 1.

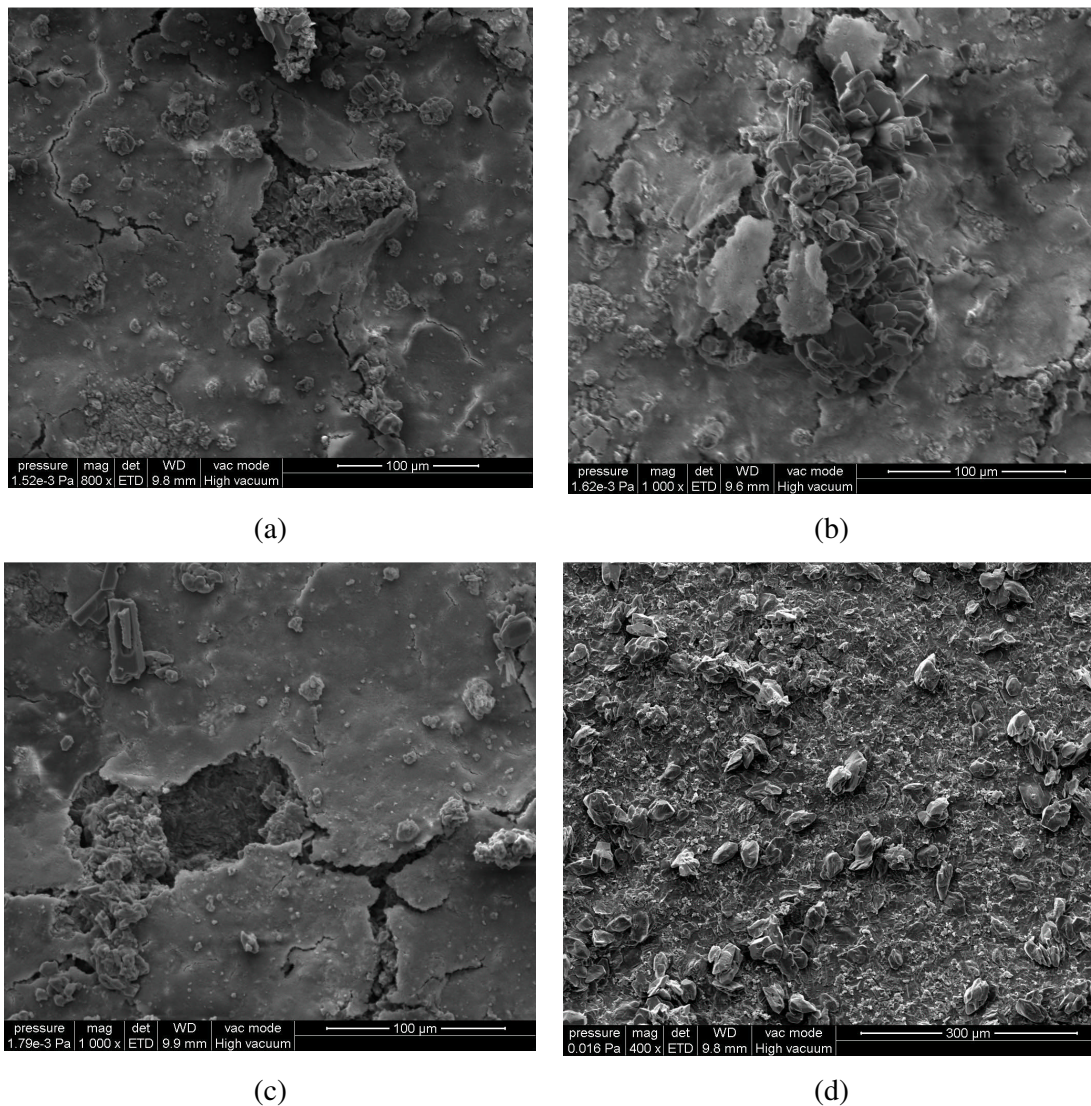
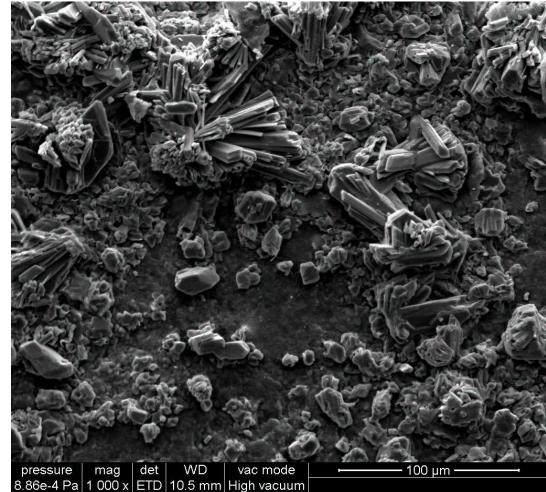


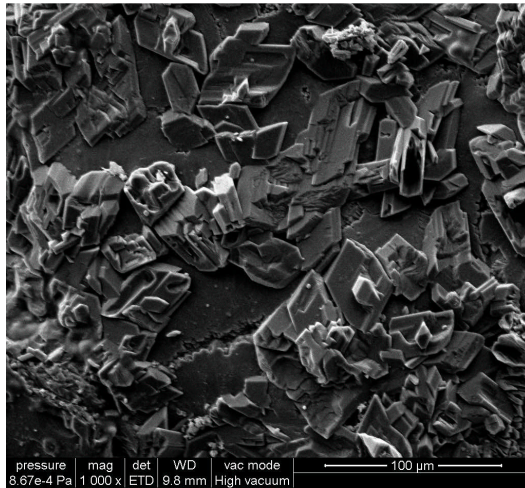
Fig. 128. Laspra – ESEM micrographs – (a) Lotexan-N; (b) Silres® BS 290; (c) Tegosivin HL 100; (d) TMSPPMA – after exposure to SO₂ contaminated atmosphere



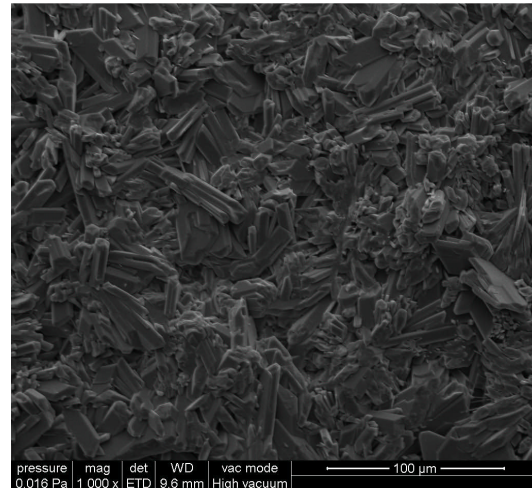
(a)



(b)



(c)



(d)

Fig. 129. Repedea – ESEM micrographs – (a) Lotexan-N; (b) Silres® BS 290; (c) Tegosivin HL 100; (d) TMSPMA – after exposure to SO₂ contaminated atmosphere

For Repedea treated with the commercially available products, the dry deposition of SO₂ leads to the formation of a higher amount of gypsum (evidenced by the higher crust thickness) as compared to the untreated samples. Due to the large molecular structures, they allow a good SO₂ penetration into stone substrates, the higher penetration, the higher in-depth sulphation (reaction between carbonate and SO₂).

The presence of epsomite in case of Laspra favors the formation within a matter of hours of a very thin water film that is responsible for the continuation of the sulphation reaction, leading to the formation of a higher amount of gypsum. This process

is evidenced by ESEM images, which reveal the sub-efflorescence of gypsum crystals onto limestone surfaces (Fig. 128).

The complete sulphation process in case of Laspra, as opposite to Repedea, can be associated with a higher susceptibility of Laspra to SO₂ action. For Repedea, only Tegosivin HL 100 and TMSPMA determined a smaller degree of sulphation and a higher resistance to SO₂ action, process evidenced by the smaller crust thickness as compared to the one obtained in case of natural Repedea (Table 28).

Table 28. Laspra and Repedea – salt crust thickness after exposure to SO₂ contaminated atmosphere

crust thickness (cm)			
Laspra		Repedea	
Laspra natural	0.0017	Repedea natural	0.00068
Laspra - Lotexan-N	0.0025	Repedea - Lotexan-N	0.00086
Laspra - Silres® BS 290	0.0020	Repedea - Silres® BS 290	0.00067
Laspra - Tegosivin HL 100	0.0041	Repedea - Tegosivin HL 100	0.00017
Laspra - TMSPMA	0.0015	Repedea - TMSPMA	0.00034

The thickness of the gypsum crust was determined by the relation

$$\delta p = W_p / A \cdot \rho_p$$

where δp = crust thickness (cm); W_p = weight of the product, gypsum (g); ρ_p = density (g cm⁻³) of gypsum, 2.32; A = surface area of the sample (cm⁻²).

As for the TMSPMA compound, the nanosized porous network inhibits SO₂ penetration ($M_{SO_2} = 64$, $M_{H_2O} = 18$), but allows water vapor to enter and exit, allowing limestones to „breathe” freely. Therefore, due to the presence of homogeneous layers of TMSPMA comprising a small amount of surfactant, the sulphation proceeds only above the surface, leading to the development of a thin gypsum crust. For Laspra treated with TMSPMA, the ESEM micrographs (Fig. 128d) show the presence of only sheet-like crystals. Taking into account that all samples have been exposed under the same conditions, the formation of a thin crust of rosette type (which corresponds to the final stage of weathering) may indicate that the sulphation process in this particular case is stopped at this level, while the appearance of needle-like crystals (initial stage) when the commercial products were used can be connected to the extension of the sulphation process by the formation of subsequent new layers of sulphite and sulphate due to the

presence of the water delivered by epsomite or by the one „entrapped” inside the stone and delivered to the surface through the fractures.

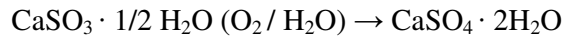
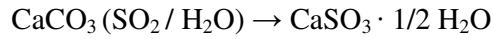
These comments are also supported by the smaller crust thickness as compared to the untreated stone subjected to SO₂ dry deposition, the absence of fractures and the visualization of sub-efflorescence of gypsum crystals. It thus appears that TMSPMA is the only water repellent (among the tested ones) that assures an efficient protectiveness (sulphation only above the surface).

In case of Repedea, the presence of predominantly sheet-like crystals as well as a small amount of calcium sulphite was evidenced by ESEM micrographs (Fig. 129d). Although crust thickness is higher in case of TMSPMA casted on Repedea as compared to Tegosivin HL 100, this result does not prove unambiguously a worst behavior, since calcium sulphite represents in fact a protective layer for stone surface. Even so, the thickness is smaller than in case of natural Repedea and Repedea treated with Lotexan-N and Silres® BS 290.

Dry deposition of SO₂ is a slow, but continuous process. When the absorption of SO₂ is low, blinded calcite particles are present. On such particles the sulphite crystals cover the limestone [148]. If water is further absent, the sulphite is not transformed into sulphate. If, however, water is present, the sulphite can be oxidized to sulphate by oxygen and some catalysts such as carbon particles and metal oxides.

The surface morphology and chemical composition of the two limestones subjected to SO₂ contaminated atmosphere were evaluated by FT-IR spectroscopy and X-ray diffraction analysis.

The experiments showed differences in the habit of the gypsum crystals formed as a consequence of the presence of a specific water repellent compound applied onto stone surface. Gypsum is produced by reaction between sulphur-containing compounds (SO₂, SO₃, H₂SO₄) and water (liquid or vapor) in the atmosphere and calcite contained in stones, is more soluble and occupies more volume than the original matrix, calcium carbonate. In case of dry deposition, the formation of gypsum from the reaction of calcium carbonate with sulfur dioxide can be schematized as



With respect to dolomite, the basic reaction is likely to imply the formation of gypsum and epsomite:



The formation of gypsum leads to the creation of cavities below the surface due to the migration of calcium ions to the surface [149]. Thus, when the soluble gypsum is washed away, it takes with it some of the stone itself, initially causing loss of surface detail but eventually leading to a loss of structural integrity.

The FT-IR spectra of natural limestones and of the stones treated with the studied compounds and subjected to SO_2 action are shown below (Fig. 130 and Fig. 131).

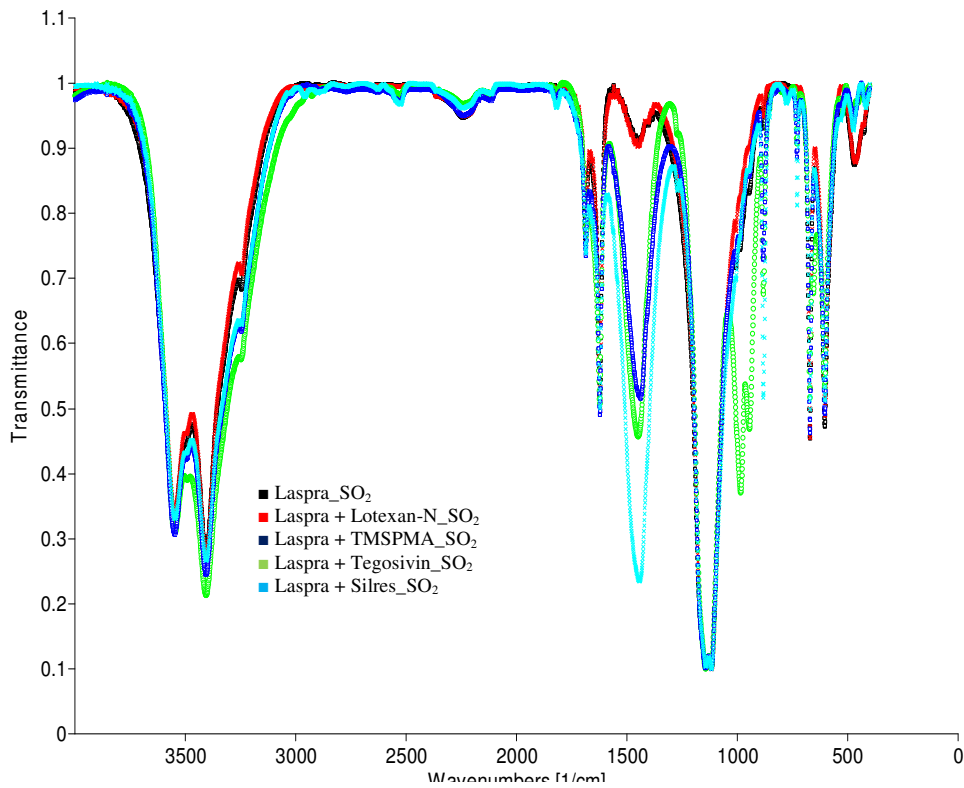


Fig. 130. FT-IR spectra of natural and treated Laspra – subjected to SO_2 action

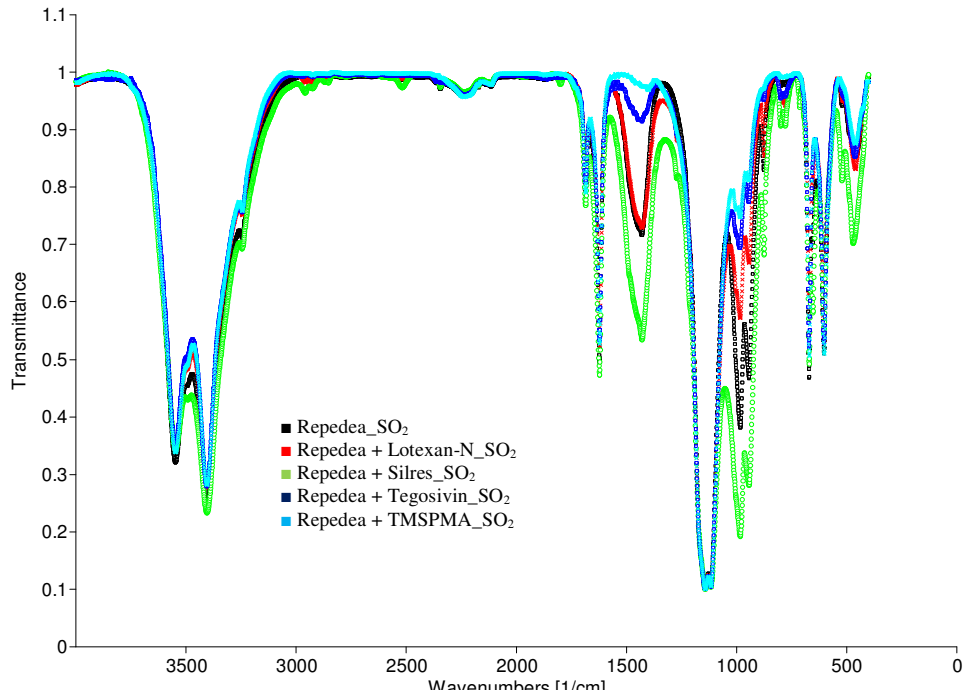


Fig. 131. FT-IR spectra of natural and treated Repedea – subjected to SO₂ action

For a better understanding of what happened after treated stone's exposure to SO₂ contaminated atmosphere, the FT-IR spectra of Laspra and Repedea and the FT-IR spectra of the two stones treated with the nanocomposite material (before the exposure) are shown below, as an example.

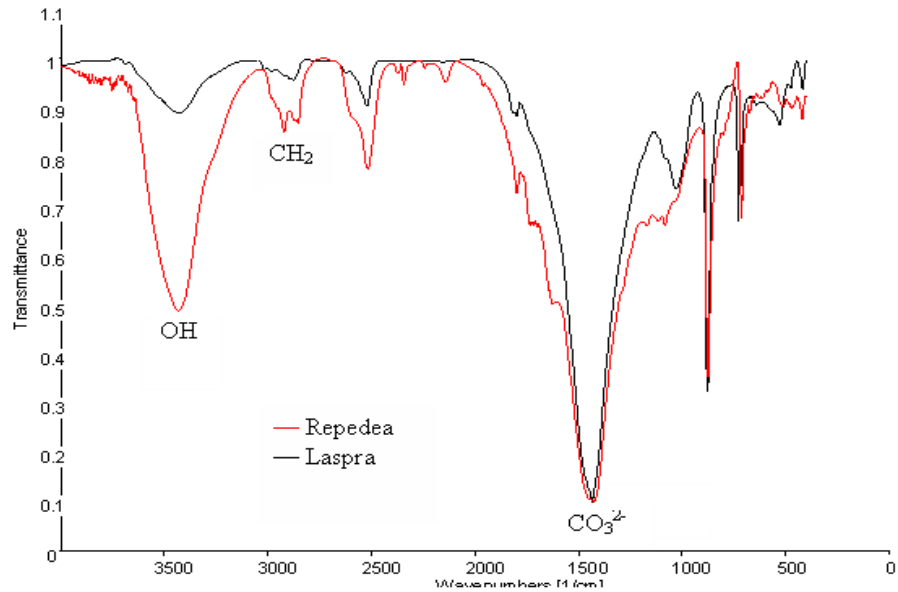


Fig. 132. FT-IR spectra of Laspra and Repedea

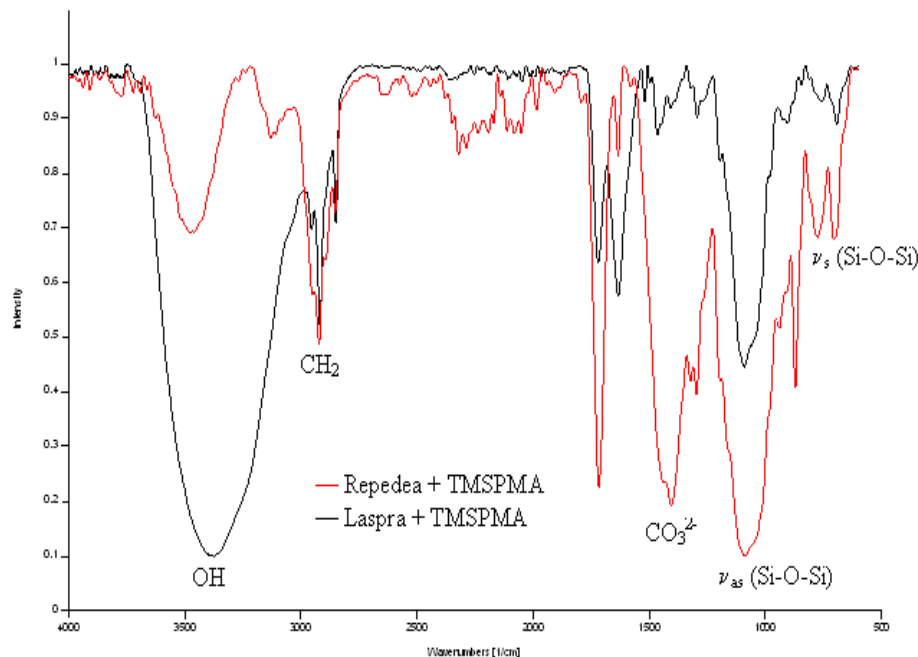


Fig. 133. FT-IR spectra of Laspra and Repedea treated with TMSPMA

In Fig. 130 and Fig. 131, the presence of OH stretching from gypsum at 3546 and 3405 cm^{-1} , as well as the O – H – O bending of the crystallization water at 1685 and 1621 cm^{-1} can be evidenced. The sulphate ions can be observed at around 1141, 1115, 670 and 602 cm^{-1} , respectively, while additional bands corresponding to sulphite ions at 983 and 944 cm^{-1} can be identified for all commercial products, as well as for the natural Repedea stone.

After SO_2 dry deposition, instead of a decrease of the CO_3^{2-} asymmetric stretching bands from calcite (1432 cm^{-1}) attributed to calcium carbonate dissolution and formation of gypsum, with the exception of Repedea treated with TMSPMA, an important increase of the intensities of the corresponding bands was evidenced, the most significant one being registered for Laspra coated with Silres® BS 290 (eight times higher). This result is quite unexpected, at least considering TMSPMA action against natural Laspra not subjected to SO_2 action (Fig. 133). As a consequence of the presence of an acidic medium (pH = 5) in case of the two limestones treated with TMSPMA, the CO_3^{2-} asymmetric stretching from calcite presented a small decrease for Repedea, while for Laspra a dramatic reduction of the same band was noticed. This behavior is attributed to the reaction between calcium carbonate and hydrochloric acid, with the formation of calcium chloride as by-product. Since dolomite (present only in Laspra) doesn't react as

easily as calcite with acids, one has to conclude that Repedea is more acid-resistant, a valuable information for the ranking of stones durability under the action of acid rains [150]. As opposed to this action, upon SO₂ dry deposition onto Laspra and Repedea coated with TMSPMA, instead of a further decrease of the CO₃²⁻ asymmetric stretching from calcite for both limestones, this process was evidenced only for Repedea, while an important increase of the carbonate region was evidenced for Laspra (five times higher as compared to the one obtained in absence of SO₂). Although FT-IR spectra indicate the higher decrease of carbonate region in case of Repedea, this does not unambiguously prove that this stone is more deteriorated due to the sulphation process. Since these measurements were performed only at the outer surface, they only confirm that the layer that lies above the original stone surface is affected by SO₂ dry deposition.

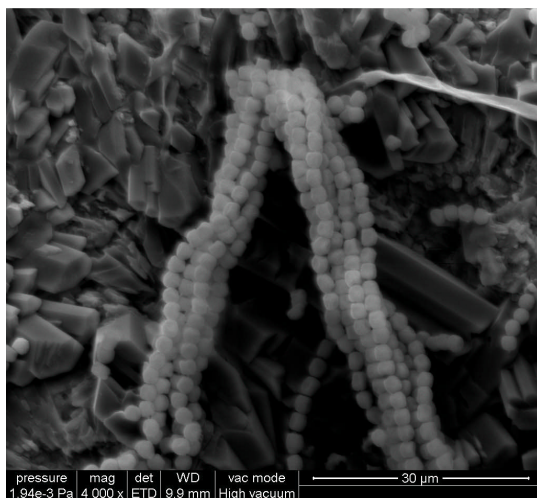
The carbonate regeneration in case of Laspra can be correlated with the presence of certain sulphur-liberating bacteria in the presence of water. Skoulikidis and Beloyannis reported that gypsum could be converted back to calcite using carbonate anions in aqueous solution [151]. They found that the gypsum layer was consolidated by newly formed calcite, which showed similar behavior to the underlying marble. Although no other authors reported success using purely chemical reactions, the use of microorganisms, a relatively recent technique, has been successful in removing sulfate from black gypsum crusts. Sulfate-reducing bacteria are able to dissociate gypsum into Ca²⁺ and SO₄²⁻ ions, and the SO₄²⁻ ions are then reduced by the bacteria, whereas the Ca²⁺ ions react with carbon dioxide to form new calcite [152]:



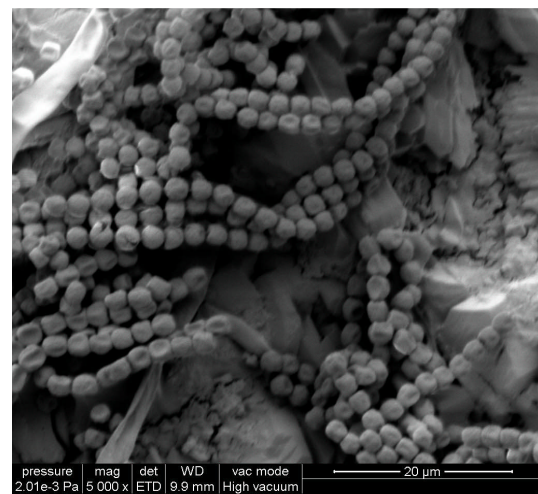
However, further investigation is necessary to attest the presence of these types of bacteria in the particular Laspra sample under study. Their presence might explain the abnormal behavior of some Laspra samples after the exposure to SO₂ atmosphere.

The bacteria might induced carbonate cementation to a depth of > 500 μm and no plugging or blocking of pores was observed, thus permitting free passage of soluble salts through the stone [153]. The newly formed carbonate might prove to be more resistant to mechanical stress, possibly due to the incorporation of organic molecules produced by bacterial metabolism into the crystals [154]. The production of a calcium carbonate layer generated by bacteria does not block the natural pore structure, thus permitting free passage of soluble salts through the stone [153]. It is already known that Laspra contains

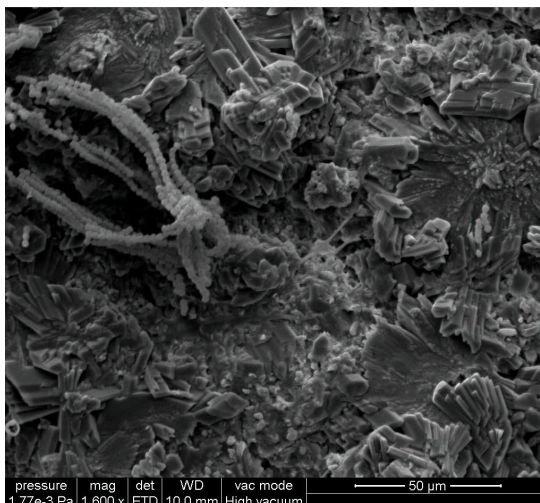
different types of bacteria and microorganisms, responsible for the biological mechanisms that contribute to Laspra deterioration. The higher intensity of the carbonate band for Laspra coated with all compounds and aged can be associated to the enhancement of stone biomineralisation by bacteria, property connected to the water vapor permeability values: the higher the amount of water „entrapped” inside the stone, the higher the amount of carbonate restoration. The smaller increase of the carbonate band in case of Laspra coated with TMSPMA as compared to the worldwide used products can be correlated with the circumstance that the „starting signal” of the carbonate region is very small (around 0.08 on the transmittance scale).



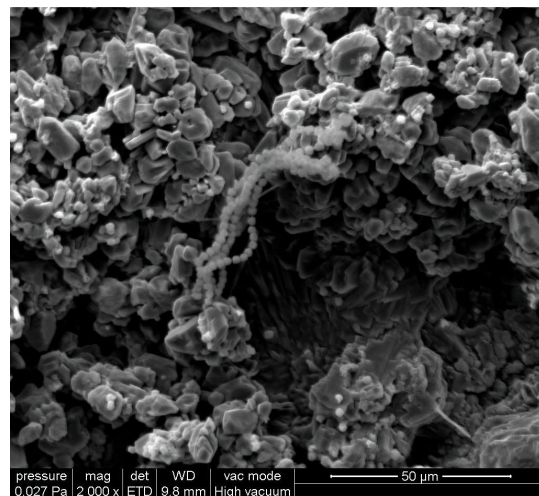
(a)



(b)



(c)



(d)

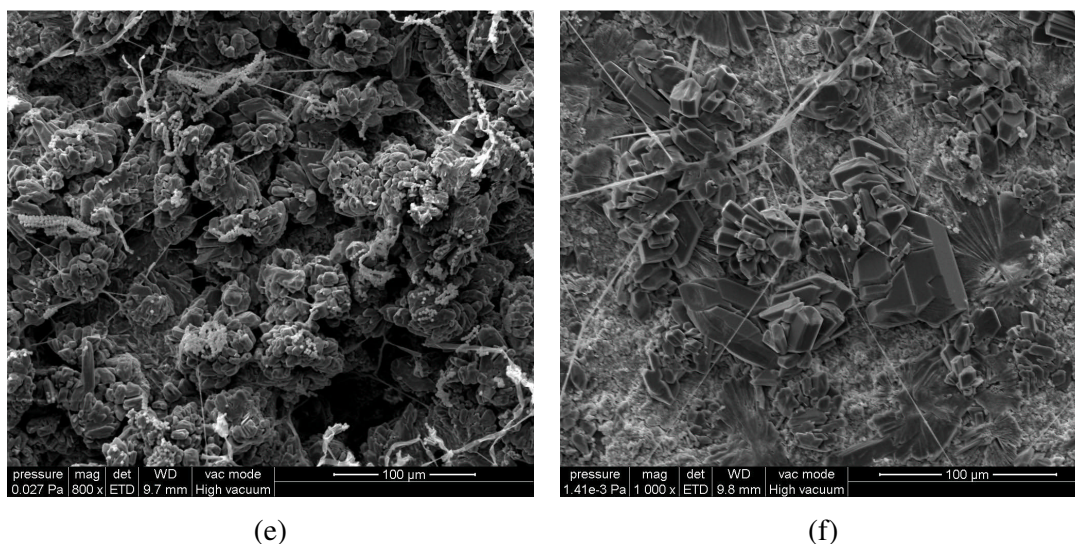


Fig. 134. ESEM micrographs – Laspra samples after exposure to SO₂ contaminated atmosphere – biological growth evidence

The X-ray measurements gave an overview on the qualitative phase identification for both limestones exposed to SO₂ action in the presence of humidity. As follows, different phases for carbonate, sulphite and sulphate species have been identified for both limestones:

Laspra: dolomite (D) – CaMg(CO₃)₂, calcite (C) – CaCO₃, ankerite (A) – CaMg_{0.32}Fe_{0.68}(CO₃)₂;

Repedea: calcite (C) – CaCO₃, magnesian calcite (CM) – Mg_{0.1}Ca_{0.9}CO₃, quartz (Q) – SiO₂;

Laspra, Repedea: hannebachite (H) – CaSO₃ · 0.5 H₂O;

Laspra: gypsum (G) – CaSO₄ · 2 H₂O, epsomite (E) – MgSO₄ · 7 H₂O, bassanite (B) – CaSO₄ · 0.5 H₂O;

Repedea: gypsum (G) – CaSO₄ · 2 H₂O, kieserite (K) – MgSO₄ · H₂O.

For Laspra (Fig. 135), the presence of the commercial products appears to favor the formation of the mineral epsomite (MgSO₄ · 7 H₂O) as one of the reaction products. The deliquescence point, i.e., the relative humidity at which epsomite goes into solution, is 88.3% at 20° C [155]. As a result, epsomite is frequently able to convert the ambient moisture into liquid water or can lose very easily one molecule of water, with the formation of hexahydrate (MgSO₄ · 6 H₂O). Other experimental results showed that after

nearly 150 h of reaction (around 6 days), when an adequate amount of epsomite has been formed, water droplets begin to appear at the surface of the specimens [156]. This thin water film allows the reaction to continue leading to a thicker salt crust development and is responsible for the enhancement of the sulphation process. Therefore, the presence of epsomite only in case of the worldwide used water repellents may be responsible for the higher amount of gypsum. In case of Laspra treated with TMSPMA, the crust is composed only of gypsum and bassanite. It seems that due to the presence of TMSPMA, SO_4^{2-} ions balance perfectly with Ca^{2+} , leading to the formation of only gypsum as a final product. Similar results have been reported by other studies.

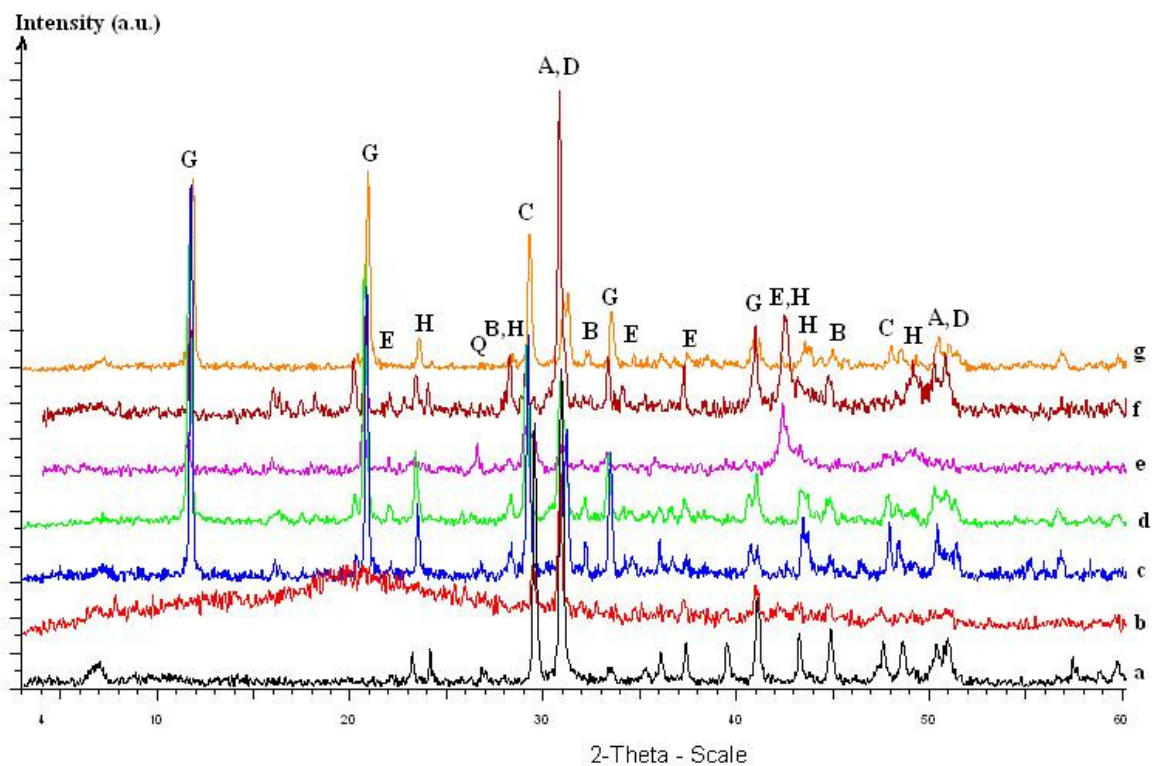


Fig 135. Laspra XRD patterns: (a) untreated; (b) Laspra + TMSPMA without being subjected to SO_2 action; (c) Laspra + SO_2 ; (d) Laspra + Lotexan-N + SO_2 ; (e) Laspra + Silres® BS 290 + SO_2 ; (f) Laspra + Tegosivin HL 100 + SO_2 ; (g) Laspra + TMSPMA + SO_2

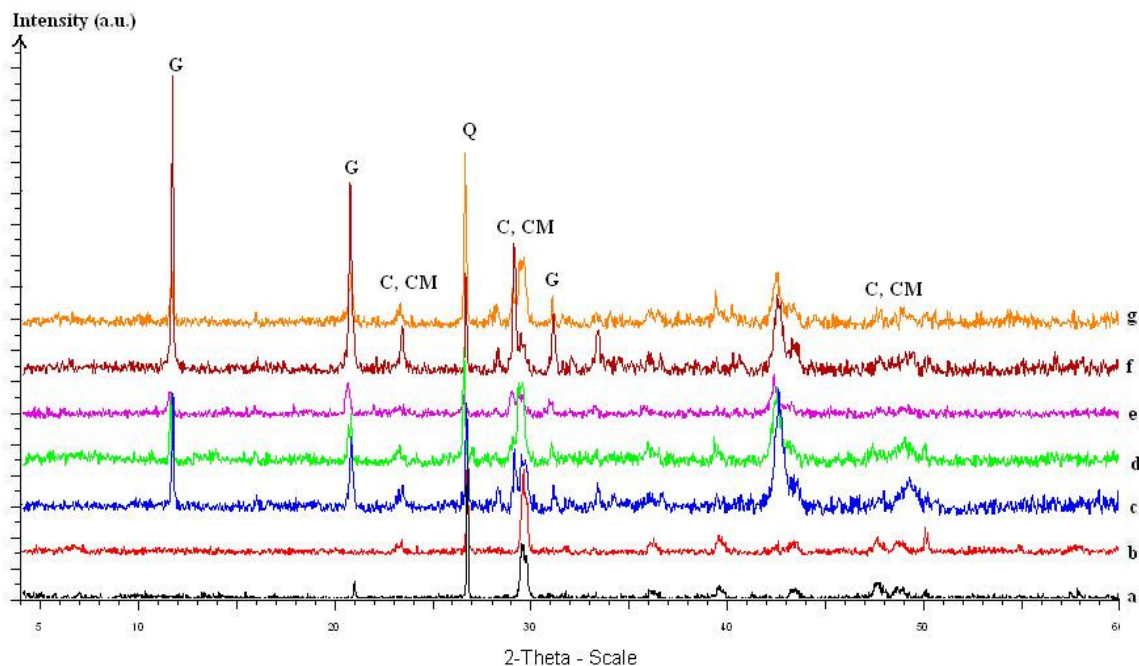


Fig. 136. Repedea XRD patterns: (a) untreated; (b) Repedea + TMSPMA without being subjected to SO₂ action; (c) Repedea + SO₂; (d) Repedea + Lotexan-N + SO₂; (e) Repedea + Silres® BS 290 + SO₂; (f) Repedea + Tegosivin HL 100 + SO₂; (g) Repedea + TMSPMA + SO₂

As opposite to Laspra, the XRD patterns of Repedea samples subjected to SO₂ dry deposition illustrate the presence of hannebachite on untreated Repedea, as well as on the one treated with all compounds (Fig. 136).

VIII. 4. 2. 2. Contact angle measurements

The measurement of the contact angle values registered by the treated limestones before and after their exposure to SO₂ contaminated atmosphere are further discussed. Table 29 lists the contact angle values exhibited by Laspra and Repedea after their treatment and before performing the resistance to SO₂ action.

Table 29. Contact angle values of Laspra and Repedea treated, but unaged

	Lotexan-N	Silres® BS 290	Tegosivin HL 100	TMSPMA
Laspra	148	151	147	120 ↓
Repedea	142	123	100 ↓	105

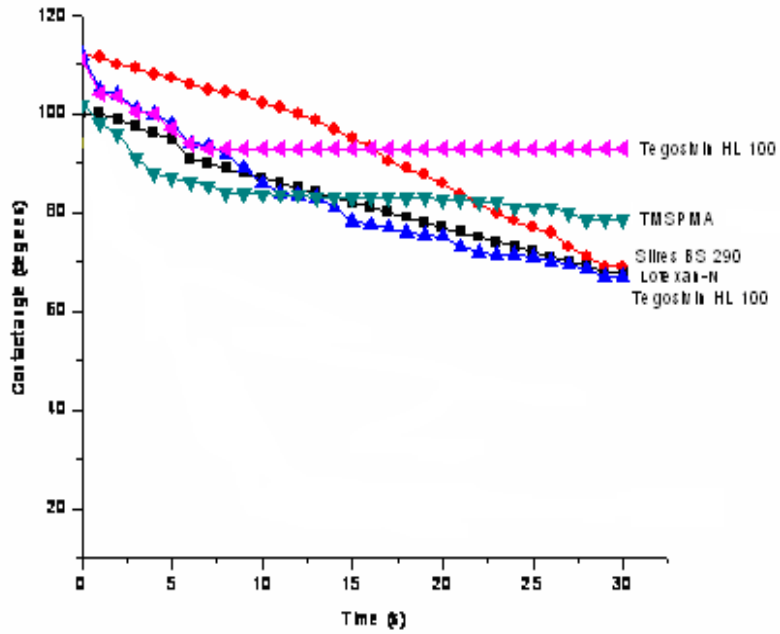


Fig. 137. Contact angle values – treated Laspra after exposure to SO₂ atmosphere

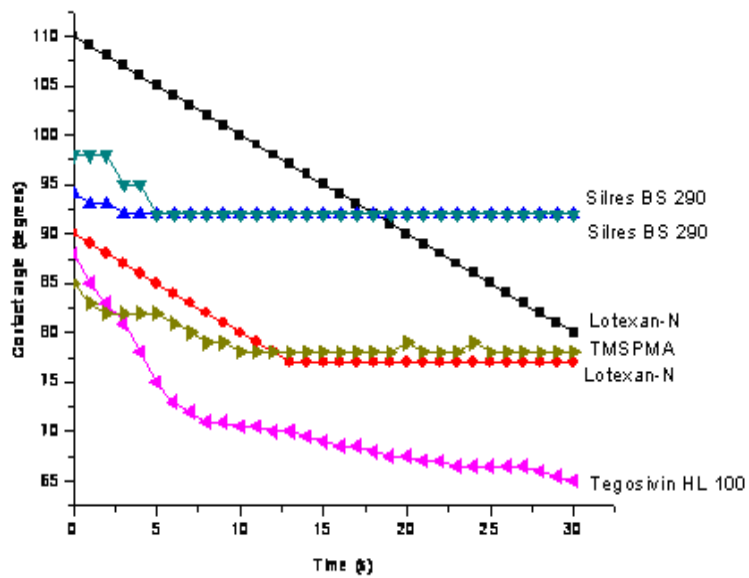


Fig. 138. Contact angle values – treated Repedea after exposure to SO₂ atmosphere

As in the case of the resistance to salt mist action, several contact angle curves (values) corresponding to the same limestone sample and therefore, to the same water repellent treatment, have been obtained in this case, as well.

It must be mentioned that the contact angle curves presented in Fig. 137 and Fig. 138 summarize a multitude of experimental values, those given in the two figures being the most representatives.

For Laspra, Tegosivin HL 100 proved to induce either the higher contact angle value, or, on the contrary, the lowest, depending on the degree of degradation of the polymeric film on the particular spot where the water drop was deposited. As for the other siloxane-based water repellents, they show a more constant behavior and this is why only a single contact angle curve was presented for each of them in Fig. 137.

In Repedea's case, Silres® BS 290 demonstrated the best performance. Figure 138 shows that both contact angle curves exhibit the highest values and the most constant behavior.

For some of the chemical products, the contact angle values registered during the first seconds of the measurement have been much higher than the ones shown by the same product after the 30 seconds of measurement. The best example is represented by Repedea treated with Lotexan-N and Tegosivin HL 100.

TMSPPMA shows a better behavior in comparison with the commercially available water repellents: the same contact angle values have been registered for a limestone sample, no matter where the water drop was deposited.

VIII. 4. 2. 3. Water vapor permeability

The data obtained after performing the water vapor permeability experiments are given in the figures below. As a general comment, one can state that for both Laspra and Repedea an increase in the water vapor permeability values is registered for all the studied samples – increase that proves to be more pronounced in some cases than in others. This behavior is mainly due to the migration of the Ca^{2+} ions towards the limestone's surface leading to the formation of small cavities, to the dissolution of the calcite to form gypsum (Fig. 127), to the cracking of the polymeric film.

The water vapor permeability data are listed in Fig. 139 and Fig. 140.

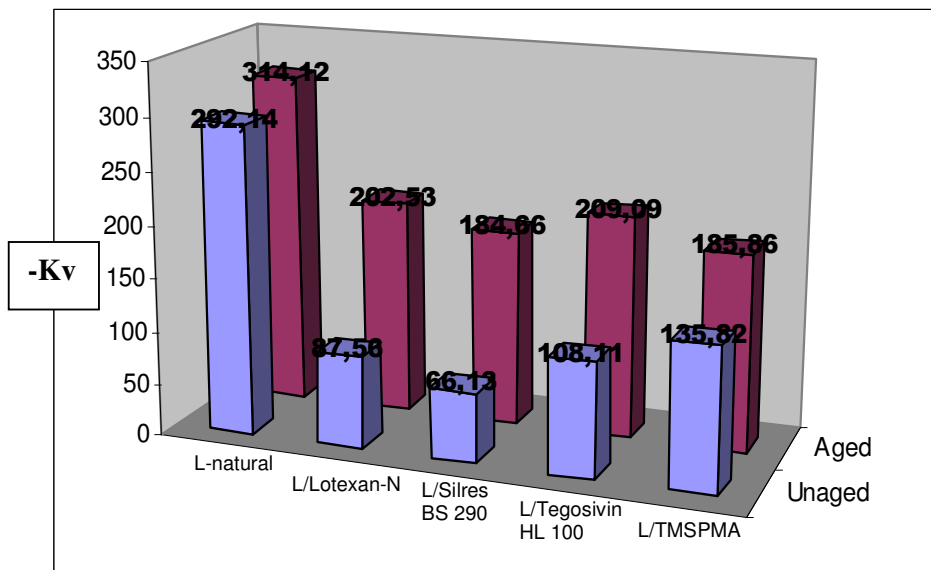


Fig. 139. Water vapor permeability – Laspra before and after exposure to SO₂ atmosphere

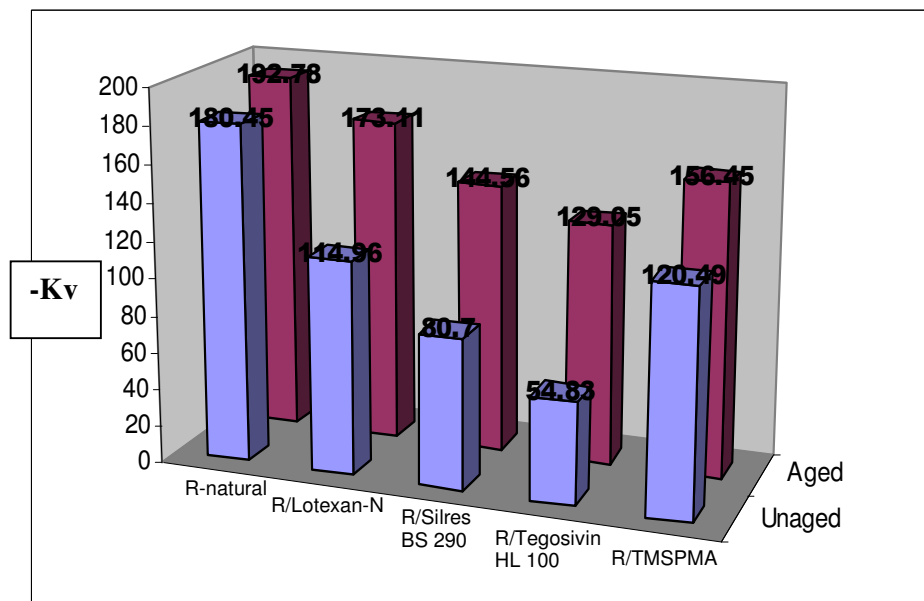


Fig. 140. Water vapor permeability – Repedea before and after exposure to SO₂ atmosphere

For Laspra, the water vapor permeability coefficients registered before and after sample exposure to SO₂ atmosphere indicate that the smallest difference appears for the samples treated with the nanocomposite material and the highest increase is shown by the samples treated with Lotexan-N and Silres® BS 290.

Repedea samples treated with TMSPMA present the lowest increase in water vapor permeability, while the highest increase is registered for the samples brushed with Tegosivin HL 100.

VIII. 4. 2. 4. Color measurements

One of the evaluation methods used in this study refers to color measurements and to the calculation, after each artificially accelerated ageing test, of the total color change, ΔE^* , that normally occurs during treated stone's weathering.

The total or global color changes exhibited by Laspra and Repedea samples after the artificially accelerated ageing under SO_2 saturated atmosphere are presented in Table 30 and Table 31.

Table 30. Total color change – Laspra – before and after the exposure to SO_2 atmosphere

	ΔE^*	ΔE^* after ageing
Laspra – untreated		7.07
Laspra – Lotexan-N	1.14	1.85
Laspra – Silres® BS 290	1.91	7.06
Laspra – Tegosivin HL 100	0.75	3.95
Laspra – TMSPMA	2.87	1.65

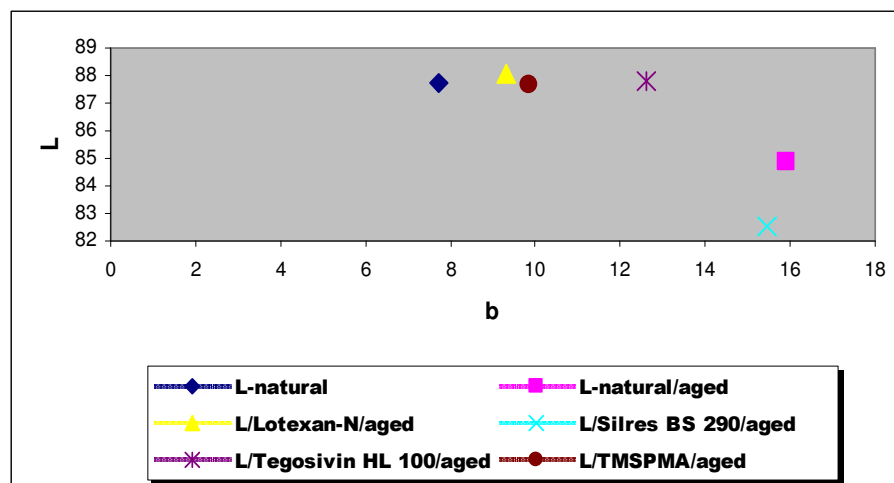


Fig. 141. Total color change – Laspra – L^* and b^* parameters

Table 31. Total color change – Repedea – before and after the exposure to SO₂ atmosphere

	ΔE^*	ΔE^* after ageing
Repedea –untreated		5.28
Repedea – Lotexan-N	10.38	4.51
Repedea – Silres® BS 290	12.18	3.36
Repedea – Tegosivin HL 100	11.92	7.02
Repedea – TMSPMA	12.15	5.14

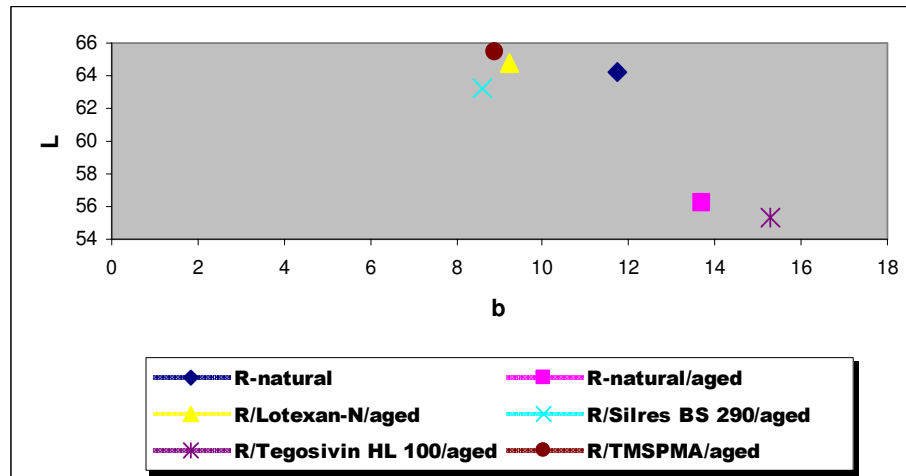


Fig. 142. Total color change – Repedea – L* and b* parameters

Table 30 lists the total color change values exhibited by Laspra (natural and treated) after performing the artificially accelerated ageing test. Judging from these data, the most pronounced difference in the total color change occurred for the samples treated with Silres® BS 290, while the samples treated with Lotexan-N, Tegosivin HL 100 and TMSPMA exhibited a small modification.



Fig. 143. Laspra treated with Tegosivin HL 100 before and after the exposure to SO_2 action (a); Repedea treated with Silres® BS 290 and TMSPMA before and after the exposure to SO_2 action (b)

Laspra samples are developing a yellowing effect after performing the resistance to SO_2 action artificially accelerated ageing test, due to the oxidation of the contained iron oxides from Fe^{2+} to Fe^{3+} . The iron oxides also act as a catalyst during the sulphation process.

Repedea samples exhibited more severe differences in the total color change values, the smallest modification being shown by the samples treated with Tegosivin HL 100.

VIII. 4. 2. 5. Weight measurements

The weight measurements have been performed in order to assess the mass changes suffered by the limestone samples after exposure to the SO_2 contaminated atmosphere.

As in the case of the resistance to salt mist artificially accelerated ageing, Laspra registered higher mass loss values than Repedea. The obtained data are presented in Fig. 144 and Fig. 145.

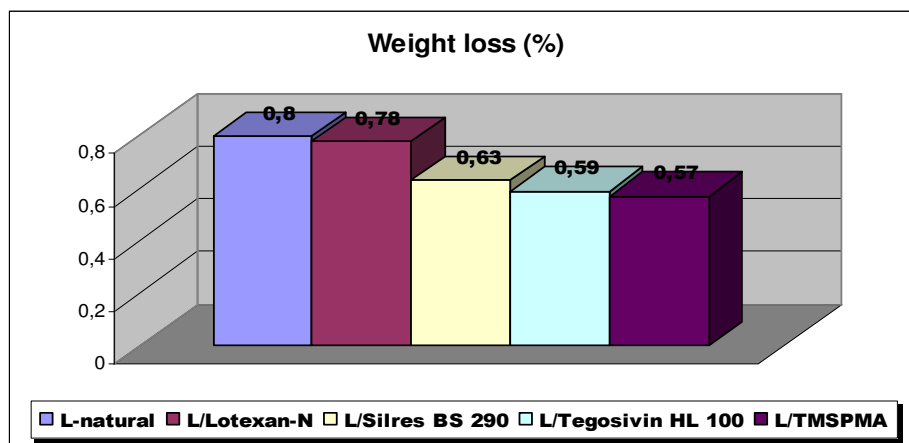


Fig. 144. Weight loss – Laspra after exposure to SO_2 saturated atmosphere

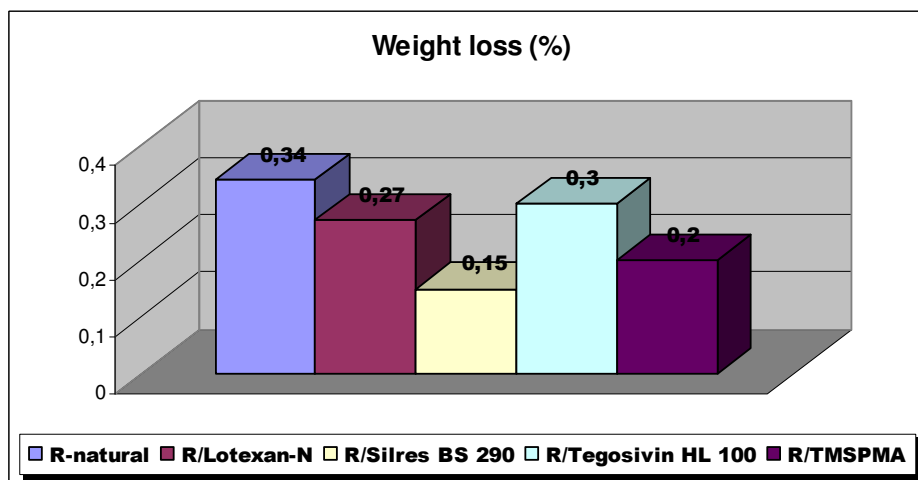


Fig. 145. Weight loss – Repedea after exposure to SO_2 saturated atmosphere

Looking at the two graphs scales, one can observe that Laspra samples have suffered a mass loss more or less twice as important as Repedea samples. It should be also mentioned that both limestones have registered the highest mass loss for the untreated samples.

In Laspra's case, the weight loss exhibited by the samples treated with the four water repellent products is not significantly different, while for Repedea the highest mass loss was manifested by the sample treated with Silres® BS 290.

VIII. 4. 3. Conclusions

The ESEM micrographs of the two types of limestones evidenced an accelerated degradation and mass loss in case of Laspra (untreated) subjected to SO₂ action. The formed salt crust thickness is about one order of magnitude higher for Laspra than for Repedea.

A comparative assessment of the data obtained in this study underlines that a better behavior of the two limestones was manifested when treated with the hybrid nanocomposite with silsesquioxane units. However, the differences in the behavior of the stone samples treated with the nanocomposite material and the ones treated with the commercial products are not that evident as in the case of the resistance to salt mist action, where TMSPMA proved to be, by far, the best choice, especially for Laspra (significantly higher durability). For the samples treated with the worldwide used water repellents, the dry deposition of SO₂ led to the formation of a higher amount of gypsum (evidenced by a higher crust thickness) as compared to the ones brushed with the TMSPMA compound.

For Laspra, the XRD patterns have shown (Fig. 135) that the presence of the worldwide used siloxane-based water repellents seems to favor the formation of epsomite (MgSO₄ · 7 H₂O) as one of the reaction products, this compound being responsible for the formation of a higher amount of gypsum. In the case of Laspra treated with TMSPMA, the crust is made only of gypsum and bassanite. Due to the presence of TMSPMA, SO₄²⁻ ions balance perfectly with Ca²⁺ ions, leading to the formation of gypsum as the only final product, similar results being obtained on previous studies on Laspra.

The evaluation methods applied to Repedea samples show that the different water repellents behave in a similar way when exposed to SO₂ artificial accelerated ageing, as also observed from the resistance against salt mist action test.

A peculiar behavior of some Laspra samples has been evidenced during their exposure to SO₂ action. Instead of a decrease of the signals corresponding to the calcite bands, the FT-IR spectra performed on aged stone samples revealed an unexpected increase in some samples. This abnormal phenomenon might be explained by the existence of the so called “sulphate-reducing” bacteria, which are able to convert sulphate into gaseous H₂S, therefore creating a sacrificial layer of new calcite and contributing to limestone’s consolidation / biocalcification. Since the block of Laspra

used in this study came from a column belonging to the oldest part of the Oviedo's cathedral, and since the literature proved that other Laspra samples showed the existence of biological growth, the theory that this particular Laspra block might be colonized is very plausible. Scientific proofs and further investigations are, nevertheless, necessary.

IX. Conclusions

The present study was concerned with the durability of two monumental stones treated with siloxane-based water repellents. The subject is of interest, considering that part of our stone-built cultural heritage, transmitted to future generations and representing different cultures, is permanently submitted to environments that yield decay phenomena.

The selected monumental limestones were Laspra – typical for the Spanish region of Asturias, used for centuries for the construction of many important cultural and religious buildings –, and Repedea, the most representative building stone in north-eastern part of Romania. Since some of the monuments that have been built from these limestones already have hundreds of years behind, their protection, conservation and eventually restoration became imperative.

In the protection of stone-based cultural heritage, water repellent products are on the front line. Water – in all its forms – is generally considered to be one of the most aggressive factors in inducing stone decay. Water penetrates inside the porous structure or fissures of the stones and through freeze-thaw cycles exerts important mechanical forces inside the stone, dissolves and transports soluble salts within the stones causing efflorescence on their surface and salt-induced spalling, carries acids in acid rains, favors the growth of microorganisms. As a result, disintegration, surface erosion, cracking, crust formation and biological films formation are the most commonly observed symptoms of stone decay, all of them being strongly related to and influenced by water.

For this research, three worldwide used siloxane-based water repellent products, namely Lotexan-N, Silres® BS 290 and Tegosivin HL 100 were investigated from the point of view of their protective ability and durability. One of the aims of the study was to better understand the action of the water repellent products applied on the two

limestones in order to be able to propose alternative, more efficient products. This is why, based on the experimental results obtained when using the three marketed products, an original compound was designed and tested. This compound is a 3-(trimethoxysilyl) propyl methacrylate-based hybrid nanocomposite (TMSPMA), whose novelty consists in its high functionality – the starting monomer contains, in a single molecule, a methacrylate group, able to thermally or photo-polymerize, and alkoxy silane groups, able to react with each other or with stone functional groups. These functional group are linked by hydrophobic short chains and form polymeric networks *via* sol-gel reactions. On the other hand, the polymer self-assembles in organized domains and the whole assembly becomes a highly crosslinked network structure.

The two components of the investigated systems, *viz.* the limestones and the water repellents, were thoroughly characterized through specific techniques.

The limestones were investigated by optical and electron microscopy, X-rays diffraction, FT-IR spectroscopy, mercury intrusion porosimetry, nitrogen adsorption on specific surface, determination of the velocity of propagation of ultrasonic waves, water absorption and water desorption at atmospheric pressure, water absorption by capillary suction, water vapor permeability and colorimetry. The results offered a clear image of the two limestones.

As for the four siloxane-based water repellents, their chemical structure was established and the thermal, rheological and film forming properties were investigated.

The coating of the two selected limestones with the four mentioned water repellents and its effect on stones durability was tested by analyzing the effect of different environmental aggressive factors on the untreated and treated limestones. Thus, the stone samples were submitted to artificially accelerated ageing tests where the influence of UV irradiation, salt mist action and SO₂ action in the presence of humidity on their durability was investigated. The evaluation of the experimental results was performed by comparing the data obtained on the untreated limestones, the treated ones and the treated and aged ones. The efficiency of the coating with the four water repellents was performed by submitting the treated / treated and aged stone samples to different tests, *viz.* microscopic investigation, contact angle measurements, water vapor

permeability measurements, color and weight loss measurements. Supplementary tests were additionally performed to answer specific questions.

All three marketed products proved their efficiency in increasing the water repellency of Laspra and Repedea. As far as the treated stones durability is concerned, no important differences among the effects of these products were noticed. All three proved to offer an efficient water protection even after prolonged UV irradiation (1000 hours, 40° C), but they induced to the treated stones only a minor protection against the aggressive action of salt mist or SO₂ in the presence of humidity.

The stone samples treated with the newly synthesized nanocomposite material showed, in most respects, a significantly higher durability as compared to the ones treated with the marketed products, especially against salt mist action, but also against prolonged UV irradiation. These improved results are due to the peculiar structure and functionality of the new compound, to its ability to form nanoaggregates able to self-assemble into a hybrid organic-inorganic polymeric network, to its ability to establish chemical or physical bonds with stone functional groups.

A summary of the durability experiments is presented below.

Resistance to salt mist action

	Laspra				Repedea			
	Lotexan-N	Silres® BS 290	Tegosivin HL 100	TMSPMA	Lotexan-N	Silres® BS 290	Tegosivin HL 100	TMSPMA
Visual observation	---	--	---	++	---	--	---	++
Contact angle	---	---	---	++	-	++	--	+
Water vapor permeability	---	---	---	++	--	--	---	-
Weight measurements	--	--	+	++	-	--	---	--
Color measurements	---	---	---	++	-	-	---	-
	-	-	-	+	-	+	-	+

Resistance to SO₂ action in the presence of humidity

	Laspra				Repedea			
	Lotexan-N	Silres® BS 290	Tegosivin HL 100	TMSPMA	Lotexan-N	Silres® BS 290	Tegosivin HL 100	TMSPMA
Visual observation	---	--	--	-	---	--	---	-
Contact angle	---	---	--	--	---	-	---	-
Water vapor permeability	---	---	--	-	--	---	---	-
Weight measurements	---	--	-	-	---	-	---	--
Color measurements	-	---	--	-	-	---	-	--
	-	-	+	+	-	+	-	+

Such a comparative table, summarizing the resistance to UV irradiation, is quite difficult to be proposed. While all four water repellents demonstrated good UV protection characteristics, no significant differences among them were noticed. The only comment consists in the fact that, while the stone samples coated with the marketed products register, after 1000 hours of UV irradiation at 40° C, a slight decrease in the contact angle values, the ones treated with TMSPMA exhibited an increase in the contact angle values.

The obtained data point out that the same treatment can afford different results and performance when applied to one limestone variety or another. As the literature generally agrees, it is very difficult and even risky to state that one specific product is the best to be used in one situation or another, but, based on this research and on its results, the conclusions would be the following ones:

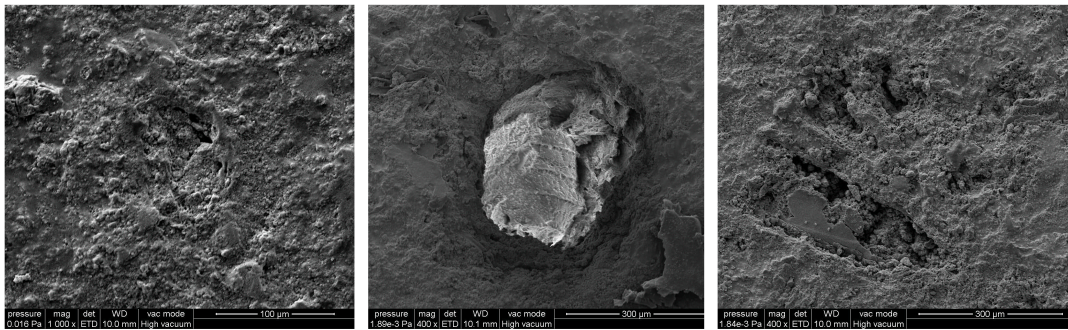
As far as the resistance to salt mist action is concerned, the product that afforded the best results when applied on Laspra is the nanocomposite material, and on Repedea Silres® BS 290 or / and TMSPMA. For the resistance to SO₂ action in the presence of humidity, it is more difficult to draw conclusions – this being the reason why no “+” can be found in the above table. Nevertheless, from the four selected water repellents,

Tegosivin HL 100 and TMSPMA proved a higher efficiency when applied on Laspra, while Silres® BS 290 and TMSPMA afforded better results in case of Repedea.

It should be mentioned that the artificially accelerated ageing, used in the present study, while offering a general overview on treatments efficiency and treated stones durability, is only a relatively reliable approach. No matter the applied treatment, it could lead to unexpected problems in the future, natural exposure providing the only “true test”.

Annex 1 – ESEM micrographs of Laspra and Repedea treated and treated / aged

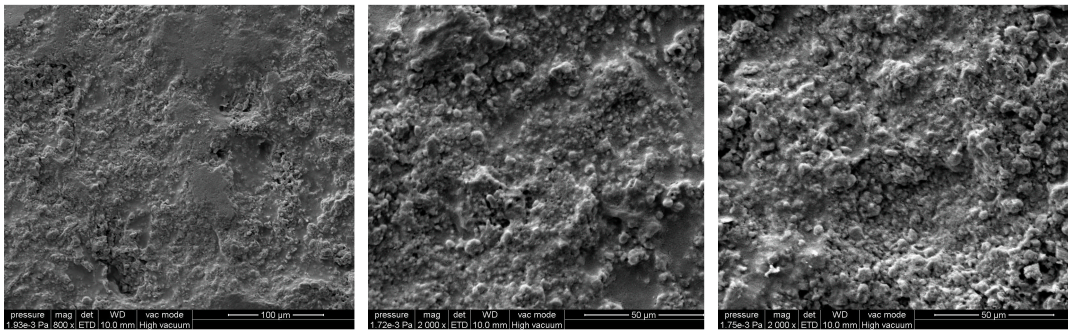
Laspra and Repedea – Treated



L – Lotexan-N

L – Lotexan-N

L – Lotexan-N



L – Lotexan-N

L – Lotexan-N

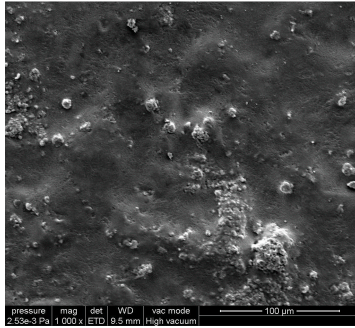
L – Lotexan-N



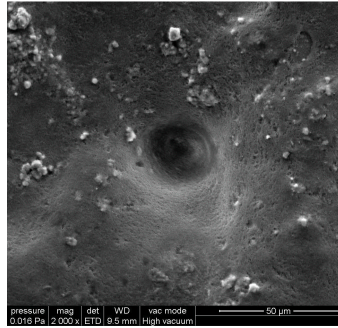
L – Silres BS 290

L – Silres BS 290

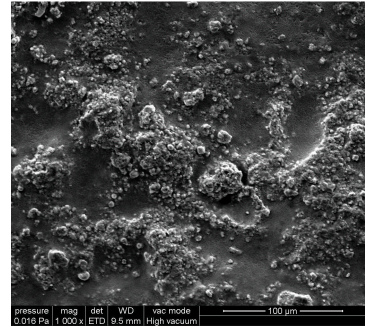
L – Silres BS 290



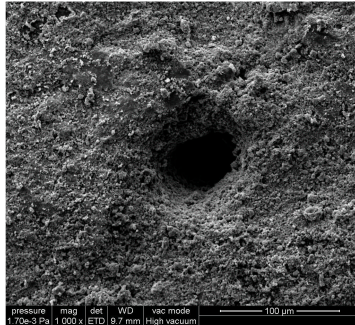
L – Silres BS 290



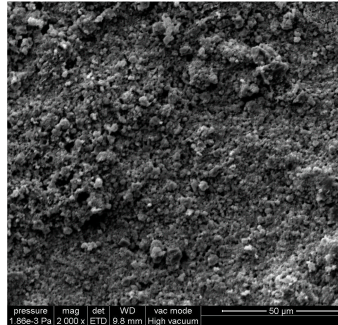
L – Silres BS 290



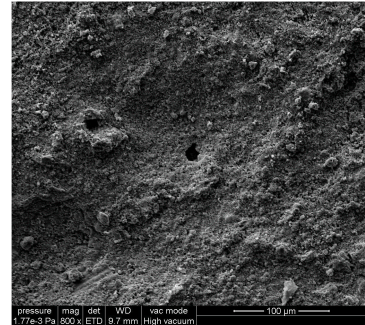
L – Silres BS 290



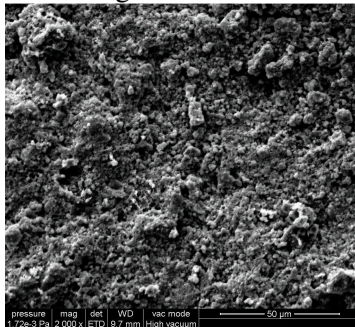
L – Tegosivin HL 100



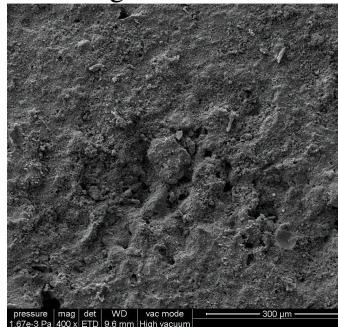
L – Tegosivin HL 100



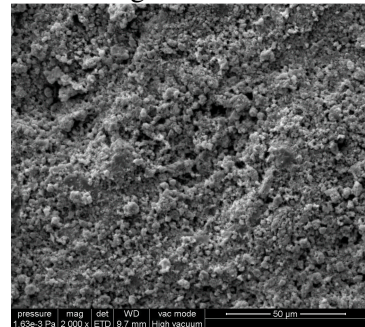
L – Tegosivin HL 100



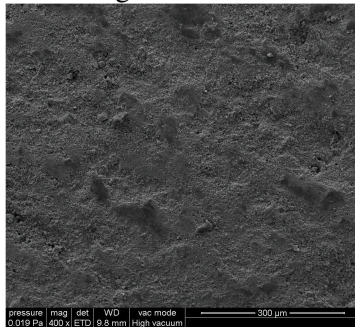
L – Tegosivin HL 100



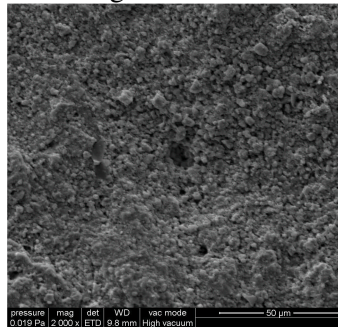
L – Tegosivin HL 100



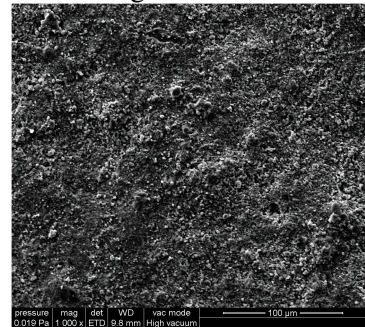
L – Tegosivin HL 100



L – TMSPMA



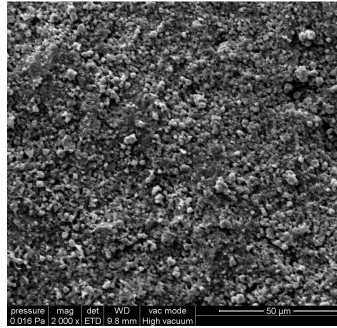
L – TMSPMA



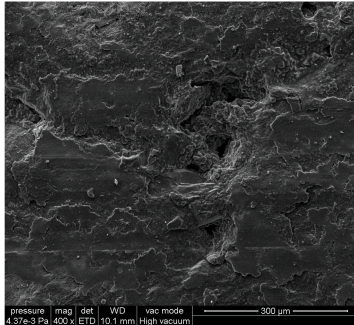
L – TMSPMA



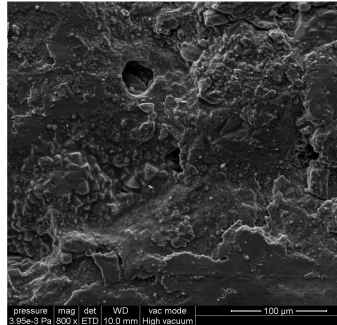
L – TMSPMA



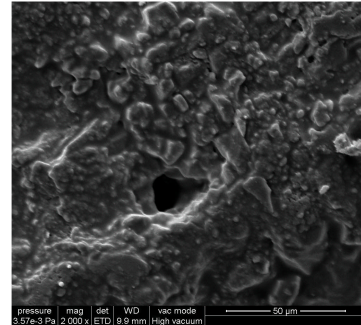
L – TMSPMA



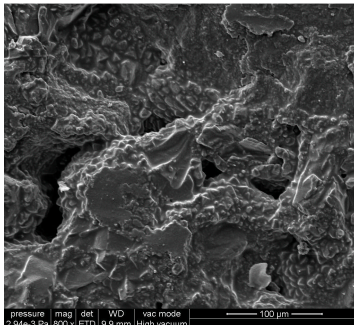
R – Lotexan-N



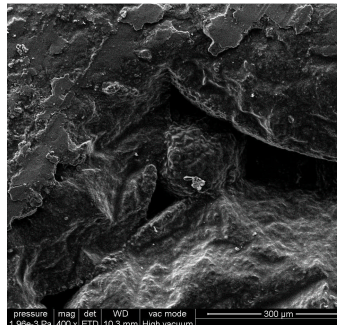
R – Lotexan-N



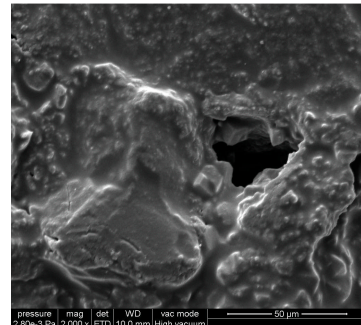
R – Lotexan-N



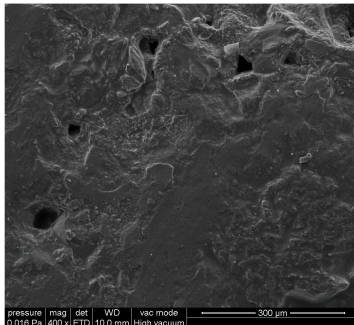
R – Lotexan-N



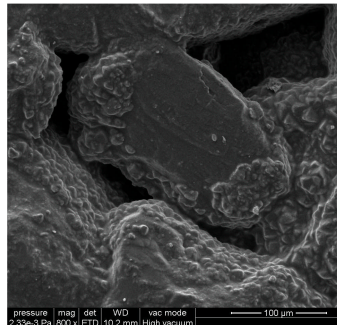
R – Lotexan-N



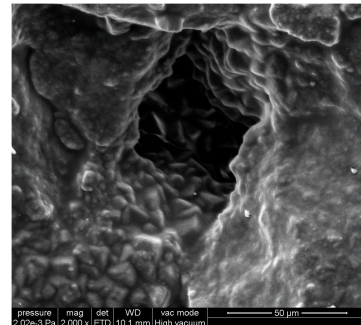
R – Lotexan-N



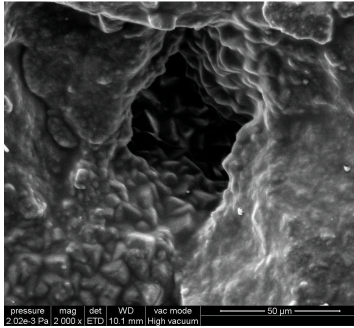
R – Silres BS 290



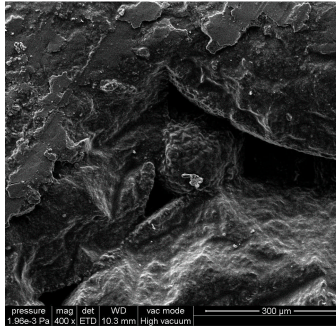
R – Silres BS 290



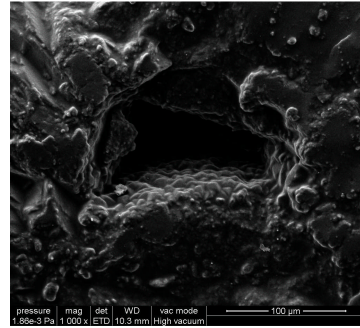
R – Silres BS 290



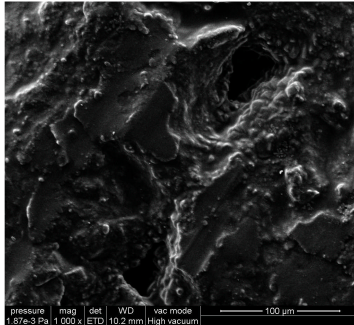
R - Silres BS 290



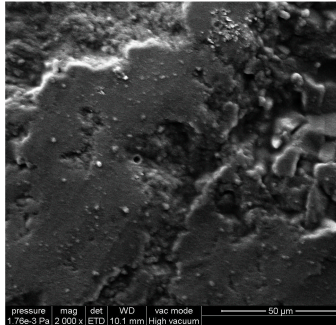
R - Silres BS 290



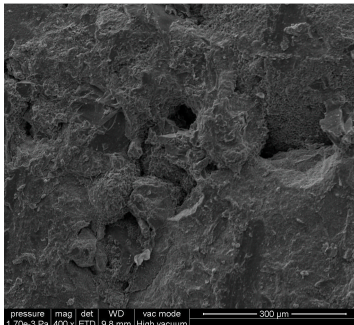
R - Silres BS 290



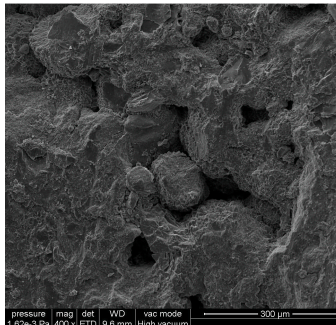
R - Silres BS 290



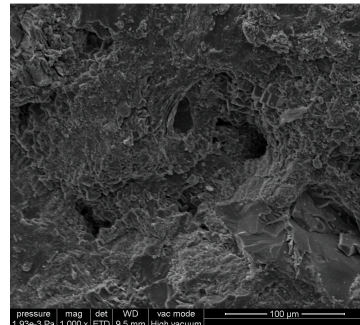
R - Silres BS 290



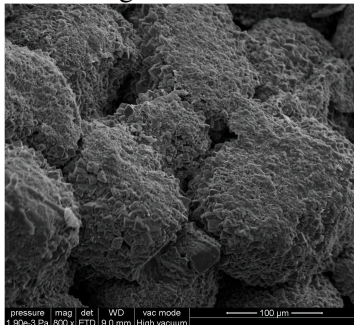
R - Tegosivin HL 100



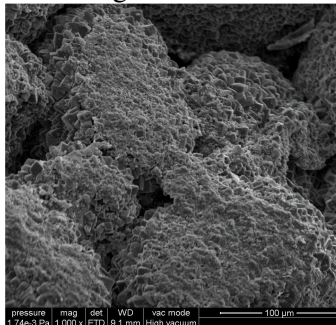
R - Tegosivin HL 100



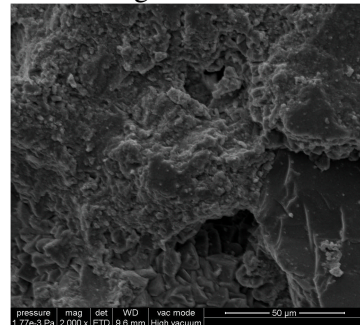
R - Tegosivin HL 100



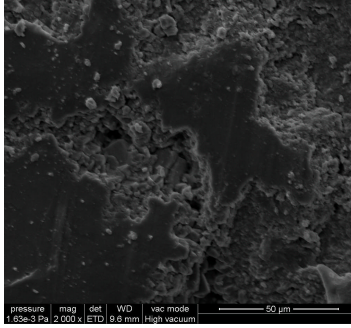
R - Tegosivin HL 100



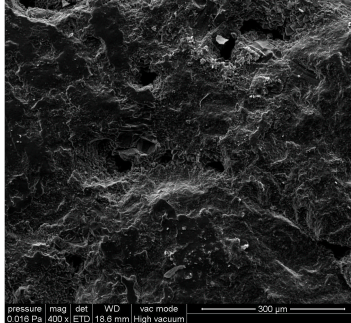
R - Tegosivin HL 100



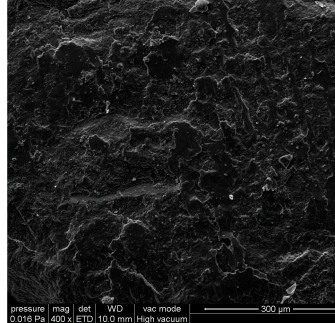
R - Tegosivin HL 100



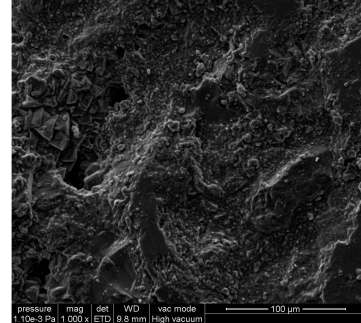
R – Tegosivin HL 100



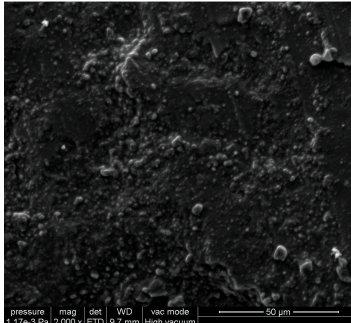
R – TMSPMA



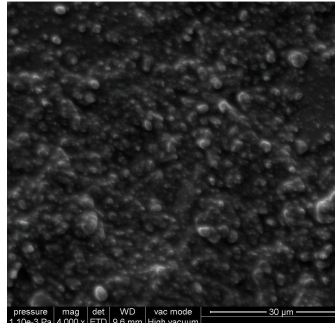
R – TMSPMA



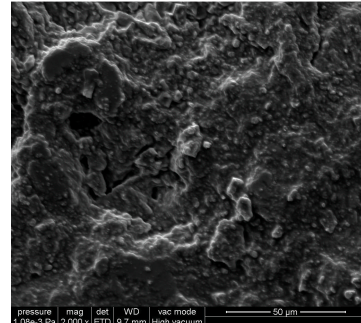
R – TMSPMA



R – TMSPMA

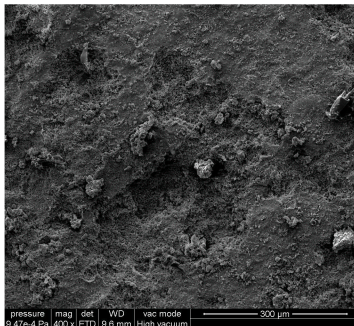


R – TMSPMA

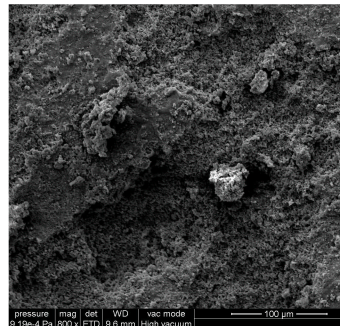


R – TMSPMA

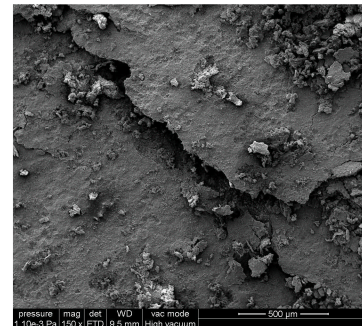
Laspra and Repedea – Treated and artificially aged – salt mist action



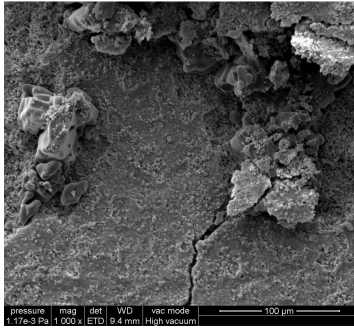
L – Lotexan-N



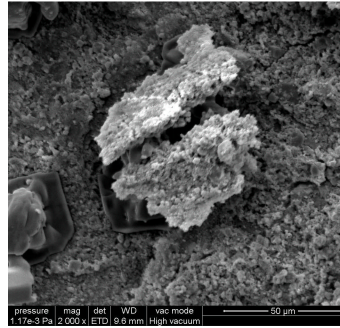
L – Lotexan-N



L – Lotexan-N



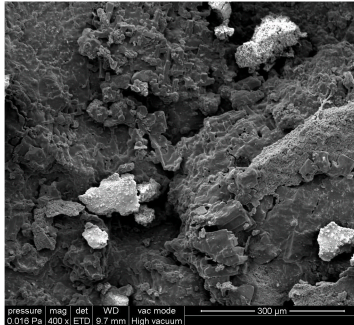
L – Lotexan-N



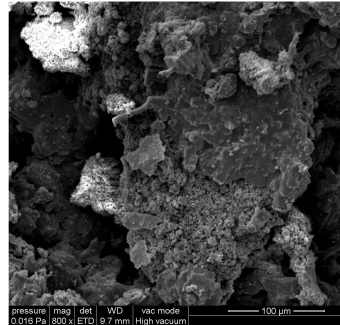
L – Lotexan-N



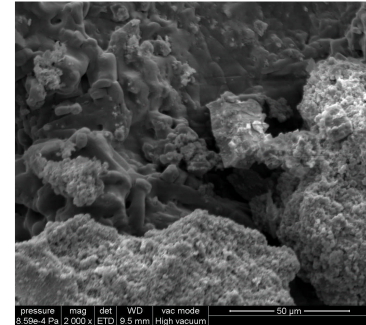
L – Lotexan-N



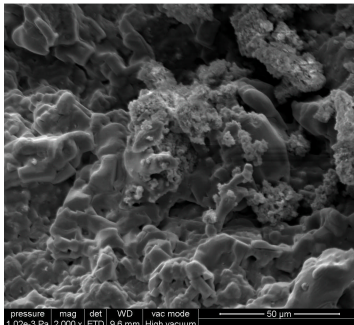
L – Silres BS 290



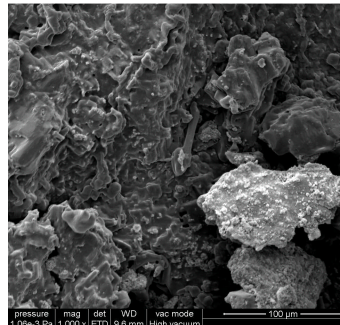
L – Silres BS 290



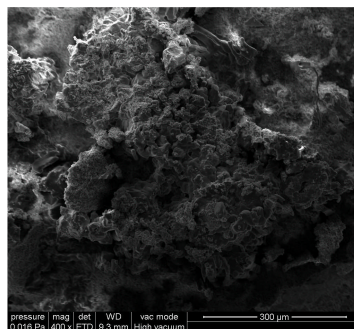
L – Silres BS 290



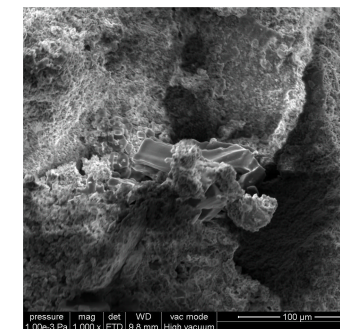
L – Silres BS 290



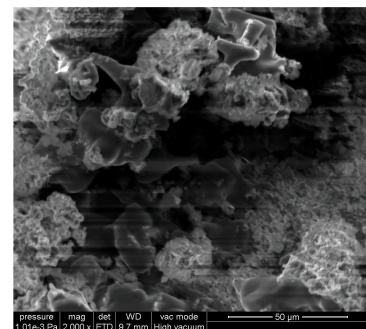
L – Silres BS 290



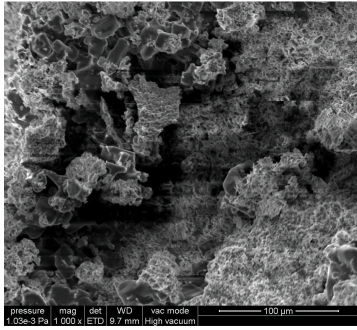
L – Tegosivin HL 100



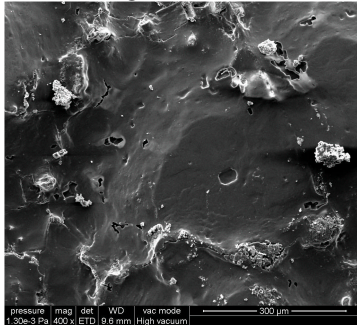
L – Tegosivin HL 100



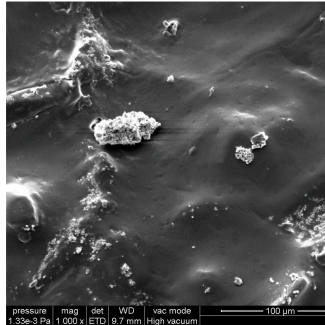
L – Tegosivin HL 100



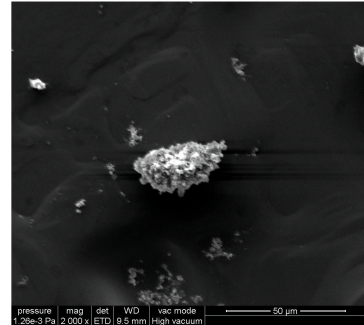
L – Tegosivin HL 100



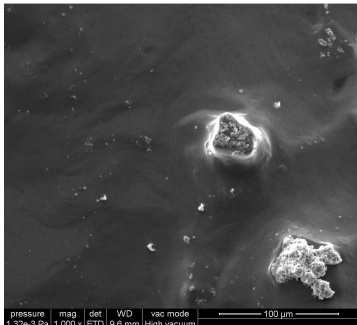
L – TMSPMA



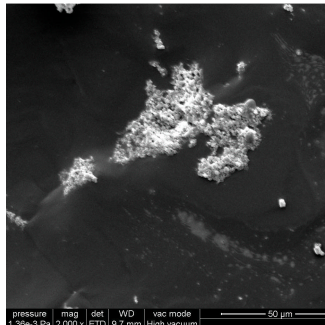
L – TMSPMA



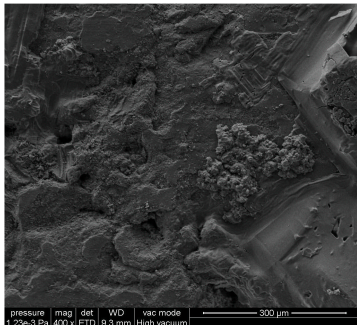
L – TMSPMA



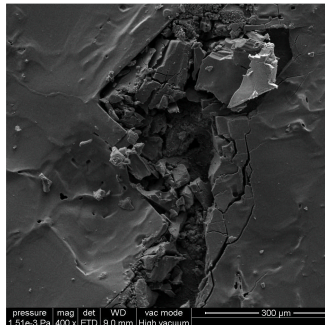
L – TMSPMA



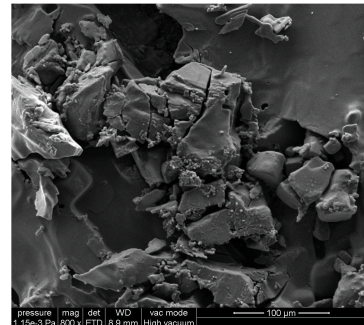
L – TMSPMA



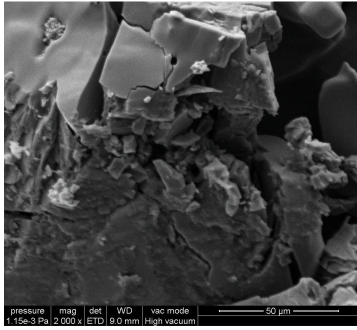
R – Lotexan-N



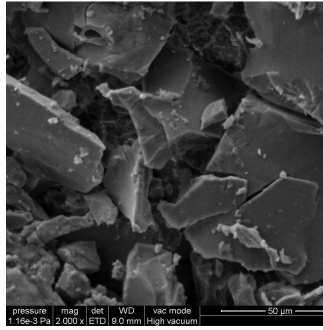
R – Lotexan-N



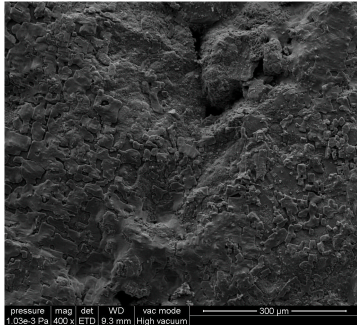
R – Lotexan-N



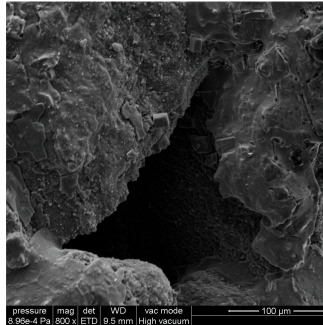
R – Lotexan-N



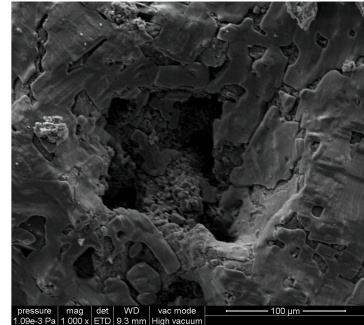
R – Lotexan-N



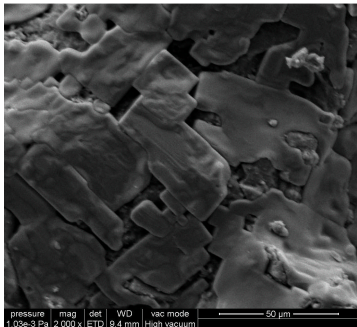
R – Silres BS 290



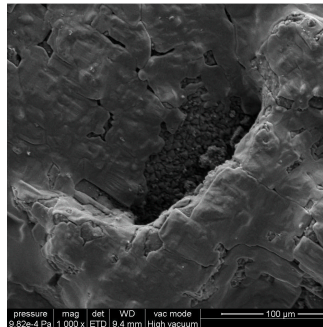
R – Silres BS 290



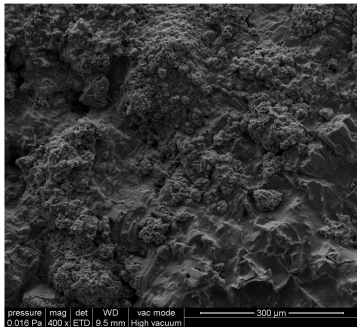
R – Silres BS 290



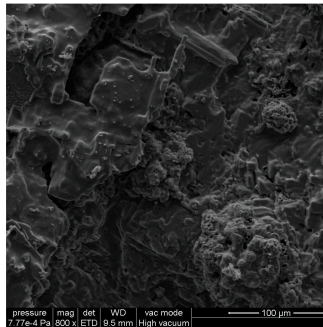
R – Silres BS 290



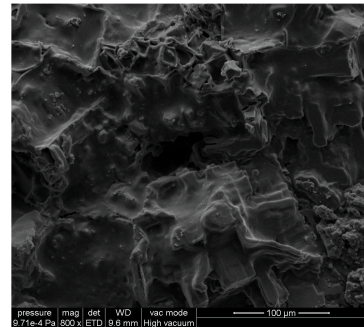
R – Silres BS 290



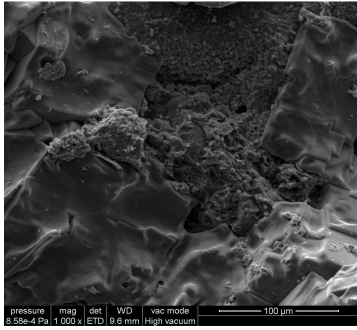
R – Tegosivin HL 100



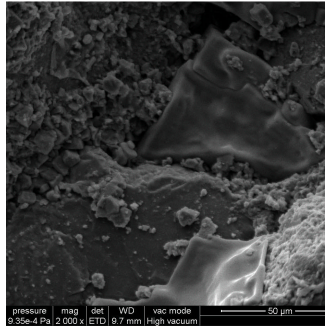
R – Tegosivin HL 100



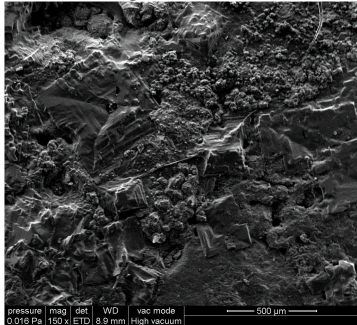
R – Tegosivin HL 100



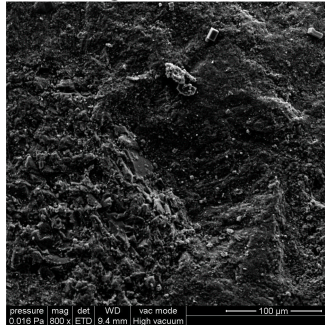
R – Tegosivin HL 100



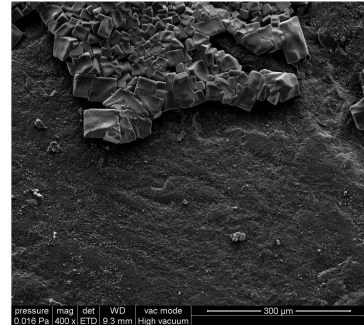
R – Tegosivin HL 100



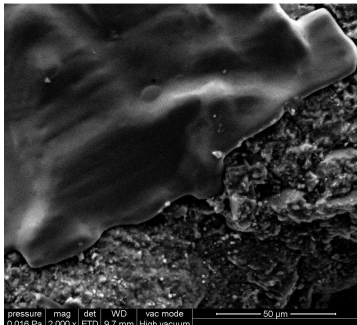
R – TMSPMA



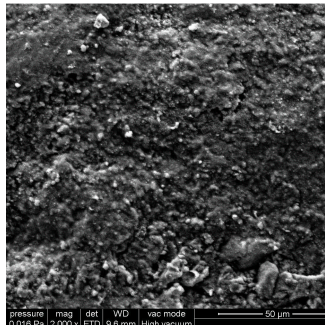
R – TMSPMA



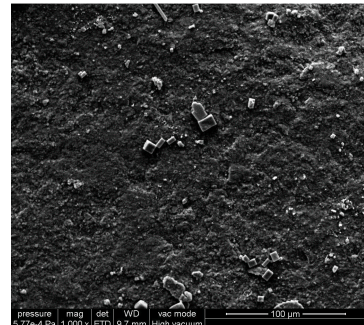
R – TMSPMA



R – TMSPMA

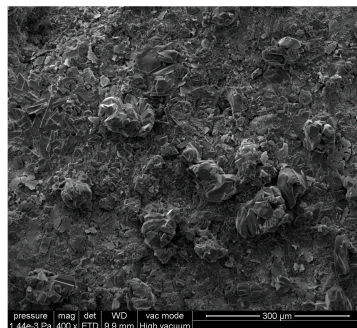


R – TMSPMA

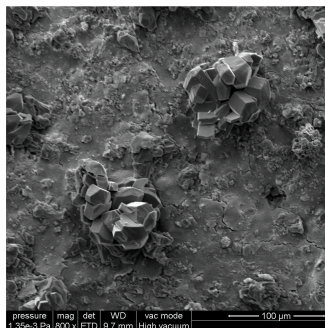


R – TMSPMA

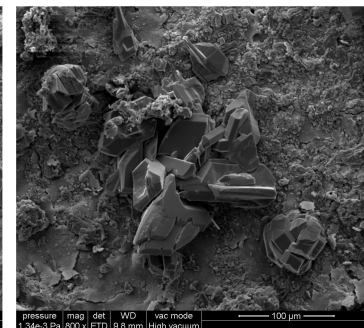
Laspra and Repedea – Treated and artificially aged – SO₂ action



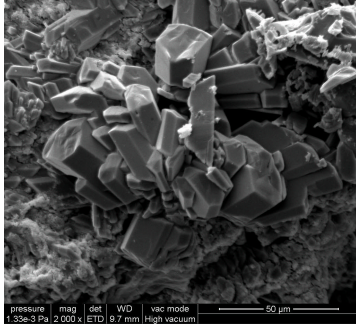
L – Lotexan-N



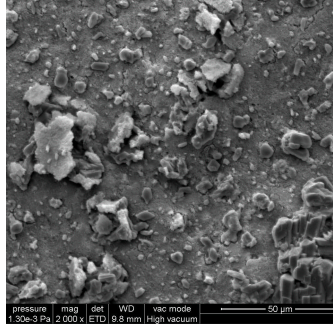
L – Lotexan-N



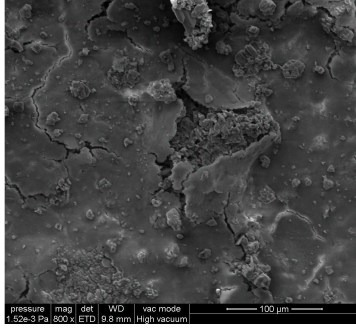
L – Lotexan-N



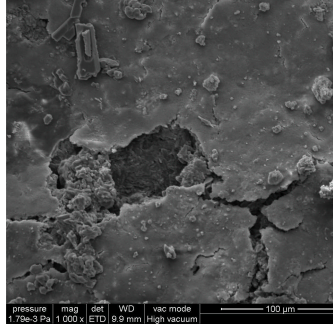
L – Lotexan-N



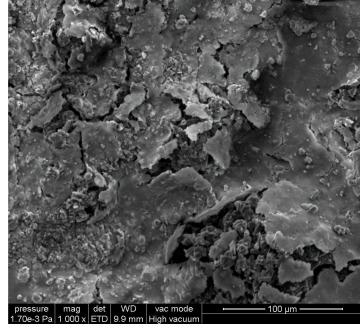
L – Lotexan-N



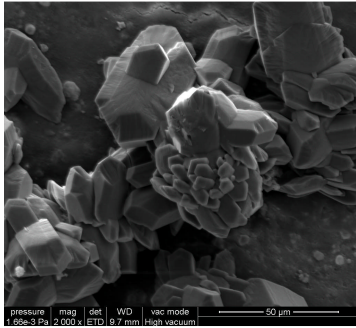
L – Silres BS 290



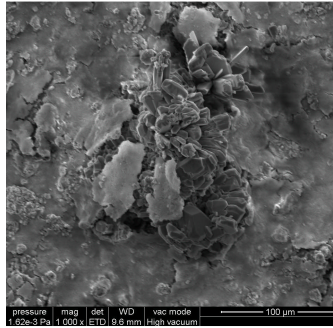
L – Silres BS 290



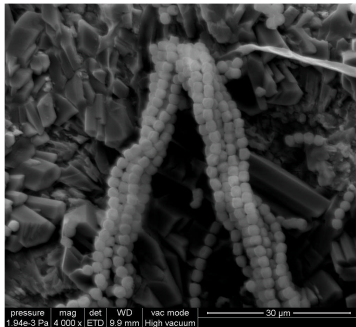
L – Silres BS 290



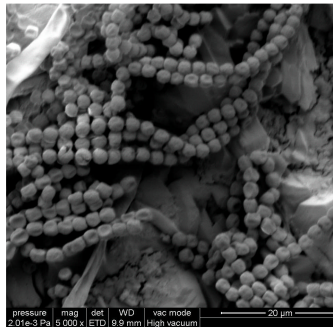
L – Silres BS 290



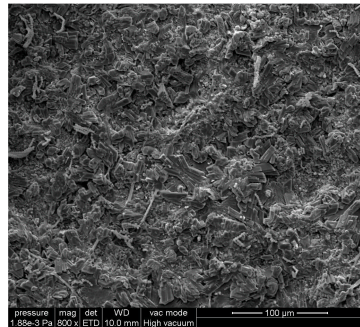
L – Silres BS 290



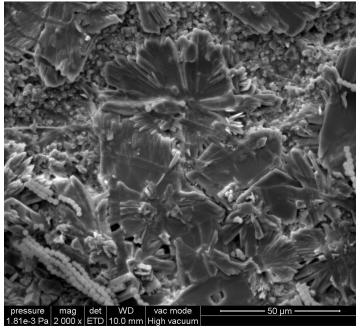
L – Tegosivin HL 100



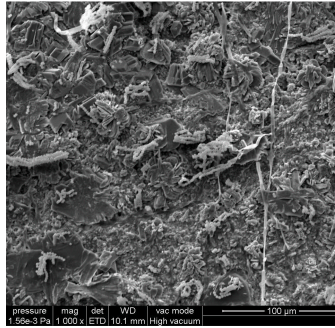
L – Tegosivin HL 100



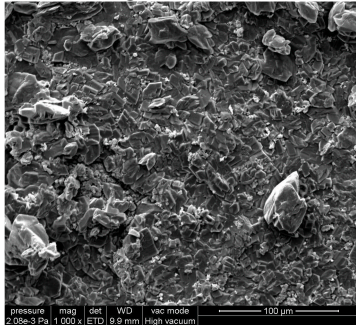
L – Tegosivin HL 100



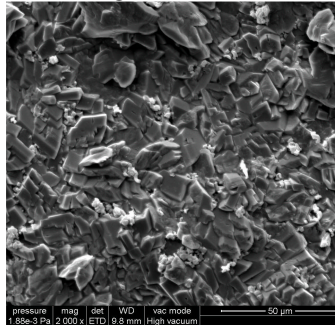
L – Tegosivin HL 100



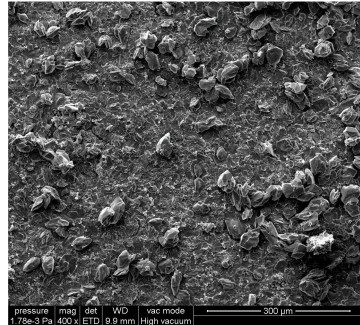
L – Tegosivin HL 100



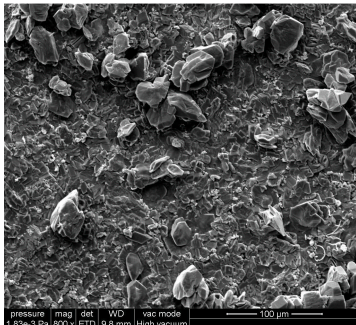
L – TMSPMA



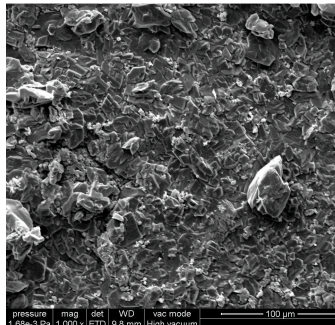
L – TMSPMA



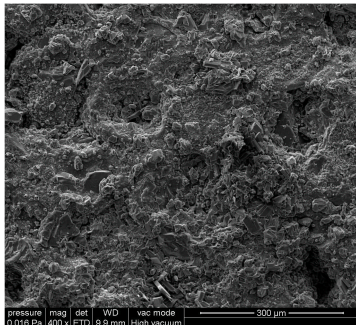
L – TMSPMA



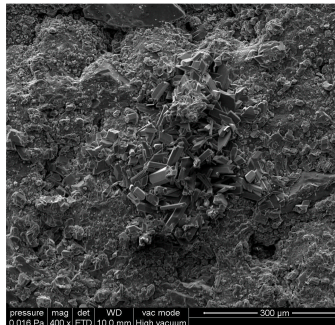
L – TMSPMA



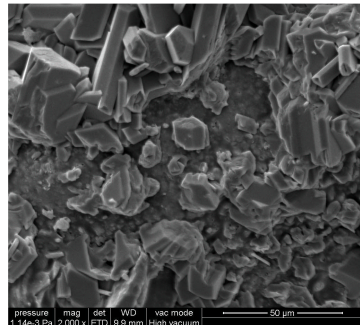
L – TMSPMA



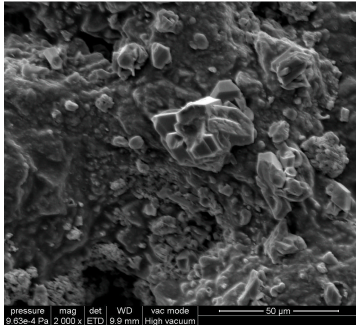
R – Lotexan-N



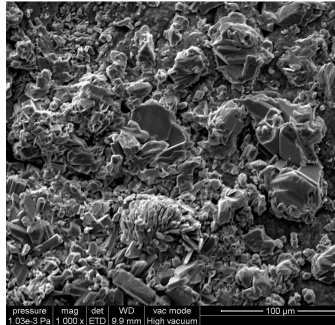
R – Lotexan-N



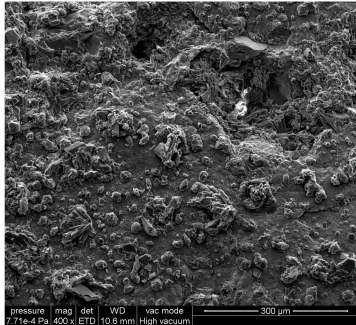
R – Lotexan-N



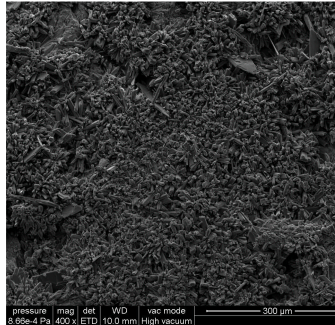
R – Lotexan-N



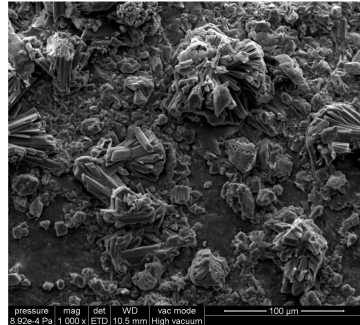
R – Lotexan-N



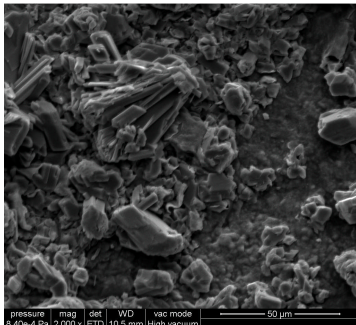
R – Silres BS 290



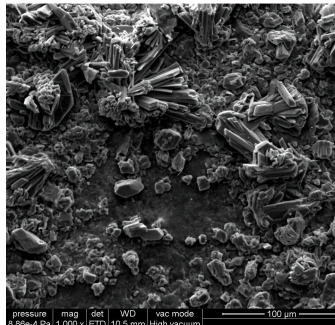
R – Silres BS 290



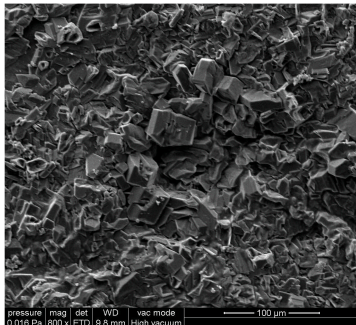
R – Silres BS 290



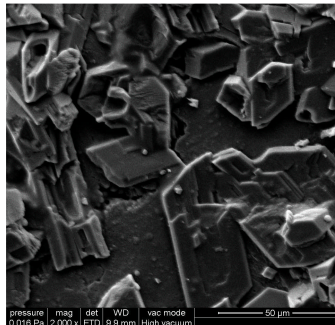
R – Silres BS 290



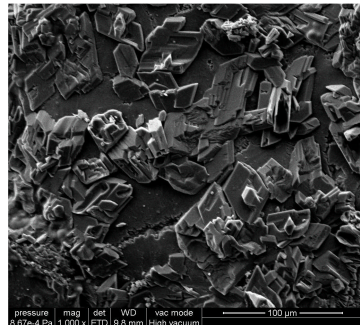
R – Silres BS 290



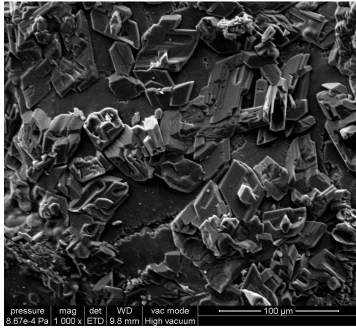
R – Tegosivin HL 100



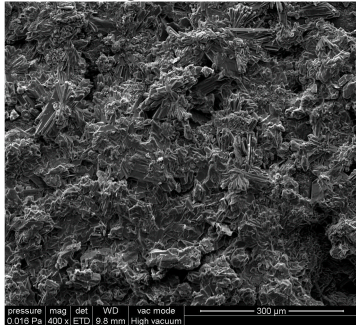
R – Tegosivin HL 100



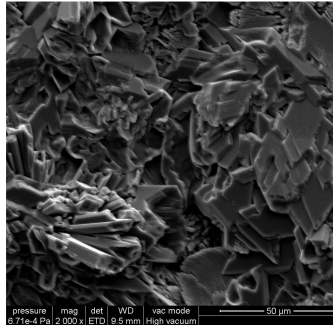
R – Tegosivin HL 100



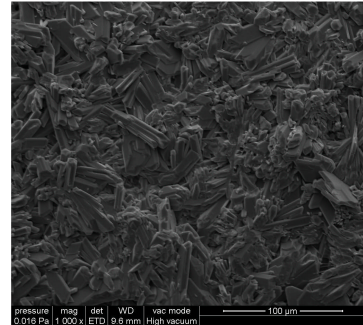
R – Tegosivin HL 100



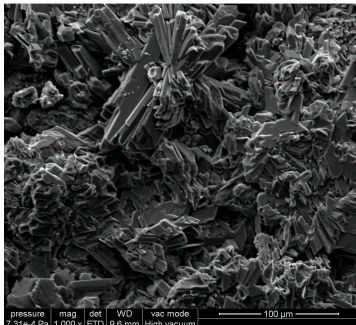
R – TMSPMA



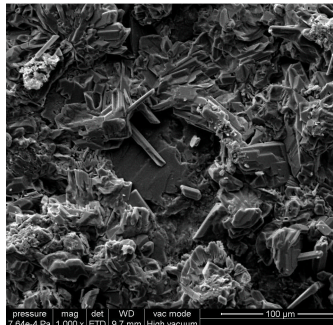
R – TMSPMA



R – TMSPMA



R – TMSPMA



R – TMSPMA

Annex 2 – Supplementary testing of 3-(trimethoxysilyl)propyl methacrylate – based nanocomposite

The newly synthesized water repellent, *viz.* the hybrid nanocomposite based on 3-(trimethoxysilyl)propyl methacrylate (TMSPMA) was tested, in the present research, as water repellent for two limestones – Laspra and Repedea. The experimental results proved that, in many respects, the hybrid nanocomposite yielded better results than the three marketed products, i. e. Lotexan-N, Silres® BS 290 and Tegosivin HL 100.

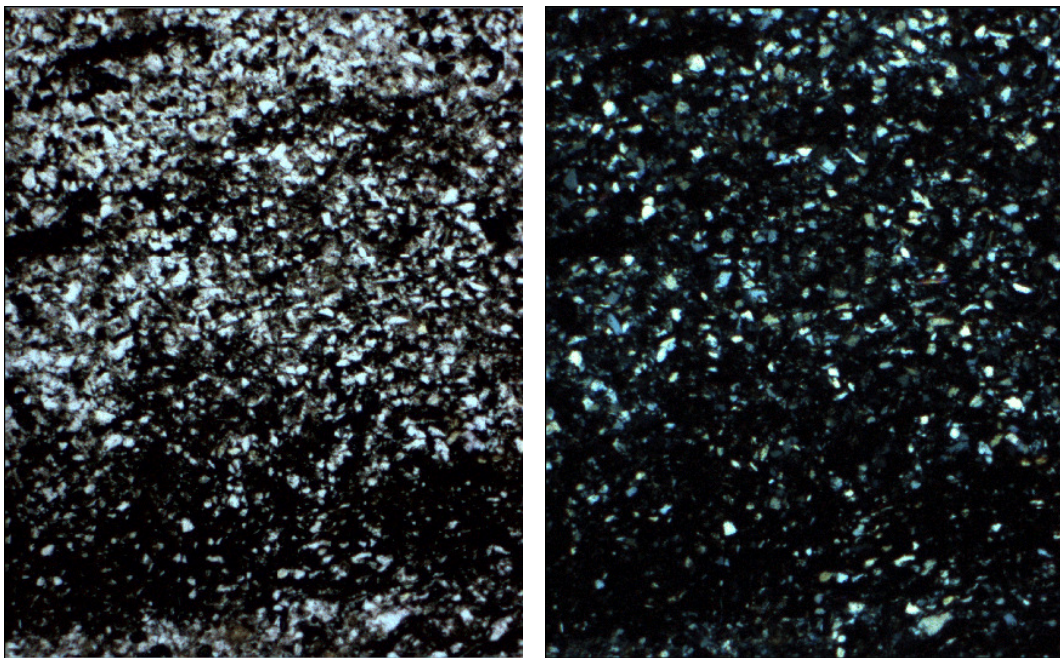
To further test the behavior of the proposed new compound, some preliminary experiments were performed²⁵ on a completely different Spanish stone, namely *Cuarcita Carioca* (trade name). A few characteristics of this stone are listed below:

- sedimentary rock, rich in iron oxides;
- porous, (micro)fissured sandstone;
- main composition: quartz (50%), clay (15%), muscovite and iron oxides;
- open porosity of about 8%;
- average pore diameter, 5 – 10 µm.

²⁵ These experiments were kindly performed by Mr. Felix J. Mateos, Group of Alteration and Durability, Department of Geology, University of Oviedo, Spain.



Macroscopic aspect of Cuarcita Carioca



*Microscopic observation of Cuarcita Carioca under polarized light microscope (POL)
(NPX25) and (NCX25)*

The stones were brushed with the nanocomposite material following the procedure previously used for Laspra and Repedea. The treated stones were then submitted to artificially accelerated ageing tests, i. e. thermic shock and freeze – thaw (these tests were required by the users).

The thermic shock and freeze – thaw artificially accelerated ageing tests were performed according to the EN – 14066 and the EN – 12371 European Standards, respectively.

The values of the contact angles measurements are listed below.

	Contact angle (degree)
<i>Cuarcita Carioca</i> treated with TMSPMA	129
<i>Cuarcita Carioca</i> treated with TMSPMA, after 7 freeze – thaw cycles	112
<i>Cuarcita Carioca</i> treated with TMSPMA, after 7 thermic shock cycles	121

These preliminary data show that the coating of *Cuarcita Carioca* stone with TMSPMA gives significantly better results – as far as the contact angle values are concerned – as compared to the results obtained for the same product applied on Laspra or Repedea. Normally, after a few ageing cycles of the mentioned type, the surface of the stones treated with usual siloxane-based water repellents loses its hydrophobic properties due to the degradation (fissures, cracks) of the superficial polymeric film.

The behavior observed for *Cuarcita Carioca* is mainly due to its different mineralogical composition (50% quartz) that determines a much better compatibilization of the polymeric treatment with the stone.

These tests prove that the newly synthesized hybrid nanocomposite could be successfully used for a wide range of building stones.

Acknowledgements

My gratitude and sincere thanks to the two promoters of this research, Prof. Rosa M. Esbert and Prof. Modesto Montoto, for their competent advices, kindness and encouragements.

The assistance of Patricia Vasquez and Felix J. Mateos during the two and a half years spent in the Department of Geology, the University of Oviedo, Spain are gratefully acknowledged.

My former professors from Iasi, Romania, Prof. Valeria Harabagiu and Prof. Constanta Ibanescu, were permanently in touch with me even after my graduation. Their constant support and faith in me meant enormously to me.

To my colleagues and friends, Mihaela Olaru, Magdalena Aflori and Raluca Darie – thank you for always being there for me.

The lectures given by the scientific advisers involved in the EPISCON project during September 2006 – February 2007 in Ravenna, Italy, introduced me to the world of science for conservation. I hope they will find in this thesis the result of their generous efforts.

To my parents for staying behind me all the way and sharing this experience with me. My father's wisdom, professional experience, patience and faith were key factors in accomplishing this PhD. Thank you, father.

This study was financially supported by EPISCON – European PhD in Science for Conservation EU Project 05-MEST-CT2005-020559.

XII. References

- [1] Verdel, T., and Chambon, C., Environmental degradation study of the Sphinx (Egypt) by the use of System Dynamics: A new approach at the disposal of specialists. In *La conservazione dei monumenti nel bacino del Mediterraneo*, ed. V. Fassina, H. Ott, and F. Zezza, 383-392. Venice: Soprintendenza ai Beni Artistici e Storici di Venezia (1994).
- [2] Brimblecombe, P., History of air pollution and deterioration of heritage. In *Weathering and Air Pollution*, 23-32. Bari: Comunità delle Università Mediterranee, Scuola Universitaria Conservazione dei Monumenti (1991).
- [3] Camuffo, D., Del Monte, M., Sabbioni, C., and Vittori, O., *Atmospheric Environment*, 16, 2253-2259 (1982).
- [4] Fassina, V., Atmospheric pollutants responsible for stone decay: Wet and dry surface deposition of air pollutants on stone and the formation of black scabs. In *Weathering and Air Pollution*, 67-86. Bari: Comunità delle Università Mediterranee, Scuola Universitaria Conservazione dei Monumenti (1991).
- [5] Ausset, P., Lefevre, R., Phillipon, J., and Venet, C., Large scale distribution of fly-ash particles inside weathering crusts on calcium carbonate substrates: Some examples on French monuments. In *La conservazione dei monumenti nel bacino del Mediterraneo*, ed. D. Decrouez, J. Chamay, and F. Zezza, 121-139. Geneva: Musée d'Histoire naturelle et Musée d'art et d'histoire (1992).
- [6] Hanna, S. B., The use of organo-silanes for the treatment of limestone in an advanced state of deterioration. In *Adhesives and Consolidants*, 171-176. London: International Institute for Conservation (1984).
- [7] Zehnder, K., and Arnold, A., *J. Crystal Growth*, 97, 513-521 (1989).
- [8] Doehne, E., In situ dynamics of sodium sulfate hydration and dehydration in stone pores: Observations at high magnification using the environmental scanning electron microscope. In *La conservazione dei monumenti nel bacino del Mediterraneo*, ed. V.

Fassina, H. Ott, and F. Zezza, 143-150. Venice: Soprintendenza ai Beni Artistici e Storici di Venezia (1994).

[9] Charola, A. E., and Weber, J., The hydration-dehydration mechanism of sodium sulfate. *7th International Congress on Deterioration and Conservation of Stone*, 581-590. Lisbon: Laboratório Nacional de Engenharia Civil (1992).

[10] McMahon, D. J., Sandberg, P., Folliard, K., and Mehta, P. K., Deterioration mechanisms of sodium sulfate. *7th International Congress on Deterioration and Conservation of Stone*, 705-714. Lisbon: Laboratório Nacional de Engenharia Civil (1992).

[11] Esbert, R. M., Montoto, M., Suarez del Río, L. M., Ruiz de Argandoña, V. G., and Grossi, C. M., Mechanical stresses generated by crystallization of salts inside treated and non-treated monumental stones: Monitoring and interpretation by acoustic mission/microseismic activity. In *Materials Issues in Art and Archaeology 2*, ed. P. B. Vandiver, J. R. Druzik, and G. S. Wheeler, 285-296. Pittsburgh: Materials Research Society (1991).

[12] Honeyborne, D. B., and Harris, P. B., The structure of porous building stone and its relation to weathering behaviour. *Proceedings of the Tenth Symposium of the Colston Research Society*, 343-359. London: Butterworths Scientific Publications (1958).

[13] Everett, D. H., *Trans. Faraday Soc.*, 57, 1541-1551 (1961).

[14] Price, C. A., Preventive conservation of salt-contaminated masonry in the Wakefield Tower, HM Tower of London. *Institute of Archaeology Bulletin*, 30, 121-133 (1993).

[15] Larson, J., The conservation of stone sculpture in museums. In *Conservation of Building and Decorative Stone*, vol. 2, ed. J. Ashurst, and F. G. Dimes, 197-207. London: Butterworth-Heinemann (1990).

[16] Fassina, V., General criteria for the cleaning of stone: Theoretical aspects and methodology of application. In *Stone Material in Monuments: Diagnosis and Conservation*, 126-132. Crete: Comunità delle Università Mediterranee, Scuola Universitaria Conservazione dei Monumenti (1993).

[17] Andrew, C., *Stonecleaning: A Guide for Practitioners*. Edinburgh: Historic Scotland and The Robert Gordon University (1994).

[18] Werner, M., Research on cleaning methods applied to historical stone monuments. In *Science, Technology and European Cultural Heritage*, ed. N. S. Baer, C. Sabbioni, and A. I. Sors, 688-691. Oxford: Butterworths-Heinemann (1991).

- [19] Young, M. E., Stonecleaning of granite buildings and monuments: The use of colour measurement in Stonecleaning trials. In *Conservation Science in the U.K.*, ed. N. H. Tennent, 20-28. London: James and James (1993).
- [20] D'Urbano, M. S., Giovannone, C., Governale, P., Pandolfi, A., and Santamaria, U., La pulitura laser di superfici lapidee: Messa a punto di una metodologia standardizzata per il controllo degli effetti. In *La conservazione dei monumenti nel bacino del Mediterraneo*, ed. V. Fassina, H. Ott, and F. Zezza, 955-962. Venice: Soprintendenza ai Beni Artistici e Storici di Venezia (1994).
- [21] Maxwell, I., Stonecleaning - for better or worse? An overview. In *Stone Cleaning and the Nature, Soiling and Decay Mechanisms of Stone*, ed. R. G. M. Webster, 3-49. London: Donhead (1992).
- [22] MacDonald, J., Thomson, B., and Tonge, K., Chemical cleaning of sandstone: Comparative laboratory studies. In *Stone Cleaning and the Nature, Soiling and Decay Mechanisms of Stone*, ed. R. G. M. Webster, 217-226. London: Donhead (1992).
- [23] Bowley, M. J., Desalination of stone: A case study. In *Building Research Establishment, Current Paper CP46/75*. Watford: Building Research Establishment (1975).
- [24] Sinner, P., Conservation of crystalline marble with the acrylic-total-impregnation process. In *Science, Technology and European Cultural Heritage*, ed. N. S. Baer, C. Sabbioni, and A. I. Sors, 700-703. Oxford: Butterworths-Heinemann (1991).
- [25] Selwitz, C. M., The use of epoxy resins for stone conservation. In *Materials Issues in Art and Archaeology 2*, ed. P. B. Vandiver, J. R. Druzik, and G. S. Wheeler, 181-191. Pittsburgh: Materials Research Society (1991).
- [26] Félix, C., and Furlan, V., Variations dimensionnelles de grès et calcaires liées à leur consolidation avec un silicate d'éthyle. In *La Conservazione dei monumenti nel bacino del Mediterraneo*, ed. V. Fassina, H. Ott, and F. Zezza, 855-859. Venice: Soprintendenza ai Beni Artistici e Storici di Venezia (1994).
- [27] Alonso, F. J., Esbert, R. M., Alonso, J., and Ordaz, J., Saline spray action on a treated dolomitic stone. In *La conservazione dei monumenti nel bacino del Mediterraneo*, ed. V. Fassina, H. Ott, and F. Zezza, 860-870. Venice: Soprintendenza ai Beni Artistici e Storici di Venezia (1994).

- [28] Piacenti, C., Camaiti, F. M., Brocchi, T., and Scala, A., New developments in perfluorinated protective agents for stone. In *Conservation of Stone and Other Materials*, ed. M.-J. Thiel, 733-739. London: E & F N Spon (1993).
- [29] Guidetti, V., Chiavarini, M., and Parrini, P., Polyfluoroethanes as stone protectives. *7th International Congress on Deterioration and Conservation of Stone*, 1279-1288. Lisbon: Laboratório Nacional de Engenharia Civil (1992).
- [30] Cimitàn, L., Rossi, P. P., and Torraca, G., Accelerated sulphation of calcareous materials in a climatic chamber: Effect of protective coatings and inhibitors. In *La conservazione dei monumenti nel bacino del Mediterraneo*, ed. V. Fassina, H. Ott, and F. Zezza, 233-241. Venice: Soprintendenza ai Beni Artistici e Storici di Venezia (1994).
- [31] Galan, E., Control of physico-mechanical parameters for determining the effectiveness of stone conservation treatments. In *Stone Material in Monuments: Diagnosis and Conservation*, 189-197. Crete: Comunità delle Università Mediterranee, Scuola Universitaria Conservazione dei Monumenti (1993).
- [32] Sasse, H. R., Honsinger, D., and Schwamborn, B., "PINS:" New technology in porous stone conservation. In *Conservation of Stone and Other Materials*, ed. M.-J. Thiel, 705-716. London: E & F N Spon (1993).
- [33] Galan, E., and Carretero, M. I., Estimation of the efficacy of conservation treatments applied to a permotriassic sandstone. In *La Conservazione dei monumenti nel bacino del Mediterraneo*, ed. V. Fassina, H. Ott, and F. Zezza, 947-954. Venice: Soprintendenza ai Beni Artistici e Storici di Venezia (1994).
- [34] Ji, X., Hampsey, J. E., Hu, Q., He, J., Yang, Z., and Lu, Y., *Chem. Mater.*, 15(19), 3656 (2003).
- [35] Wight, A. P. and Davis, M. E., *Chem. Rev.*, 102(10), 3589 (2002).
- [36] Simionescu, B., Olaru, M., Aflori, M., Buruiana, E. C., and Cotofana, C., *Solid State Phenom.*, 151, 17-23 (2009).
- [37] Simionescu, B., Olaru, M., Aflori, M., Buruiana, E. C., and Cotofana, C., *High Perform. Polym.*, DOI: 10.1177/0954008308100905 (2009).
- [38] Winkler, E. M., *Stone: Properties, Durability in Man's Environment*, 2nd ed., Springer-Verlag, New York (1975).
- [39] Wheeler, G. S., Schein, A., Sherrer, G., Su, S. H., and Blackwell, C. Scott, *Anal. Chem.*, 64(5), 347 (1992).

- [40] Wheeler, G. S., Fleming, S. A., and Ebersole, S., Comparative Strengthening Effect of Several Consolidants on Wallace Sandstone and Indiana Limestone, 1033, 7th *International Congress on Deterioration and Conservation of Stone*, Lisbon (1992).
- [41] Montoto, M., *Estratos*, 40, 12-17 (1996).
- [42] Bello, M. A., Martin, L., and Martin, A., *Studies in Conservation*, 37, 193-200 (1992).
- [43] Zhang, S., Paterson, M. S., and Cox, S. F., *Tectonophysics*, 335, 17-36 (2001).
- [44] Rodriguez Navarro, C., and Sebastian Pardo, E., Applications of scanning electronic microscopy in the porometric analysis of ornamental calcareous material. *Electron Microscopy. Eurem 92*, Vol. 2, 799-800. Granada (1992).
- [45] Royer-Carfagni, G. F., *Int. J. Rock Mechanics and Mining Sciences*, 36, 119-126 (1999).
- [46] Badan, B., Cavaletti, R., and Marchesini, L., Intervento sulle sculture in marmo Marco in Venecia. 3rd *Congresso Internazionale sul Deterioramento e la Conservazione della Pietra*, 623-627. Venecia (1979).
- [47] Lazzarini, L., and Fascina, V., Studio scientifico sullo stato di conservazione delle pietre e dei marmi della Porta della Carta di Venecia. 3rd *Congresso Internazionale sul Deterioramento e la Conservazione della Pietra*, 645-660. Venecia (1979).
- [48] Garcia-Valles, M., Vendrell-Saz, M., Wolfgang, E., and Urzi, C., *Appl. Geochem.*, 12, 255-266 (1997).
- [49] Aldrovandi, A., Lalli, C., Lanterna, G., and Matteini, M., *J. Cultural Heritage*, vol. 1, supplement 1, s55-s60 (2000).
- [50] Esbert, R. M., Grossi, C. M., Rojo, A., Alonso, F. J., Montoto, M., Ordaz, J., Perez de Andres, M. C., Escudero, C., Barrera, M., Sebastian, E., Rodriguez Navarro, C., and Elert, K., *J. Cultural Heritage*, 4, s50-s55 (2002).
- [51] Thompson, B. R., and Thompson, D. O., Ultrasonic in non-destructive evaluation. *Proc. IEEE*, 73, 1716-1755 (1985).
- [52] Abell, A. B., Willis, K. L., Lange, D. A., *J. Coll. Interface Sci.*, 211, 39-44 (1999).
- [53] Alonso, F. J., Esbert, R. M., and Ordaz, J., *Bol. Geol. y Min. de Espana*, 98 (2) 226-237 (1987).
- [54] Newman, A. W., *Micrometrics. Physical characterization of pharmaceutical solids*, ed. H. G. Brittain, 253-280. New York: Marcel Decker (1995).
- [55] Suarez, D. L., and Wood, J. D., *Chemical Geol.*, 132(1-4), 143-150 (1996).

- [56] Zezza, U., Massa, V., and Bortolaso, G., Non destructive on site spectrometric color testing building stones. *3rd Int. Conf. Non-Destructive Testing, Microanalytical and Environmental Evaluation for Study and Conservation of Work of Art*, 539-553. Viterbo (1992).
- [57] Simon, S., Boehm, H. P., and Snethlage, R., A surface-chemical approach to marble conservation. *7th International Congress on Deterioration and Conservation of Stone*, 851-859. Lisbon (1992).
- [58] Toniolo, L., Poli, T., Castelvetro, V., Manariti, A., Chiantore, O., and Lazzari, M., *J. Cultural Heritage*, 3, 309-316 (2002).
- [59] Davis, S. N., Porosity and Permeability of Natural Materials in Flow through Porous Materials, ed. R. J. M. DeWiest, 54-89. New York: Academic Press (1969).
- [60] Johnson, A. I., and Morris, D. A., Physical and hydrologic properties of water bearing deposits from core – holes in the Los Banos – Kettleman City area, California, U.S. *Geol. Survey, Open. File Rept.* Denver, Col. (1962).
- [61] Domenico, P. A., and Schwartz, W., *Physical and Chemical Hydrogeology*. John Wiley & Sons Inc. (1998)
- [62] Choquette, P. W., and Pray, L. C., *Am. Assoc. Petrol. Geol. Bull.*, 54, 207-259 (1970).
- [63] Boucher, E. A., *J. Mater. Sci.*, 11, 1734-1750 (1976).
- [64] Andriani, G., and Walsh, N., *Bull. Eng. Geol. Environment*, 62, 77-84 (2003).
- [65] Valdeon, L., Esbert, R. M., and Grossi, C. M., Hydric properties of some spanish building stones: a petrophysical interpretation. *Material issues in art and archeology III, Material Research Society Proc.*, 267, 911-916 (1992).
- [66] Montoto, M., and Esbert, R. M., *Trabajos de Geologia*, 21, 239-252 (1999).
- [67] Torraca, G., Porous building materials: Materials science for architectural conservation. *Int. Center for the Preservation and Restoration of Cultural Property, ICCROM, Roma*, 141 (1982).
- [68] Montoto, M., *Petrophysics at the rock matrix scale: hydraulic properties and petrographic interpretation*, 116 (2003).
- [69] Brown, C. E., *J. Hydrology*, 147, 169-195 (1993).
- [70] Petreus, I., unpublished data (2007).
- [71] Dürrast, H., Siegesmund, S., *Int. J. Earth Sci.*, 88, 392-408 (1999).

- [72] Winkler, E. M., *Stone in architecture: Properties, durability*. Berlin: Springer-Verlag (1997).
- [73] Amoroso, G. G., and Fassina, V., Stone Decay and Conservation: Atmospheric Pollution. Cleaning. Consolidation and Protection. *Materials Science Monographs* 11, 224-225. New York: Elsevier Science Publishers B.V. (1983).
- [74] Torraca, G., *Porous Building Materials: Materials Science for Architectural Conservation*, 3rd edition, 134. Rome: ICCROM (1988).
- [75] Clifton, J. R., Stone Consolidating Materials – A Status Report, 24 (1992).
- [76] Motakef, S., Suratwala, T., Roncone, R. L., Boulton, J. M., Teowee, G., and Uhlmann, D. R., *J. Non-Cryst. Solids*, 178, 37-43 (1994).
- [77] Yoshida, M., and Prasad, P. N., *Appl. Optics*, 35(9), 1500-1506 (1996).
- [78] Xu, C., Eldada, L., Wu, C., Norwood, R. A., Shacklette, L. W., Yardley, J. T., and Wei, Y., *Chem. Mater. (Commun.)*, 8(12), 2701-2703 (1996).
- [79] Dave, B. C., Dunn, B., Valentine, J. S., and Zink, J. I., *Anal. Chem.*, 66(22), 1120-1127 (1996).
- [80] Davies, B. L., Samoc, M., and Woodruff, M., *Chem. Mater.*, 8(11), 2586-2594 (1996).
- [81] Ji, X., Hampsey, J. E., Hu, Q., He, J., Yang, Z., and Lu, Y., *Chem. Mater.*, 15(19), 3656-3662 (2003).
- [82] Wight, A. P., and Davis, M. E., *Chem. Rev.*, 102(10), 3589-3614 (2002).
- [83] Pescarmona, P. P., and Maschmeyer, T., *Austr. J. Chem.*, 54(9-10), 583-596 (2001).
- [84] Eisenberg, P., Erra-Balsells, R., Ishikawa, Y., Lucas, J. C., Mauri, A. N., Nonami, H., Riccardi, C. C., and Williams, R. J. J., *Macromolecules*, 33(6), 1940-1947 (2000).
- [85] Feher, F. J., and Budzichowski, T. A., *Polyhedron*, 14(22), 3239-3253 (1995).
- [86] Park, J. W., and Thomas, E. L., *J. Am. Chem. Soc.*, 124(4), 514-515 (2002).
- [87] Du, J., and Chen, Y., *Macromol. Rapid Commun.*, 26(6), 491-494 (2005).
- [88] Du, J., and Chen, Y., *Macromolecules*, 37(15), 5710-5716 (2004).
- [89] Du, J., Chen, Y., Zhang, Y., Han, C. C., Fischer, K., and Schmidt, M., *J. Am. Chem. Soc.*, 125(48), 14710-14711 (2003).
- [90] Du, J., and Chen, Y., *Angew. Chem. Int. Ed.*, 43(38), 5084-5087 (2004).
- [91] Medda, S. K., Kundu, D., and De, G., *J. Non-Cryst. Solids*, 318(1-2), 149-156 (2003).
- [92] Liu, H., Zheng, S., and Nie, K., *Macromolecules*, 38, 5088-5097 (2005).

- [93] Bharadwaj, R. K., Berry, R. J., and Farmer, B. L., *Polymer*, 41, 7209-7221 (2000).
- [94] Rumo-Urbe, A., Mather, P. T., Haddad, T. S., and Lichtenhan, J. D., *J. Polym. Sci., Part B: Polym. Phys.*, 36, 1857-1872 (1998).
- [95] Appolonia, L., Fassina, V., Matteoli, U., Mecchi, A. M., Nugari, M. P., Pinna, D., Peruzzi, R., Salvadori, O., Santamaria, U., Scala, A., and Tiano, P., Methodology for the evaluation of protective products for stone materials. Part II: experimental tests on treated materials. *Proc. Int. Coll. on Methods of Evaluating Products for the Conservation of Porous Building Material in Monuments*, 301-312. Rome (1995).
- [96] Castelvetro, V., Aglietto, M., Ciardelli, F., Chiantore, O., Lazzari, M., and Toniolo L., *J. Coat. Technol.*, 74, 57-61 (2002).
- [97] Tsakalof, A., Manoudis, P., Karapanagiotis, I., Chrysoulakis, I., and Panayiotou, C., *J. Cultural Heritage*, 8, 69-72 (2007).
- [98] Alvarez de Buergo Ballester, M., and Fort González, R., *Progr. Organic Coatings*, 43, 258-266 (2001).
- [99] Hansen, C. M., *Progr. Organic Coatings*, 42, 167-173 (2001).
- [100] Simon, S., and Sneathlge, R., Marble weathering in Europe. Results of EURO CARE-EUROMARBLE Exposure Programme 1992-1994. *Proc. 8th International Congress on Deterioration and Conservation of Stone*, 159. Berlin (1996).
- [101] Lewin, S. Z., *The mechanism of masonry decay through crystallization*. Washington DC: National Academy of Sciences (1981).
- [102] Young, A. R. M., *Geology*, 15, 962-969 (1987).
- [103] Pye, K., and Mottershead, D. N., *J. Eng. Geol.*, 28, 333-338 (1995).
- [104] Zezza, F., Marine spray and polluted atmosphere as factors of damage to monuments in the Mediterranean coastal environment. *E. C. Project, Report 4*, 3 (1996).
- [105] Zezza, F., and Macri, F., *Sci. Total Environ.*, 123 (1995).
- [106] Moropoulou, A., Theoulakis, P., and Chrysophakis, T., *Atm. Environ.*, 895 (1995).
- [107] Rodriguez-Navarro, C., and Doehne, E., *Earth Surf. Proc. Land.*, 24, 191-209 (1999).
- [108] Rodriguez-Navarro, C., Doehne, E., and Sebastian, E., *Cem. Concr. Res.*, 30, 1527-1533 (2000).
- [109] Flatt, R. J., *J. Cryst. Growth*, 242, 435-454 (2002).
- [110] Thaulow, N., and Sahu, S., *Mat. Charact.*, 53, 123-127 (2004).
- [111] Scherer, G. W., *Cem. Concr. Res.*, 29, 1347-1358 (1999).

- [112] Scherer, G. W., *Cem. Concr. Res.*, 34, 1613-1624 (2004).
- [113] Steiger, M., *J. Cryst. Growth*, 282, 455-469 (2005).
- [114] Steiger, M., *J. Cryst. Growth*, 282, 470-481 (2005).
- [115] Coussy, O., *J. Mech. Phys. Solids*, 54, 1517-1547 (2006).
- [116] Goudie, A. S., and Viles, H. A., *Salt weathering hazard*. London: Wiley (1997).
- [117] Winkler, E. M., and Singer, P. C., *Geol. Soc. Am. Bull.*, 83, 3509-3513 (1972).
- [118] La Iglesia, A., Gonzalez, V., Lopez-Acevedo, V., and Viedma, C., *J. Cryst. Growth*, 177, 111-118 (1997).
- [119] Dei, L. M., Mauro, M., Baglioni, P., Del Fa, C. M., and Fratini, F., *Langmuir*, 15, 8915-8922 (1999).
- [120] Wellman, H. W., and Wilson, A. T., *Nature*, 205, 1097-1098 (1965).
- [121] Fitzer, B., and Sneath, R., *G. P. Newsletter*, 3, 13-18 (1982).
- [122] Gauri, K. L., Chowdhury, A. N., Kulshreshtha, N. P., and Punuru, A. R., *Engineering Geology of Ancient Works, Monuments and Historical Sites*. Rotterdam: Balkema, 723 (1988).
- [123] Benavente, D., Garcia del Cura, M. A., Fort, R., and Ordonez, S., *J. Cryst. Growth*, 204, 168-177 (1999).
- [124] Scherer, G. W., *Ninth International Congress on Deterioration and Conservation of Stone*, Venice, 187 (2000).
- [125] Price, C. A., *Stone Conservation: An Overview of Current Research*, The Getty Conservation Institute, CA (1996).
- [126] Mosquera, M. J., de los Santos, D. M., Montes, A., and Valdez-Castro, L., *Langmuir*, 24, 2772-2784 (2008).
- [127] Sperling, C. H. B., and Cooke, R. U., *Earth Surf. Proc. Land.*, 10, 541-549 (1985).
- [128] Goudie, A. S., *Earth Surf. Proc. Land.*, 18, 368-378 (1993).
- [129] Lubelli, B., Van Hees, R. P. J., Huinink, H. P., and Groot, C. J. W. P., *Cem. Concr. Res.*, 36(4), 678-687 (2006).
- [130] Lubelli, B. A., *Salt chloride damage to porous building materials*. Ph.D. thesis, Delft University of Technology (2006).
- [131] Pel, L., Huinink, H., Kopinga, K., Van Hees, R. P. J., and Zezza, F., *Proc. 13th Int. Brick and Block Masonry Conf.* Amsterdam (2004).
- [132] Lubelli, B., and De Rooij, M. R., *Constr. Build. Mat.* doi:10.1016/j. conbuildmat. 2008.09.010 (2008).

- [133] Welton, R. G., *Environ. Geochem. Health*, 25, 139-145 (2003).
- [134] Malaga-Starzec, J. K., *J. Cultural Heritage*, 4, 313-318 (2003).
- [135] Rodriguez-Navarro, C., and Dohne, E., *Earth Surf. Process. Land.*, 24, 19-23 (1999).
- [136] Sunagawa, I., *Bull. Mineral.*, 104, 81-91 (1981).
- [137] Arnold, A., and Zehnder, K., Crystallization and habits of salt efflorescences on walls. II. Conditions of crystallization. In *5th International congress on the deterioration and conservation of stone*, 269. Lausanne: Presses Polytechniques Romandes (1985).
- [138] Furlan, V., and Girardet, F., Considerations on the Rate of Accumulation and Distribution of Sulphurous Pollutants in Exposed Stones. In: *Materials Science and Restoration*, ed. F. H. Wittmann, 285-290. Filderstadt: Lack und Chemie (1983).
- [139] Amorosso, G. G., and Fassina, V., *Stone decay and conservation - Atmospheric pollution, cleaning, consolidation and protection. Materials Science Monographs*, vol. 11. Amsterdam: Elsevier (1983).
- [140] Gauri, K. L., and Holdren, G. C., *Environ. Sci. Technol.*, 15, 386-392 (1981).
- [141] Baedeker, P. A., Reddy, M. M., Reimann, K. J., and Sciammarella, C. A., *Atmos. Environ.*, 26B, 147-158 (1992).
- [142] Camuffo, D., del Monte, M., and Sabbioni, C., *Water, Air, Soil Poll.*, 19, 351-360 (1983).
- [143] Elfving, P., The initial steps in the air pollution induced deterioration of calcareous stone. In: *Proceedings of the 1995 LCP congress*, ed. R. Pancella, 421-427. Montreaux (1995).
- [144] Gauri, K. L., Popli, R., and Sarma, A. C., *Durability Build. Mat.*, 1, 209-217 (1982).
- [145] Derbez, M., and Lefevre, R. A., *8th Intern. Congr. Deterioration and Conservation of Stone*, 459-370. Berlin (1996).
- [146] (a) Cody, R. D., and Cody, A. M., *J. Sed. Petrol.*, 58, 247-255 (1987); (b) Amit, R., and Yaalon, D. H., *Earth Surface Proc. Land.*, 21, 1127-1143 (1996).
- [147] Edinger, S. E., *J. Cryst. Growth*, 18, 217-224 (1973).
- [148] Amoroso, G. G., and Fassina, V., *Stone Decay and Conservation, Materials Science Monographs*, 11, 151-172 (1983).
- [149] Gauri, K. L., *Studies in Conservation*, 34, 201-206 (1989).

- [150] (a) Simionescu, B., Aflori, M., and Olaru, M., *Constr. Build. Mat.*, 23, 3426-3430 (2009), doi: 10.1016/j.conbuildmat.2009.06.032 (2009); (b) Simionescu, B., and Olaru, M., *Eur. J. Sci. Theol.*, 5(1), 59-67 (2009); (c) Simionescu, B., Aflori, M., and Olaru, M., *Z. Kristallogr. Suppl.* 30, 471-476 (2009).
- [151] Skoulikidis, T. N., and Beloyannis, N., *Studies in Conservation*, 29, 197-204 (1984).
- [152] Gauri, K. L., and Bandyopadhyay, J. K., *Carbonate Stone, Chemical Behaviour, Durability, and Conservation*. John Wiley & Sons (1999).
- [153] Doornkamp, J. C., and Ibrahim, H. A. M., *Prog. Phys. Geogr.*, 14, 335-348 (1990).
- [154] Rodriguez-Navarro, C., *Appl. Environ. Microbiol.*, 69, 2182-2193 (2003).
- [155] Arnold, A., and Zehnder, K., In: *The Conservation of Monuments in the Mediterranean Basin*, ed. F. Zezza, 30-58. Proceedings, 1st International Symposium. Bari (1989).
- [156] Sanjeev Tambe, K., Gauri, L., Li, S., and Cobourn W. G., *Environ. Sci. Technol.*, 25(12), 2071-2075 (1991).

Personal contributions

- [1] Simionescu, B., Olaru, M., Aflori, M., Buruiana, E. C., Cotofana, C., *Silsesquioxane-based Hybrid Nanocomposites of Polymethacrylate Type with Self-assembling Properties*, *Solid State Phenomena*, 151, 17-23 (2009).
- [2] Simionescu, B., Olaru, M., *Assesment of Siloxane-Based Polymeric Matrices as Water Repellent Coatings for Stone Monuments*, *Eur. J. Sci. Theol.*, 5(1), 59-67 (2009)
- [3] Simionescu, B., *European PhD in Science for Conservation – EU Project EPISCON*, *EEMJ*, 8(1), 80 (2009).
- [4] Simionescu, B., Olaru, M., Aflori, M., Buruiana, E. C., Cotofana, C., *Silsesquioxane-based Hybrid Nanocomposite with Self-assembling Properties for Porous Limestones Conservation*, *High Perform. Polym.*, DOI: 10.1177/0954008308100905 (2009).
- [5] Simionescu, B., Aflori, M., Olaru, M., *Protective coatings based on silsesquioxane nanocomposite films for building limestones*, *Constr. Build. Mat.*, 23, 3426-3430 (2009), doi: 10.1016/j.conbuildmat.2009.06.032 (2009).
- [6] Aflori, M., Simionescu, B., Olaru, M., Cotofana, C., *Studii privind actiunea consolidantilor pe baza de derivati de silan asupra rocilor Laspra (Catedrala Oviedo din Spania) si Repedea (Manastirea Dobrovat din Romania)*, *Monumentul IX – Lucrarile celei de a IX-a editii a Simpozionului National Monumentul – Traditie si Viitor*, Iasi – 2008, ArtStudio Iasi 2008 ISSN 1844-9042, 595-609 (2008).
- [7] Simionescu, B., Aflori, M., Olaru, M., *Mineral composition and stone conservation of cultural heritage building materials studied by PXRD*, *Z. Kristallogr. Suppl.* 30, 471-476 (2009).
- [8] Theodoridou, M., Simionescu, B., *EPISCON – Project, European PhD in Science for Conservation*, *International Symposium “Stone Consolidation in Cultural Heritage”*, Lisbon, Portugal, May 6-7, 2008 – poster.

- [9] Simionescu, B., Olaru, M., Aflori, M., Buruiana, E. C., Cotofana, C., ***Silsesquioxane-based Hybrid Nanocomposites of Polymethacrylate Type with Self-assembling Properties***, E-MRS Fall Meeting, Warsaw University of Technology, Warsaw, Poland, September 15-19, 2008 – oral presentation.
- [10] Simionescu, B., Doroftei, F., Olaru, M., Aflori, M., Cotofana, C., ***Salt-induced decay in limestones treated with siloxane-based water repellents***, International Conference on Material Science & Engineering, February 26-28, 2009, Brasov, Romania – oral presentation; submitted to *J. Optoelectronics Adv. Mat.*
- [11] Olaru, M., Simionescu, B., ***Tayloring New Nanomaterials for Stone Conservation***, *New Materials Forum*, March 5-6, 2009, Valencia, Spain – oral presentation.